Adaptive Resummation of Markovian Quantum Dynamics

Dissertation zur Erlangung des Grades Doktor der Naturwissenschaften an der Fakultät für Physik der Universität Duisburg-Essen durchgeführt am Max-Planck-Institut für Physik komplexer Systeme

vorgelegt von Felix Lucas

aus Berlin

Jena, den 27.03.2014

1. Gutachter: Prof. Dr. Klaus Hornberger

2. Gutachter: Prof. Dr. Christiane Koch

3. Gutachter: Prof. Dr. Peter Entel

Tag der mündlichen Prüfung: 06.08.2014

Zusammenfassung

In der Praxis wechselwirken fast alle Quantensysteme auf die ein oder andere Weise mit ihrer Umgebung. Die komplexen Bewegungs- oder Mastergleichungen solcher offener Quantensysteme sind jedoch nur in den seltensten Fällen analytisch lösbar, und es ist daher schwer, prägnante und allgemeingültige Aussagen über sie zu treffen. Solche wären aber wiederum notwendig, um die spezifische Dynamik offener Quantensysteme wie Dekohärenz, Dissipation oder stationäre Zustände gezielt ausnutzen zu können.

In dieser Dissertation leiten wir eine hochkonvergente, nichtperturbative Reihendarstellung für Markow'sche Mastergleichungen her. Sie basiert auf einer Entwicklung der Markow'schen Dynamik in kontinuierliche Abschnitte und abrupte Sprünge und erhält ihre vorteilhaften Konvergenzeigenschaften durch eine adaptive Resummierung dieser sogenannten *Jump-Expansion*. Anhand der Dynamik zweier namhafter Modellsysteme, der räumlichen Detektion eines freien Teilchens und dem Landau-Zener-Problem mit Umgebungskopplung, zeigen wir, dass durch die hohe Konvergenz der Reihendarstellung und die mathematische Flexibilität der Resummierung neue, hochgenaue analytische Näherungen ermöglicht werden. Basierend auf der analytischen Beschreibung des offenen Landau-Zener-Problems schlagen wir eine effiziente und robuste inkohärente Kontrollmethode für die Isomerisierung des menschlichen Sehproteins Rhodopsin vor. Die Resummierung der Jump-Expansion ermöglicht aber nicht nur hochpräzise analytische Näherungslösungen für Markow'sche Mastergleichungen, sie impliziert auch eine neue, effiziente Methode für deren numerische Simulation. Den dazugehörigen Simulationsalgorithmus formulieren wir mit Hilfe der Monte-Carlo-Integration der involvierten Entwicklungsterme und demonstrieren ihn anhand einiger ausgewählter, paradigmatischer offener Quantensysteme.

Abstract

In this thesis we derive a highly convergent, nonperturbative expansion of Markovian open quantum dynamics. It is based on a splitting of the incoherent dynamics into periods of continuous evolution and abrupt jumps and attains its favorable convergence properties from an adaptive resummation of this so-called *jump expansion*. By means of the long-standing problems of spatial particle detection and Landau-Zener tunneling in the presence of dephasing, we show that this adaptive resummation technique facilitates new highly accurate analytic approximations of Markovian open systems. The open Landau-Zener model leads us to propose an efficient and robust incoherent control technique for the isomerization reaction of the visual pigment protein rhodopsin. Besides leading to approximate analytic descriptions of Markovian open quantum dynamics, the adaptive resummation of the jump expansion implies an efficient numerical simulation method. We spell out the corresponding numerical algorithm by means of Monte Carlo integration of the relevant terms in the jump expansion and demonstrate it in a set of paradigmatic open quantum systems.

Ich danke Klaus Hornberger für seine umsichtige und gewissenhafte Betreuung. Durch ihn erlernte ich eine tiefgründige wissenschaftliche Arbeitsweise und erhielt einen Einblick in einige der interessantesten und fundamentalsten Probleme der modernen Physik. In den entscheidenden Momenten gab er mir immer wieder neue, erfolgversprechende Impulse und ließ mir dennoch genügend Freiheit um meine eigenen Gedanken zu verfolgen.

Besonders danken möchte ich Marie, deren moralischer Rückhalt von unschätzbarem Wert ist, und natürlich Frieda und Kuno, die mir zugleich innerer Ausgleich und persönlicher Ansporn sind. Darüber hinaus danke ich meiner ganzen Familie ohne deren langjährige Unterstützung ich niemals so weit gekommen wäre.

Contents

1 Introduction

The notion that the behavior of the macroscopic objects around us are determined by the properties and interrelations of their basic constituents is deeply rooted in our modern, educated world view, to the extent of being almost common sense. For example, we find it reasonable that a billiard ball obtains its mass and rigidity from the mass and electromagnetic forces of its constituent molecules, although the exact underlying physical mechanism might be complicated. Our classical intuition would, however, firmly protest if someone were to claim that the billiard ball can be found in both the upper left and the lower right pocket at the same time, just as quantum mechanics predicts for the constituent molecules. In other words, the fundamental contradictions between classical physics and quantum mechanics imply a serious dilemma which most of our contemporaries choose to ignore.

To be more precise, in classical physics one assumes that an object is completely determined by a set of well defined, measurable physical properties. In contrast, the behavior of a quantum particle is governed by a catalog of what *could* be measured, which is called the wave function. The wave function does not allow for a straightforward realistic interpretation: It prescribes that all measurements are inherently probabilistic and, consequently, that our way of perceiving the objects around us defines their physical reality. Most notably, this opens up the possibility for quantum systems to be in two distinct, classically allowed states at the same time which is called the quantum superposition principle.

The apparent contradictions between classical and quantum mechanics have bothered physicists for decades until, in the 1980s, a genuine quantum solution to this dilemma was proposed. The so-called decoherence theory suggests to view the emergence of classical properties on the macroscopic scale as resulting from a continuous monitoring of an open quantum system by its environment [1–4]. The line of thought employed is that information about the open quantum system leaks out into the surroundings, which continuously pins down the physical reality of the system just as in a conventional quantum measurement. This is what is called *decoherence*. Moreover, the inevitable information leakage occurs ever more strongly as the system size increases. This decoherence mechanism for describing the quantum to classical transition has so far withstood all experimental tests [5, 6].

Besides explaining the fundamental difference between quantum and classical behavior, decoherence theory has quite a few practical implications as well. For example, it states that, if we want to exploit the quantum nature of a given system, for example for information processing, we better isolate it from the environment or reduce the induced classicality in some other way [7, 8]. Also, the much richer incoherent dynamics of an open quantum system implies new levers for controlling its dynamics [9–11], for example

for steering a given chemical reaction [12]. What is more, a properly designed incoherent control scheme can be much more robust than the conventional coherent control techniques [11, 13].

Although the basic principles of decoherence theory are well established, an intuitive understanding as well as an accurate analytical description of its dynamics are underdeveloped at present. A deeper understanding of decoherence is, however, necessary for avoiding its detrimental impact and for using it in quantum control. The problem is that the description of open quantum systems is conceptually more difficult than that of closed quantum systems: On the one hand, it must incorporate different possible outcomes of the monitoring by the environment, which introduces a stochastic component to the system dynamics. On the other hand, the description of the open system necessarily involves references to the properties of the complex environment. For practical purposes those references should ideally be concise and in closed form, which calls for a simple, approximate description of the environment. These aspects make an analytic description and intuitive understanding of the decoherence of a given open quantum system quite challenging. In particular, the emergence of specific classical properties from an underlying quantum description through decoherence has so far been shown only for a limited set of model systems with model environments [14–16].

1.1 Scope of the Thesis

In the present thesis we outline a new method for the analytical and numerical investigation of open quantum systems based on a highly convergent, nonperturbative expansion of their dynamics called the *jump expansion* [17–21]. In order to facilitate an analytical treatment we focus on the simplest conceivable open systems which are those immersed in a memoryless environment. The time evolution of these so-called *Markovian* open systems is completely determined by a master equation for the system degrees of freedom without explicit reference to the dynamics of the environment.

The jump expansion decomposes the Markovian system dynamics into periods of continuous evolution and discontinuous jumps [17–19]. This structure is very similar to that of a Dyson series for a weakly perturbed closed quantum system. In contrast to the Dyson series, the nonperturbative jump expansion does not involve a small parameter. While this enables us to cover the complete range of parameters involved, it makes the convergence properties of the jump expansion doubtful. The convergence of the jump expansion can, however, be enhanced by performing an adaptive resummation based on the invariance properties of Markovian master equations [20, 21]. We derive various such resummations, for example one which optimizes the convergence by maximizing the weights of the lowest order expansion terms, and others which combine a strong convergence with a simple algebraic structure. The latter ones are specifically suited for deriving approximate analytic descriptions.

This adaptive resummation method enables us to derive highly accurate analytic approximations to two long-standing nontrivial open quantum systems: (i) the spatial monitoring of a free particle, and (ii) the open Landau-Zener system [20]. In both cases,

the adaptive resummation method supplies a compelling intuitive picture of the open system dynamics. While the evolution in the spatial detection setting can be viewed as the repeated quantum scattering at an imaginary potential step, the open Landau-Zener system is mapped to a classical alternating Markov chain. The gained intuition can then be used for designing robust incoherent control techniques, as we show by means of the isomerization reaction in the visual pigment protein rhodopsin [22].

Besides facilitating new approximate analytic descriptions of open quantum systems, the adaptive resummation method provides a novel scheme for their efficient numerical simulation [21]. It is based on the numerical approximation of the terms of the jump expansion by classical Monte Carlo integration with importance sampling. The high convergence of the resummed jump expansion implies that one obtains successive estimates of the system evolution, with the most important contributions evaluated first. In this sense it complements the standard quantum Monte Carlo simulation method which calculates all contributions indiscriminately. The validity and efficiency of the classical Monte Carlo simulation method is verified in a set of paradigmatic Markovian master equations.

1.2 Structure

This thesis is structured as follows. We start by introducing the basic concepts of open quantum systems and their dynamics in Chapter 2. This chapter may well be skipped by the informed reader already familiar with the topic. We outline, in particular, how one formally divides a large quantum compound into a system part and an environmental part and show that disregarding the environmental degrees of freedom leads to density matrices for the open system state. Focusing on Markovian open systems, we then write down a master equation for the time evolution of the system density matrix in terms of a time-local generator, without explicit reference of the of the environmental dynamics. Respecting the physical constraints for density matrices, we see that the dynamical generator takes on a particularly simple form involving a set of positive rates and associated jump operators acting on the system degrees of freedom. We conclude this chapter by demonstrating a possible interpretation of the open system dynamics in terms of a stochastic time evolution on Hilbert space composed of periods of deterministic evolution interspersed with random jumps.

After deriving the time evolution equation for general Markovian open systems from first principles, in Chapter 3 we apply it to three paradigmatic open quantum models: (i) the damped harmonic oscillator, (ii) the motion of a Brownian test particle in a thermal background gas, and (iii) the time evolution induced by a continuous non-selective measurement. These models allow us to demonstrate the genuine features of open quantum dynamics that distinguish them from the closed system evolution under the Schrödinger equation. They also serve as testbeds for our newly derived numerical simulation scheme later on.

Chapter 4 is entirely devoted to the jump expansion of the Markovian time evolution and its properties and resummations. The jump expansion is formally derived in analogy

to Dyson series for closed quantum systems by splitting the Markovian generator into two parts. This leads to a decomposition of the dynamics into periods of continuous evolution of the density matrix and abrupt transformations. The jump expansion yields a formal solution to general Markovian master equations even though it is not guaranteed to converge due to its nonperturbative character, *i.e.* the absence of a small parameter.

One can, however, ensure the convergence of the jump expansion in a second step, which makes it useful also for practical applications. Using the invariance of Markovian master equations under complex shifts of the jump operators, first we see that there exists a multitude of expansions of one and the same open system dynamics. They can be viewed as arising from different resummations of the original jump expansion. Then, we quantify the convergence of a specific expansion by means of suitably defined weights of the respective expansion terms. It shows that the resummations differ in how fast they converge with the number of expansion orders. Based on this quantification of convergence, we derive the optimally convergent resummation by maximizing the weights of the lowest order expansion terms. We find that the optimal resummation is adaptive in the sense that the involved optimal complex shifts of the jump operators are conditioned on the types of all previous jump transformations and on the times when they occurred. From this optimal adaptive resummation one can derive other strongly convergent resummations that have a simpler algebraic structure, *i.e.* which involve fewer dependencies. Those are particularly useful for deriving analytical approximations for Markovian open systems.

In Chapter 5 we derive approximate analytical descriptions of two exemplary master equations based on the adaptive resummation method. The first model system describes a free particle in one dimension undergoing spatial detection. While in the original jump expansion with unshifted jump operators, the jump transformations amount to projections of the particle onto the left and right half space, the adaptive resummation associates them with transits across the coordinate origin. It also shows that influence of the spatial detection is equivalent to a sequence of quantum scatterings at an imaginary potential step, which is readily accessible with analytical means. This enables us to derive an approximate analytical expression for the probability of reflection at the measurement boundary, which is accurate to the per mil level. In the second open system, the Landau-Zener problem with dephasing, the adaptive resummation method suggests a mapping of the original quantum dynamics involving tunnelings and jumps to a classical alternating Markov chain which, in turn, is analytically accessible. Again we obtain a highly accurate analytic approximation, this time for the open Landau-Zener tunneling probability.

Chapter 6 shows that, besides facilitating accurate analytic approximations, the adaptive resummation method opens up a new way to simulate open quantum systems efficiently. In particular, it yields a numerical algorithm that successively approximates the expansion terms by Monte Carlo integration with importance sampling. The maximization of the lowest order weights by the optimal resummation implies here that one can assess the contributions to a given evolved state term by term, in the order of their importance. This simulation method is briefly compared to the standard approach based on quantum trajectories. We then apply the Monte Carlo integration scheme to the

exemplary Markovian master equations from Chapter 3, to prove its validity and illustrate the efficiency implied by the optimal resummation. In particular, the numerical examples show that the optimal resummation generally converges within the lowest two to five orders.

Using the analytic open Landau-Zener model from Chapter 5, in Chapter 7 we propose an incoherent control scheme based on the back action dynamics due to a nonselective continuous measurement. To show that incoherent control can surpass conventional coherent control techniques in terms of performance and robustness, we apply it to the isomerization reaction of the biological pigment protein rhodopsin. The isomerization of rhodopsin not only constitutes the primary event in human vision, but it is also used for light harvesting in certain bacteria. While the relatively large rhodopsin molecule exhibits only a limited susceptibility to intricately shaped coherent laser pulses [23], we demonstrate that a purposeful switching on and off of an infrared measurement enhances the isomerization yield incoherently up to values close to unity. Also, a simple on-off sequence is much less prone to experimental imperfections than a laser pulse that is shaped in the time and frequency domain.

2 Dynamics of Open Quantum Systems

One of the original fundamental postulates of quantum mechanics is this [24, 25]: all measurements of quantum systems yield probabilistic outcomes; the quantum state after the measurement is conditioned on the recorded outcome. The quantum state of a system, in turn, is represented by a so-called *wave function* which can be viewed as a catalog that contains all possible measurement outcomes and their probabilities. This postulate, which defines quantum mechanics as an intrinsically probabilistic theory, is in plain contradiction to our classical physical intuition—namely, that objects have well defined, *i.e.* deterministically measurable properties and that those properties exist independent of whether they have been measured or not. This discrepancy led Einstein to conjecture that quantum mechanics must be incomplete and culminated in his famous declaration that "God does not play dice!"

Nevertheless, the completeness of quantum theory and the fundamental properties of quantum measurements were repeatedly verified with different experimental setups [5, 26, 27]. What is more, our modern understanding of quantum mechanics puts us in a position to deduce the probabilistic nature of quantum measurements and the associated state transformation from the mathematical properties of the state space of composite systems [25, 28]. The underlying mechanism can be briefly described as follows: In the generic measurement setting, the relevant quantum object to be described is composed of the system under scrutiny and the measurement apparatus. Prior to a measurement, the two must interact and the apparatus will then assume one of several predefined states that we can read off as one specific outcome. This is, however, insufficient for reconstructing the full system state before the interaction faithfully, as it turns out [25]. In fact, the impossibility to obtain complete information about the system is manifest in a probabilistic occurrence of the outcomes and the only way to extract more information is by repeating the measurement.

The generic quantum measurement setting is very similar to that of an open quantum system in contact with its environment. Here, the environment continuously extracts information about the open system. The difference is that one generally cannot switch on and off the system-environment interaction nor can one directly read off the state of the environment which is, by definition, large and inaccessible. Making use of the measurement analogy, one would therefore expect the open system to evolve in a way that can be described as the average over some stochastic dynamics. This continuous averaging process degrades the characteristic ability of quantum systems to form coherent superpositions especially for large systems that interact strongly with their environment. Therefore, the same mechanism that results in the probabilistic nature of quantum measurements can consistently describe the emergence of classical properties on the macroscopic scale. This so-called *decoherence theory* [4] has so far withstood all experimental

tests [6, 29]. What is more, only the dynamics of open quantum systems can explain such important phenomena as energy dissipation [28, 30] or quantum Brownian motion [19, 31].

In this chapter, we will lay the ground for the ensuing study of open quantum dynamics by working out the above concepts. First, we describe the mathematical structure of the states and associated state space of quantum systems, which naturally accounts for their probabilistic quantum properties. Then we introduce the formal concept of a quantum measurement. Finally, we outline the derivation of a differential evolution equation for open quantum systems. Specifically, we concentrate on the important subclass of time-local Markovian evolution equations [28], which are particularly suited for systems in contact with a large number of environmental degrees of freedom.

2.1 Quantum Fundamentals

2.1.1 The Density Matrix

In quantum mechanics, the physical states of a system are described by normalized vectors $|\psi\rangle$ that belong to a Hilbert space $\mathcal{H}$. Assuming that vectors $\{|\chi_i\rangle\}$ form an orthonormal basis of $\mathcal{H}$, one can expand each vector as

$$|\psi\rangle = \sum_{i=1}^{d} c_i |\chi_i\rangle, \tag{2.1}$$

with the expansion coefficients $c_i = \langle\chi_i|\psi\rangle$ and the Hilbert space dimension $\dim(\mathcal{H}) = d$. Here we have made use of the scalar product $\langle\cdot|\cdot\rangle$ associated with $\mathcal{H}$ or, equivalently, of the dual vectors $\langle\psi|$ of $|\psi\rangle$. The absolute square of the expansion coefficient c_i is postulated as the probability to find the system in the basis state $|\chi_i\rangle$, which means that state vectors must be of unit norm, $\langle\psi|\psi\rangle = 1$.

Furthermore, all measurable quantities of a given quantum system are described by Hermitian operators A called *observables*. The possible outcomes of an idealized measurement of A are given by the eigenvalues a_i[1], where $\mathsf{A} = \sum_i a_i |a_i\rangle\langle a_i|$. The probability to record outcome a_i is determined by the overlap of the corresponding eigenvector $|a_i\rangle$ with the state vector $|\psi\rangle$,

$$\mathrm{Prob}(a_i|\psi) \equiv |\langle a_i|\psi\rangle|^2. \tag{2.2}$$

As a consequence, the expectation value of the observable A is given by

$$\langle\mathsf{A}\rangle_\psi = \sum_i a_i \,\mathrm{Prob}(a_i|\psi) = \sum_i a_i \langle\psi|a_i\rangle\langle a_i|\psi\rangle = \langle\psi|\mathsf{A}|\psi\rangle. \tag{2.3}$$

After detecting the outcome a_i, the state vector $|\psi\rangle$ is projected onto the corresponding

[1] For a more general definition of quantum measurements that is applicable to realistic measurement scenarios, see Sec. 2.1.3.

eigenvector

$$|\psi\rangle \mapsto |\psi_{a_i}\rangle = \mathrm{Prob}(a_i|\psi)^{-1/2}\langle a_i|\psi\rangle|a_i\rangle. \tag{2.4}$$

Here, the prefactor $\mathrm{Prob}(a_i|\psi)^{-1/2}$ ensures the normalization of $|\psi_{a_i}\rangle$.

If the quantum system under consideration allows for statistical ensembles of state vectors, one must resort to a more general definition of quantum states. Imagine, for example, that a given quantum device prepares either one of the state vectors $|\psi_j\rangle$ ($j = 1, 2, \ldots$), each with a corresponding probability $p_j \geq 0$ where $\sum_j p_j = 1$. Then, the resulting quantum state is represented by the so-called *density matrix*

$$\rho = \sum_j p_j |\psi_j\rangle\langle\psi_j|. \tag{2.5}$$

The convention here is that the symbol $|\psi_j\rangle\langle\psi_j|$ is to be read as an outer product of a vector $|\psi_j\rangle$ with its dual vector $\langle\psi_j|$. It is a projector onto the vector $|\psi_j\rangle$, *i.e.* $|\psi_j\rangle\langle\psi_j||\psi_j\rangle\langle\psi_j| = |\psi_j\rangle\langle\psi_j|$, which is why we refer to ρ as a matrix[2]. State vectors or so-called *pure states* $|\psi\rangle$ are incorporated in the above definition as the specific density matrices $\rho = |\psi\rangle\langle\psi|$. All density matrices that cannot be written in this form are called *mixed states*.

The density matrix ρ of a mixed state incorporates our classical (Bayesian) uncertainty about the true state vector. This can be seen in the corresponding definitions of measurement probabilities and expectation values of observables A,

$$\mathrm{Prob}(a_i|\rho) \equiv \langle a_i|\rho|a_i\rangle = \sum_j p_j |\langle a_i|\psi_j\rangle|^2 = \sum_j p_j \,\mathrm{Prob}(a_i|\psi_j), \tag{2.6}$$

$$\langle\mathsf{A}\rangle_\rho = \sum_i a_i \,\mathrm{Prob}(a_i|\rho) = \sum_{i,j} a_i p_j \,\mathrm{Prob}(a_i|\psi_j) = \sum_{i,j} p_j \langle\mathsf{A}\rangle_{\psi_j} = \mathrm{Tr}(\mathsf{A}\rho), \tag{2.7}$$

where we have used Eqs. (2.2), (2.3), and (2.5). Equivalent to the pure state case, a detection of the outcome a_i results in a projection onto the corresponding eigenvector

$$\rho \mapsto \rho_{a_i} = \mathrm{Prob}(a_i|\rho)^{-1}\langle a_i|\rho|a_i\rangle|a_i\rangle\langle a_i|. \tag{2.8}$$

It is important to note that different ensembles, say $\{p_j, |\psi_j\rangle\}$ and $\{w_j, |\varphi_j\rangle\}$, may lead to exactly the same density matrix[3]. Therefore, all conclusions about the physical properties of a given system must be drawn from ρ, not from a specific ensemble of state vectors.

There are two main requirements that any physically meaningful density matrix must fulfill. The consistency arguments that the measurement of any observable A should produce an outcome *at all* and that the probability for any outcome should be nonnegative

[2] The use of the symbols $|\cdot\rangle$ and $\langle\cdot|$ for vectors and dual vectors, which is called the *bra-ket* notation, is quite powerful. It allows us to immediately identify $\langle\cdot|\cdot\rangle$ and $|\cdot\rangle\langle\cdot|$ as complex numbers and matrices, respectively, and it is in agreement with the notation of scalar products and expectation values, see Eqs. (2.1) and (2.3).

[3] Take, for example, the ensembles $\{3/4, |0\rangle; 1/4, |1\rangle\}$ and $\{1/2, \sqrt{3/4}|0\rangle + \sqrt{1/4}|1\rangle; 1/2, \sqrt{3/4}|0\rangle - \sqrt{1/4}|1\rangle\}$ that both lead to the density matrix $\rho = 3/4|0\rangle\langle 0| + 1/4|1\rangle\langle 1|$.

imply that ρ must have unit trace and be positive,

$$\operatorname{Tr}\rho = 1, \tag{2.9}$$

$$\rho \geq 0. \tag{2.10}$$

The meaning of positivity in this context is that all eigenvalues λ_j in the spectral decomposition

$$\rho = \sum_j \lambda_j |e_j\rangle\langle e_j| \tag{2.11}$$

are real and positive. The positivity of ρ implies that ρ is Hermitian. Also note that the spectral decomposition, Eq. (2.11) defines one specific ensemble of state vectors, Eq. (2.5), for the density matrix ρ. In general, there are infinitely many equivalent ensembles.

In a specific Hilbert space basis, such as $\{|\chi_i\rangle\}$, ρ can be represented by a complex, Hermitian matrix (ρ_{ij}) as

$$\rho = \sum_{i,j=1}^{d} \rho_{ij} |\chi_i\rangle\langle\chi_j|, \qquad \text{with } \rho_{ij} = \langle\chi_i|\rho|\chi_j\rangle. \tag{2.12}$$

The nonnegative entries ρ_{ii} on the diagonal of this matrix, the so-called *populations*, are the probabilities to find the system in the basis states $|\chi_i\rangle$. The off-diagonal elements ρ_{ij} with $i \neq j$ are called *coherences* since they are responsible for quantum mechanical interference effects that appear, for example, in the famous double-slit experiment [24]. One can show that for positive density matrices, they are bounded from above by

$$|\rho_{ij}|^2 \leq \rho_{ii}\rho_{jj}. \tag{2.13}$$

For infinite dimensional Hilbert spaces and a continuous (improper) basis such as the position basis of a free particle, Eq. (2.12) reads

$$\rho = \int \rho(x,x')|x\rangle\langle x'|\mathrm{d}x\mathrm{d}x', \qquad \text{with } \rho(x,x') = \langle x|\rho|x'\rangle. \tag{2.14}$$

The space of all physical density matrices is convex, which means that any two physical states ρ_1 and ρ_2 can be admixed with the classical probabilities p and $1-p$ to give a new valid density matrix

$$\rho = p\rho_1 + (1-p)\rho_2. \tag{2.15}$$

ρ then incorporates our additional (classical) uncertainty about the prescribed mixing process. Conversely, any density matrix ρ can be decomposed into a sum of two density matrices ρ_1 and ρ_2. A necessary condition for pure states $\rho = |\psi\rangle\langle\psi|$ is now that $\rho_1 = \rho_2$. Pure states are hence the only states that involve no classical uncertainty. The degree of purity of a density matrix ρ can be quantified by the von Neumann entropy

$$S_{\mathrm{N}}(\rho) = -\operatorname{Tr}[\rho\ln\rho] = -\sum_j \lambda_j \ln\lambda_j, \tag{2.16}$$

where we have used the spectral decomposition (2.11) of ρ. The von Neumann entropy ρ of is therefore simply the Shannon entropy of its eigenvalues. It vanishes if and only if ρ is a pure state and it takes on its maximum value $S_{\mathrm{N}}(\rho) = \ln d$ for the maximally mixed state $\rho = d^{-1}\mathbb{1}$. Alternatively, the purity can be measured by the linear entropy

$$S_{\mathrm{lin}}(\rho) = 1 - \mathrm{Tr}\,\rho^2. \tag{2.17}$$

The linear entropy is bounded by $0 \leq S_{\mathrm{lin}}(\rho) \leq 1 - 1/d$ and, similar to the von Neumann entropy, attains its extreme values for a pure state and the maximally mixed state.

2.1.2 Composite Quantum Systems and Entanglement

Let us now consider two quantum systems with respective Hilbert spaces $\mathcal{H}^{(1)}$ and $\mathcal{H}^{(2)}$. They may represent, for example, two distinguishable particles or two degrees of freedom of the same particle. The Hilbert space of the joint system is given by the tensor product $\mathcal{H} = \mathcal{H}^{(1)} \otimes \mathcal{H}^{(2)}$ of the two constituent Hilbert spaces[4]. For such a composite Hilbert space, the state vectors are written as

$$|\psi\rangle = \sum_{i,j} c_{ij} |\psi_i^{(1)}\rangle \otimes |\psi_j^{(2)}\rangle, \qquad \text{with } |\psi_i^{(k)}\rangle \in \mathcal{H}^{(k)}, \tag{2.18}$$

and, as before, density matrices are statistical ensembles of these state vectors, see Eq. (2.5).

For a composite pure state, Eq. (2.18), we can diagonalize the coefficient matrix (c_{ij}) using the singular singular value decomposition $c_{ij} = \sum_k u_{ik} d_{kk} v_{kj}$, where (u_{ij}) and (v_{ij}) are unitary matrices. In the present context, this is called the Schmidt-decomposition and it allows to rewrite the state as $|\psi\rangle = \sum_k d_{kk} |\phi_k^{(1)}\rangle \otimes |\phi_k^{(2)}\rangle$, with $|\phi_k^{(1)}\rangle = \sum_i u_{ik} |\psi_i^{(1)}\rangle$ and $|\phi_k^{(2)}\rangle = \sum_j v_{jk} |\psi_j^{(2)}\rangle$. State vectors whose Schmidt-decomposition has more than one term, *i.e.* states which *cannot* be written in the form $|\psi\rangle = |\psi^{(1)}\rangle \otimes |\psi^{(2)}\rangle$, are called *entangled states* [25, 32]. Analogously, mixed states are called entangled if they cannot be written as a so-called *product state* $\rho = \rho^{(1)} \otimes \rho^{(2)}$ or as a statistical mixture of product states.

Entanglement is a genuine quantum property originating from the superposition principle of composite quantum systems. Crucially, measurements on the constituent subsystems of an entangled system are correlated. Take, for example, a pair of two-level systems in the entangled pure state[5]

$$\rho_{\mathrm{e}} = |\psi_{\mathrm{e}}\rangle\langle\psi_{\mathrm{e}}| \equiv \frac{1}{2}(|00\rangle + |11\rangle)(\langle 00| + \langle 11|) = \frac{1}{2}(|00\rangle\langle 00| + |00\rangle\langle 11| + |11\rangle\langle 00| + |11\rangle\langle 11|). \tag{2.19}$$

Applying Eq. (2.6), we see that the probabilities to detect the first subsystem in state $|0\rangle$ or $|1\rangle$ are both $1/2$. If we follow the conditional update rule, Eq. (2.8), after detecting

[4] In contrast, the classical state space of a composite system is the *direct sum* of the constituent state spaces [32].

[5] Here, we use the abbreviated notation $|i^{(1)}\rangle \otimes |j^{(2)}\rangle = |ij\rangle$.

the first subsystem in state $|0\rangle$ (state $|1\rangle$), however, we find that the probability to detect the second subsystem in the same state $|0\rangle$ ($|1\rangle$) is unity. The same holds true for the classically correlated but unentangled mixed state

$$\rho_{\mathrm{c}} = \frac{1}{2}(|00\rangle\langle 00| + |11\rangle\langle 11|). \tag{2.20}$$

By *classical* correlations we mean that the above correlations are statistical in nature and not due to a quantum superposition. The difference between ρ_{e} and ρ_{s} is that only ρ_{e} exhibits perfect correlations in the distinct measurement basis $\{(|0\rangle + |1\rangle)/\sqrt{2}, (|0\rangle - |1\rangle)/\sqrt{2}\}$ as well. In this sense, entangled states exhibit stronger correlations than any classically correlated state [25, 32].

These strong correlations result in another property of entangled states which is particularly important for the study of open quantum systems. Assume that our access is limited to one subsystem of the pure entangled state $\rho_{\mathrm{e}} = |\psi_{\mathrm{e}}\rangle\langle\psi_{\mathrm{e}}|$, Eq. (2.19), and we know nothing about the other subsystem. This is equivalent the partial trace over the degrees of freedom of the second subsystem [25],

$$\rho_1 = \mathrm{Tr}_2[\rho_{\mathrm{e}}] = \langle 0^{(2)}|\rho_{\mathrm{e}}|0^{(2)}\rangle + \langle 1^{(2)}|\rho_{\mathrm{e}}|1^{(2)}\rangle = \frac{1}{2}\left(|0^{(1)}\rangle\langle 0^{(1)}| + |1^{(1)}\rangle\langle 1^{(1)}|\right), \tag{2.21}$$

which is a balanced statistical mixture of $|0^{(1)}\rangle$ and $|1^{(1)}\rangle$. By symmetry, the partial trace over the first subsystem gives $\rho_2 = (|0^{(2)}\rangle\langle 0^{(2)}| + |1^{(2)}\rangle\langle 1^{(2)}|)/2$. In addition, one can check that the classically correlated state ρ_{c} yields exactly the same partial traces. We can conclude that an entangled state contains more information than the sum of its parts and that the ignorance of one of the constituent subsystems induces a classical statistical uncertainty about the other subsystem part.

This has important implications both for quantum measurements and for open quantum systems. In the generic measurement setup, one brings the quantum system into contact with a measurement apparatus. The interaction between the measured system and the apparatus generally leads to joint entangled states and in the end one reads off the outcomes only from the apparatus part, see Sec. 2.1.3. Therefore, the probabilistic character of quantum measurements stems from our inability to read out the total system-apparatus state and can hence be regarded as intrinsic. Very similarly, an open quantum system interacts with its environment so that their joint state is generally entangled as well. Here, it is our ignorance of the large and inaccessible environment which induces a statistical uncertainty in the open system state, see Sec. 2.2.

2.1.3 Measurements in Quantum Mechanics

Projective Measurements

Let us first briefly summarize and formalize the above postulate on idealized projective measurements of quantum states ρ, see Eqs. (2.6)–(2.8). The outcome a of a projective measurement of an observable $\mathsf{A} = \sum_i a_i |a_i\rangle\langle a_i|$ with a nondegenerate spectrum is

obtained with probability

$$\mathrm{Prob}(a|\rho) = \mathrm{Tr}(\mathsf{P}_a\rho) = \langle a|\rho|a\rangle, \tag{2.22}$$

where $\mathsf{P}_a = |a\rangle\langle a|$ is the projector onto the corresponding eigenstate. As a result of detecting a, ρ is projected with P_a and, hence, the map

$$\mathcal{M} : \rho \mapsto \mathcal{M}(\rho|a) = \frac{\mathsf{P}_a\rho\mathsf{P}_a}{\mathrm{Tr}(\mathsf{P}_a\rho)}, \tag{2.23}$$

takes the pre- to the post-measurement state. As a consequence, a second measurement of A, carried out immediately after detecting a, will again yield a with probability one.

A measurement of A is consistent in the sense that the measurement probabilities sum up to unity,

$$\sum_a \mathrm{Prob}(a|\rho) = \sum_a \mathrm{Tr}(\mathsf{P}_a\rho) = 1, \tag{2.24}$$

where we have used Eq. (2.9) and the fact that eigenvectors $|a\rangle$ of Hermitian operators form an orthonormal basis of $\mathcal{H}$, $\sum_a \mathsf{P}_a = \mathbb{1}$. The expectation value for a measurement of A is simply given by $\mathrm{Tr}(\mathsf{A}\rho)$. This can be seen by averaging over all possible outcomes

$$\langle\mathsf{A}\rangle_\rho = \sum_a a\,\mathrm{Prob}(a|\rho) = \sum_a a\,\mathrm{Tr}(\mathsf{P}_a\rho) = \mathrm{Tr}\left[\left(\sum_a a\mathsf{P}_a\right)\rho\right] = \mathrm{Tr}(\mathsf{A}\rho), \tag{2.25}$$

where we have inserted the spectral decomposition of A in the last equality.

Generalized Measurements

Projective measurements serve to translate the classical concept of measurable quantities to quantum observables. A more general formulation is necessary, however, to account for realistic measurements relying on non-ideal detectors with finite resolution. To do that, we consider the outcomes a as classical random numbers, whose probability distribution can be represented by a set of positive operators F_a called *effects*,

$$\mathrm{Prob}(a|\rho) = \mathrm{Tr}(\mathsf{F}_a\rho). \tag{2.26}$$

Based on the above probability, we can generalize the mapping (2.23) from pre- to post-measurement states using the so-called *measurement operators* $\mathsf{M}_{a,i}$,

$$\mathcal{M} : \rho \mapsto \mathcal{M}(\rho|a) = \frac{1}{\mathrm{Prob}(a|\rho)}\sum_i \mathsf{M}_{a,i}\rho\mathsf{M}_{a,i}^\dagger = \frac{1}{\mathrm{Tr}(\mathsf{F}_a\rho)}\sum_i \mathsf{M}_{a,i}\rho\mathsf{M}_{a,i}^\dagger. \tag{2.27}$$

In Sec. 2.2 we will see that the expression $\sum_i \mathsf{M}_{a,i}\rho\mathsf{M}_{a,i}^\dagger$, appearing in Eq. (2.27), represents the most general, physically allowed transformation of a density matrix ρ, see Eq. (2.48). The unconditional or *nonselective* post-measurement state is obtained by

averaging over all outcomes,

$$\rho \mapsto \sum_a \mathrm{Prob}(a|\rho)\mathcal{M}(\rho|a) = \sum_{a,i} \mathsf{M}_{a,i}\rho\mathsf{M}_{a,i}^\dagger. \tag{2.28}$$

In order to be consistent with the unit trace of the post-measurement state $\mathcal{M}(\rho|a)$, the operators $\mathsf{M}_{a,i}$ must satisfy $\mathrm{Tr}\left(\sum_i \mathsf{M}_{a,i}^\dagger \mathsf{M}_{a,i}\rho\right) = \mathrm{Tr}(\mathsf{F}_a\rho)$ for any ρ, and therefore

$$\mathsf{F}_a = \sum_i \mathsf{M}_{a,i}^\dagger \mathsf{M}_{a,i}. \tag{2.29}$$

Furthermore, the normalization condition for the probability distribution, $\sum_a \mathrm{Tr}(\mathsf{F}_a\rho) = 1$, requires that

$$\sum_a \mathsf{F}_a = \sum_{a,i} \mathsf{M}_{a,i}^\dagger \mathsf{M}_{a,i} = \mathbb{1}. \tag{2.30}$$

In this way, the positive operator-valued measure $\mathrm{Tr}(\mathsf{F}_a\cdot)$ is associated with a general measurement and we recognize the special case of a projection-valued measure in the projective measurements described in the previous section.

A generalized measurement which introduces no classical noise, *i.e.* which maps pure states to pure states, is called *efficient*. This is the case if the operator decompositions (2.29) of all F_a have only one term

$$\mathsf{F}_a = \mathsf{M}_a^\dagger \mathsf{M}_a. \tag{2.31}$$

With the help of the polar decomposition we can then write the measurement operators M_a as a product of a unitary operator U_a and a Hermitian operator $\sqrt{\mathsf{F}_a}$

$$\mathsf{M}_a = \mathsf{U}_a\sqrt{\mathsf{F}_a}. \tag{2.32}$$

The mapping associated with an efficient measurement is then given by

$$\mathcal{M}(\rho|a) = \mathsf{U}_a \frac{\sqrt{\mathsf{F}_a}\rho\sqrt{\mathsf{F}_a}}{\mathrm{Tr}(\mathsf{F}_a\rho)}\mathsf{U}_a^\dagger. \tag{2.33}$$

It looks somewhat similar to the mapping due to a projective measurement (2.23). The effect of the "raw measurement" under operators $\sqrt{\mathsf{F}_a}$ is to "squeeze" the state in a specific direction just like a projection, and then U_a rotates the state conditioned on the outcome of the "raw measurement".

Indirect Measurements

Most experimentally relevant measurements are more specific than the above general setting: they involve the measured quantum system, plus an additional probe or measurement apparatus that is coupled to it. This so-called *indirect measurement* setting is in accord with our intuition about a practical implementation of a measurement and it

serves to bridge the gap between the previously discussed ideal, projective and the completely general measurements. It also makes use of the concept of composite quantum systems developed in Sec. 2.1.2.

Let us denote the Hilbert spaces of system and apparatus by $\mathcal{H}^{\mathrm{S}}$ and $\mathcal{H}^{\mathrm{A}}$, respectively. Assuming that the apparatus can initially be prepared in the state $|\psi^{\mathrm{A}}\rangle \in \mathcal{H}^{\mathrm{A}}$, irrespective of the system state ρ, we have the joint initial state

$$\rho_0^{\mathrm{tot}} = \rho \otimes |\psi^{\mathrm{A}}\rangle\langle\psi^{\mathrm{A}}|. \tag{2.34}$$

Now, the experimenter may let system and apparatus interact for some time τ. The state ρ_0^{tot} therefore evolves under the joint time evolution operator $\mathsf{U}_\tau = \exp[-i\tau\mathsf{H}^{\mathrm{SA}}/\hbar]$ due to the system-apparatus-Hamiltonian H^{SA}, and one obtains

$$\rho_\tau^{\mathrm{tot}} = \mathsf{U}_\tau \rho_0^{\mathrm{tot}} \mathsf{U}_\tau^\dagger. \tag{2.35}$$

Finally, the apparatus is measured projectively with projectors P_a. This implies the measurement operators $\mathbb{1} \otimes \mathsf{P}_a$ on the joint system-apparatus state space and the probability to obtain outcome a for the initial system state ρ reads

$$\mathrm{Prob}(a|\rho) = \mathrm{Tr}([\mathbb{1} \otimes \mathsf{P}_a]\rho_\tau^{\mathrm{tot}}) = \mathrm{Tr}\left([\mathbb{1} \otimes \mathsf{P}_a]\mathsf{U}_\tau[\rho \otimes |\psi^{\mathrm{A}}\rangle\langle\psi^{\mathrm{A}}|]\mathsf{U}_\tau^\dagger\right). \tag{2.36}$$

Using the cyclic invariance of the trace, we obtain

$$\mathrm{Prob}(a|\rho) = \mathrm{Tr}(\mathsf{U}_\tau^\dagger[\mathbb{1} \otimes \mathsf{P}_a]\mathsf{U}_\tau[\rho \otimes |\psi^{\mathrm{A}}\rangle\langle\psi^{\mathrm{A}}|]) = \mathrm{Tr}(\mathsf{F}_a\rho). \tag{2.37}$$

In Eq. (2.37) we have inserted the definition (2.26) for the system effect F_a, since we are ultimately interested in S and not in A. F_a is therefore given by

$$\mathsf{F}_a = \mathrm{Tr}_{\mathrm{A}}(\mathsf{U}_\tau^\dagger[\mathbb{1} \otimes \mathsf{P}_a]\mathsf{U}_\tau[\mathbb{1} \otimes |\psi^{\mathrm{A}}\rangle\langle\psi^{\mathrm{A}}|]). \tag{2.38}$$

In order to derive the transformation of the system state ρ under the prescribed indirect measurement, we use the usual projective state-reduction (2.23) on ρ_τ^{tot} and trace out the apparatus

$$\mathcal{M}(\rho|a) = \mathrm{Tr}_{\mathrm{A}}\left(\frac{[\mathbb{1} \otimes \mathsf{P}_a]\mathsf{U}_\tau[\rho \otimes |\psi^{\mathrm{A}}\rangle\langle\psi^{\mathrm{A}}|]\mathsf{U}_\tau^\dagger[\mathbb{1} \otimes \mathsf{P}_a]}{\mathrm{Tr}(\mathsf{F}_a\rho)}\right). \tag{2.39}$$

In comparison with Eq. (2.27), one can extract the system measurement operators

$$\mathsf{M}_a = \mathrm{Tr}_{\mathrm{A}}(\mathsf{P}_a\mathsf{U}_\tau|\psi^{\mathrm{A}}\rangle\langle\psi^{\mathrm{A}}|) = \langle a|\mathsf{U}_\tau|\psi^{\mathrm{A}}\rangle. \tag{2.40}$$

We see that if we can prepare the A in a pure state $|\psi^{\mathrm{A}}\rangle$ the above indirect measurement is efficient. In contrast, for a mixed state $\rho^A = \sum_k p_k|\varphi_k\rangle\langle\varphi_k|$ one obtains an inefficient measurement with an additional classical uncertainty about the post measurement state.

This completes our short overview of the theory of quantum measurements. It will

enable us to interpret the evolution of open quantum systems as a continuous measurement of the open system by its environment, see Sec. 2.3. The indirect measurement of a cavity field will also serve as a model system for the study of Markovian open quantum dynamics, see Secs. 3.3 and 6.2.1.

2.2 Markovian Dynamics of Open Quantum Systems

2.2.1 Closed Quantum Dynamics

The Schrödinger equation and the Liouville-von Neumann equation describe how pure and mixed states $|\psi_t\rangle$ and ρ_t of a *closed* quantum system evolve in time. They read

$$\partial_t|\psi_t\rangle = -\frac{i}{\hbar}\mathsf{H}(t)|\psi_t\rangle \tag{2.41}$$

$$\text{and} \quad \partial_t\rho_t = -\frac{i}{\hbar}[\mathsf{H}(t),\rho_t], \tag{2.42}$$

respectively. They describe the dynamics as being generated by the Hermitian operator H, called the Hamiltonian. As an observable, H is associated with the physical quantity energy, *i.e.* its expectation value $\mathrm{Tr}(\mathsf{H}\rho)$ gives the mean system energy in state ρ.

The solutions of the Schrödinger equation can be expressed in terms of unitary operators $\mathsf{U}(t,t_0)$ by

$$|\psi_t\rangle = \left(\mathcal{T}_+ \exp\left[-\frac{i}{\hbar}\int_{t_0}^{t}\mathsf{H}(t')\mathrm{d}t'\right]\right)|\psi_{t_0}\rangle \equiv \mathsf{U}(t,t_0)|\psi_{t_0}\rangle. \tag{2.43}$$

Here, the exponential of an operator is defined in terms of its Taylor expansion $\exp(\mathsf{A}) = \sum_{n=0}^{\infty}\mathsf{A}^n/n!$, and the time ordering operator $\mathcal{T}_+$ ($\mathcal{T}_-$, see below) ensures that time arguments of the Hamiltonian in this expansion are in ascending (descending) order. The introduction of $\mathcal{T}_+$ ($\mathcal{T}_-$) is necessary since $\mathsf{H}(t_1)$ may not commute with $\mathsf{H}(t_2)$ for $t_1 \neq t_2$. Equivalently, solutions to the Liouville-von Neumann equation read

$$\rho_t = \left(\mathcal{T}_+ \exp\left[-\frac{i}{\hbar}\int_{t_0}^{t}\mathsf{H}(t')\mathrm{d}t'\right]\right)\rho_{t_0}\left(\mathcal{T}_- \exp\left[\frac{i}{\hbar}\int_{t_0}^{t}\mathsf{H}(t')\mathrm{d}t'\right]\right) = \mathsf{U}(t,t_0)\rho_{t_0}\mathsf{U}^\dagger(t,t_0), \tag{2.44}$$

and we will usually set $t_0 = 0$ in the following. The unitarity of the time evolution operator $\mathsf{U}(t,t_0)$ implies that its inverse is given by its adjoint or conjugate transpose, *i.e.* $\mathsf{U}^{-1}(t,t_0) = \mathsf{U}^\dagger(t,t_0)$, which, in turn, means that any closed quantum evolution is invertible. In other words, Eqs. (2.41) and (2.42) do not naturally distinguish an arrow of time (positive or negative).

As we have argued in the previous section, the state of a quantum system is affected decisively by its coupling to an inaccessible environment. Let $\mathcal{H}^{\mathrm{S}}$ and $\mathcal{H}^{\mathrm{E}}$ be the respective Hilbert spaces of system and environment, which gives the joint Hilbert space $\mathcal{H}^{\mathrm{tot}} = \mathcal{H}^{\mathrm{S}}\otimes\mathcal{H}^{\mathrm{E}}$. Assuming that the compound of open system and environment forms a closed quantum system, it is straightforward to apply the time evolution operator $\mathsf{U}(t,0)$

to the initial compound system-environment state ρ_0^{tot}. The evolved state ρ_t of the system alone is then obtained by disregarding the environment using the partial trace, as prescribed by Eq. (2.21),

$$\rho_t = \text{Tr}_{\text{E}}\left[\mathsf{U}(t,0)\rho_0^{\text{tot}}\mathsf{U}^\dagger(t,0)\right]. \tag{2.45}$$

This equation of motion is, however, not particularly helpful since one needs to specify the exact initial system-environment state and the joint time evolution operator. We usually want to describe the open system time evolution in a closed form analogous to Eq. (2.42), *i.e.* without explicit reference to the environment.

2.2.2 Dynamical Maps

In order to arrive at an evolution equation for the open system alone, one takes a different approach. Assuming that one can prepare the system in an initial state ρ_0 that is not correlated with the state of the environment ρ_{E}, the time evolution is given by a one-parameter family of so-called *dynamical maps* that take the initial state to a state at later times

$$\mathcal{W}_t : \rho_0 \mapsto \rho_t, \quad \text{for } t \geq 0, \tag{2.46}$$

with $\mathcal{W}_0 = \text{Id}$. Crucially, one demands of any dynamical map that it yields physical states, meaning that $\mathcal{W}_t$ should be trace-preserving, convex linear, and completely positive. Trace preservation ensures that $\text{Tr}(\rho_t) = \text{Tr}(\mathcal{W}_t\rho_0) = 1$ at all times, as required by Eq. (2.9). Convex linearity of $\mathcal{W}_t$ is defined as

$$\mathcal{W}_t(p\rho + (1-p)\sigma) = p\mathcal{W}_t(\rho) + (1-p)\mathcal{W}_t(\sigma), \tag{2.47}$$

which implies that if the initial state is given by ρ with probability $p \in [0,1]$, we should end up in $\mathcal{W}_t\rho$ with the same probability. Finally, complete positivity means that the extension $\mathcal{W}_t \otimes \mathbb{1}$ of the dynamical map to any higher dimensional state space, for example that of system and another correlated degree of freedom, should take positive states (in the sense of Eq. (2.10)) to positive states.

The subsequent derivation of an open system evolution equation hinges crucially on the so-called *Kraus decomposition* of completely positive maps [33]. Namely, any completely positive map can be specified in terms of a set of system operators $\{\mathsf{W}_k(t)\}$ in the form

$$\mathcal{W}_t\rho = \sum_{k=1}^{N} \mathsf{W}_k(t)\rho\mathsf{W}_k^\dagger(t). \tag{2.48}$$

Conversely, any map that can be written in the form (2.48) is completely positive if the Kraus operators $\mathsf{W}_k(t)$ fulfill

$$\sum_{k=1}^{N} \mathsf{W}_k^\dagger(t)\mathsf{W}_k(t) \leq \mathbb{1}, \tag{2.49}$$

which means that $\mathbb{1} - \sum_k \mathsf{W}_k^\dagger(t)\mathsf{W}_k(t)$ is a positive operator. Here, the equality holds for trace-preserving maps $\mathcal{W}_t$, and in all other cases $\mathcal{W}_t$ is trace decreasing. The Kraus decomposition is not unique and the number N of required operators is limited by the Hilbert space dimension by $N \leq \dim(\mathcal{H})^2$.

2.2.3 The Markov Assumption

In Sec. 2.1.2 we have seen that disregarding one part of a composite quantum system generally leads to mixed states ρ, which can be interpreted as comprising an uncertainty about the true quantum state $|\psi\rangle$. The dynamics of an open system should hence involve stochasticity in one way or another, if its environment is ignored.

Generally, causality implies that the system properties at time t depend on the system and environmental state at earlier times $t' \leq t$. Our experience from classical stochastic processes tells us, however, that many realistic systems quickly forget about their past time evolution so that the state change at time t does *not* depend on earlier times. These so-called *Markovian* systems are well-described by a time-local equation of motion or *master equation*, as we will see shortly. For the dynamics of open quantum systems Markovianity implies that a dynamical map $\mathcal{W}_t$ is *divisible* into two completely positive maps,

$$\mathcal{W}_t = \mathcal{W}_{t,s} \circ \mathcal{W}_s, \tag{2.50}$$

for any intermediate time $0 \leq s \leq t$. It is understood that $\mathcal{W}_{t,s}$ is that dynamical map which takes system states ρ_s at time s to states ρ_t at time t (this naturally extends the previous definition (2.46) of dynamical maps with initial time 0). For dynamical maps $\mathcal{W}_{t,s}$ that do not depend on s and t separately but only on the difference $t-s$, divisibility implies that the set of dynamical maps has semigroup structure, *i.e.* $\mathcal{W}_{t+s} = \mathcal{W}_t \circ \mathcal{W}_s$.

Recall that dynamical maps were introduced to describe only the system part of an underlying joint evolution of the system and its environment. This means that, in an operational sense, $\mathcal{W}_t$ is equivalent to taking the initial system and environmental state, propagating them jointly for time t, and then tracing out the environment, see Eq. (2.45). Eq. (2.50) then tells us that one may disregard the environment at any intermediate instant s and take the resulting system state again as input for the described operation, without changing the final state at time t. In other words, the environment contains no information about earlier system states which would act back on the system at later times. The environment is in this sense memoryless. Note however, that there exists no precise definition of Markovianity in the literature [34]. Some authors adopt the criterion (2.50) of divisibility [35, 36], whereas others use the notion of backflow of information from the environment to the open system [37]. Interestingly, both concepts were shown to be mathematically inequivalent [38]: whereas divisibility of the dynamical maps implies the absence of a backflow of information, the converse is not true (there exist systems that exhibit no information backflow but have indivisible dynamical maps).

Due to the divisibility (2.50) of Markovian dynamical maps, the system time evolution

is described by a differential equation for ρ_t that involves a time dependent generator $\mathcal{L}(t)$,

$$\partial_t \rho_t = \mathcal{L}(t)\rho_t. \tag{2.51}$$

The symbol $\mathcal{L}$ is here chosen in analogy to the classical Liouville operator[6]. The dynamical maps $\mathcal{W}_t$ describing a Markovian time evolution can hence be written in the form

$$\mathcal{W}_{t,s} = \mathcal{T}_+ \exp\left[\int_s^t \mathcal{L}(t')\mathrm{d}t'\right], \tag{2.52}$$

analogous to the time evolution operator $\mathsf{U}(t,s)$, Eq. (2.43), for closed quantum systems.

It is clear that the Markov assumption (2.50) is a rather strong condition which can only be fulfilled approximately in reality. Generally, it is only fulfilled on a time scale that is coarse-grained with respect to the environment correlation time in which the memory of earlier states is lost. Nevertheless, Markovian master equations have turned out to be a very accurate approximation to the dynamics of many open quantum systems, especially those coupled to many external degrees of freedom. In Sec. 2.2.5 we will specify the precise physical conditions underlying the Markov assumption.

2.2.4 The Standard Form of Markovian Master Equations

Being a rather strong condition on the dynamics of an open quantum system, the Markov assumption considerably narrows down the set of conceivable generators $\mathcal{L}(t)$. This leads to the fact that $\mathcal{L}(t)$ can be written out quite explicitly: its standard form can be expressed in terms of a set of system operators $\{\mathsf{L}_j\}$ similar to the Kraus decomposition (2.48) for the dynamical maps $\mathcal{W}_t$. The standard form was derived in 1976 independently by Gorini, Kossakovski, and Sudarshan [39] and by Lindblad [40] for finite dimensional Hilbert spaces and for bounded operators in infinite dimensions, respectively. For simplicity, we will here demonstrate the standard form for the finite dimensional case.

A d-dimensional Hilbert space $\mathcal{H}$ admits a d^2-dimensional space $L(\mathcal{H})$ of Hilbert-Schmidt operators acting on the elements of $\mathcal{H}$. Denoting an orthonormal Hilbert-Schmidt basis by $\{\mathsf{E}_i\}$ we have

$$(\mathsf{E}_i, \mathsf{E}_j) \equiv \mathrm{Tr}[\mathsf{E}_i^\dagger \mathsf{E}_j] = \delta_{i,j}, \tag{2.53}$$

where $(\mathsf{A},\mathsf{B}) = \mathrm{Tr}[\mathsf{A}^\dagger\mathsf{B}]$ denotes the natural scalar product on $L(\mathcal{H})$. In particular, the E_i can be chosen in such a form that the d^2-th basis operator is proportional to the identity matrix,

$$\mathsf{E}_{d^2} = \frac{1}{\sqrt{d}}\mathbb{1}, \tag{2.54}$$

and all other basis operators are traceless,

$$\mathrm{Tr}\,\mathsf{E}_i = 0, \qquad \text{for } i \neq d^2. \tag{2.55}$$

[6] To be precise, the generator $\mathcal{L}(t)$ in Eq. (2.51) just like the dynamical map $\mathcal{W}_t$ in Eq. (2.46) are *super operators* acting on the set of density operators.

We can now represent any operator A in this basis by

$$\mathsf{A} = \sum_{i=1}^{d^2} (\mathsf{E}_i, \mathsf{A})\mathsf{E}_i. \tag{2.56}$$

In order to express the Markovian generator $\mathcal{L}(t)$ in terms of operators acting on the open system, let us first expand the operators $\mathsf{W}_k(t,s)$ in the Kraus decomposition (2.48) of $\mathcal{W}_{t,s}$ in the basis $\{\mathsf{E}_i\}$,

$$\mathcal{W}_{t,s}\rho_s = \sum_{i,j=1}^{d^2} c_{ij}(t,s)\mathsf{E}_i\rho_s\mathsf{E}_j^\dagger. \tag{2.57}$$

Here, the expansion coefficients $c_{ij}(t,s)$ are given by

$$c_{ij}(t,s) = \sum_{k=1}^{N} (\mathsf{E}_i, \mathsf{W}_k(t,s))(\mathsf{E}_j, \mathsf{W}_k(t,s))^*, \tag{2.58}$$

and the matrix $(c_{ij}(t,s))$ is positive Hermitian since $c_{ij}(t,s) = c_{ji}^*(t,s)$, and $c_{ii}(t,s)$ is a sum of absolute values. Note that, in contrast to Eq. (2.48), we have used the initial time $s \neq 0$ resulting in t- and s-dependent Kraus operators. Based on this representation, we can now calculate the differential quotient of the map $\mathcal{W}_{t+\Delta t,t}$ which yields the generator $\mathcal{L}(t)$ in the limit $\Delta t \to 0$,

$$\begin{aligned}
\mathcal{L}(t)\rho_t &= \lim_{\Delta t\to 0} \frac{\mathcal{W}_{t+\Delta t,t}\rho_t - \rho_t}{\Delta t} \\
&= \left[\lim_{\Delta t\to 0} \frac{\frac{1}{d}c_{d^2d^2}(t+\Delta t,t) - 1}{\Delta t}\right]\rho_t + \left[\lim_{\Delta t\to 0} \sum_{j=1}^{d^2-1} \frac{c_{jd^2}(t+\Delta t,t)}{\sqrt{d}\Delta t}\mathsf{E}_j\right]\rho_t \\
&\quad + \rho_t\left[\lim_{\Delta t\to 0} \sum_{j=1}^{d^2-1} \frac{c_{d^2j}(t+\Delta t,t)}{\sqrt{d}\Delta t}\mathsf{E}_j^\dagger\right] + \sum_{i,j=1}^{d^2-1}\left[\lim_{\Delta t\to 0} \frac{c_{ij}(t+\Delta t,t)}{\sqrt{d}\Delta t}\right]\mathsf{E}_i\rho_t\mathsf{E}_j^\dagger \\
&= c(t)\rho_t + \mathsf{B}(t)\rho_t + \rho_t\mathsf{B}^\dagger(t) + \sum_{i,j=1}^{d^2-1} \alpha_{ij}(t)\mathsf{E}_i\rho_t\mathsf{E}_j^\dagger.
\end{aligned} \tag{2.59}$$

Here, we have inserted the d^2-th basis operator, Eq. (2.54). For the last equality we have also substituted the expressions in square brackets by the real number $c(t)$, by Hilbert-Schmidt operators $\mathsf{B}(t)$ and $\mathsf{B}^\dagger(t)$, and by complex numbers $\alpha_{ij}(t)$, in that order. Using a second substitution with the Hermitian operators

$$\mathsf{G}(t) = \frac{\hbar}{2}(\mathsf{B}(t) + \mathsf{B}^\dagger(t) + c(t)), \tag{2.60}$$

$$\mathsf{H}(t) = \frac{\hbar}{2i}(\mathsf{B}(t) - \mathsf{B}^\dagger(t)), \tag{2.61}$$

we can recast the generator $\mathcal{L}(t)$ into the form

$$\mathcal{L}(t)\rho_t = -\frac{i}{\hbar}[\mathsf{H}(t), \rho_t] + \frac{1}{\hbar}(\mathsf{G}(t)\rho_t + \rho_t\mathsf{G}(t)) + \sum_{i,j=1}^{d^2-1} \alpha_{ij}(t)\mathsf{E}_i\rho_t\mathsf{E}_j^\dagger. \tag{2.62}$$

Due to the conservation of the trace of ρ under $\mathcal{W}_{t,s}$ we have $\mathrm{Tr}[\mathcal{L}(t)\rho_t] = 0$, which implies that we can relate the operator G with the complex coefficients α_{ij} via

$$0 = \mathrm{Tr}[\mathcal{L}(t)\rho_t] = \mathrm{Tr}\left[\left(\frac{2}{\hbar}\mathsf{G}(t) + \sum_{i,j=1}^{d^2-1} \alpha_{ij}(t)\mathsf{E}_j^\dagger\mathsf{E}_i\right)\rho_t\right]. \tag{2.63}$$

Using the cyclic invariance of the trace we have here eliminated the commutator of $\mathsf{H}(t)$ and ρ_t and rearranged the factors in the last summand. Since Eq. (2.63) must hold for any ρ_t, we have

$$\mathsf{G}(t) = -\frac{\hbar}{2}\sum_{i,j=1}^{d^2-1} \alpha_{ij}(t)\mathsf{E}_j^\dagger\mathsf{E}_i. \tag{2.64}$$

Substituting this expression for $\mathsf{G}(t)$ back into Eq. (2.62) results in the *first standard form* for the generator

$$\mathcal{L}(t)\rho_t = -\frac{i}{\hbar}[\mathsf{H}(t), \rho_t] + \sum_{i,j=1}^{d^2-1} \alpha_{ij}(t)\left(\mathsf{E}_i\rho_t\mathsf{E}_j^\dagger - \frac{1}{2}\mathsf{E}_j^\dagger\mathsf{E}_i\rho_t - \frac{1}{2}\rho_t\mathsf{E}_j^\dagger\mathsf{E}_i\right). \tag{2.65}$$

The complex coefficient matrix $(\alpha_{ij}(t)) = (\lim_{\Delta t\to 0} c_{ij}(t+\Delta t, t)/\sqrt{d}\Delta t)$, as defined by Eq. (2.59), is positive Hermitian due to the positivity of $(c_{ij}(t,s))$, see Eq. (2.58).

The first standard form (2.65) can hence be further simplified by diagonalizing the coefficient matrix $\alpha(t)$ with the help of a suitable unitary matrix, $U(t)\alpha(t)U^\dagger(t) = \mathrm{diag}(\gamma_1(t), \ldots, \gamma_{d^2-1}(t))$, with positive rates $\gamma_k(t)$. Relabeling the linear combinations $\sqrt{\gamma_k(t)}\sum_{j=1}^{d^2-1} U_{jk}^\dagger(t)\mathsf{E}_j$ of basis vectors by $\mathsf{L}_k(t)$, we finally obtain the *second standard form*, or short the *standard form* of a general time-dependent Markovian generator

$$\mathcal{L}(t)\rho_t = \partial_t\rho_t = -\frac{i}{\hbar}[\mathsf{H}(t), \rho_t] + \sum_{k=1}^{N}\left\{\mathsf{L}_k(t)\rho_t\mathsf{L}_k^\dagger(t) - \frac{1}{2}\mathsf{L}_k^\dagger(t)\mathsf{L}_k(t)\rho_t - \frac{1}{2}\rho_t\mathsf{L}_k^\dagger(t)\mathsf{L}_k(t)\right\}, \tag{2.66}$$

with $N \leq d^2 - 1$. Note that the operators L_k are here defined to include the square roots of the rates $\gamma_k(t)$.

In the first summand on the right hand side of Eq. (2.66) we recognize the Liouville-von Neumann equation (2.42) for closed quantum systems which results in unitary dynamics. The Hermitian operator $\mathsf{H}(t)$ is, however, not necessarily the same as the closed system Hamiltonian. Similar to the dressed states in quantum optics it may involve a shift of the closed system energy levels by the coupling to the environmental degrees of freedom.

In the fine structure of atoms, for example, this effect goes by the name of *Lamb shift*. In contrast, the second part on the right hand side of Eq. (2.66) involving the so-called *Lindblad* or *jump operators* L_k is solely due to the influence of the environment. It leads to non-unitary dynamics of the open system. In particular, it changes the system entropy or purity, as can be seen by inserting Eq. (2.66) into the time derivative of the linear entropy (2.17),

$$\partial_t S_{\text{lin}}(\rho_t) = -2\,\text{Tr}[\rho_t(\partial_t\rho_t)] = 2\,\text{Tr}\left[\sum_k \left\{\rho_t^2 \mathsf{L}_k^\dagger(t)\mathsf{L}_k(t) - \rho_t \mathsf{L}_k(t)\rho_t \mathsf{L}_k^\dagger(t)\right\}\right]. \tag{2.67}$$

A pure state $\rho_t = |\psi\rangle\langle\psi|$, for example, experiences an increase of entropy $\partial_t S_{\text{lin}} = \sum_k \langle \mathsf{L}_k^\dagger(t)\mathsf{L}_k(t)\rangle_\psi - |\langle \mathsf{L}_k(t)\rangle_\psi|^2$ unless it is a simultaneous eigenstate of all jump operators. This indicates that, in contrast to the closed system dynamics we saw in Sec. 2.2.1, a non-unitary open system time evolution is generally not invertible and that it acts contractively on the state space.

An important property of Markovian master equations, which will be used in particular in Chap. 4 to find convergent expansions for ρ_t, is that its jump operators are not unique. In particular, Eq. (2.66) is invariant under a shift of the L-operators and a suitable transformation of the Hamiltonian,

$$\mathsf{L}_k(t) \to \mathsf{L}_{k,\boldsymbol{\alpha}}(t) \equiv \mathsf{L}_k(t) + \alpha_k(t), \tag{2.68}$$

$$\mathsf{H}(t) \to \mathsf{H}_{\boldsymbol{\alpha}}(t) \equiv \mathsf{H}(t) - \frac{i\hbar}{2}\sum_k (\alpha_k(t)\mathsf{L}_k^\dagger(t) - \alpha_k^*(t)\mathsf{L}_k(t)), \tag{2.69}$$

where $\boldsymbol{\alpha}(t) = (\alpha_1(t), \ldots, \alpha_N(t)) \in \mathbb{C}^N$. The invariance of Eq. (2.66) under the transformations (2.68), (2.69) is verified straightforwardly. As a natural result of the diagonalization of the coefficient matrix $\alpha_{ij}(t)$ in Eq. (2.65) one has the additional freedom to apply any unitary mixing of the L-operators without changing the master equation (2.66),

$$\mathsf{L}_k(t) \to \sum_j U_{jk}(t)\mathsf{L}_k(t), \tag{2.70}$$

where U is a unitary matrix.

While Eq. (2.66) was derived for finite dimensional systems and for bounded operators in infinite dimensions, a completely general derivation remains an open problem. The Hilbert space of a moving particle with its continuous basis of position eigenstates $|x\rangle$, for example, does not fulfill the above conditions. Nevertheless all physically motivated Markovian master equations studied so far are in standard form, or can be cast into standard form by slight modifications. With its relatively simple structure[7] and wide applicability, Eq. (2.66) is therefore the ideal starting point for studying the dynamics of open quantum systems.

[7] Although Eq. (2.66) gives the simplest realistic approximate description of open quantum dynamics, it is known to have analytic solutions only for extremely simple concrete models such as two level systems with phase noise [25] or the damped quantum harmonic oscillator [28].

2.2.5 Microscopic Derivations

In the previous section, we have derived the standard form for the generator $\mathcal{L}(t)$ of any Markovian quantum evolution on a purely axiomatic basis: we demanded that it should be memoryless and behave according to the laws of quantum composite systems. Now we want to show that this quite abstract Markovian evolution equation is indeed realized for realistic physical assumptions about the microscopic nature of the open system and its environment. In particular, we will thereby obtain an expression for the jump operators L_k in terms of the physical properties of the environment.

The Weak Coupling Limit

The most common way to obtain a Markovian system evolution is by assuming that the system is only weakly coupled to its environment [28]. More specifically, if we assume that the Hamiltonians H for the system, H_E for the environment, and H_int for their interaction are known microscopically, we have the total Hamiltonian

$$\mathsf{H}_\mathrm{tot} = \mathsf{H} + \mathsf{H}_\mathrm{E} + \mathsf{H}_\mathrm{int}. \tag{2.71}$$

Note that, throughout this and the following section, we assume time-independent Hamiltonians for simplicity. The time evolution of the joint system-environment state ρ_t^tot under H_tot is given by the von Neumann equation (2.42),

$$\partial_t \tilde{\rho}_t^\mathrm{tot} = -\frac{i}{\hbar}\left[\widetilde{\mathsf{H}}_\mathrm{int}(t), \tilde{\rho}_t^\mathrm{tot}\right], \tag{2.72}$$

whose integral form is given by

$$\tilde{\rho}_t^\mathrm{tot} = \tilde{\rho}_0^\mathrm{tot} - \frac{i}{\hbar}\int_0^t \mathrm{d}s \left[\widetilde{\mathsf{H}}_\mathrm{int}(s), \tilde{\rho}_s^\mathrm{tot}\right]. \tag{2.73}$$

The tilde indicates that the equations are stated in the interaction picture, which is defined by

$$\tilde{\rho}_t^\mathrm{tot} = e^{i(\mathsf{H}+\mathsf{H}_\mathrm{E})t/\hbar}\rho_t^\mathrm{tot}e^{-i(\mathsf{H}+\mathsf{H}_\mathrm{E})t/\hbar}, \tag{2.74}$$

$$\widetilde{\mathsf{H}}_\mathrm{int}(t) = e^{i(\mathsf{H}+\mathsf{H}_\mathrm{E})t/\hbar}\mathsf{H}_\mathrm{int}e^{-i(\mathsf{H}+\mathsf{H}_\mathrm{E})t/\hbar}. \tag{2.75}$$

By reinserting the integral form (2.73) into the differential form (2.72) and tracing out the environment, we obtain the time derivative of the system state at time t,

$$\partial_t \tilde{\rho}_t = \mathrm{Tr}_\mathrm{E}\left[-\frac{1}{\hbar^2}\int_0^t \mathrm{d}s \left[\widetilde{\mathsf{H}}_\mathrm{int}(t), \left[\widetilde{\mathsf{H}}_\mathrm{int}(s), \tilde{\rho}_s^\mathrm{tot}\right]\right]\right]. \tag{2.76}$$

Without loss of generality, we have assumed that $\mathrm{Tr}_\mathrm{E}\left[\widetilde{\mathsf{H}}_\mathrm{int}(t), \tilde{\rho}_0^\mathrm{tot}\right] = 0$ (it may always be achieved by choosing a suitable H_E).

While Eq. (2.76) is still exact, it can be simplified by assuming a small system-

environment-coupling $\mathsf{H}_{\rm int}$, which implies an uncorrelated joint state up to second order in $\mathsf{H}_{\rm int}$ both initially and also for $t > 0$,

$$\rho_t^{\rm tot} = \rho_t \otimes \rho^{\rm E}. \tag{2.77}$$

Here, $\rho^{\rm E}$ is a stationary state of the environment, *i.e.* $\left[\mathsf{H}_{\rm E}, \rho^{\rm E}\right] = 0$. This so-called *Born approximation* implies that the system has a negligible influence on the environment and, in particular, that correlations between the two decay completely on the coarse grained time scale of interest. By expanding the interaction picture coupling operator $\widetilde{\mathsf{H}}_{\rm int}(t)$ in any Hilbert-Schmidt basis,

$$\widetilde{\mathsf{H}}_{\rm int}(t) = \sum_k \widetilde{\mathsf{A}}_k(t) \otimes \widetilde{\mathsf{B}}_k(t), \tag{2.78}$$

with $\widetilde{\mathsf{A}}_k = \widetilde{\mathsf{A}}_k^\dagger$, $\widetilde{\mathsf{B}}_k = \widetilde{\mathsf{B}}_k^\dagger$, we can now rewrite Eq. (2.76) with the help of the approximation (2.77) as

$$\partial_t \tilde{\rho}_t = -\frac{1}{\hbar^2} \sum_{k,l} \int_0^t {\rm d}s C_{kl}(t-s) \left\{ \widetilde{\mathsf{A}}_k(t)\widetilde{\mathsf{A}}_l(s)\tilde{\rho}_s - \widetilde{\mathsf{A}}_l(s)\tilde{\rho}_s\widetilde{\mathsf{A}}_k(t) + {\rm h.c.} \right\} \equiv \int_0^t {\rm d}s \mathcal{K}(t-s)\tilde{\rho}_s. \tag{2.79}$$

The complete information about the environment is now contained in the environment correlation functions

$$C_{kl}(\tau) = {\rm Tr}_{\rm E}\left[e^{i\mathsf{H}_{\rm E}\tau}\mathsf{B}_k e^{-i\mathsf{H}_{\rm E}\tau}\mathsf{B}_l \rho^{\rm E} \right]. \tag{2.80}$$

Equation (2.79) already transpires the standard form (2.66) but it is still non-local in time and not Markovian.

A truly Markovian master equation is obtained after two additional steps. First, one replaces the system state $\tilde{\rho}_s$ with $\tilde{\rho}_t$ in Eq. (2.79), which is admissible under the above assumption that $\mathsf{H}_{\rm int}$ is small. This leads to the time-local *Redfield equation*

$$\partial_t \tilde{\rho}_t = \left[\int_0^t {\rm d}s \mathcal{K}(t-s) \right] \tilde{\rho}_t. \tag{2.81}$$

The Redfield equation is, however, not yet Markovian since the involved generator depends on the elapsed time interval $[0, t]$ since the initial preparation. Second, the rapid decay of the environment correlation functions $C_{kl}(\tau)$ allows one to extend the upper integration limit in Eq. (2.81) to infinity, after substituting the integration variable s with $t - s$. This leads to the Markovian master equation

$$\partial_t \tilde{\rho}_t = \left[\int_0^\infty {\rm d}s \mathcal{K}(s) \right] \tilde{\rho}_t, \tag{2.82}$$

which involves a generator that is not dependent on the past. It is clear that this approximation is only valid on a time scale that is coarse grained with respect to the environment correlation times. The two approximations leading to Eqs. (2.81) and (2.82)

are together called the *Born-Markov approximation*.

Although Eq. (2.82) has the desired form of a Markovian master equation, it is not guaranteed to yield a completely positive evolution[8] since we have performed various approximations along the way from Eq. (2.76). In order to obtain a completely positive master equation out of Eq. (2.82) we need to make one final approximation called the *rotating wave* or *secular approximation*. It is applicable if the system Hamiltonian has a discrete, non-degenerate spectrum and it relies on the specific representation $\mathsf{A}_k = \sum_\omega \mathsf{A}_k(\omega)$ of the system-part of the system-environment interaction (*cf.* Eq. (2.78)), with

$$\mathsf{A}_k(\omega) = \sum_{E'-E=\hbar\omega} \langle E|\mathsf{A}_k|E'\rangle |E\rangle\langle E'| = \mathsf{A}_k^\dagger(\omega). \tag{2.83}$$

Expressing the interaction picture representation of A_k in terms of the elements $\mathsf{A}_k(\omega)$

$$\widetilde{\mathsf{A}}_k(t) = \sum_\omega e^{-i\omega t}\mathsf{A}_k(\omega), \tag{2.84}$$

we can recast Eq. (2.79) as

$$\partial_t\tilde{\rho}_t = \sum_{k,l}\sum_{\omega,\omega'} e^{i(\omega-\omega')t}\Gamma_{kl}(\omega')\left\{\mathsf{A}_l(\omega')\tilde{\rho}_t\mathsf{A}_k^\dagger(\omega) - \mathsf{A}_k^\dagger(\omega)\mathsf{A}_l(\omega')\tilde{\rho}_t + \text{h.c.}\right\}, \tag{2.85}$$

with

$$\Gamma_{kl}(\omega) = \frac{1}{\hbar^2}\int_0^\infty e^{i\omega s}C_{kl}(s)\mathrm{d}s. \tag{2.86}$$

The rotating wave approximation neglects all terms in Eq. (2.85) with $\omega \neq \omega'$, *i.e.* with a non-stationary phase, since they will average out on time scales that are large compared the smallest system energy spacing. Finally, we obtain the first standard form (2.65) for the Markovian time evolution

$$\partial_t\tilde{\rho}_t = -\frac{i}{\hbar}\left[\mathsf{H}_{\text{Lamb}},\tilde{\rho}_t\right] + \sum_{k,l,\omega}\gamma_{kl}(\omega)\left\{\mathsf{A}_l(\omega)\tilde{\rho}_t\mathsf{A}_k^\dagger(\omega) - \frac{1}{2}\mathsf{A}_k^\dagger(\omega)\mathsf{A}_l(\omega)\tilde{\rho}_t - \frac{1}{2}\tilde{\rho}_t\mathsf{A}_k^\dagger(\omega)\mathsf{A}_l(\omega)\right\}, \tag{2.87}$$

with the Hermitian operator $\mathsf{H}_{\text{Lamb}} = \hbar/2i\sum_{k,l,\omega}(\Gamma_{kl}(\omega) - \Gamma_{kl}^*(\omega))\mathsf{A}_k^\dagger(\omega)\mathsf{A}_l(\omega)$. H_{Lamb} effects a renormalization of the closed system energies through the environment coupling known as the Lamb shift. The rates $\gamma_{kl} = \Gamma_{kl}(\omega) + \Gamma_{lk}^*(\omega)$ are given by the Fourier transform of the environment correlation functions $C_{kl}(\tau)$ and they form a Hermitian matrix. Using Bochner's theorem on the Fourier transform of positive functions [41], one can show that (γ_{kl}) is also positive. The usual second standard form (2.66) is now obtained straightforwardly by diagonalizing rate matrix (γ_{kl}) and switching back to the Schrödinger picture, which adds the system Hamiltonian H to H_{Lamb} in the commutator of Eq. (2.87).

[8] One example is the Caldeira-Leggett master equation discussed in Chap. 3.

The Monitoring Approach

In the previous section we have derived the standard form of a Markovian open system evolution by approximating the system-environment dynamics in the *joint limit* of weak coupling and short environment correlation times. Intuitively one would expect, however, that a short correlation time by itself already implies a memoryless evolution (*i.e.* the Markov assumption). Indeed, one can derive the Markovian standard form (2.66) from microscopic considerations without any assumption about the coupling strength in the so-called *monitoring approach* [19, 42], as we will show in the following.

In the monitoring approach one assumes that the system-environment interaction can be described by a series of individual interaction events or collisions[9]. In other words, the environment is thought of as randomly sending probe particles that extract information about the system. The rate at which collisions take place depends both on the system state ρ and on the state ρ_{E} of the incoming probe particle. It is therefore best expressed as the expectation value of an operator G acting on the joint state $\rho_{\mathrm{tot}} = \rho \otimes \rho_{\mathrm{E}}$, and one obtains for the probability for a collision in a time interval Δt

$$\mathrm{Prob}\left(\mathrm{C}_{\Delta t}|\rho_{\mathrm{tot}}\right) = \Delta t \,\mathrm{Tr}\left[\mathsf{G}\rho_{\mathrm{tot}}\right]. \tag{2.88}$$

Therefore, if a collision is about to take place, one needs to update ρ_{tot} with

$$\mathcal{M}\left(\rho_{\mathrm{tot}}|\mathrm{C}_{\Delta t}\right) = \mathrm{Prob}\left(\mathrm{C}_{\Delta t}|\rho_{\mathrm{tot}}\right)^{-1} \Delta t \mathsf{G}^{1/2}\rho_{\mathrm{tot}}\mathsf{G}^{1/2}, \tag{2.89}$$

as prescribed by the theory of generalized measurements (*cf.* Eqs. (2.26) and (2.27)). Conversely, if no collision takes place within Δt one updates with

$$\mathcal{M}\left(\rho_{\mathrm{tot}}|\overline{\mathrm{C}}_{\Delta t}\right) = \mathrm{Prob}\left(\overline{\mathrm{C}}_{\Delta t}|\rho_{\mathrm{tot}}\right)^{-1}\left(\rho_{\mathrm{tot}} - \Delta t \mathsf{G}^{1/2}\rho_{\mathrm{tot}}\mathsf{G}^{1/2}\right), \tag{2.90}$$

since $\mathrm{Prob}\left(\overline{\mathrm{C}}_{\Delta t}|\rho_{\mathrm{tot}}\right) = 1 - \Delta t\,\mathrm{Tr}\left[\mathsf{G}\rho_{\mathrm{tot}}\right]$. We see that one needs a fictitious generalized measurement to describe a series of random scattering events. Assuming the scattering interaction of system and probe to be governed by the S-matrix S, the probabilistic change of ρ_{tot} within Δt is given by

$$\rho'_{\mathrm{tot}} = \Delta t \mathsf{S}\mathsf{G}^{1/2}\rho_{\mathrm{tot}}\mathsf{G}^{1/2}\mathsf{S}^{\dagger} + \rho_{\mathrm{tot}} - \Delta t \mathsf{G}^{1/2}\rho_{\mathrm{tot}}\mathsf{G}^{1/2}. \tag{2.91}$$

In terms of the nontrivial part T of the S-matrix, $\mathsf{S} = \mathbb{1} + i\mathsf{T}$, the difference quotient of ρ_{tot} takes the form

$$\begin{aligned}\frac{\rho'_{\mathrm{tot}} - \rho_{\mathrm{tot}}}{\Delta t} = {} & \mathsf{T}\mathsf{G}^{1/2}\rho_{\mathrm{tot}}\mathsf{G}^{1/2}\mathsf{T}^{\dagger} - \frac{1}{2}\mathsf{T}^{\dagger}\mathsf{T}\mathsf{G}^{1/2}rho_{\mathrm{tot}}\mathsf{G}^{1/2} \\ & -\frac{1}{2}\mathsf{G}^{1/2}\rho_{\mathrm{tot}}\mathsf{G}^{1/2}\mathsf{T}^{\dagger}\mathsf{T} + \frac{i}{2}\left[\mathsf{T} + \mathsf{T}^{\dagger}, \mathsf{G}^{1/2}\rho_{\mathrm{tot}}\mathsf{G}^{1/2}\right],\end{aligned} \tag{2.92}$$

where we used the relation $\mathsf{T} + \mathsf{T}^{\dagger} = i\mathsf{T}^{\dagger}\mathsf{T}$ that is due to the unitarity of S. If we assume

[9] The paradigm for this type of interaction is a Brownian particle in an ideal gas environment.

the probe part ρ_{E} of $\rho_{\mathrm{tot}} = \rho \otimes \rho_{\mathrm{E}}$ to be unaffected by the sequential scattering events, one can take the limit $\Delta t \to 0$ and obtains a differential equation for the system state ρ by tracing out the probe,

$$\begin{aligned}\partial_t \rho = &-\frac{i}{\hbar}\left[\mathsf{H}, \rho\right] + i\,\mathrm{Tr}_{\mathrm{E}}\left(\left[\mathsf{G}^{1/2}\,\mathrm{Re}\left(\mathsf{T}\right)\mathsf{G}^{1/2}, \rho \otimes \rho_{\mathrm{E}}\right]\right) + \mathrm{Tr}_{\mathrm{E}}\left(\mathsf{T}\mathsf{G}^{1/2}\left[\rho \otimes \rho_{\mathrm{E}}\right]\mathsf{G}^{1/2}\mathsf{T}^{\dagger}\right) \\ &-\frac{1}{2}\,\mathrm{Tr}_{\mathrm{E}}\left(\mathsf{G}^{1/2}\mathsf{T}^{\dagger}\mathsf{T}\mathsf{G}^{1/2}\left[\rho \otimes \rho_{\mathrm{E}}\right]\right) - \frac{1}{2}\,\mathrm{Tr}_{\mathrm{E}}\left(\left[\rho \otimes \rho_{\mathrm{E}}\right]\mathsf{G}^{1/2}\mathsf{T}^{\dagger}\mathsf{T}\mathsf{G}^{1/2}\right). \end{aligned} \tag{2.93}$$

Here, we added the coherent system time evolution under H between the scattering events and approximated $\mathrm{Tr}_{\mathrm{E}}\left(\left[\mathrm{Re}\left(\mathsf{T}\right), \mathsf{G}^{1/2}\rho \otimes \rho_{\mathrm{E}}\mathsf{G}^{1/2}\right]\right)$ by $\mathrm{Tr}_{\mathrm{E}}\left(\left[\mathsf{G}^{1/2}\,\mathrm{Re}\left(\mathsf{T}\right)\mathsf{G}^{1/2}, \rho \otimes \rho_{\mathrm{E}}\right]\right)$. The Markovian standard form of Eq. (2.93), which is a result of demanding uncorrelated collisions (*i.e.* $\rho_{\mathrm{E}} = \mathrm{const}$), is manifest. Again, no assumptions about the magnitude of system-environment interactions were made.

2.3 Quantum Trajectories

In Sec. 2.1 we have argued that mixed states ρ are interpreted as involving a classical uncertainty about the pure quantum state $|\psi\rangle$ of the considered system. We also saw that pure initial states generally evolve into mixed states if the system is in contact with its environment. It is therefore natural to expect that any evolution equation for density matrices ρ such as Eqs. (2.66), (2.87), or (2.93) can be represented by a properly defined classical stochastic process in the Hilbert space of pure states. This is indeed the case [43–46], and such a representation is called an *unraveling* of the master equation into *quantum trajectories*, *i.e.* into realizations of the stochastic process. Such an unraveling not only yields a deeper insight into open quantum dynamics by explaining experimental observations such as the random telegraph signal of trapped ions caused by quantum jumps [47, 48]. It can also be used as an efficient technique for the notoriously difficult numerical solution of open quantum systems [44, 45], as we will see in Chap. 6.

The fundamental idea of an unraveling of the master equation is to define a stochastic differential equation for pure states,

$$|\mathrm{d}\psi_t\rangle = |a(\psi_t; t)\rangle \mathrm{d}t + \sum_i |b_i(\psi_t; t)\rangle \mathrm{d}N_i(t). \tag{2.94}$$

The so-called *drift* $|a(\psi_t; t)\rangle$ of the state $|\psi_t\rangle$ is deterministic and proportional to the usual time differential $\mathrm{d}t$, whereas the state change $|b_i(\psi_t; t)\rangle$ is applied depending on classical stochastic process $N_i(t)$. The stochastic pure state solutions $|\psi_t\rangle$ of Eq. (2.94) define a valid unraveling of the master equation

$$\partial_t \rho_t = -\frac{i}{\hbar}[\mathsf{H}, \rho_t] + \sum_i \gamma_i(t)\left(\mathsf{L}_i \rho_t \mathsf{L}_i^{\dagger} - \frac{1}{2}\mathsf{L}_i^{\dagger}\mathsf{L}_i\rho_t - \frac{1}{2}\rho_t \mathsf{L}_i^{\dagger}\mathsf{L}_i\right), \tag{2.95}$$

if their ensemble average is equal to the mixed state ρ_t at all times,

$$\rho_t = \mathbb{E}[|\psi_t\rangle\langle\psi_t|]. \tag{2.96}$$

Here, $\mathbb{E}$ denotes the arithmetic mean over infinitely many realizations of stochastic pure states $|\psi_t\rangle$. In practice, ρ is approximated by the ensemble average of a *finite* number of realizations. Note that Eq. (2.95) is a general Markovian master equation in standard form, except that the jump rates $\gamma_i(t)$ are not included in L_i as in Eq. (2.66).

Generally, there are two different types of stochastic processes that lead to a Markovian evolution of $|\psi_t\rangle$ and therefore of ρ_t: diffusive processes and piecewise deterministic processes. We will here restrict our attention to piecewise deterministic processes (PDP). Crucially, any PDP can be written in terms of a set of statistically independent Poisson processes $N_i(t)$, whose probability densities $p_i(n,t)$ for n jumps within time t satisfy the differential equation

$$\partial_t p_i(n,t) = r_i(t)p_i(n-1,t) - r_i(t)p_i(n,t). \tag{2.97}$$

Here, $r_i(t)$ denotes the time-dependent jump rate of the process $N_i(t)$ so that the expectation value of the increment $\Delta N_i(t)$ is given by

$$\mathbb{E}[\Delta N_i(t)] = r_i(t)\Delta t \quad (\text{for } \Delta t \to 0). \tag{2.98}$$

The solution of Eq. (2.97) is the well known Poissonian probability distribution

$$p_i(n,t) = \frac{[\mu_i(t)]^n}{n!} e^{-\mu_i(t)}, \tag{2.99}$$

with the integrated jump rate $\mu_i(t) = \int_0^t r_i(s)\mathrm{d}s$. The mean and variance of $N_i(t)$ is given by

$$\langle N_i(t)\rangle = \mathrm{Var}[N_i(t)] = \mu_i(t). \tag{2.100}$$

Before we can find a suitable unraveling of the Markovian master equation (2.95), we must clarify the meaning of the stochastic differential equation (SDE) (2.94) and, in particular, the meaning of the symbol $\mathrm{d}N_i(t)$ involved. We therefore need to make a short excursion into the theory of classical stochastic calculus.

2.3.1 Stochastic Calculus for PDPs

A classical PDP $X(t)$ is said to obey an SDE of the form (2.94) if it fulfills the corresponding integral equation[10] [28]

$$X(t) = X(0) + \int_0^t a[X(t');t']\mathrm{d}t' + \sum_i \int_0^t b_i[X(t');t']\mathrm{d}N_i(t'). \tag{2.101}$$

[10] Since we are considering a classical stochastic process here, we substituted the quantum state $|\psi_t\rangle$ with classical process variable X, and $|a(\psi_t;t)\rangle$ and $|b_i(\psi_t;t)\rangle$ with $a[X(t'),t']$ and $b_i[X(t'),t']$, as compared to quantum counterpart, Eq. (2.94).

The stochastic integral in Eq. (2.101), in turn, is defined by

$$\int_0^t f[X(t');t']\mathrm{d}N_i(t') \equiv \sum_{k=1}^{n} f[X(s_k);s_k]\Delta N_{i,k}, \tag{2.102}$$

for an arbitrary real function f of the stochastic process $X(t)$ and time t[11]. Here, s_k are the random jump times ($0 \leq s_1 \leq \ldots s_n \leq t$) for one realization of the Poisson process and $\Delta N_{i,k} = 1$ since the Poisson process $N_i(t)$ increases stepwise. Strictly speaking, the symbol $\mathrm{d}N_i(t)$ is therefore only defined under an integral and all equations where it appears in its own right as in Eq. (2.94) are understood to hold true when integrating over an arbitrary function f.

With this definition of a stochastic integral we can derive the properties of the differential $\mathrm{d}N_i(t)$, *i.e.* the unique calculus or *Ito calculus* for the differentiation and integration of PDPs. First, consider the integral

$$\begin{aligned}\int_0^t f[X(t');t']\mathrm{d}N_i(t')^2 &= \sum_{k=1}^{n} f[X(s_k);s_k]\Delta N_{i,k}^2 = \sum_{k=1}^{n} f[X(s_k);s_k]\Delta N_{i,k} \\ &= \int_0^t f[X(t');t']\mathrm{d}N_i(t'),\end{aligned} \tag{2.103}$$

where we have used that $\Delta N_{i,k} = 1$. Therefore it is legitimate to write

$$\mathrm{d}N_i(t)^2 = \mathrm{d}N_i(t), \tag{2.104}$$

or, more generally, $\mathrm{d}N_i(t)\mathrm{d}N_j(t) = \delta_{ij}\mathrm{d}N_i(t)$ for two statistically independent Poisson processes. Equation (2.104) implies that higher orders of $\mathrm{d}N_i(t)$ cannot be neglected in the Taylor expansion of functions of PDPs or, equivalently, that $\mathrm{d}N_i(t)$ does not vanish for $\mathrm{d}t \to 0$ in Eq. (2.94) (it is either zero or one). In particular, this results in a different chain rule for the differentiation of functions $f[X(t)]$ of PDPs,

$$\begin{aligned}\mathrm{d}f[X(t)] &= f\left(X + a[X;t]\mathrm{d}t + \sum_i b_i[X;t]\mathrm{d}N_i(t)\right) - f(X) \\ &= \partial_X f(X) a[X;t]\mathrm{d}t + f\left(X + \sum_i b_i[X;t]\mathrm{d}N_i(t)\right) - f(X),\end{aligned} \tag{2.105}$$

where it is not permissible to expand the second summand any further.

2.3.2 The Monte Carlo Unraveling

Based on the general form (2.94) for the stochastic evolution of pure states and by applying the differentiation rule (2.105) for PDPs, we can now write down one specific

[11] Causality implies that $f[X(t);t]$ must also be non-anticipating, *i.e.* it must be independent of $N_i(s) - N_i(t)$ for $s > t$.

unraveling of the master equation (2.95)—the so-called *Monte Carlo unraveling*. Note that, generally, infinitely many unravelings with the *same* ensemble average (2.96) but with *different* stochastic trajectories (2.94) are conceivable, since the pure state decomposition (2.5) of a density matrix ρ_t is not unique. If we are concerned about the open system alone, all these different unravelings are equivalent since its physical properties are completely determined by the density matrix. If, however, we were able continuously extract information from the environment, *e.g.* by complete, projective measurements, then it would be possible to know the system state with certainty. In this case, the system follows a pure state evolution and undergoes random jumps when a probabilistic measurement outcome is recorded. Each trajectory then corresponds to one measurement record and the different unravelings are distinguished by different types of measurements.

First, let us assume that the initial state is pure, $\rho = |\psi\rangle\langle\psi|$. The time derivative of the ensemble average (2.96) is then written as

$$\begin{aligned}\partial_t\rho &= \frac{1}{\mathrm{d}t}\mathbb{E}[|\mathrm{d}\psi\rangle\langle\psi| + |\psi\rangle\langle\mathrm{d}\psi| + |\mathrm{d}\psi\rangle\langle\mathrm{d}\psi|] \\ &= |a(\psi)\rangle\langle\psi| + |\psi\rangle\langle a(\psi)| + \sum_i r_i(0)\{|b_i(\psi)\rangle\langle\psi| + |\psi\rangle\langle b_i(\psi)| + |b_i(\psi)\rangle\langle b_i(\psi)|\},\end{aligned} \tag{2.106}$$

where we inserted the general pure state SDE (2.94). According to the chain rule (2.105) for functions of PDPs, we took care to include all orders of the stochastic part while using only the first order of the deterministic part (*i.e.* only part of the term $|\mathrm{d}\psi\rangle\langle\mathrm{d}\psi|$). In addition, we used the expectation value of the increment $\mathbb{E}[\mathrm{d}N_i(t)] = r_i(t)\mathrm{d}t$, Eq. (2.98).

For the Monte Carlo unraveling, one now uses the stochastic state changes or jumps

$$|b_i(\psi)\rangle = \frac{\mathsf{L}_i|\psi\rangle}{\langle\psi|\mathsf{L}_i^\dagger\mathsf{L}_i|\psi\rangle} - |\psi\rangle, \tag{2.107}$$

given in terms of the jump operators L_i of the master equation (2.95) that we want to unravel. The deterministic drift $|a(\psi)\rangle$, in turn, should be in agreement with the Schrödinger equation if the system is closed, *i.e.* we set

$$|a(\psi)\rangle = -\frac{i}{\hbar}\mathsf{H}|\psi\rangle + |\tilde{a}\rangle, \tag{2.108}$$

with the unknown state $|\tilde{a}\rangle$. Inserting the deterministic and stochastic terms (2.108) and (2.107) into Eq. (2.106), we obtain

$$\begin{aligned}\partial_t\rho = -\frac{i}{\hbar}[\mathsf{H}, |\psi\rangle\langle\psi|] + |\tilde{a}\rangle\langle\psi| + |\psi\rangle\langle\tilde{a}| + \sum_i r_i(0)\Bigg\{&\left[\frac{\mathsf{L}_i}{\langle\mathsf{L}_i^\dagger\mathsf{L}_i\rangle_\psi} - \mathbb{1}\right]|\psi\rangle\langle\psi| \\ &+ |\psi\rangle\langle\psi|\left[\frac{\mathsf{L}_i^\dagger}{\langle\mathsf{L}_i^\dagger\mathsf{L}_i\rangle_\psi} - \mathbb{1}\right] + \left[\frac{\mathsf{L}_i}{\langle\mathsf{L}_i^\dagger\mathsf{L}_i\rangle_\psi} - \mathbb{1}\right]|\psi\rangle\langle\psi|\left[\frac{\mathsf{L}_i^\dagger}{\langle\mathsf{L}_i^\dagger\mathsf{L}_i\rangle_\psi} - \mathbb{1}\right]\Bigg\},\end{aligned} \tag{2.109}$$

which simplifies to

$$\partial_t \rho = -\frac{i}{\hbar}\left[\mathsf{H}, |\psi\rangle\langle\psi|\right] + |\tilde{a}\rangle\langle\psi| + |\psi\rangle\langle\tilde{a}| + \sum_i r_i(0)\left[\frac{\mathsf{L}_i|\psi\rangle\langle\psi|\mathsf{L}_i^\dagger}{\langle\mathsf{L}_i^\dagger\mathsf{L}_i\rangle_\psi^2} - |\psi\rangle\langle\psi|\right]. \tag{2.110}$$

Finally, in order for this expression of $\partial_t\rho$ to be equal to the master equation (2.95) at $t = 0$ one chooses [28]

$$r_i(0) = \gamma_i(0)\langle\mathsf{L}_i^\dagger\mathsf{L}_i\rangle_\psi^2, \tag{2.111}$$

and

$$|\tilde{a}\rangle = \sum_i \gamma_i(0)\left[\frac{1}{2}\langle\mathsf{L}_i^\dagger\mathsf{L}_i\rangle_\psi - \frac{1}{2}\mathsf{L}_i^\dagger\mathsf{L}_i\right]|\psi\rangle. \tag{2.112}$$

In fact, this argument also holds true for later times $t > 0$. Therefore, the stochastic differential equation

$$\begin{aligned}|\mathrm{d}\psi_t\rangle = &-\frac{i}{\hbar}\mathsf{H}|\psi_t\rangle\mathrm{d}t - \frac{1}{2}\sum_i \gamma_i(t)\left[\mathsf{L}_i^\dagger\mathsf{L}_i - \langle\mathsf{L}_i^\dagger\mathsf{L}_i\rangle_\psi\right]|\psi_t\rangle\mathrm{d}t \\ &+\sum_i\left[\frac{\mathsf{L}_i|\psi_t\rangle}{\langle\psi_t|\mathsf{L}_i^\dagger\mathsf{L}_i|\psi_t\rangle} - |\psi_t\rangle\right]\mathrm{d}N_i(t),\end{aligned} \tag{2.113}$$

with average Poisson increments $\mathbb{E}[\mathrm{d}N_i(t)] = \gamma_i(t)\langle\mathsf{L}_i^\dagger\mathsf{L}_i\rangle\mathrm{d}t$, defines an unraveling of the master equation (2.95) via the ensemble average, Eq. (2.96).

As mentioned above, infinitely many unravelings of the same master equation (2.95) exist. For example, other piecewise deterministic unravelings can be found by using L-operators with a complex shift in the definition (2.107) of the stochastic part of the SDE[12]. There are also infinitely many unravelings of Eq. (2.95) based on diffusive stochastic processes [28].

[12] While the master equation (2.95) is invariant under complex shifts of the L-operators (see Eq. (2.68)), the SDE (2.113) of the Monte Carlo unraveling is not.

3 Exemplary Master Equations

In Chap. 2 we gave a short introduction to the theory of open quantum systems and described their general dynamical behavior in terms of a Markovian master equation for the evolution of the density matrix. In the present chapter we will consider three specific paradigmatic model systems that display the basic features of Markovian open quantum dynamics. While these models serve to build intuition for the behavior of open quantum systems, they are also the numerical testbeds for the expansion and resummation technique developed in the following chapter. Specifically, we consider (i) the Harmonic oscillator immersed in a bosonic heat bath [14, 28, 49], (ii) a Brownian particle moving within an environmental background gas [2, 19, 50–53], and (iii) a quantum system monitored by a continuous, nonselective measurement [28, 54]. First, we will deduce the corresponding master equations from their specific microscopic descriptions by applying the derivation schemes outlined in Sec. 2.2.5. Second, we will briefly discuss the most important dynamical properties displayed by the solutions of the master equations.

3.1 The Damped Harmonic Oscillator

A prominent method to derive a Markovian master equation for specific quantum systems is based on the assumption of a weak system-environment coupling, see Sec. 2.2.5. A typical situation in where this is very well satisfied is the quantum optical setting of a few-level system coupled to a surrounding field of electromagnetic modes [28]. In this case, the environmental part H_E of the total Hamiltonian

$$\mathsf{H}_\mathrm{tot} = \mathsf{H} + \mathsf{H}_\mathrm{E} + \mathsf{H}_\mathrm{int}, \tag{3.1}$$

reads, in second quantization,

$$\mathsf{H}_\mathrm{E} = \int_0^\infty g(\omega)\hbar\omega\mathsf{b}^\dagger(\omega)\mathsf{b}(\omega)\mathrm{d}\omega. \tag{3.2}$$

Here, ω represents the frequencies of the electromagnetic modes in the environment and $g(\omega)$ the spectral density [28]. $\mathsf{b}(\omega)$ and $\mathsf{b}^\dagger(\omega)$ are the respective creation and annihilation operators satisfying the commutation relation $\left[\mathsf{b}(\omega), \mathsf{b}^\dagger(\omega')\right] = \delta(\omega-\omega')$. In the following, we will consider the open system to be a quantum harmonic oscillator,

$$\mathsf{H} = \hbar\omega_0\mathsf{a}^\dagger\mathsf{a}. \tag{3.3}$$

Without loss of generality, we omitted the vacuum energy both in H_E and in H. The environmental electromagnetic field E couples to the dipole operator d of the harmonic

oscillator, which is proportional to its position $\mathsf{a} + \mathsf{a}^\dagger$ and its charge q. Therefore the interaction Hamiltonian reads

$$\mathsf{H}_{\text{int}} = \mathsf{d} \otimes \mathsf{E} = q \left(\mathsf{a} + \mathsf{a}^\dagger\right) \otimes \int_0^\infty g(\omega) \left(\mathsf{b}(\omega) - \mathsf{b}^\dagger(\omega)\right) \mathrm{d}\omega. \tag{3.4}$$

Assuming that system and environment are weakly coupled, we can immediately write down the master equation (2.87) based on the above microscopic model. Specifically, we use $\mathsf{A}(\omega_0) = q\mathsf{a}$ and $\mathsf{A}(-\omega_0) = q\mathsf{a}^\dagger$ as jump operators, see Eq. (2.83), and neglect the Lamb shift to obtain the master equation for the damped harmonic oscillator,

$$\begin{aligned}\partial_t \rho_t = &-i\left[\omega_0 \mathsf{a}^\dagger\mathsf{a}, \rho_t\right] + \gamma(\omega_0)\left\{\mathsf{a}\rho_t\mathsf{a}^\dagger - \frac{1}{2}\mathsf{a}^\dagger\mathsf{a}\rho_t - \frac{1}{2}\rho_t\mathsf{a}^\dagger\mathsf{a}\right\} \\ &+\gamma(-\omega_0)\left\{\mathsf{a}^\dagger\rho_t\mathsf{a} - \frac{1}{2}\mathsf{a}\mathsf{a}^\dagger\rho_t - \frac{1}{2}\rho_t\mathsf{a}\mathsf{a}^\dagger\right\}.\end{aligned} \tag{3.5}$$

Consequently, jumps of the damped harmonic oscillator correspond to a creation or an annihilation of a photon, which increases or decreases the system energy by $\hbar\omega_0$. The associated jump rates are designated $\gamma(\omega_0)$ and $\gamma(-\omega_0)$, respectively.

In addition, we assume the electromagnetic field to be in a thermal state,

$$\rho_{\text{E}} = \frac{1}{Z_{\text{E}}} \exp\left[-\beta \mathsf{H}_{\text{E}}\right] = \int_0^\infty \mathrm{d}\omega (1 - \exp[-\beta\hbar\omega]) \exp\left[-\beta\hbar\omega \mathsf{b}^\dagger(\omega)\mathsf{b}(\omega)\right], \tag{3.6}$$

with the inverse temperature factor $\beta = (k_B T)^{-1}$. The absorption and emission rates $\gamma(\omega_0)$ and $\gamma(-\omega_0)$ in Eq. (3.5) are now determined by the electromagnetic field correlations $\langle \widetilde{\mathsf{E}}(t)\widetilde{\mathsf{E}}(0)\rangle_{\rho_{\text{E}}}$ in the interaction picture through Eqs. (2.80) and (2.86), and therefore by the correlation functions

$$\langle \mathsf{b}(\omega)\mathsf{b}^\dagger(\omega')\rangle_{\rho_{\text{E}}} = \delta(\omega - \omega')(1 + N(\omega)), \tag{3.7}$$

$$\langle \mathsf{b}^\dagger(\omega)\mathsf{b}(\omega')\rangle_{\rho_{\text{E}}} = \delta(\omega - \omega')N(\omega). \tag{3.8}$$

Here, $N(\omega)$ denotes the average number of photons in the mode ω, *i.e.* the Planck distribution

$$N(\omega) = \frac{1}{\exp[\beta\hbar\omega] - 1}. \tag{3.9}$$

This leads to the absorption and emission rates [28]

$$\gamma(-\omega_0) = N(\omega_0)\gamma_0 \quad \text{and} \quad \gamma(\omega_0) = (1 + N(\omega_0))\gamma_0 m \tag{3.10}$$

with the spontaneous emission rate

$$\gamma_0 = 2\pi g(\omega)|q|^2. \tag{3.11}$$

In the following, we will devote particular attention to the zero temperature limit of the heat bath surrounding the harmonic oscillator. In this limit, the average number of

photons N in the ω_0-mode vanishes, see Eq. (3.9), and the master equation (3.5) reduces to

$$\partial_t \rho_t = -i\left[\omega_0 \mathsf{a}^\dagger \mathsf{a}, \rho_t\right] + \gamma_0 \left\{ \mathsf{a}\rho_t \mathsf{a}^\dagger - \frac{1}{2}\mathsf{a}^\dagger \mathsf{a}\rho_t - \frac{1}{2}\rho_t \mathsf{a}^\dagger \mathsf{a} \right\}. \tag{3.12}$$

As one expects intuitively, with no excitations in the bath, the harmonic oscillator can only lose energy via spontaneous emission events, which are described by the jump operator a and rate γ_0. Remarkably, Eq. (3.12) is one of the few Markovian master equations that can be solved analytically. Therefore, it is convenient to discuss the dynamical properties of the damped harmonic oscillator based on the analytic solution of Eq. (3.12) and thereby illustrate the behavior of Markovian open quantum systems in general.

3.1.1 Dissipation and Decoherence

The master equation (3.12) of the harmonic oscillator in a zero temperature environment can be solved in terms of the eigenstates $|\alpha\rangle$ of the annihilation operator (*i.e.* $\mathsf{a}|\alpha\rangle = \alpha|\alpha\rangle$), the so-called *coherent states*. Here, α is a complex number which represents the position of the quantum state in the analog of the two-dimensional classical phase space. The coherent state $|\alpha\rangle$ is constructed from the vacuum state $|0\rangle$ with the help of the displacement operator

$$\mathsf{D}(\alpha) = \exp\left(\alpha \mathsf{a}^\dagger - \alpha^* \mathsf{a}\right) = e^{-\frac{1}{2}|\alpha|^2} e^{\alpha \mathsf{a}^\dagger} e^{-\alpha^* \mathsf{a}} \tag{3.13}$$

via

$$|\alpha\rangle = \mathsf{D}(\alpha)|0\rangle = e^{-\frac{1}{2}|\alpha|^2} e^{\alpha \mathsf{a}^\dagger}|0\rangle. \tag{3.14}$$

An initial coherent state $\rho_0 = |\alpha_0\rangle\langle\alpha_0|$ evolves under the master equation (3.12) as

$$\rho_t = |\alpha_t\rangle\langle\alpha_t|, \tag{3.15}$$

with an oscillating but exponentially damped amplitude

$$\alpha_t = \alpha_0 \exp\left(-i\omega_0 t - \frac{\gamma_0}{2}t\right). \tag{3.16}$$

This can be verified by taking the time derivative of Eq. (3.15)[1],

$$\begin{aligned}
\partial_t \rho_t &= \left(\left[\frac{\partial}{\partial \alpha_t}|\alpha_t\rangle\right]\langle\alpha_t| + |\alpha_t\rangle\left[\frac{\partial}{\partial \alpha_t}\langle\alpha_t|\right]\right)\partial_t \alpha_t + \left(\left[\frac{\partial}{\partial \alpha_t^*}|\alpha_t\rangle\right]\langle\alpha_t| + |\alpha_t\rangle\left[\frac{\partial}{\partial \alpha_t^*}\langle\alpha_t|\right]\right)\partial_t \alpha_t^* \\
&= \left(-\alpha_t^* + \mathsf{a}^\dagger\right)\rho_t\left(-i\omega_0 - \frac{\gamma_0}{2}\right)\alpha_t + \rho_t\left(-\alpha_t + \mathsf{a}\right)\left(i\omega_0 - \frac{\gamma_0}{2}\right)\alpha_t^* \\
&= -i\omega_0\left(\mathsf{a}^\dagger \alpha_t \rho_t - \rho_t \alpha_t^* \mathsf{a}\right) + \gamma_0\left(\alpha_t \rho_t \alpha_t^* - \frac{1}{2}\mathsf{a}^\dagger \alpha_t \rho_t - \frac{1}{2}\rho_t \alpha_t^* \mathsf{a}\right),
\end{aligned} \tag{3.17}$$

[1]Note that in Eq. (3.17), we treat $|\alpha\rangle$ as a vector depending on the independent variables α and α^* instead of depending on the real and imaginary parts of α. Both cases can be shown to be equivalent by writing out the so-called Wirthinger derivatives, $\partial_\alpha = (\partial_x - i\partial_y)/2$ and $\partial_{\alpha^*} = (\partial_x + i\partial_y)/2$, with x the real and y the imaginary part of α [55].

which is equal to the master equation (3.12).

The evolution equations (3.15) and (3.16) state that an initial coherent state spirals towards the origin of the complex plane under the influence of a zero temperature electromagnetic field. Since the energy of the harmonic oscillator is quantified by the mean distance from the origin, it therefore asymptotically dissipates all of its energy to the environment. More generally, one can show that for an environment at $T \geq 0$, any initial state of the harmonic oscillator is contracted to the fixed point or steady state ρ_{ss} given by the thermal state at the temperature of the environment [28],

$$\rho_{\mathrm{ss}} = \frac{1}{Z} \exp\left[-\beta \mathsf{H}\right] = \left(1 - \exp[-\beta\hbar\omega_0]\right) \exp\left[-\beta\hbar\omega_0 \mathsf{a}^\dagger \mathsf{a}\right]. \tag{3.18}$$

This dissipation process which leads asymptotically to ρ_{ss}, occurs on a time scale inversely proportional to the spontaneous emission rate,

$$\tau_{\mathrm{dis}} = \gamma_0^{-1}. \tag{3.19}$$

In addition to τ_{dis}, the master equation (3.12) defines another, less obvious time scale. To see this, note that coherent initial states remain pure during the entire open system evolution, see Eq. (3.15) and Sec. 3.1.2. Our observation from Sec. 2.2 that a pure initial state generally evolves into a mixed state remains true, however. Consider, for example, an initial superposition of coherent states,

$$|\psi_0\rangle = c_1|\alpha_0\rangle + c_2|\beta_0\rangle, \tag{3.20}$$

corresponding to the density matrix

$$\rho_0 = |c_1|^2|\alpha_0\rangle\langle\alpha_0| + |c_2|^2|\beta_0\rangle\langle\beta_0| + c_1c_2^*|\alpha_0\rangle\langle\beta_0| + c_2c_1^*|\beta_0\rangle\langle\alpha_0|. \tag{3.21}$$

The evolution of this initial state under the master equation (3.12) is given by [28]

$$\rho_t = |c_1|^2|\alpha_t\rangle\langle\alpha_t| + |c_2|^2|\beta_t\rangle\langle\beta_t| + c_1c_2^*D_t|\alpha_t\rangle\langle\beta_t| + c_2c_1^*D_t|\beta_t\rangle\langle\alpha_t|, \tag{3.22}$$

where the coherent states $|\alpha_t\rangle$ and $|\beta_t\rangle$ evolve according to Eq. (3.16) and the evolution of the off-diagonal coefficients is governed by

$$D_t = \exp\left[\left(-\frac{1}{2}|\alpha_0 - \beta_0|^2 + i\,\mathrm{Im}[\alpha_0\beta_0^*]\right)\left(1 - e^{-\gamma_0 t}\right)\right]. \tag{3.23}$$

On time scales which are short compared to the dissipation time scale $\tau_{\mathrm{dis}} = \gamma_0^{-1}$, the off-diagonal terms, or coherences, of ρ_t therefore decay with

$$|D_t| \simeq \exp\left[-\frac{\gamma_0}{2}|\alpha_0 - \beta_0|^2 t\right], \quad \text{for } t \ll \gamma_0^{-1}. \tag{3.24}$$

This process is known by the name of *decoherence* and the associated time scale,

$$\tau_{\mathrm{dec}} = \frac{2}{\gamma_0 |\alpha_0 - \beta_0|^2} = \frac{2\tau_{\mathrm{dis}}}{|\alpha_0 - \beta_0|^2}, \tag{3.25}$$

is generally much shorter than the dissipation time scale τ_{dis}. In particular, the efficiency of decoherence grows with the size of the open system, here quantified by the distance $|\alpha_0 - \beta_0|^2$ of the initially superposed coherent states. Once the coherences have decayed completely, the harmonic oscillator finds itself in a probabilistic mixture of the two coherent states of the initial coherent superposition,

$$\rho_t \simeq |c_1|^2 |\alpha_t\rangle\langle\alpha_t| + |c_2|^2 |\beta_t\rangle\langle\beta_t|, \quad \text{for } t \gg \tau_{\mathrm{dec}}. \tag{3.26}$$

The statistical weights of $|\alpha_t\rangle\langle\alpha_t|$ and $|\beta_t\rangle\langle\beta_t|$ in ρ_t are equal to the probabilities of detecting the initial superposition in either $|\alpha_0\rangle$ or $|\beta_0\rangle$.

In conclusion, we saw that two dynamical regimes associated with different time scales can be distinguished in the evolution of the damped harmonic oscillator. On a short time scale τ_{dec} one observes decoherence, *i.e.* the system looses its ability to form quantum superpositions. On a longer time scale τ_{dis} processes such as energy dissipation or diffusion take place, which we already know from classical open systems. This separation of time scales into two regimes is typical for most realistic open quantum systems.

3.1.2 The Pointer Basis

In the previous section we learned that decoherence distinguishes a set of states which remain pure for a relatively long time, whereas their coherent superpositions get mixed rapidly. These states are called *pointer states* or *robust states* [1, 2] and they ideally form a basis of the Hilbert space. It is the basis in which ρ becomes diagonal so that after the time τ_{dec} an observer probabilistically detects the system in either one or the other pointer state with probabilities given by the Born rule for the initial state. The facts that this is what we classically expect, and that τ_{dec} decreases with the system size and practically vanishes on the macroscopic scale, suggest that decoherence is a promising candidate to explain the long-debated quantum to classical transition [3, 4]. Furthermore, the pointer states of specific model systems were found to exhibit classically expected properties [4, 28, 53]: For example, the coherent states $|\alpha\rangle$ (the pointer states of the damped harmonic oscillator, see previous section) have a well defined, though unsharp, position, momentum, and energy and evolve along the classical phase space trajectories.

Motivated by the above observations, one may say that a given open quantum system has the pointer states $\mathsf{P}_\alpha = |\pi_\alpha\rangle\langle\pi_\alpha|$ if it exhibits a separation of time scales $\tau_{\mathrm{dec}} \ll \tau_{\mathrm{dis}}$, so that at intermediate times $\tau_{\mathrm{dec}} \ll t \ll \tau_{\mathrm{dis}}$ the system state ρ_t is well approximated by a mixture of the P_α,

$$\rho_t \simeq \int \mathrm{d}\alpha \, \mathrm{Tr}\left[\mathsf{P}_\alpha \rho_0\right] \mathsf{P}_\alpha, \quad \text{for } \tau_{\mathrm{dec}} \ll t \ll \tau_{\mathrm{dis}}. \tag{3.27}$$

The pointer states P_α are determined by the environment coupling and are therefore independent of the initial state ρ_0 of the open system [4]. Furthermore, the P_α generally depend only weakly on time [53]. The definition (3.27) states that an initial pointer state remains approximately pure during the entire decoherence process. Therefore, pointer states are those pure states which become mixed most slowly, *i.e.* which are most robust to decoherence.

Although the definition of pointer states is relatively straightforward, a general method to determine the pointer states of a given open system is still missing. The most obvious ansatz is to sort all pure states according to their entropy production rate [4]. This, however, implies an optimization problem which is very hard to solve in general [53]. Another approach, which we will follow here, is to find a nonlinear evolution equation for pure states whose solitons are the pointer states [14, 49].

More specifically, we demand this evolution equation to be non-linear in order to be able to distinguish between pointer states and their coherent superpositions and it should, in addition, follow the true mixed state evolution under the master equation as closely as possible. On the decoherence time scale, an initial pointer state $\rho_0 = \mathsf{P}_\alpha$ is then best approximated by the same pure state P_α, even though it may become mixed slowly, see Eq. (3.27). Recall from Chap. 2 that the physical states ρ form a convex set with the pure states lying on the surface. Therefore, while an initially pure state located on the surface dives into this convex set as it becomes mixed under the master equation, the nonlinear equation retains it in that point of the surface that is closest to the evolved mixed state.

The most general nonlinear equation that conserves the trace and the purity is given by [49]

$$\partial_t \mathsf{P}_t = -i\,[\mathsf{A}_t, \mathsf{P}_t] + [\mathsf{P}_t, [\mathsf{P}_t, \mathsf{B}_t]]\,, \tag{3.28}$$

with general Hermitian operators A_t and B_t, and the pure state projector $\mathsf{P}_t^2 = \mathsf{P}_t$. Its first, linear part is equivalent to the von Neumann equation (2.42) for closed systems. We can verify that the purity, quantified by the linear entropy (2.17), is conserved under Eq. (3.28) by taking the time derivative of Eq. (2.17),

$$\begin{aligned}\partial_t \operatorname{Tr}\left[\mathsf{P}_t^2\right] &= 2\operatorname{Tr}\left[\mathsf{P}_t\,(\partial_t \mathsf{P}_t)\right] = 2\operatorname{Tr}\left[\mathsf{P}_t\,(-i\,\{\mathsf{A}_t\mathsf{P}_t - \mathsf{P}_t\mathsf{A}_t\} + \mathsf{P}_t\mathsf{P}_t\mathsf{B}_t - 2\mathsf{P}_t\mathsf{B}_t\mathsf{P}_t + \mathsf{B}_t\mathsf{P}_t\mathsf{P}_t)\right] \\ &= -i\operatorname{Tr}\left[\mathsf{P}_t^2\mathsf{A}_t - \mathsf{P}_t^2\mathsf{A}_t\right] + \operatorname{Tr}\left[\mathsf{P}_t^3\mathsf{B}_t - 2\mathsf{P}_t^3\mathsf{B}_t + \mathsf{P}_t^3\mathsf{B}_t\right] = 0,\end{aligned} \tag{3.29}$$

where the cyclic invariance of the trace was used. Using the Hermitian operator $\mathsf{X}_t = -i\,[\mathsf{A}_t, \mathsf{P}_t] + \mathsf{B}_t$, Eq. (3.28) can be simplified to

$$\partial_t \mathsf{P}_t = [\mathsf{P}_t, [\mathsf{P}_t, \mathsf{X}_t]]\,. \tag{3.30}$$

As described above, this nonlinear equation leads asymptotically to the pointer states if it follows the full open system master equation as closely as possible. Therefore, we minimize the distance between Eq. (3.30) and $\partial_t \mathsf{P}_t = \mathcal{L}(t)\mathsf{P}_t$, where distance in state

space is quantified by the Hilbert-Schmidt norm $\|\mathsf{A}\|^2 = \mathrm{Tr}\left[\mathsf{A}^\dagger\mathsf{A}\right]$,

$$\|\underbrace{\mathcal{L}(t)\mathsf{P}_t}_{\equiv \mathsf{Z}_t} - \partial_t \mathsf{P}_t\|^2 = \mathrm{Tr}\left[(\mathsf{Z}_t - [\mathsf{P}_t,[\mathsf{P}_t,\mathsf{X}_t]])^2\right] = \mathrm{Tr}\left[\mathsf{Z}_t^2 - 2\left(\mathsf{Z}_t^2\mathsf{P}_t - (\mathsf{Z}_t\mathsf{P}_t)^2\right)\right]$$
$$+2\,\mathrm{Tr}\left[(\mathsf{Z}_t - \mathsf{X}_t)^2\,\mathsf{P}_t - ((\mathsf{Z}_t - \mathsf{X}_t)\,\mathsf{P}_t)^2\right]. \tag{3.31}$$

Noting that the first summand is independent of X_t and that the second summand is nonnegative, the above equation is obviously minimized by $\mathsf{X}_t = \mathsf{Z}_t = \mathcal{L}(t)\mathsf{P}_t$. The desired nonlinear equation for pointer states thus reads

$$\partial_t \mathsf{P}_t = [\mathsf{P}_t,[\mathsf{P}_t,\mathcal{L}(t)\mathsf{P}_t]]\,. \tag{3.32}$$

This evolution equation for the projectors P_t can be recast in a more intuitive form by inserting $\mathsf{P}_t = |\chi\rangle\langle\chi|$,

$$\partial_t|\chi\rangle = [\{\mathcal{L}(t)|\chi\rangle\langle\chi|\} - \langle\chi|\{\mathcal{L}(t)|\chi\rangle\langle\chi|\}|\chi\rangle]|\chi\rangle. \tag{3.33}$$

Note that the curly brackets are necessary since $\mathcal{L}(t)$ is a superoperator acting on $|\chi\rangle\langle\chi|$. For a Markovian generator $\mathcal{L}(t)$ given in standard form (2.66), Eq. (3.33) reads

$$\begin{aligned}\partial_t|\chi\rangle &= \Bigg[-\frac{i}{\hbar}\left([\mathsf{H},|\chi\rangle\langle\chi|] - [\langle\mathsf{H}\rangle,|\chi\rangle\langle\chi|]\right)\\ &\quad + \sum_j \mathsf{L}_j|\chi\rangle\langle\chi|\mathsf{L}_j^\dagger - \frac{1}{2}\mathsf{L}_j^\dagger\mathsf{L}_j|\chi\rangle\langle\chi| - \frac{1}{2}|\chi\rangle\langle\chi|\mathsf{L}_j^\dagger\mathsf{L}_j - \langle\mathsf{L}_j\rangle\langle\mathsf{L}_j^\dagger\rangle + \langle\mathsf{L}_j^\dagger\mathsf{L}_j\rangle\Bigg]|\chi\rangle\\ &= \left[-\frac{i}{\hbar}\left(\mathsf{H} - \langle\mathsf{H}\rangle\right) + \sum_j\left\{\langle\mathsf{L}_j^\dagger\rangle\left(\mathsf{L}_j - \langle\mathsf{L}_j\rangle\right) - \frac{1}{2}\left(\mathsf{L}_j^\dagger\mathsf{L}_j - \langle\mathsf{L}_j^\dagger\mathsf{L}_j\rangle\right)\right\}\right]|\chi\rangle,\end{aligned} \tag{3.34}$$

where expectation values are with respect to $|\chi\rangle$, and $\langle\mathsf{H}\rangle$ can be neglected since it only induces a global phase.

To demonstrate that Eq. (3.34) is solved by the pointer states of the harmonic oscillator found in Sec. 3.1.1, we set $\mathsf{L} = \sqrt{\gamma_0}\mathsf{a}$ and $\mathsf{H} = \hbar\omega_0\mathsf{a}^\dagger\mathsf{a}$. Equation (3.34) then reads

$$\partial_t|\chi\rangle = -i\omega_0\mathsf{a}^\dagger\mathsf{a}|\chi\rangle + \gamma_0\left[\langle\mathsf{a}^\dagger\rangle\left(\mathsf{a} - \langle\mathsf{a}\rangle\right) - \frac{1}{2}\left(\mathsf{a}^\dagger\mathsf{a} - \langle\mathsf{a}^\dagger\mathsf{a}\rangle\right)\right]|\chi\rangle. \tag{3.35}$$

The first term in square bracket vanishes for a coherent state $|\chi\rangle = |\alpha_t\rangle$. The remaining differential equation,

$$\partial_t|\alpha_t\rangle = \left[\left(-i\omega_0 - \frac{\gamma_0}{2}\right)\alpha_t\mathsf{a}^\dagger + \frac{\gamma_0}{2}|\alpha_t|^2\right]|\alpha_t\rangle, \tag{3.36}$$

is solved by $\alpha_t = \alpha_0\exp(-i\omega_0 t - \gamma_0/2t)$, as can be verified by taking the time derivative of $|\alpha_t\rangle = \exp\left(-|\alpha_t|^2/2 + \alpha_t\mathsf{a}^\dagger\right)|0\rangle$. This shows that, in agreement with our previous

observations, the stationary states of Eq. (3.34) and therefore the pointer states of the damped harmonic oscillator are the coherent states $|\alpha_t\rangle$, see Eqs. (3.15) and (3.16).

3.2 Quantum Brownian Motion

Brownian motion is the random movement of a heavy particle due to collisions with background gas particles. In quantum mechanics, the problem of Brownian motion is a paradigm to describe frictional dissipation and spatial decoherence of the considered particle. It can be described phenomenologically by two different microscopic models which were conceived in the framework of the Markovian approximation schemes described in Sec. 2.2.5. The two models make quantitatively different predictions that apply to distinct experimental settings: the first was confirmed in solid state physics [30] and the second in matter wave interference [6].

3.2.1 The Caldeira-Leggett Master Equation

The first, so-called *Caldeira-Leggett model* [50] considers a particle of mass m moving in a potential $V(x)$. The background particles are modeled by a bath of harmonic oscillators in the thermal state ρ_{E} just like for the previous example of the damped harmonic oscillator, see Eq. (3.6). The coupling between the particle and background gas is assumed to be proportional to both the particle position operator x and the amplitudes $\mathsf{x}(\omega)$ of the environmental harmonic oscillators,

$$\mathsf{x}(\omega) = \sqrt{\frac{\hbar}{2m_{\mathrm{ho}}\omega}}\left[\mathsf{b}(\omega) + \mathsf{b}^\dagger(\omega)\right]. \tag{3.37}$$

The joint system-environment Hamiltonian $\mathsf{H}_{\mathrm{tot}} = \mathsf{H} + \mathsf{H}_{\mathrm{E}} + \mathsf{H}_{\mathrm{int}}$ is therefore determined by

$$\mathsf{H} = \frac{\mathsf{p}^2}{2m} + V(\mathsf{x}), \tag{3.38}$$

$$\mathsf{H}_{\mathrm{E}} = \int g(\omega)\hbar\omega\mathsf{b}^\dagger(\omega)\mathsf{b}(\omega)\mathrm{d}\omega, \tag{3.39}$$

$$\mathsf{H}_{\mathrm{int}} = -\mathsf{x}\int g(\omega)\kappa(\omega)\mathsf{x}(\omega)\mathrm{d}\omega. \tag{3.40}$$

As before, $g(\omega)$ stands for the density of modes in the environment and $\kappa(\omega)$ for the mode dependent coupling constant.

The above microscopic model allows one to perform the Born-Markov approximation directly, see Eq. (2.82), *i.e.* to write the sytem dynamics in terms of a suitable superoperator $\mathcal{K}$ as

$$\partial_t\rho_t = -\frac{i}{\hbar}\left[\mathsf{H} + \mathsf{H}_{\mathrm{c}}, \rho_t\right] + \mathcal{K}\rho_t, \tag{3.41}$$

with

$$\mathcal{K}\rho_t = -\frac{1}{\hbar^2}\int_0^\infty \mathrm{Tr}_\mathrm{E}\left[\mathsf{H}_\mathrm{int}, \left[e^{-i(\mathsf{H}+\mathsf{H}_\mathrm{E})t'/\hbar}\mathsf{H}_\mathrm{int}e^{i(\mathsf{H}+\mathsf{H}_\mathrm{E})t'/\hbar}, \rho_t\otimes\rho_\mathrm{E}\right]\right]\mathrm{d}t'. \tag{3.42}$$

In contrast to Eq. (2.82), we use the Schrödinger picture here for brevity and include an additional, environment-induced renormalization H_c of the closed system energy levels [28],

$$\mathsf{H}_\mathrm{c} = \mathsf{x}^2\int g(\omega)\frac{\kappa(\omega)^2}{2m_\mathrm{ho}\omega^2}\mathrm{d}\omega \equiv \mathsf{x}^2\int\frac{J(\omega)}{\omega}\mathrm{d}\omega, \tag{3.43}$$

with $J(\omega)$ denoting the spectral density of the bath. To further specify the superoperator $\mathcal{K}$ and find out under which conditions the Born-Markov approximation (3.41) is justified, we assume an Ohmic spectral density with Lorenz-Drude cutoff,

$$J(\omega) = \frac{2m\gamma}{\pi}\frac{\Omega^2}{\Omega^2+\omega^2}\omega. \tag{3.44}$$

This spectral density increases linearly for $\omega \ll \Omega$ and goes to zero for $\omega \gg \Omega$. It guarantees an ω-independent damping rate γ of the Brownian particle. For this choice of $J(\omega)$, $\mathcal{K}$ takes the form of an integral over two terms [28],

$$\begin{aligned}\mathcal{K}\rho_t = \frac{1}{\hbar^2}\int_0^\infty \mathrm{d}t'\Bigg(&im\gamma\hbar\Omega^2 e^{-\Omega t'}\left[\mathsf{x}, \left\{e^{-i(\mathsf{H}+\mathsf{H}_\mathrm{E})t'/\hbar}\mathsf{x}e^{i(\mathsf{H}+\mathsf{H}_\mathrm{E})t'/\hbar}, \rho_t\right\}\right]\\ &-2m\gamma k_B T\Omega^2\left[\sum_{n=-\infty}^{\infty}\frac{\Omega e^{-\Omega t'} - |\nu_n|e^{-|\nu_n|t'}}{\Omega^2-\nu_n^2}\right]\left[\mathsf{x}, \left[e^{-i(\mathsf{H}+\mathsf{H}_\mathrm{E})t'/\hbar}\mathsf{x}e^{i(\mathsf{H}+\mathsf{H}_\mathrm{E})t'/\hbar}, \rho_t\right]\right]\mathrm{d}t'\Bigg),\end{aligned} \tag{3.45}$$

where the $\nu_n = 2\pi n k_B T/\hbar$ are called *Matsubara frequencies*. Inscribed in the weights of the above integrand are the inverse correlation times Ω and ν_n (with $n \neq 0$) of the environment. Our initial Markov assumption, Eq. (3.41), is only admissible if the dissipation time scale $1/\gamma$ of the system is large compared to either of the environmental correlation time scales, *i.e.* if

$$\hbar\gamma \ll \min\{\hbar\Omega, 2\pi k_B T\}. \tag{3.46}$$

Similar to the previous example of the damped harmonic oscillator, we consider the limit of slow coherent system dynamics compared to rapid environment correlation time scales. Denoting by ω_0 a typical system time scale, we can write this condition as

$$\hbar\omega_0 \ll \min\{\hbar\Omega, 2\pi k_B T\}. \tag{3.47}$$

In this limit we can now approximate the time evolved system position operator x in Eq. (3.45) by its free dynamics and use its respective expansion up to first order in t',

$$e^{-i(\mathsf{H}+\mathsf{H}_\mathrm{E})t'/\hbar}\mathsf{x}e^{i(\mathsf{H}+\mathsf{H}_\mathrm{E})t'/\hbar} \approx e^{-i\mathsf{H}t'/\hbar}\mathsf{x}e^{i\mathsf{H}t'/\hbar} \approx \mathsf{x} - \frac{i}{\hbar}\left[\mathsf{H}, \mathsf{x}\right]t' = \mathsf{x} - \frac{\mathsf{p}}{m}t'. \tag{3.48}$$

Substituting the above approximation into Eq. (3.45), we obtain a sum of four terms; the corresponding t'-integrals can be evaluated analytically for high temperatures $k_B T \gtrsim \Omega\hbar$ [28]. While the first term involving $[\mathsf{x}, \{\mathsf{x}, \rho_t\}]$ exactly cancels the anticipated environmental shift H_c of the system energies, see Eq. (3.43), the last term involving $[\mathsf{x}, [\mathsf{p}, \rho_t]]$ is proportional to ω_0/Ω and can hence be neglected in the limit (3.47). The master equation for the system evolution ρ_t finally reads

$$\partial_t \rho_t = -\frac{i}{\hbar}\left[\mathsf{H}, \rho_t\right] - \frac{i\gamma}{\hbar}\left[\mathsf{x}, \{\mathsf{p}, \rho_t\}\right] - \frac{4\pi\gamma}{\Lambda_\mathrm{th}^2}\left[\mathsf{x}, [\mathsf{x}, \rho_t]\right], \tag{3.49}$$

with $\Lambda_\mathrm{th} \equiv \sqrt{2\pi\hbar^2/mk_BT}$ the thermal de Broglie wavelength of the particle. Equation (3.49) is called the *Caldeira-Leggett master equation*. While the first term of the Caldeira-Leggett master equation describes the usual closed quantum dynamics of a particle in a potential, the second and third term describe frictional dissipation and decoherence due to thermal fluctuations, respectively. Dissipation and decoherence are genuine open system phenomena that were already encountered in the damped harmonic oscillator, see Sec. 3.1.1.

Looking at the Caldeira-Leggett master equation, one notices that it cannot be cast into standard form, Eq. (2.66), *i.e.* the generated time evolution is not completely positive. Complete positivity can be ensured, however, by subtracting $(\gamma/8mk_BT)\,[\mathsf{p}, [\mathsf{p}, \rho_t]]$ [28], which, for high temperatures, is small compared to the other terms (this is called a minimally invasive modification of Eq. (3.49)). Hence, the dynamics of a quantum Brownian particle that is coupled weakly to a hot background gas is described by the Markovian master equation

$$\partial_t \rho_t = -\frac{i}{\hbar}\left[\frac{\mathsf{p}^2}{2m} + \frac{\gamma}{2}(\mathsf{xp}+\mathsf{px}) + V(\mathsf{x}), \rho_t\right] + \gamma\left(\mathsf{L}\rho_t\mathsf{L}^\dagger - \frac{1}{2}\mathsf{L}^\dagger\mathsf{L}\rho_t - \frac{1}{2}\rho_t\mathsf{L}^\dagger\mathsf{L}\right), \tag{3.50}$$

with

$$\mathsf{L} = \frac{\sqrt{8\pi}}{\Lambda_\mathrm{th}}\mathsf{x} + i\frac{\Lambda_\mathrm{th}}{\sqrt{8\pi}}\mathsf{p}. \tag{3.51}$$

Dissipation & Decoherence

Let us investigate the dynamical regimes of dissipation and decoherence in the Caldeira-Leggett model, *i.e.* how the particle exchanges energy with the environment and gradually loses its ability to form coherent superpositions.

To quantify the transfer of energy between the Brownian particle and the environment, we consider the expectation value of kinetic energy operator $\mathsf{T} = \mathsf{p}^2/2m$. Its time derivative reads

$$\partial_t\langle\mathsf{T}\rangle_t = \mathrm{Tr}\left[\frac{\mathsf{p}^2}{2m}\partial_t\rho_t\right] = -\frac{i\gamma}{2m\hbar}\,\mathrm{Tr}\left(\mathsf{p}^2\left[\mathsf{x}, \mathsf{p}\rho_t + \rho_t\mathsf{p}\right]\right) - \frac{4\pi\gamma}{2m\Lambda_\mathrm{th}^2}\,\mathrm{Tr}\left(\mathsf{p}^2\left[\mathsf{x}, \mathsf{x}\rho_t - \rho_t\mathsf{x}\right]\right), \tag{3.52}$$

where we have inserted the Caldeira-Leggett master equation (3.49). Using the canonical

commutation relation $[\mathsf{x}, \mathsf{p}] = i\hbar$, one obtains the differential equation [28]

$$\partial_t \langle \mathsf{T} \rangle_t = -4\gamma \langle \mathsf{T} \rangle_t + 2\gamma k_B T, \tag{3.53}$$

which is solved by

$$\langle \mathsf{T} \rangle_t = \frac{k_B T}{2} + \left(\langle \mathsf{T} \rangle_0 - \frac{k_B T}{2} \right) e^{-4\gamma t}. \tag{3.54}$$

We see that the kinetic energy of the particle approaches the thermal energy $k_B T/2$ asymptotically, with the dissipation time scale given by $\tau_{\rm dis} = 1/4\gamma$. Furthermore, one can show that the steady state of the Caldeira-Leggett master equation (3.49) and of its completely positive version (3.50) is indeed the thermal state $\rho = \exp[-\beta \mathsf{H}]/Z^{-1}$ [56]. The time evolution equation (3.53) also shows that the frictional decay of the kinetic energy is due to the second term of the Caldeira-Leggett master equation.

To study the phenomenon of decoherence, we now consider the short time dynamics of the Caldeira-Leggett model, for which we can approximate the environmental influence by the third term of Eq. (3.49) [2, 3, 57],

$$\partial_t \rho_t = -\frac{i}{\hbar} [\mathsf{H}, \rho_t] - \frac{4\pi\gamma}{\Lambda_{\rm th}^2} [\mathsf{x}, [\mathsf{x}, \rho_t]] \,. \tag{3.55}$$

We will call this simplified Caldeira-Leggett model the *linear coupling limit* of quantum Brownian motion [19]. After switching to the interaction picture, $\tilde{\rho}_t = e^{i\mathsf{H}t/\hbar} \rho_t e^{-i\mathsf{H}t/\hbar}$, and to the position representation, $\langle x|\tilde{\rho}_t|x'\rangle = \tilde{\rho}_t(x, x')$, Eq. (3.55) reads

$$\partial_t \tilde{\rho}_t = -\frac{4\pi\gamma}{\Lambda_{\rm th}^2} (x - x')^2 \tilde{\rho}_t(x, x'). \tag{3.56}$$

We see that, in the position representation, the off-diagonal elements of $\tilde{\rho}_t$ decay under the environmental influence. For example, a coherent superposition of two position eigenstates, $\tilde{\rho}_t = |\psi\rangle\langle\psi|$ with $|\psi\rangle = (|x_1\rangle + |x_2\rangle)/\sqrt{2}$, decays to their probabilistic mixture on the decoherence time scale

$$\tau_{\rm dec} = \frac{\Lambda_{\rm th}^2}{\pi (x_1 - x_2)^2} \tau_{\rm dis}. \tag{3.57}$$

Similar to the decoherence time scale of the damped harmonic oscillator, Eq. (3.25), $\tau_{\rm dec}$ is inverse-proportional to the square of the difference of the two positions, so that $\tau_{\rm dec}$ is generally much smaller than $\tau_{\rm dis}$.

The pointer basis of the linear coupling master equation (3.55) is *not* the position basis, however, as one would expect in analogy to the damped harmonic oscillator. This is evident from the fact that a position eigenstate or delta-function $\psi(x) = \delta(x)$ disperses quickly and the resulting broad wave packet again becomes mixed, see Eq. (3.56)[2]. Here, the pointer states, *i.e.* those states that exhibit the lowest entropy production rate *on average*, can be identified from the steady states of the nonlinear equation (3.34) from

[2] The underlying reason is that here, in contrast to the damped harmonic oscillator, the Hamiltonian $\mathsf{H} = \mathsf{p}^2/2m + V(\mathsf{x})$ and jump operator $\mathsf{L} = \mathsf{x}$ do not commute.

Sec. 3.1.2. It turns out that the pointer states of the linear coupling model are those localized wave packets $\pi_t(x)$ of finite width σ, for which the dispersive effect of H and the localizing effect of x are in equilibrium [14, 51, 53]. They are given by

$$\pi_t(x) = \mathcal{N} \exp\left[-\frac{1-i}{4\sigma^2}\left(x - \langle \mathsf{x}\rangle_t\right)^2 + \frac{i}{\hbar}\left(x - \langle \mathsf{x}\rangle_t\right)\langle \mathsf{p}\rangle + i\phi_t\right], \tag{3.58}$$

with the time dependent phase $\phi_t = \left(\langle \mathsf{p}\rangle^2/2\hbar m - \hbar/4m\sigma^2\right)t$. They move with constant momentum, $\langle \mathsf{x}\rangle_t = \langle \mathsf{p}\rangle t/m + \langle \mathsf{x}\rangle_0$, and their width is given by $\sigma = \left(\hbar\Lambda_{\mathrm{th}}^2/\pi\gamma\right)^{1/4}/2$. Since they are not eigenstates of the jump operator, they exhibit a small but nonvanishing entropy increase, *i.e.* they do not remain pure states.

3.2.2 Collisional Decoherence

The second microscopic model for quantum Brownian motion assumes that background gas particles scatter off the Brownian particle sequentially [19, 52]. As before, the background gas is assumed to be in a thermal state ρ_{E} which is diagonal in the momentum basis in the case of ideal, non-interacting gas particles ($\mathsf{H}_{\mathrm{E}} = \mathsf{p}^2/2m$),

$$\rho_{\mathrm{E}} = \frac{1}{Z_{\mathrm{E}}}\exp\left[-\beta\mathsf{H}_{\mathrm{E}}\right] = \int \mathrm{d}p\mu(p)|p\rangle\langle p|. \tag{3.59}$$

For uncorrelated scattering events, the reduced dynamics of the Brownian particle is Markovian by definition, *i.e.* without the need to make any further assumptions on the interaction strength between particle and gas. Therefore, we can start out from Eq. (2.93) which, in momentum representation, $\langle P|\rho_t|P'\rangle = \rho_t(P,P')$, reads

$$\begin{aligned}\partial_t\rho_t(P,P') = &-\frac{i}{\hbar}\frac{P^2-(P')^2}{2M}\rho_t(P,P') + \int \mathrm{d}P_0\mathrm{d}P_0'\rho_t(P_0,P_0')M(P,P';P_0,P_0')\\ &-\frac{1}{2}\int \mathrm{d}P_0\rho(P_0,P')\int \mathrm{d}P_f M(P_f,P_f;P_0,P)\\ &-\frac{1}{2}\int \mathrm{d}P_0'\rho(P,P_0')\int \mathrm{d}P_f M(P_f,P_f;P',P_0'),\end{aligned} \tag{3.60}$$

with

$$M(P,P';P_0,P_0') = \langle P|\,\mathrm{Tr}_{\mathrm{E}}\left[\mathsf{T}\mathsf{G}^{1/2}(|P_0\rangle\langle P_0'|\otimes\rho_{\mathrm{E}})\mathsf{G}^{1/2}\mathsf{T}^\dagger\right]|P'\rangle. \tag{3.61}$$

Note that the second term on the right hand side of Eq. (2.93) vanishes for the diagonal state ρ_{E}, given by Eq. (3.59). Here and in the follwing we use the capital letters M and P to denote the mass and the momentum of the Brownian particle, while the small letters m and p denote the respective parameters of the gas particles.

Generally, a collision keeps the center of mass of the colliding particles invariant and only changes their relative coordinates. It is therefore convenient to express the scattering

matrix S in terms of the center of mass scattering matrix S_0 as [58]

$$\mathsf{S}|P\rangle|p\rangle = \int \mathrm{d}Q|P-Q\rangle|p+Q\rangle\langle\frac{m_*}{m}p - \frac{m_*}{M}P + Q|\mathsf{S}_0|\frac{m_*}{m}p - \frac{m_*}{M}P\rangle, \tag{3.62}$$

with the reduced mass $m_* = Mm/(M+m)$. While for a general Brownian particle one obtains the so-called quantum linear Boltzmann equation from Eq. (3.60) [59], we will here consider the much simpler limiting case where the Brownian particle is much heavier than the gas particles, $M \gg m$. This limit is called *collisional decoherence* since here Brownian and background gas particles do not exchange energy (no dissipation but only decoherence takes place). The scattering matrix S therefore reduces to

$$\mathsf{S}|P\rangle|p\rangle = \int \mathrm{d}Q|P-Q\rangle|p+Q\rangle\langle p+Q|\mathsf{S}_0|p\rangle, \quad \text{for} M \gg m. \tag{3.63}$$

The operator G, in turn, is given by the product of gas-particle-density n_{gas}, absolute relative velocity $|\mathsf{v}_{\mathrm{rel}}| = |\mathsf{p}/m - \mathsf{P}/M|$, and scattering cross section $\sigma(\mathsf{p}_{\mathrm{rel}})$, so that its expectation value is equal to the scattering rate. In the limit of collisional decoherence, G simplifies to

$$\mathsf{G} = n_{\mathrm{gas}}\frac{|\mathsf{p}|}{m}\sigma(\mathsf{p}). \tag{3.64}$$

With the environmental state ρ_{E}, the scattering matrix S, and the rate operator G given by Eqs. (3.59), (3.63), and (3.64), respectively, the complex function $M(P,P';P_0,P_0')$, Eq. (3.61), reads [19]

$$\begin{aligned} M(P,P';P-Q,P'-Q') &= \int \mathrm{d}p_0\mathrm{d}p_1\mu(p_0)\delta(Q+p_1-p_0)\delta(Q'-p_1+p_0) \\ &\quad \times \frac{n_{\mathrm{gas}}}{m}|p_0|\sigma(p_0)|\langle p_1|\mathsf{T}_0|p_0\rangle|^2 \\ &= \delta(Q-Q')\int \mathrm{d}p_0\mu(p_0)\frac{n_{\mathrm{gas}}}{m}|p_0|\sigma(p_0)|\langle p_0-Q|\mathsf{T}_0|p_0\rangle|^2 \\ &\equiv \delta(Q-Q')M_{\mathrm{in}}(Q). \end{aligned} \tag{3.65}$$

Substituting this back into the master equation (3.60), we see that collisions with background gas particles simply lead to momentum kicks of the Brownian particle,

$$\begin{aligned} \partial_t\rho_t(P,P') = -\frac{i}{\hbar}\frac{P^2-(P')^2}{2M}\rho_t(P,P') + \int \mathrm{d}Q\rho_t(P-Q,P'-Q)M_{\mathrm{in}}(Q) \\ -\rho_t(P,P')\int \mathrm{d}Q M_{\mathrm{in}}(Q). \end{aligned} \tag{3.66}$$

Equation (3.66) also shows that $M_{\mathrm{in}}(Q)$ quantifies the rate of collisions that lead to a change of momentum by Q, which can be written as the total collision rate γ times the probability for a momentum change by Q, $M_{\mathrm{in}}(Q) = \gamma G(Q)$ with $\int G(Q)\mathrm{d}Q = 1$. The momentum transfer distribution $G(Q)$ can be related to microscopic quantities of the

background gas [52]. In many realistic scenarios, it is well approximated by a Gaussian of fixed width. Finally, writing the master equation (3.66) in a more familiar fashion without reference to the momentum representation, we obtain

$$\begin{aligned}\partial_t \rho_t &= -\frac{i}{\hbar}\left[\frac{\mathsf{P}^2}{2M}, \rho_t\right] + \gamma \int G(Q) e^{iQ\mathsf{X}/\hbar} \rho_t e^{-iQ\mathsf{X}/\hbar} \mathrm{d}Q - \gamma \rho_t \\ &\equiv -\frac{i}{\hbar}\left[\frac{\mathsf{P}^2}{2M}, \rho_t\right] + \gamma \int \mathrm{d}Q \left(\mathsf{L}_Q \rho_t \mathsf{L}_Q^\dagger - \frac{1}{2}\mathsf{L}_Q^\dagger \mathsf{L}_Q \rho_t - \frac{1}{2}\rho_t \mathsf{L}_Q^\dagger \mathsf{L}_Q\right). \end{aligned} \tag{3.67}$$

Again, this collisional decoherence master equation describes the open quantum dynamics of a heavy particle that undergoes sequential, uncorrelated collisions with light background gas particles with rate γ.

Decoherence

As in the previous examples, we now discuss the phenomenon of decoherence in the collisional decoherence model, Eq. (3.67) (as mentioned above, collisional decoherence does not involve energy dissipation). Since the eigenstates of the jump operators L_Q are again the position eigenstates $|x\rangle$, the position basis will be the preferred basis of decoherence. In the position representation and in the interaction picture, Eq. (3.67) reads

$$\partial_t \tilde{\rho}_t(x, x') = \gamma \int \mathrm{d}Q G(Q)(e^{iQ(x-x')/\hbar} - 1)\tilde{\rho}_t(x, x'). \tag{3.68}$$

Equation (3.68) is solved by

$$\tilde{\rho}_t(x, x') = \exp\left[-\gamma\left(1 - \int \mathrm{d}Q G(Q) e^{iQ(x-x')/\hbar}\right)\right] \tilde{\rho}_0(x, x'). \tag{3.69}$$

This shows that, like in the Caldeira-Leggett model for Brownian motion, the off-diagonal terms in the position representation of the density matrix ρ_t decay so that the state tends towards a probabilistic mixture of spatially localized wave packets. Here, the time scale of spatial decoherence depends on the Fourier transform of the momentum transfer distribution $G(Q)$,

$$\tau_{\mathrm{dec}} = \frac{1}{\gamma[1 - \tilde{G}(x - x')]}. \tag{3.70}$$

If $G(Q)$ can be approximated with a normalized Gaussian of fixed width, the decoherence rate τ_{dec}^{-1} shows a quadratic behavior for small $x - x'$ and saturates at γ for large $x - x'$. One can say that the Fourier transform of the environmental momentum transfer distribution determines what differences in position the background gas is able to resolve [19]. While coherent superpositions of wave packets that are closer than this threshold remain unaffected, the background gas can distinguish perfectly those that are much farther apart and thus decoherence occurs on a time scale given by the collision rate γ. This saturation of the decoherence rate is relevant in interference experiments with large molecules [6, 60]. In contrast, the decoherence rate in the Caldeira-Leggett model,

Eq. (3.57), shows a simple quadratic behavior and therefore grows beyond all bounds for coherent superpositions of macroscopic size.

The pointer states of collisional decoherence are again those localized wave packets for which the dispersive effect of the free particle Hamiltonian and the localizing effect of decoherence are in equilibrium [53]. They are exponentially localized wave packets that move with a constant momentum, $\langle \mathsf{x} \rangle_t = \langle \mathsf{p} \rangle / m + x_0$, and have a fixed width σ [16, 53, 61],

$$\pi_t(x) = \exp\left[-\frac{1}{\sigma}\left|x - \langle \mathsf{x} \rangle_t\right|\right] \exp\left[\frac{i}{\hbar}\left(\langle \mathsf{p} \rangle + m\gamma a\sigma\right)\left|x - \langle \mathsf{x} \rangle_t\right|\right]. \tag{3.71}$$

The spatial extension can be approximated with $\sigma \approx a\hbar/\sigma_G + \sigma_G/4am\gamma$, where σ_G is the width of the momentum transfer distribution $G(Q)$ and the parameter a must be determined numerically.

3.3 Dynamics under Continuous, Nonselective Measurements

The above discussion of the collisional decoherence model suggests that decoherence depends on which open system states the environment can resolve via the system-environment interaction. In other words, in analogy to a measurement apparatus in contact with a quantum system and the mixing induced by the extraction of information, we can interpret the increasing statistical uncertainty about the state of an open system as due to a continuous monitoring by the environment, see Secs. 2.1.3 and 4.2.2. Being hence a paradigm for the description of open quantum systems, we will now consider the generic measurement situation and discuss the resulting dynamics of the measured system.

As we saw in Sec. 2.1.3, a general quantum measurement is formulated in terms of measurement operators $\mathsf{M}_{a,i}$ which act on the measured quantum system. When outcome a is obtained, the system state ρ is transformed with

$$\mathcal{M}(\rho|a) = \frac{1}{\mathrm{Tr}\left[\mathsf{F}_a \rho\right]} \sum_i \mathsf{M}_{a,i} \rho \mathsf{M}_{a,i}^\dagger, \tag{3.72}$$

where $\mathsf{F}_a = \sum_i \mathsf{M}_{a,i}^\dagger \mathsf{M}_{a,i}$. The expectation value $\mathrm{Tr}\left[\mathsf{F}_a \rho\right] \geq 0$ is the probability $\mathrm{Prob}(a)$ for outcome a to be detected. The F_a must therefore fulfill the consistency condition $\sum_a \mathsf{F}_a = \mathbb{1}$.

Equation (3.72) states that a measurement leads to an abrupt state transformation that is conditioned on the measurement outcome. In case of our ignorance of the obtained outcome a, we must average over all possible transformations $\mathcal{M}(\rho|a)$ so that the post-measurement state is independent of a,

$$\rho' = \sum_a \mathrm{Prob}(a) \mathcal{M}(\rho|a) = \sum_{a,i} \mathsf{M}_{a,i} \rho \mathsf{M}_{a,i}. \tag{3.73}$$

By definition, this so-called nonselective measurement scenario fulfills the main property of a Markovian system transformation, namely that of being memoryless, see Sec. 2.2.

To study the dynamics of the measured system and not only a single instantaneous measurement transformation, we furthermore assume that the measurement is performed continuously in time. The simplest way to measure continuously and in a memoryless fashion is to apply the nonselective measurement, Eq. (3.73), probabilistically with a constant rate γ. The continuous nonselective measurement is hence described by a homogeneous Poisson process with rate γ and the probability for performing a measurement within an infinitesimal time interval $\mathrm{d}t$ is $\gamma \mathrm{d}t$. The associated infinitesimal time evolution of ρ_t reads

$$\tilde{\rho}_{t+\mathrm{d}t} = \gamma \mathrm{d}t \sum_{a,i} \widetilde{\mathsf{M}}_{a,i} \tilde{\rho}_t \widetilde{\mathsf{M}}_{a,i}^\dagger + (1 - \gamma \mathrm{d}t) \tilde{\rho}_t. \tag{3.74}$$

We use the Heisenberg picture, $\widetilde{\mathsf{A}} = e^{i\mathsf{H}t/\hbar} \mathsf{A} e^{-i\mathsf{H}t/\hbar}$, indicated by the tilde, to account for the continuous coherent dynamics of ρ_t between the measurements. Solving Eq. (3.74) for the difference quotient $(\tilde{\rho}_{t+\mathrm{d}t} - \tilde{\rho}_t)/\mathrm{d}t$, and taking the limit $\mathrm{d}t \to 0$ leads to

$$\partial_t \tilde{\rho}_t = \gamma \left(\sum_{a,i} \widetilde{\mathsf{M}}_{a,i} \tilde{\rho}_t \widetilde{\mathsf{M}}_{a,i}^\dagger - \tilde{\rho}_t \right). \tag{3.75}$$

After transforming Heisenberg picture operators back to the Schrödinger picture, we obtain the evolution equation

$$\partial_t \rho_t = -\frac{i}{\hbar} [\mathsf{H}, \rho_t] + \gamma \left(\sum_{\alpha,i} \mathsf{M}_{a,i} \rho_t \mathsf{M}_{a,i}^\dagger - \rho_t \right). \tag{3.76}$$

Taking into account the consistency condition $\sum_a \mathsf{F}_a = \sum_{a,i} \mathsf{M}_{a,i}^\dagger \mathsf{M}_{a,i} = \mathbb{1}$, we see that Eq. (3.76) constitutes a Markovian master equation in standard form (2.66) with jump operators proportional to the measurement operators, $\mathsf{L}_{a,i} = \sqrt{\gamma} \mathsf{M}_{a,i}$. In contrast to the previous examples, the Markov property is here fulfilled by definition, *i.e.* without any approximations about the nature of the system-environment coupling.

Let us make a few remarks concerning dissipation and decoherence in a general measurement setup. First, in contrast to the previously considered open systems, the measured system is not in contact with a thermal bath. Therefore, the exchange of energy between system and measurement apparatus, which occurs if the operators $\mathsf{M}_{a,i}$ do not commute with H, is somewhat different from the aforementioned dissipation in its thermodynamic sense. Second, a measurement setup is generally intended to provide information about a physical system quantity, associated with an observable A. In this case, ideally the measurement operators are diagonal in the eigenbasis of A, see the specific example in the following section. The measurement operators can then distinguish between different eigenstates of A and successive measurements yield the same outcome if they are applied without time delay. In that case, decoherence obviously occurs in the

eigenbasis of A and the pointer states[3] are the eigenstates of A.

3.3.1 Indirect Measurement Setup in Cavity QED

To fill the above, completely general measurement concept with life, let us now consider a specific cavity QED setup which can be used to implement the described Markovian dynamics under nonselective measurements. It consists of a microwave cavity and a two-level atom, which is sent through the cavity to probe the state of its electromagnetic field mode. This setup was used to demonstrate the fundamental mechanism of decoherence [5], to implement a quantum non-demolition measurement [62], and to execute quantum feedback loops [63, 64]. It is a prototype of the indirect measurement scheme derived in Sec. 2.1.3.

To specify the implemented indirect measurement, let us assume that the cavity is initially in a coherent superposition of Fock states $|\psi\rangle = \sum_n c_n|n\rangle$. The probe atoms are prepared in a superposition of ground and excited state, $|+\rangle = (|0\rangle + |1\rangle)/\sqrt{2}$ (the second, orthogonal single atom basis state is $|-\rangle = (|0\rangle - |1\rangle)/\sqrt{2}$). The joint initial state of cavity and probe thus reads

$$\left|\psi_0^{\text{tot}}\right\rangle = \left[\sum_n c_n|n\rangle\right] \otimes |+\rangle. \tag{3.77}$$

By sending an atom through the cavity, it acquires an n-dependent phase through its interaction with the cavity field,

$$|\psi_t^{\text{tot}}\rangle = \sum_n \left[c_n|n\rangle \otimes \exp\left(-\frac{i}{\hbar} n\kappa t \sigma_z\right)|+\rangle\right]. \tag{3.78}$$

Here κ denotes the coupling constant between atom and field and σ_z the third Pauli matrix. The interaction time t can be tuned by adjusting the velocity of the atoms to map a total number of d Fock states onto the full unit circle,

$$|\psi_\tau^{\text{tot}}\rangle = \sum_n [c_n|n\rangle \otimes |+_n\rangle], \tag{3.79}$$

$$|\pm_n\rangle \equiv \exp\left(\frac{i\pi}{2}\frac{n}{d}\sigma_z\right)|\pm\rangle. \tag{3.80}$$

After the atom has left the cavity, it can be subjected to a projective measurement in any of the atomic bases $\{|+_k\rangle, |-_k\rangle\}$ labeled by k, which acts as the identity on the cavity degrees of freedom. For a specific k, the joint atom-cavity projectors read $|\pm_k\rangle\langle\pm_k| \otimes \mathbb{1}$, with $\mathbb{1} = \sum_n |n\rangle\langle n|$. Eliminating the atomic degrees of freedom, a projection of the

[3] As a side remark: the term "pointer state" originated from its interpretation in the measurement situation. The pointer states are those states in which the macroscopic pointer of the measurement apparatus probabilistically ends up.

state (3.79) hence implements the measurement operators

$$\mathsf{M}_{\pm,k} = \sum_n \langle \pm_k | +_n \rangle |n\rangle\langle n| \tag{3.81}$$

for the cavity field. The post-measurement cavity state after detecting the outcome $\pm$ in the atomic basis k is therefore given by

$$\mathcal{M}(\pm,k||\psi\rangle\langle\psi|) = \frac{\mathsf{M}_{\pm,k}|\psi\rangle\langle\psi|\mathsf{M}_{\pm,k}^\dagger}{\langle\psi|\mathsf{M}_{\pm,k}^\dagger\mathsf{M}_{\pm,k}|\psi\rangle} = \frac{\sum_{nm} c_n c_m^* \langle\pm_k|+_n\rangle|n\rangle\langle m|\langle +_m|\pm_k\rangle}{\sum_n |\langle\pm_k|+_n\rangle|^2|c_n|^2} = |\psi_{\pm,k}\rangle\langle\psi_{\pm,k}| \tag{3.82}$$

$$\text{with } |\psi_{\pm,k}\rangle = \sum_n \frac{c_n\langle\pm_k|+_n\rangle}{\sqrt{\sum_n |\langle\pm_k|+_n\rangle|^2|c_n|^2}}|n\rangle = \sum_n c'_n|n\rangle. \tag{3.83}$$

This shows that the coefficients in the coherent superposition $|\psi\rangle = \sum c_n|n\rangle$ are enhanced or suppressed in $|\psi_{\pm,k}\rangle$, depending on their overlap with the measured basis state $|\pm_k\rangle$,

$$|c'_n|^2 = \frac{|\langle\pm_k|+_n\rangle|^2}{\mathrm{Prob}(\pm,k)}|c_n|^2 = \frac{\cos^2\left[\frac{\pi}{2}\left(\frac{n-k}{d}\right) - \frac{\pi}{4} \pm \frac{\pi}{4}\right]}{\mathrm{Prob}(\pm,k)}|c_n|^2. \tag{3.84}$$

For example, if we detect $(+,k)$, the $(k+d)$-th coefficient is maximally suppressed, $c'_{k+d} = 0$, while the k-th coefficient is maximally enhanced, $c'_k = c_k/\sqrt{\mathrm{Prob}(+,k)}$. If one repeats such measurements while changing the measurement basis k, one may probabilistically enhance one of the coefficients approximately to unity so that all other coefficients vanish. In other words, this setup allows one to successively pin down the Fock state $|n\rangle$ inside the cavity[4].

Measurements with Feedback

A quantum measurement not only allows one to extract information about the measured system; it can also be used to manipulate the system state by applying system transformations depending on the previous measurement outcomes. Formally, one way to apply such a *feedback operation* is by including an additional unitary part in the measurement operators,

$$\mathsf{M}^{\mathrm{fb}}_{a,i} = \mathsf{U}_a\mathsf{M}_{a,i}. \tag{3.85}$$

This leaves the detection probabilities unchanged,

$$\mathrm{Tr}\left[\left(\sum_i \left(\mathsf{M}^{\mathrm{fb}}_{a,i}\right)^\dagger \mathsf{M}^{\mathrm{fb}}_{a,i}\right)\rho\right] = \mathrm{Tr}\left[\left(\sum_i \mathsf{M}^\dagger_{a,i}\underbrace{\mathsf{U}_a^{-1}\mathsf{U}_a}_{\mathbb{1}}\mathsf{M}_{a,i}\right)\rho\right] = \mathrm{Tr}\left[\mathsf{F}_a\rho\right] = \mathrm{Prob}(a), \tag{3.86}$$

[4]To be precise, for $n \geq d$ one determines the number $n \bmod d$ since $\mathsf{M}_{\pm,k}$ has the same effect on $|n\rangle$ as on $|n+d\rangle$.

and a system under a nonselective measurement with feedback still exhibits Markovian dynamics, Eq. (3.76), with jump operators $\mathsf{M}^{\mathrm{fb}}_{a,i}$ instead of $\mathsf{M}_{a,i}$. Without going into further details on feedback control theory here [54], we just shortly mention two possible feedback loops for the present system.

In the present setup one can, for example, inject a classical microwave pulse into the cavity, effectively a displacement $\mathsf{D}(\alpha)$ of the cavity field, see Eq. (3.13), that minimizes the distance between the conditional post-measurement state $|\psi_{\pm,k}\rangle$, Eq. (3.83), and a desired Fock state $|n\rangle$. It was shown that this allows stabilizing the cavity in state $|n\rangle$ after a certain number of iterations, irrespective of the initial state [63]. This stabilization can also be achieved with a somewhat simpler feedback operation which can be described by the creation operator $\mathsf{a}^\dagger$. In reality, the operation $\mathsf{a}^\dagger$ could be implemented by injecting an excited state atom in resonance with the cavity mode which deposits its quantum with unit probability. Specifically, assume we apply $\mathsf{a}^\dagger$ only when the outcome $(+,0)$ is detected,

$$\mathsf{M}^{\mathrm{fb}}_{+,0} = \mathsf{a}^\dagger \mathsf{M}_{+,0}, \tag{3.87}$$

while all other measurement operators are left unchanged. The probability to detect $+$ in the atomic basis $k=0$, given a general cavity state $|\psi\rangle = \sum_n c_n |n\rangle$, is

$$\mathrm{Prob}(+,0) = \sum_n |\langle \pm_0 +_n \rangle|^2 |c_n|^2 = \sum_n \cos^2\left[\frac{\pi}{2}\frac{n}{d}\right] |c_n|^2. \tag{3.88}$$

We see that $\mathrm{Prob}(+,0)$ vanishes if $|\psi\rangle = |d\rangle$. Therefore, once the cavity falls into the state $|d\rangle$, no more feedback operation is applied so that the cavity state remains unchanged. This will be confirmed numerically in Chap. 6.

4 The Jump Expansion

The idea to expand complex physical quantities into an asymptotic sum over simpler, more accessible terms has a long history in theoretical physics. Understanding the expansion term by term allows one to develop an intuition for the expanded quantity and, if the series is convergent, facilitates its quantitative approximation. For example, expansions of a periodic function into a series of harmonics helped the French mathematician Joseph Fourier to understand the propagation of heat in solids in 1822 [65]. In 1860 Charles Delaunay applied Brook Taylor's power series expansion from 1715 [66] to study the movement of the moon as part of the three-body problem and found evidence for chaotic dynamics [67].

In the present chapter we will show how to find an expansion for the open quantum dynamics ρ_t under an arbitrary Markovian master equation (2.66) [17–19]. The approach is guided by the derivation of the Dyson series for closed systems [68]. Just like the Dyson series, the so-called *jump expansion* for open systems features a decomposition of the entire dynamics into periods of continuous, unperturbed evolution and instantaneous perturbations, or jumps. As opposed to the Dyson series, however, the jump expansion is intrinsically nonperturbative which has the drawback that it is not guaranteed to converge. We will therefore ensure its convergence in a second step, by performing a resummation of the jump expansion in an optimal, adaptive fashion [20, 21].

We start by presenting a derivation of the Dyson series [68] and then extend this formalism to Markovian open systems to obtain the jump expansion. Subsequently, we perform a resummation to optimize its convergence. For practical purposes, especially to obtain analytically tractable terms, we also derive suboptimal resummations that greatly simplify the optimally convergent form of the jump expansion.

4.1 Derivation

4.1.1 The Dyson Series for Closed Systems

The evolution of any closed quantum system with the initial state $|\psi_0\rangle$ is governed by the system Hamiltonian H_0 through the time-dependent Schrödinger equation,

$$\partial_t|\psi_t\rangle = -\frac{i}{\hbar}\mathsf{H}_0(t)|\psi_t\rangle. \tag{4.1}$$

Here we assume a general time-dependent Hamiltonian, as this will become relevant in the following. Formally, solutions of this differential equation can be expressed with the

help of the time evolution operator U_0 as

$$|\psi_t\rangle = \mathsf{U}_0(t,0)|\psi_0\rangle, \tag{4.2}$$

$$\mathsf{U}_0(t,0) = \mathcal{T}\exp\left(-\frac{i}{\hbar}\int_0^t \mathsf{H}_0(t')\mathrm{d}t'\right). \tag{4.3}$$

By inserting the operator U_0 into the Schrödinger equation, it can be recast as

$$\partial_t \mathsf{U}_0(t,0) = -\frac{i}{\hbar}\mathsf{H}_0(t)\mathsf{U}_0(t,0). \tag{4.4}$$

In Eq. (4.3), $\mathcal{T}$ is the time ordering operator which ensures that in each term of the formal expansion $\exp[-i/\hbar\int \mathsf{H}_0(t')\mathrm{d}t'] = \sum_n[-i/\hbar\int \mathsf{H}_0(t')\mathrm{d}t']^n/n!$, the time arguments of the Hamiltonian are in decreasing order. This is necessary for Eq. (4.4) to hold true even in the case that $[\mathsf{H}_0(t), \mathsf{H}_0(t')] \neq 0$ for $t \neq t'$. If a small perturbation $\varepsilon\mathsf{V}$, with $\varepsilon \ll 1$, is added to this problem,

$$\mathsf{H} = \mathsf{H}_0(t) + \varepsilon\mathsf{V}, \tag{4.5}$$

the time evolution of the perturbed system can be expanded in terms of the unperturbed Hamiltonian and the perturbation in the so-called Dyson series. This is achieved by switching to the interaction picture via the transformation $|\widetilde{\psi}_t\rangle = \mathsf{U}_0^\dagger(t,0)|\psi_t\rangle$, so that the Schrödinger equation takes the form

$$\partial_t|\widetilde{\psi}_t\rangle = \partial_t\left[\mathsf{U}_0^\dagger(t,0)|\psi_t\rangle\right] = \frac{i}{\hbar}\left[\mathsf{U}_0^\dagger(0,t)\mathsf{H}_0(t) - \mathsf{U}_0^\dagger(0,t)(\mathsf{H}_0(t)+\varepsilon\mathsf{V})\right]|\psi_t\rangle = -\frac{i}{\hbar}\varepsilon\widetilde{\mathsf{V}}(t)|\widetilde{\psi}_t\rangle, \tag{4.6}$$

with $\widetilde{\mathsf{V}}(t) = \mathsf{U}_0^\dagger(t,0)\mathsf{V}\mathsf{U}_0(t,0)$. The time evolution operator in the interaction picture $\widetilde{\mathsf{U}}(t,0)$ therefore satisfies the differential equation

$$\partial_t\widetilde{\mathsf{U}}(t,0) = -\frac{i}{\hbar}\varepsilon\widetilde{\mathsf{V}}(t)\widetilde{\mathsf{U}}(t,0), \tag{4.7}$$

which can be formally recast as an integral equation,

$$\widetilde{\mathsf{U}}(t,0) = \mathbb{1} - \frac{i}{\hbar}\varepsilon\int_0^t \widetilde{\mathsf{V}}(t')\widetilde{\mathsf{U}}(t',0)\mathrm{d}t'. \tag{4.8}$$

Here, we have used that $\widetilde{\mathsf{U}}$ satisfies $\widetilde{\mathsf{U}}(t,t) = \mathbb{1}$. Upon iterative reinsertion of $\widetilde{\mathsf{U}}$ on the right hand side, we obtain the Dyson series,

$$\widetilde{\mathsf{U}}(t,0) = \mathbb{1} - \frac{i\varepsilon}{\hbar}\int_0^t \mathrm{d}t_1\widetilde{\mathsf{V}}(t_1) - \frac{\varepsilon^2}{\hbar^2}\int_0^t \mathrm{d}t_2\int_0^{t_2}\mathrm{d}t_1\widetilde{\mathsf{V}}(t_2)\widetilde{\mathsf{V}}(t_1) + \ldots, \tag{4.9}$$

which converges for sufficiently small parameters ε and bounded operators $\widetilde{\mathsf{V}}(t)$. In the Schrödinger picture it reads

$$\begin{aligned}\mathsf{U}(t,0) = \mathsf{U}_0(t,0) - \frac{i\varepsilon}{\hbar}\int_0^t \mathrm{d}t_1 \mathsf{U}_0(t,t_1)\mathsf{V}\mathsf{U}_0(t_1,0) \\ -\frac{\varepsilon^2}{\hbar^2}\int_0^t \mathrm{d}t_2 \int_0^{t_2} \mathrm{d}t_1 \mathsf{U}_0(t,t_2)\mathsf{V}\mathsf{U}_0(t_2,t_1)\mathsf{V}\mathsf{U}_0(t_1,0)\ldots\end{aligned} \tag{4.10}$$

We see that the time evolution of the perturbed system can be seen as a series of intervals of unperturbed evolution, interspersed with applications of the small perturbation $\varepsilon\mathsf{V}$.

4.1.2 Decomposing the Dynamical Generator of Open Systems

In Sec. 2.2.4 of the previous chapter we saw that the dynamics of a Markovian open quantum system is governed by a master equation (2.66) in Lindblad form. It naturally incorporates the Schrödinger equation (4.1) as a limiting case, but it also gives rise to incoherent dynamics featuring new phenomena such as fixed points. Whereas the Schrödinger equation is an evolution equation for state vectors $|\psi\rangle$ belonging to the Hilbert space $\mathcal{H}$, the master equation governs the evolution of density matrices ρ, *i.e.* operators belonging to the associated Liouville space. In spite of these differences, Eqs. (2.66) and (4.1) are formally equivalent in the sense that the change of the state at time t is proportional both to a time-local generator and the state itself. This suggests that the same formalism of Sec. 4.1.1, which resulted in an expansion for the time evolution under the Schrödinger equation, may give rise to an expansion for the dynamics of Markovian open systems as well.

Analogously to Eq. (4.5), we consider a decomposition of the generator $\mathcal{L}(t)$ of the master equation $\partial_t\rho_t = \mathcal{L}(t)\rho_t$ into a sum of two parts

$$\mathcal{L}(t) = \mathcal{L}_\mu(t) + \mathcal{J}_\mu(t). \tag{4.11}$$

At this point, the decomposition is arbitrary and the index μ simply labels the different conceivable choices for the two summands. $\mathcal{L}(t)$ generates the semigroup of propagators

$$\mathcal{U}(t,t_0) = \mathcal{T}\exp\left(\int_{t_0}^t \mathcal{L}(t')\mathrm{d}t'\right), \tag{4.12}$$

which map the initial state ρ_{t_0} to the state ρ_t at later times, $\rho_t = \mathcal{U}(t,t_0)\rho_{t_0}$. Proceeding in the same way as for the Dyson series, we will derive an expansion for $\mathcal{U}(t,0)$, where we use the initial time $t_0 = 0$ for brevity. First, we note that, by definition, the differential equation for the propagator is

$$\partial_t\mathcal{U}(t,0) = \mathcal{L}(t)\mathcal{U}(t,0) = \mathcal{L}_\mu(t)\mathcal{U}(t,0) + \mathcal{J}_\mu(t)\mathcal{U}(t,0), \tag{4.13}$$

where we have already made use of the decomposition (4.11).

Due to the irreversible character of incoherent dynamics, propagators $\mathcal{U}(t,0)$ are in

general not invertible. It is therefore impossible to switch to an "interaction picture" and back as one does for closed systems, see Eq. (4.6). Nevertheless, avoiding the detour via the interaction picture, we can rewrite Eq. (4.13) *directly* in integral form as

$$\mathcal{U}(t,0) = \mathcal{U}_\mu(t,0) + \int_0^t \mathcal{U}_\mu(t,t')\mathcal{J}_\mu(t')\mathcal{U}(t',0)\mathrm{d}t'. \tag{4.14}$$

Here $\mathcal{U}_\mu(t,t_0)$ is defined analogous to $\mathcal{U}(t,t_0)$, Eq. (4.12), $\mathcal{U}_\mu(t,t_0) = \mathcal{T}\exp(\int_{t_0}^t \mathcal{L}_\mu(t')\mathrm{d}t')$. The equivalence of Eqs. (4.13) and (4.14) can be checked by taking the time derivative of Eq. (4.14),

$$\begin{aligned}\partial_t\mathcal{U}(t,0) &= \partial_t\mathcal{U}_\mu(t,0) + \int_0^t \left(\partial_t\mathcal{U}_\mu(t,t')\right)\mathcal{J}_\mu(t')\mathcal{U}(t',0)\mathrm{d}t' + [\mathcal{U}_\mu(t,t')\mathcal{J}_\mu(t')\mathcal{U}(t',0)]_{t'=t} \\ &= \mathcal{L}_\mu(t)\mathcal{U}_\mu(t,0) + \mathcal{L}_\mu(t)\int_0^t \mathcal{U}_\mu(t,t')\mathcal{J}_\mu(t')\mathcal{U}(t',0)\mathrm{d}t' + \mathcal{J}_\mu(t)\mathcal{U}(t,0) \\ &= \mathcal{L}_\mu(t)\mathcal{U}(t,0) + \mathcal{J}_\mu(t)\mathcal{U}(t,0).\end{aligned} \tag{4.15}$$

In the second line we used that $\mathcal{U}_\mu(t,t) = \mathrm{id}$ and then substituted Eq. (4.14) for $\mathcal{U}(t,0)$ to obtain the third line.

We can now solve Eq. (4.14) iteratively,

$$\begin{aligned}\mathcal{U}(t,0) = \mathcal{U}_\mu(t,0) &+ \int_0^t \mathrm{d}t_1\mathcal{U}_\mu(t,t_1)\mathcal{J}_\mu(t_1)\mathcal{U}_\mu(t_1,0) \\ &+ \int_0^t \mathrm{d}t_2\int_0^{t_2} \mathrm{d}t_1\mathcal{U}_\mu(t,t_2)\mathcal{J}_\mu(t_2)\mathcal{U}_\mu(t_2,t_1)\mathcal{J}_\mu(t_1)\mathcal{U}_\mu(t_1,0) + \ldots\end{aligned} \tag{4.16}$$

By letting this expanded form of the propagator act on the initial state ρ_0, we obtain the jump expansion for the solution of the master equation $\partial_t\rho_t = \mathcal{L}(t)\rho_t$,

$$\rho_t = \sum_{n=0}^{\infty}\rho_t^{(n)}, \text{ with} \tag{4.17}$$

$$\rho_t^{(n)} = \int_0^t \mathcal{U}_\mu(t,t')\mathcal{J}_\mu(t')\rho_{t'}^{(n-1)}\mathrm{d}t', \tag{4.18}$$

and $\rho_t^{(0)} = \mathcal{U}_\mu(t,0)\rho_0$. More explicitly, this expansion reads

$$\rho_t = \sum_{n=0}^{\infty}\int_0^t \mathrm{d}t_n\int_0^{t_n}\mathrm{d}t_{n-1}\ldots\int_0^{t_2}\mathrm{d}t_1\mathcal{U}_\mu(t,t_n)\mathcal{J}_\mu(t_n)\mathcal{U}_\mu(t_n,t_{n-1})\mathcal{J}_\mu(t_{n-1})\ldots\mathcal{J}_\mu(t_1)\mathcal{U}_\mu(t_1,0)\rho_0. \tag{4.19}$$

In analogy to the usual Dyson series for unitary propagators, the full time evolution $\mathcal{U}(t,0)$ can be seen as comprising intervals of unperturbed evolutions under $\mathcal{U}_\mu$, interspersed with perturbations, or jumps $\mathcal{J}_\mu$. The jumps $\mathcal{J}_\mu$, in turn, are distributed over the entire propagation interval as indicated by the integral from 0 to t. The series

$\rho_t = \sum_n \rho_t^{(n)}$, Eq. (4.19), is ordered according to the number of jump super operators $\mathcal{J}_\mu$ involved and we will call the constituent terms $\rho_t^{(n)}$ *jump terms* in the following. The main difference of the jump expansion with respect to the Dyson series is the absence of a small parameter. Its convergence properties are therefore at best dubious, rendering the formal expansion (4.19) of little practical use. In spite of this missing small parameter, we will see that convergence can be ensured in a different way, namely by choosing optimal decompositions μ in Eq. (4.11).

4.1.3 Freedom in the $\mathcal{L}$-Decomposition

For the purpose of optimizing the convergence of the jump expansion (4.19), it is sensible to restrict our attention to a physically meaningful subset of all arbitrary decompositions (4.11) and then perform the optimization within this subset. To parametrize this physically meaningful subset, note that the master equation (2.66) is invariant under the transformation

$$\mathsf{L}_j(t) \to \mathsf{L}_{j,\boldsymbol{\alpha}(t)}(t) \equiv \mathsf{L}_j(t) + \alpha_j(t), \tag{4.20}$$

$$\mathsf{H}(t) \to \mathsf{H}_{\boldsymbol{\alpha}(t)}(t) \equiv \mathsf{H}(t) + \frac{\hbar}{2i}\sum_{j=1}^{N}(\alpha_j^*(t)\mathsf{L}_j(t) - \alpha_j(t)\mathsf{L}_j^\dagger(t)), \tag{4.21}$$

where $\boldsymbol{\alpha}(t) = (\alpha_1(t), \ldots, \alpha_N(t)) \in \mathbb{C}^N$ is a complex vector. For brevity, we will mostly omit the t argument of $\boldsymbol{\alpha}$ since the operators that involve $\boldsymbol{\alpha}$ are explicitly time-dependent in any case. To check the invariance of the master equation arithmetically, one substitutes $\mathsf{H}_{\boldsymbol{\alpha}}$ and $\mathsf{L}_{j,\boldsymbol{\alpha}}$ into the Eq. (2.66) and simplifies the obtained expression. We omit this somewhat lengthy calculation, since it is not particularly illuminating. As will be explained below, a physically meaningful decomposition of the generator in terms of the operators $\mathsf{H}_{\boldsymbol{\alpha}}(t)$ and $\mathsf{L}_{j,\boldsymbol{\alpha}}(t)$ is given by $\mathcal{L}(t) = \mathcal{L}_{\boldsymbol{\alpha}}(t) + \mathcal{J}_{\boldsymbol{\alpha}}(t)$, with

$$\mathcal{J}_{\boldsymbol{\alpha}}(t)\rho = \sum_{j=1}^{N}\mathsf{L}_{j,\boldsymbol{\alpha}}(t)\rho\mathsf{L}_{j,\boldsymbol{\alpha}}^\dagger(t) \equiv \sum_{j=1}^{N}\mathcal{J}_{j,\boldsymbol{\alpha}}(t)\rho, \tag{4.22}$$

$$\mathcal{L}_{\boldsymbol{\alpha}}(t)\rho = -\frac{i}{\hbar}\left(\mathsf{H}_{\boldsymbol{\alpha}}^{\text{eff}}(t)\rho - \rho\mathsf{H}_{\boldsymbol{\alpha}}^{\text{eff}\dagger}(t)\right). \tag{4.23}$$

Here, $\mathsf{H}_{\boldsymbol{\alpha}}^{\text{eff}}(t)$ is an effective, non-Hermitian Hamiltonian,

$$\mathsf{H}_{\boldsymbol{\alpha}}^{\text{eff}}(t) = \mathsf{H}_{\boldsymbol{\alpha}}(t) - \frac{i\hbar}{2}\sum_j \mathsf{L}_{j,\boldsymbol{\alpha}}^\dagger(t)\mathsf{L}_{j,\boldsymbol{\alpha}}(t), \tag{4.24}$$

with a negative imaginary part. In addition, we have decomposed the jumps $\mathcal{J}_{\boldsymbol{\alpha}}$ into "different kinds" of jumps $\mathcal{J}_{j,\boldsymbol{\alpha}}$, each corresponding to one jump operator $\mathsf{L}_{j,\boldsymbol{\alpha}}$. This will allow us to further break down the jump expansion into more elementary parts as we proceed.

For a decomposition of $\mathcal{L}$ into $\mathcal{J}_{j,\boldsymbol{\alpha}}$, Eq. (4.22), and $\mathcal{L}_{\boldsymbol{\alpha}}$, Eq. (4.23), all transformations

in the corresponding jump expansion—*i.e.* the jumps $\mathcal{J}_{j,\boldsymbol{\alpha}}$ and the unperturbed evolution $\mathcal{U}_{\boldsymbol{\alpha}}$ generated by $\mathcal{L}_{\boldsymbol{\alpha}}$—are completely positive, norm decreasing maps and, hence, take physical states ρ to other physically allowed density matrices. This can be seen by comparing $\mathcal{J}_{j,\boldsymbol{\alpha}}$ and $\mathcal{U}_{\boldsymbol{\alpha}}$ to the Kraus decomposition (2.48). The Kraus-map structure of $\mathcal{J}_{j,\boldsymbol{\alpha}}$ is manifest in its definition (4.22), and $\mathcal{U}_{\boldsymbol{\alpha}}$ can be cast into the Kraus-map form,

$$\mathcal{U}_{\boldsymbol{\alpha}}(t,t_0)\rho = \left[\mathcal{T}\exp\left(-\frac{i}{\hbar}\int_{t_0}^{t}\mathsf{H}_{\boldsymbol{\alpha}}^{\mathrm{eff}}(t')\mathrm{d}t'\right)\right]\rho\left[\mathcal{T}\exp\left(\frac{i}{\hbar}\int_{t_0}^{t}\mathsf{H}_{\boldsymbol{\alpha}}^{\mathrm{eff}\dagger}(t')\mathrm{d}t'\right)\right], \tag{4.25}$$

by analogy of the continuous generator $\mathcal{L}_{\boldsymbol{\alpha}}(t)$, Eq. (4.23), to the Liouville-von Neumann equation (2.42) and its respective solutions (2.44). The completely positive, norm decreasing property of $\mathcal{J}_{j,\boldsymbol{\alpha}}$ and $\mathcal{U}_{\boldsymbol{\alpha}}$ implies that all terms $\rho_t^{(n)}$ of the jump expansion $\rho_t = \sum_n \rho_t^{(n)}$ are valid, *i.e.* positive, density matrices with trace $\mathrm{Tr}\,\rho_t^{(n)} \leq 1$. By substituting Eqs. (4.22) and (4.25) into Eq. (4.19), the jump terms take the form

$$\begin{aligned}\rho_t^{(n)} &= \int_0^t \mathrm{d}t_n \int_0^{t_n}\mathrm{d}t_{n-1}\ldots\int_0^{t_2}\mathrm{d}t_1 \mathcal{U}_{\boldsymbol{\alpha}}(t,t_n)\mathcal{J}_{\boldsymbol{\alpha}}(t_n)\mathcal{U}_{\boldsymbol{\alpha}}(t_n,t_{n-1})\mathcal{J}_{\boldsymbol{\alpha}}(t_{n-1})\ldots\mathcal{J}_{\boldsymbol{\alpha}}(t_1)\mathcal{U}_{\boldsymbol{\alpha}}(t_1,0)\rho_0 \\ &= \sum_{j_1\ldots j_n=1}^{N}\int_0^t \mathrm{d}t_n \int_0^{t_n}\mathrm{d}t_{n-1}\ldots\int_0^{t_2}\mathrm{d}t_1 \mathcal{U}_{\boldsymbol{\alpha}}(t,t_n)\mathcal{J}_{j_n,\boldsymbol{\alpha}}(t_n)\mathcal{U}_{\boldsymbol{\alpha}}(t_n,t_{n-1})\mathcal{J}_{j_{n-1},\boldsymbol{\alpha}}(t_{n-1})\ldots \\ &\quad\times\mathcal{J}_{j_1,\boldsymbol{\alpha}}(t_1)\mathcal{U}_{\boldsymbol{\alpha}}(t_1,0)\rho_0.\end{aligned} \tag{4.26}$$

Note that we have dropped the time-ordering operator for brevity here. Substituting the superoperators $\mathcal{J}_{j,\boldsymbol{\alpha}}$ and $\mathcal{U}_{\boldsymbol{\alpha}}$ with the corresponding expressions in terms of the jump operators and the effective Hamiltonian, Eqs. (4.22) and (4.25), we obtain

$$\begin{aligned}\rho_t^{(n)} = \sum_{j_1\ldots j_n=1}^{N}\int_0^t \mathrm{d}t_n \int_0^{t_n}\mathrm{d}t_{n-1}\ldots\int_0^{t_2}\mathrm{d}t_1 e^{-i/\hbar\int_{t_n}^{t}\mathsf{H}_{\boldsymbol{\alpha}}^{\mathrm{eff}}(t')\mathrm{d}t'}\mathsf{L}_{j_n,\boldsymbol{\alpha}}(t_n)\ldots\mathsf{L}_{j_1,\boldsymbol{\alpha}}(t_1) \\ \times e^{-i/\hbar\int_0^{t_1}\mathsf{H}_{\boldsymbol{\alpha}}^{\mathrm{eff}}(t')\mathrm{d}t'}\rho_0 e^{i/\hbar\int_0^{t_1}\mathsf{H}_{\boldsymbol{\alpha}}^{\mathrm{eff}\dagger}(t')\mathrm{d}t'}\mathsf{L}_{j_1,\boldsymbol{\alpha}}^{\dagger}(t_1)\ldots\mathsf{L}_{j_n,\boldsymbol{\alpha}}^{\dagger}(t_n)e^{i/\hbar\int_{t_n}^{t}\mathsf{H}_{\boldsymbol{\alpha}}^{\mathrm{eff}\dagger}(t')\mathrm{d}t'}.\end{aligned} \tag{4.27}$$

Inspecting Eqs. (4.20)–(4.24), we see that the complex vectors $\boldsymbol{\alpha}$ parametrize those $\mathcal{L}$-decompositions (4.11) that lead to physical density matrices $\rho_t^{(n)}$ in the jump expansion $\rho_t = \sum_n \rho_t^{(n)}$. We emphasize that these decompositions are equivalent in the sense that they all lead to the same solutions of the master equation (2.66). Exploiting this freedom to decompose the generator in different, physically equivalent ways, we will optimize the convergence of the series (4.19) over the complex vectors $\boldsymbol{\alpha}$. Before doing so in Sec. 4.3, we deduce the relevant properties of the jump expansion in order to build some intuition that will become useful later on.

4.2 Properties of the Jump Expansion

4.2.1 The Jump Record

The jump expansion (4.27) inclines us to view the time evolution ρ_t of an open quantum system as a sum of terms $\rho_t^{(n)}$, that originate from the initial state ρ_0 through a sequence of elementary transformation events or jumps $\mathcal{J}_{j,\boldsymbol{\alpha}}(t)$ with a continuous evolution in between. This sequence is characterized completely by specifying the sequence of ordered times $t_1 < \ldots < t_n < t$ at which these transformations took place, and by the information "which kind" of transformation was applied, as given by the corresponding indices $j_1, \ldots j_n$. The term $\rho_t^{(n)}$ then comprises sequences of length n with all possible combinations of jump times and jump indices, which means that we must sum over all indices and integrate over all times.

We can collect the information about each sequence in the so-called *jump record*

$$\mathfrak{R}^n = (j_1, t_1; j_2, t_2 \ldots; j_n, t_n). \tag{4.28}$$

This allows us to define the total transformation under the corresponding sequence as

$$\mathcal{K}_{\mathfrak{R}^n}(t) \equiv \mathcal{U}_{\boldsymbol{\alpha}}(t, t_n)\mathcal{J}_{j_n,\boldsymbol{\alpha}}(t_n)\mathcal{U}_{\boldsymbol{\alpha}}(t_n, t_{n-1})\mathcal{J}_{j_{n-1},\boldsymbol{\alpha}}(t_{n-1}) \ldots \mathcal{J}_{j_1,\boldsymbol{\alpha}}(t_1)\mathcal{U}_{\boldsymbol{\alpha}}(t_1, 0), \tag{4.29}$$

whose action on ρ_0 can be written out using Eq. (4.27),

$$\begin{aligned}\mathcal{K}_{\mathfrak{R}^n}(t)\rho_0 &= e^{-i/\hbar \int_{t_n}^{t} \mathsf{H}_{\boldsymbol{\alpha}}^{\mathrm{eff}}(t')\mathrm{d}t'} \mathsf{L}_{j_n,\boldsymbol{\alpha}}(t_n) \ldots \mathsf{L}_{j_1,\boldsymbol{\alpha}}(t_1) e^{-i/\hbar \int_0^{t_1} \mathsf{H}_{\boldsymbol{\alpha}}^{\mathrm{eff}}(t')\mathrm{d}t'} \rho_0 \\ &\quad \times e^{i/\hbar \int_0^{t_1} \mathsf{H}_{\boldsymbol{\alpha}}^{\mathrm{eff}\dagger}(t')\mathrm{d}t'} \mathsf{L}_{j_1,\boldsymbol{\alpha}}^{\dagger}(t_1) \ldots \mathsf{L}_{j_n,\boldsymbol{\alpha}}^{\dagger}(t_n) e^{i/\hbar \int_{t_n}^{t} \mathsf{H}_{\boldsymbol{\alpha}}^{\mathrm{eff}\dagger}(t')\mathrm{d}t'} \\ &\equiv \mathsf{K}_{\mathfrak{R}^n}(t)\rho_0\mathsf{K}_{\mathfrak{R}^n}^{\dagger}(t).\end{aligned} \tag{4.30}$$

One can now read Eq. (4.27) as a decomposition of $\rho_t^{(n)}$ into the *record-conditioned branches*, $\rho_t^{(\mathfrak{R}^n)} \equiv \mathcal{K}_{\mathfrak{R}^n}(t)\rho_0$, given by

$$\rho_t^{(n)} = \sum_{j_1 \ldots j_n = 1}^{N} \int_0^t \mathrm{d}t_n \ldots \int_0^{t_2} \mathrm{d}t_1 \mathcal{K}_{\mathfrak{R}^n}(t)\rho_0 \equiv \sum_{\{\mathfrak{R}^n\}} \mathcal{K}_{\mathfrak{R}^n}(t)\rho_0 = \sum_{\{\mathfrak{R}^n\}} \rho_t^{(\mathfrak{R}^n)}. \tag{4.31}$$

Here, we introduced the summation symbol $\sum_{\{\mathfrak{R}^n\}}$ as a short form for the multi-integral over $t_1, \ldots, t_n$ and the sum over $j_1, \ldots, j_n$. In the above definitions it is understood that the "sequence of length zero" is simply the unperturbed propagation $\mathcal{K}_{\mathfrak{R}^0}(t) = \mathcal{U}_{\boldsymbol{\alpha}}(t, 0)$.

The jump record allows one to view the jump expansion in a slightly new light. While the jump expansion still provides a decomposition of the entire dynamics into a continuous evolution and n spontaneous jumps, the jump record further breaks down the n-jump term into a series of transformations for which specific jumps have occurred at specific times, see schematic diagram in Fig. 4.1. We will see in the following section that with each record we can associate a probability so that one may interpret the final state ρ_t of the open system evolution as arising from a stochastic process that describes a random

occurrence of different "types" of jumps at random times and a deterministic evolution in between. The sum over all these different "trajectories" in ρ_t would then reflect our ignorance of exactly which record is realized in one instance of the evolution.

4.2.2 Relation to Quantum Trajectories and Measurement Interpretation

As we mentioned, with the above definition of a jump record we can now take the interpretation of the jump expansion (4.27) one step further. We noted in Sec. 4.1.3 that the super-operators $\mathcal{J}_{j,\boldsymbol{\alpha}}$ and $\mathcal{U}_{\boldsymbol{\alpha}}$, making up the transformation sequence $\mathcal{K}_{\mathfrak{R}^n}$ in Eq. (4.29), are completely positive maps. Therefore, all record-conditioned branches $\rho_t^{(\mathfrak{R}^n)}$ and, equivalently, all jump terms $\rho_t^{(n)}$ are unnormalized density matrices with positive traces or weights,

$$w_{\mathfrak{R}^n}(t) \equiv \operatorname{Tr} \rho_t^{(\mathfrak{R}^n)} = \operatorname{Tr}[\mathcal{K}_{\mathfrak{R}^n}(t)\rho_0], \tag{4.32}$$

$$w_n(t) \equiv \operatorname{Tr} \rho_t^{(n)}. \tag{4.33}$$

Noting that the weights $w_{\mathfrak{R}^n}(t)$, and analogously $w_n(t)$, always add up to unity due to the normalization of ρ_t,

$$\operatorname{Tr} \rho_t = \sum_n \underbrace{\operatorname{Tr} \rho_t^{(n)}}_{w_n(t)} = \sum_n \sum_{\{\mathfrak{R}^n\}} \underbrace{\operatorname{Tr} \rho_t^{(\mathfrak{R}^n)}}_{w_{\mathfrak{R}^n}(t)} = 1, \tag{4.34}$$

they can be given the meaning of probabilities.

To substantiate this interpretation, note that the trace of $\rho_t^{(0)}$ starts with $\operatorname{Tr}[\rho_0^{(0)}] = 1$ and decays with t due to the continuous evolution $\mathcal{U}_{\boldsymbol{\alpha}}(t,0)$. The initial value is due to the fact that $\mathcal{U}_{\boldsymbol{\alpha}}(0,0) = \mathrm{id}$, see Eq. (4.25), and the norm decay is seen by taking the time derivative of $w_0(t)$,

$$\begin{aligned} \partial_t w_0(t) &= \partial_t \operatorname{Tr} \rho_t^{(0)} = \partial_t \operatorname{Tr}[\mathcal{U}_{\boldsymbol{\alpha}}(t,0)\rho_0] = \operatorname{Tr}[\mathcal{L}_{\boldsymbol{\alpha}}(t)\mathcal{U}_{\boldsymbol{\alpha}}(t,0)\rho_0] \\ &= \operatorname{Tr}\left[-\frac{i}{\hbar}\left(\mathsf{H}_{\boldsymbol{\alpha}}^{\mathrm{eff}}(t)\rho_t^{(0)} - \rho_t^{(0)}\mathsf{H}_{\boldsymbol{\alpha}}^{\mathrm{eff}\,\dagger}(t)\right)\right] = -\operatorname{Tr}\left[\sum_j \mathsf{L}_{j,\boldsymbol{\alpha}}^\dagger(t)\mathsf{L}_{j,\boldsymbol{\alpha}}(t)\rho_t^{(0)}\right]. \end{aligned} \tag{4.35}$$

In the last equality, we eliminated the commutator of $\rho_t^{(0)}$ with the Hermitian part $\mathsf{H}_{\boldsymbol{\alpha}}$ of the effective Hamiltonian through the cyclic invariance of the trace. Now we see that $\partial_t w_0 \leq 0$ since both $\rho_t^{(0)}$ and the operators $\mathsf{L}_{j,\boldsymbol{\alpha}}^\dagger(t)\mathsf{L}_{j,\boldsymbol{\alpha}}(t)$ are positive. Due to the above properties of the weight $w_0(t)$, it is naturally interpreted as the probability that no jump occurs between 0 and t. Analogously, the weight $w_1(t)$ can be interpreted as the probability for a single jump, and the weight $w_{\mathfrak{R}^n}(t)$ would be the probability for the occurrence of n jumps with the jump record $\mathfrak{R}^n$.

We can now establish a connection between the jump expansion and the normalized quantum trajectories from Chap. 2 by normalizing the record conditioned branches with

their respective weights,

$$\frac{1}{w_{\mathfrak{R}^n}(t)}\rho_t^{(\mathfrak{R}^n)} = \frac{1}{w_{\mathfrak{R}^n}(t)}\mathcal{K}_{\mathfrak{R}^n}\rho_0 = \frac{1}{w_{\mathfrak{R}^n}(t)}\mathcal{U}_{\boldsymbol{\alpha}}(t,t_n)\mathcal{J}_{j_n,\boldsymbol{\alpha}}(t_n)\dots\mathcal{J}_{j_1,\boldsymbol{\alpha}}(t_1)\mathcal{U}_{\boldsymbol{\alpha}}(t_1,0)\rho_0. \tag{4.36}$$

In fact, for a pure initial state $\rho_0 = |\psi_0\rangle\langle\psi_0|$, the normalized branch (4.36) is a pure state trajectory $|\psi_t^{(\mathfrak{R}^n)}\rangle\langle\psi_t^{(\mathfrak{R}^n)}|$ that corresponds to the jump record $\mathfrak{R}^n$,

$$\begin{aligned}|\psi_t^{(\mathfrak{R}^n)}\rangle &= \frac{1}{\sqrt{w_{\mathfrak{R}^n}(t)}}e^{-\frac{i}{\hbar}\int_{t_n}^t \mathsf{H}_{\boldsymbol{\alpha}}^{\mathrm{eff}}(t')\mathrm{d}t'}\mathsf{L}_{j_n,\boldsymbol{\alpha}}(t_n)\dots\mathsf{L}_{j_1,\boldsymbol{\alpha}}(t_1)e^{-\frac{i}{\hbar}\int_0^{t_1}\mathsf{H}_{\boldsymbol{\alpha}}^{\mathrm{eff}}(t')\mathrm{d}t'}|\psi_0\rangle \\ &= \frac{\mathsf{K}_{\mathfrak{R}^n}(t)}{\sqrt{w_{\mathfrak{R}^n}(t)}}|\psi_0\rangle,\end{aligned} \tag{4.37}$$

where we have used the explicit expression (4.30) for $\mathcal{K}_{\mathfrak{R}^n}$. This means that $|\psi_t^{(\mathfrak{R}^n)}\rangle$ is that particular quantum trajectory, which has experienced jumps at times $t_1,\dots,t_n$ with operators $\mathsf{L}_{j_n,\boldsymbol{\alpha}},\dots,\mathsf{L}_{j_1,\boldsymbol{\alpha}}$, all registered in the jump record. The jump expansion can therefore be seen as a sum over all possible trajectories $|\psi_t^{(\mathfrak{R}^n)}\rangle$, weighted with their respective probabilities $w_{\mathfrak{R}^n}(t)$.

What is more, comparing Eq. (4.36) with Eq. (2.27) we are inclined to view the normalized record-conditioned branches $|\psi_t^{(\mathfrak{R}^n)}\rangle$ as outcomes of a hypothetical time-dependent and efficient measurement. The associated measurement operators are here the $\mathsf{K}_{\mathfrak{R}^n}(t)$ as defined in Eq. (4.30), and the corresponding measurement transformation is given by

$$\rho_0 \mapsto \frac{\mathsf{K}_{\mathfrak{R}^n}(t)\rho_0\mathsf{K}_{\mathfrak{R}^n}^\dagger(t)}{\mathrm{Tr}[\mathsf{K}_{\mathfrak{R}^n}^\dagger(t)\mathsf{K}_{\mathfrak{R}^n}(t)\rho_0]} = \frac{1}{w_{\mathfrak{R}^n}(t)}\rho_t^{(\mathfrak{R}^n)}. \tag{4.38}$$

In this interpretation, $t_1,\dots,t_n$ are the times at which the hypothetical measurement apparatus has registered outcomes $j_1,\dots,j_n$. Here, the environment can be viewed as the measurement apparatus and the loss of purity can be attributed to the fact that the environment continuously gathers information about the open system through their mutual interaction. Full access to this information would allow one to reconstruct the pure system state $|\psi_t^{(\mathfrak{R}^n)}\rangle$, conditioned on the measurement record $\mathfrak{R}^n$, see Sec. 2.3. In the absence of this information, however, we account for our ignorance about the system state by averaging over all outcomes, weighted with their respective probabilities.

4.2.3 Convergence of the Jump Expansion

In practice, one usually approximates a given infinite series with its truncated form unless an exact analytic expression for the infinite series exists. Such an approximation is, however, only useful if the studied series is convergent. Let us therefore assess the convergence of the jump expansion derived in Sec. 4.1, since it is not guaranteed to converge *a priori*. Generally, one can characterize the convergence of an expansion by considering the weights w_n of its constituent terms. For example, a highly convergent series is characterized by a strongly increasing cumulative sum $\sum_{n=0}^m w_n$, *i.e.* by strong

weights of its lowest order terms and a rapid decrease of the weights with increasing expansion order. In contrast, the weights in a series with low convergence are expected to show a slowly increasing cumulative sum. In this sense, the convergence of a given series can be optimized by maximizing the lowest order weights. In case of the jump expansion, $\rho_t = \sum_n \rho_t^{(n)}$, the weight $w_n(t)$ of a given term $\rho_t^{(n)}$ is naturally quantified by its trace, see Eq. (4.33). In the present section we will see that the $w_n(t)$ implicitly depend on the decomposition of the generator parametrized by complex tuples $\boldsymbol{\alpha}$, and we will see how the $w_n(t)$ evolve in time. In the following section, we will then optimize the convergence of the jump expansion by dynamically adjusting the tuples $\boldsymbol{\alpha}$.

The weights $w_n(t)$ given by Eq. (4.33) show two particularities that will greatly simplify this optimization task. On the one hand, as already mentioned above, the unperturbed propagator $\mathcal{U}_{\boldsymbol{\alpha}}(t, t_0)$ from Eq. (4.25) is the identity map for $t = t_0$,

$$\mathcal{U}_{\boldsymbol{\alpha}}(t_0, t_0)\rho = \rho. \tag{4.39}$$

Therefore we have $\rho_n^{(0)} = \delta_{n,0}\rho_0$, so that the weights satisfy the initial condition $w_n(0) = \delta_{n,0}$. On the other hand, we expect the jump count to grow stepwise in time since jumps happen only one at a time, increasing the count by exactly one. Therefore, we expect the time evolution of the $w_n(t)$ to be cascaded in the sense that the n-th order term gains weight from the $(n-1)$-th order while loosing weight to the $(n+1)$-th order. As we will see shortly, this cascading time evolution can be described in terms of a suitably defined positive, time-dependent rate operator $\Gamma_{\boldsymbol{\alpha}}(t)$ as

$$\partial_t w_n(t) = \partial_t \operatorname{Tr}[\rho_t^{(n)}] = \operatorname{Tr}\left[\Gamma_{\boldsymbol{\alpha}}(t)\rho_t^{(n-1)}\right] - \operatorname{Tr}\left[\Gamma_{\boldsymbol{\alpha}}(t)\rho_t^{(n)}\right], \tag{4.40}$$

see Eqs. (4.45) and (4.46) below. The expectation values $\operatorname{Tr}[\Gamma_{\boldsymbol{\alpha}}(t)\rho_t^{(n)}]$ are thus positive real numbers describing the absolute rates at which weight is transferred from $\rho_t^{(n)}$ to $\rho_t^{(n+1)}$. Since $\rho_t^{(n)}$ and $\rho_t^{(n+1)}$ involve n and $n+1$ jump superoperators, respectively, see Eq. (4.27), we call the $\operatorname{Tr}[\Gamma_{\boldsymbol{\alpha}}(t)\rho_t^{(n)}]$ *jump rates*. In the following, we will omit the time-argument of $\Gamma_{\boldsymbol{\alpha}}(t)$ for brevity . The above considerations together imply that the lowest order weights $w_n(t)$ at a given time t are maximized by minimizing the jump rates at all times $t' \leq t$.

To verify the evolution equation (4.40) for the $w_n(t)$ and to find an explicit expression for $\Gamma_{\boldsymbol{\alpha}}$, we take the time derivative of Eq. (4.26) for a general parametrization $\boldsymbol{\alpha}$,

$$\begin{aligned}
\partial_t \rho_t^{(n)} &= \partial_t \int_0^t \mathrm{d}t_n \int_0^{t_n} \mathrm{d}t_{n-1} \ldots \int_0^{t_2} \mathrm{d}t_1 \mathcal{U}_{\boldsymbol{\alpha}}(t, t_n)\mathcal{J}_{\boldsymbol{\alpha}}(t_n)\mathcal{U}_{\boldsymbol{\alpha}}(t_n, t_{n-1})\mathcal{J}_{\boldsymbol{\alpha}}(t_{n-1})\ldots\mathcal{U}_{\boldsymbol{\alpha}}(t_1, 0)\rho_0 \\
&= \int_0^{t_n} \mathrm{d}t_{n-1} \ldots \int_0^{t_2} \mathrm{d}t_1 \mathcal{U}_{\boldsymbol{\alpha}}(t, t_n)\mathcal{J}_{\boldsymbol{\alpha}}(t_n)\mathcal{U}_{\boldsymbol{\alpha}}(t_n, t_{n-1})\mathcal{J}_{\boldsymbol{\alpha}}(t_{n-1})\ldots\mathcal{U}_{\boldsymbol{\alpha}}(t_1, 0)\rho_0\Big|_{t_n=t} + \\
&\quad \int_0^t \mathrm{d}t_n \int_0^{t_n} \mathrm{d}t_{n-1} \ldots \int_0^{t_2} \mathrm{d}t_1 [\partial_t \mathcal{U}_{\boldsymbol{\alpha}}(t, t_n)]\, \mathcal{J}_{\boldsymbol{\alpha}}(t_n)\mathcal{U}_{\boldsymbol{\alpha}}(t_n, t_{n-1})\mathcal{J}_{\boldsymbol{\alpha}}(t_{n-1})\ldots\mathcal{U}_{\boldsymbol{\alpha}}(t_1, 0)\rho_0.
\end{aligned} \tag{4.41}$$

Note that the derivative of the integration limit eliminated the t_n-integration in the first summand. Now we can use that $\mathcal{U}_{\boldsymbol{\alpha}}(t,t) = \mathrm{id}$ in the first term and, in the second term, that the time derivative of the exponential in $\mathcal{U}_{\boldsymbol{\alpha}}(t,t_n) = \exp[\int_{t_n}^{t} \mathcal{L}_{\boldsymbol{\alpha}}(t')\mathrm{d}t']$ brings down $\mathcal{L}_{\boldsymbol{\alpha}}(t)$,

$$\begin{aligned}\partial_t \rho_t^{(n)} = \mathcal{J}_{\boldsymbol{\alpha}}(t) \int_0^t \mathrm{d}t_{n-1} \ldots \int_0^{t_2} \mathrm{d}t_1 \mathcal{U}_{\boldsymbol{\alpha}}(t,t_{n-1}) \mathcal{J}_{\boldsymbol{\alpha}}(t_{n-1}) \ldots \mathcal{U}_{\boldsymbol{\alpha}}(t_1,0)\rho_0 + \\ \mathcal{L}_{\boldsymbol{\alpha}}(t) \int_0^t \mathrm{d}t_n \int_0^{t_n} \mathrm{d}t_{n-1} \ldots \int_0^{t_2} \mathrm{d}t_1 \mathcal{U}_{\boldsymbol{\alpha}}(t,t_n) \mathcal{J}_{\boldsymbol{\alpha}}(t_n) \mathcal{U}_{\boldsymbol{\alpha}}(t_n,t_{n-1}) \ldots \mathcal{U}_{\boldsymbol{\alpha}}(t_1,0)\rho_0.\end{aligned} \tag{4.42}$$

Substituting back $\rho_t^{(n-1)}$ and $\rho_t^{(n)}$, given by Eq. (4.26), for the multi-integrals in the first and in the second term, respectively, we obtain

$$\partial_t \rho_t^{(n)} = \mathcal{J}_{\boldsymbol{\alpha}}(t)\rho_t^{(n-1)} + \mathcal{L}_{\boldsymbol{\alpha}}(t)\rho_t^{(n)}. \tag{4.43}$$

We can use this expression in the time derivative of the weights,

$$\partial_t w_n(t) = \mathrm{Tr}\left[\partial_t \rho_t^{(n)}\right] = \mathrm{Tr}\left[\mathcal{J}(t)_{\boldsymbol{\alpha}}\rho_t^{(n-1)} + \mathcal{L}_{\boldsymbol{\alpha}}(t)\rho_t^{(n)}\right], \tag{4.44}$$

and insert the explicit form of the $\mathcal{L}$-decomposition, Eqs. (4.22) and (4.23),

$$\begin{aligned}\partial_t w_n(t) &= \mathrm{Tr}\left[\sum_j \mathsf{L}_{j,\boldsymbol{\alpha}}(t)\rho_t^{(n-1)}\mathsf{L}_{j,\boldsymbol{\alpha}}^\dagger(t) - \frac{i}{\hbar}\left(\mathsf{H}_{\boldsymbol{\alpha}}^{\mathrm{eff}}(t)\rho_t^{(n)} - \rho_t^{(n)}\mathsf{H}_{\boldsymbol{\alpha}}^{\mathrm{eff}\dagger}(t)\right)\right] \\ &= \mathrm{Tr}\left[\sum_j \mathsf{L}_{j,\boldsymbol{\alpha}}^\dagger(t)\mathsf{L}(t)_{j,\boldsymbol{\alpha}}\rho_t^{(n-1)} - \frac{i}{\hbar}\left[\mathsf{H}_{\boldsymbol{\alpha}}(t), \rho_t^{(n)}\right]\right. \\ &\quad \left. -\frac{1}{2}\sum_j (\mathsf{L}_{j,\boldsymbol{\alpha}}^\dagger(t)\mathsf{L}_{j,\boldsymbol{\alpha}}(t)\rho_t^{(n)} - \rho_t^{(n)}\mathsf{L}_{j,\boldsymbol{\alpha}}^\dagger(t)\mathsf{L}_{j,\boldsymbol{\alpha}}(t))\right] \\ &= \sum_j \mathrm{Tr}\left[\mathsf{L}_{j,\boldsymbol{\alpha}}^\dagger(t)\mathsf{L}_{j,\boldsymbol{\alpha}}(t)\rho_t^{(n-1)} - \mathsf{L}_{j,\boldsymbol{\alpha}}^\dagger(t)\mathsf{L}_{j,\boldsymbol{\alpha}}(t)\rho_t^{(n)}\right].\end{aligned} \tag{4.45}$$

Here, the cyclic invariance of the trace was used multiple times, in particular to eliminate the commutator of $\rho_t^{(n)}$ with the Hermitian part $\mathsf{H}_{\boldsymbol{\alpha}}$ of the effective Hamiltonian. Comparing Eqs. (4.40) and (4.45), we see that the rate operator $\Gamma_{\boldsymbol{\alpha}}$ is properly defined as

$$\Gamma_{\boldsymbol{\alpha}} \equiv \sum_j \mathsf{L}_{j,\boldsymbol{\alpha}}^\dagger(t)\mathsf{L}_{j,\boldsymbol{\alpha}}(t) = \sum_j \mathrm{Tr}[(\mathsf{L}_j^\dagger(t) + \alpha_j^*(t))(\mathsf{L}_j(t) + \alpha_j(t))\rho_t^{(n)}] \equiv \sum_j \Gamma_{j,\boldsymbol{\alpha}}, \tag{4.46}$$

with the additional splitting of $\Gamma_{\boldsymbol{\alpha}}$ into the rate operators $\Gamma_{j,\boldsymbol{\alpha}}$ associated with different jump types. In Eq. (4.46) we have used the definition (4.20) for $\mathsf{L}_{j,\boldsymbol{\alpha}}$. The positivity of $\Gamma_{\boldsymbol{\alpha}}$

and $\Gamma_{j,\boldsymbol{\alpha}}$ is guaranteed by the fact that they have the form of a completely positive map, see Eq. (2.48). Let us finally note that the non-Hermitian part the effective Hamiltonian $\mathsf{H}^{\text{eff}}_{\boldsymbol{\alpha}}$, Eq. (4.24), which defines the continuous between-jump evolution $\mathcal{U}_{\boldsymbol{\alpha}}(t_{i+1}, t_i)$, is given by $-\frac{i\hbar}{2}\sum_j \mathsf{L}^\dagger_{j,\boldsymbol{\alpha}}(t)\mathsf{L}_{j,\boldsymbol{\alpha}}(t)$. Therefore the jump rate $\mathrm{Tr}[\Gamma_{\boldsymbol{\alpha}}\rho^{(n)}_t]$ is proportional to the norm decrease of $\rho^{(n)}_t$ under $\mathsf{H}^{\text{eff}}_{\boldsymbol{\alpha}}$.

4.3 Resummation of the Jump Expansion

In Sec. 4.1.2 we derived the formal expansion (4.19) for the open system time evolution in analogy to the Dyson series for closed systems. Despite their formal similarity, the Dyson series is a perturbative expansion whereas the jump expansion is not. This makes the latter a lot more versatile, but it also casts its convergence into doubt. In Sec. 4.1.3 we then saw that a physically motivated subset of all possible jump expansions can be parametrized by complex vectors $\boldsymbol{\alpha}$ and, in Sec. 4.2.3, we described how the convergence can be assessed for a given $\boldsymbol{\alpha}$. Since all expansions are equivalent in the sense that they give the same ρ_t independent of $\boldsymbol{\alpha}$, they are actually just formal resummations of one and the same jump expansion, say for $\boldsymbol{\alpha} = 0$. In other words, by changing $\boldsymbol{\alpha}$ we simply regroup the terms of the expansion. It is intuitively clear that we want to regroup the terms in such a way that the most important terms appear first since this would allow us to truncate the jump expansion and thereby obtain a reliable estimate of ρ_t.

In this section, we aim at achieving this goal by optimizing the convergence of the series over the parameter $\boldsymbol{\alpha}$ [20, 21]. It will turn out that the *optimal* resummation is not realized by a constant vector $\boldsymbol{\alpha}$ but by one which changes from one expansion term to the next, see schematic diagram in Fig. 4.1. Since this *adaptive* form of the jump expansion with its intricate structure is not always suitable for practical applications, especially for obtaining analytical approximations to ρ_t, we will also derive suboptimal resummations that combine high convergence with a simpler algebraic structure [20].

4.3.1 The Optimally Convergent Resummation

As we argued in the previous section, the jump expansion initially comprises only the lowest order term, *i.e.* $w_0(0) = 1$, and higher order terms are then sequentially populated according to Eq. (4.40). In order to maximize the lowest order weights and thereby optimize the series' convergence, it is therefore sufficient to minimize the rates $\mathrm{Tr}[\Gamma_{\boldsymbol{\alpha}}\rho^{(n)}_t]$ at which $w_n(t)$ decreases in favor of $w_{n+1}(t)$.

Before we proceed with the task of minimizing $\mathrm{Tr}[\Gamma_{\boldsymbol{\alpha}}\rho^{(n)}_t]$ by choosing the right $\boldsymbol{\alpha}$, we must account for the fact that each jump term $\rho^{(n)}_t$ can be further decomposed into the record-conditioned branches $\rho^{(\mathfrak{R}^n)}_t$, see Eq. (4.31). Using the additional splitting of $\Gamma_{\boldsymbol{\alpha}}$ into $\Gamma_{j,\boldsymbol{\alpha}}$, see Eq. (4.46), we note that the jump rate $\mathrm{Tr}[\Gamma_{\boldsymbol{\alpha}}\rho^{(n)}_t]$ is actually composed of

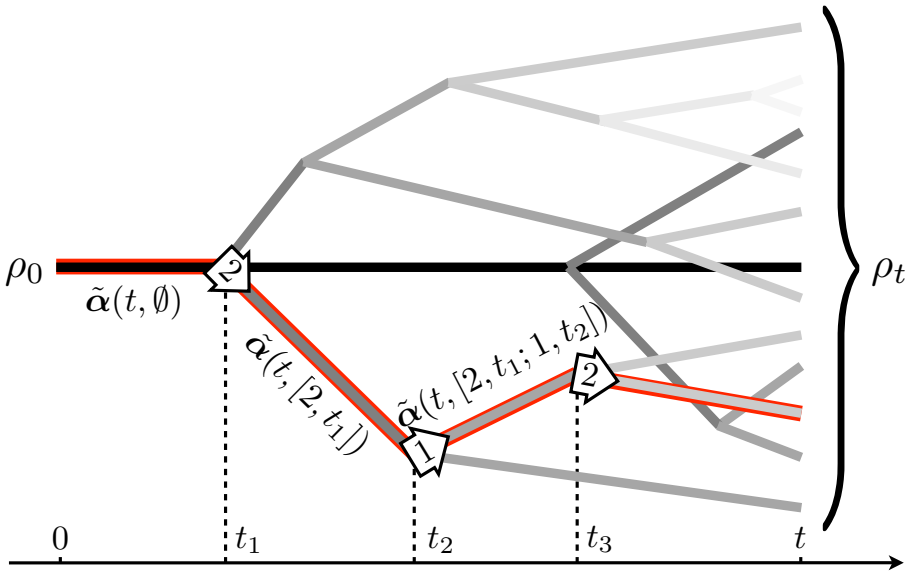

Figure 4.1: Schematic diagram of the optimally convergent jump expansion: The time evolution from ρ_0 to ρ_t is decomposed into branches that consist of a series of continuous and jump-transformations, $\mathcal{U}_{\tilde{\boldsymbol{\alpha}}}(t_{i+1},t_i)$ and $\mathcal{J}_{j,\tilde{\boldsymbol{\alpha}}}$, represented by straight lines and branching points, respectively. The branches are distinguished by the times t_i and the types j of the involved jump transformations, *i.e.* by the jump record $\mathfrak{R}^n$ (see exemplary branch $\mathfrak{R}^3 = (2,t_1;1,t_2;2,t_3)$ traced in the picture, with t_i and j marked on the time axis on the bottom and inside the arrows at the branching points, respectively). ρ_t is given by the sum over all possible branches $\rho_t^{(\mathfrak{R}^n)}$, see Eqs. (4.29) and (4.31). The convergence of this expansion is optimized or, in other words, the number of branches that contribute appreciably to ρ_t is minimized by adapting the transformations $\mathcal{U}_{\tilde{\boldsymbol{\alpha}}}(t_{i+1},t_i)$ and $\mathcal{J}_{j,\tilde{\boldsymbol{\alpha}}}$ to each specific branch by means of the time-dependent complex numbers $\tilde{\boldsymbol{\alpha}}(t,\mathfrak{R}^n)$, see Eqs. (4.51), (4.22), and (4.23): $\tilde{\boldsymbol{\alpha}}(t,\emptyset)$, $\tilde{\boldsymbol{\alpha}}(t,[2,t_1])$, $\tilde{\boldsymbol{\alpha}}(t,[2,t_1;1,t_2])$, and $\tilde{\boldsymbol{\alpha}}(t,[2,t_1;1,t_2;2,t_3])$ are used in the respective intervals $[t_i,t_{i+1}]$ in the marked exemplary branch.

the record-specific partial jump rates $\mathrm{Tr}[\Gamma_{j,\boldsymbol{\alpha}}\rho_t^{(\mathfrak{R}^n)}]$,

$$\mathrm{Tr}\left[\Gamma_{\boldsymbol{\alpha}}\rho_t^{(n)}\right] = \mathrm{Tr}\left[\sum_j \Gamma_{j,\boldsymbol{\alpha}} \sum_{\{\mathfrak{R}^n\}} \rho_t^{(\mathfrak{R}^n)}\right] = \sum_{j,\{\mathfrak{R}^n\}} \mathrm{Tr}\left[\Gamma_{j,\boldsymbol{\alpha}}\rho_t^{(\mathfrak{R}^n)}\right]. \tag{4.47}$$

The partial jump rates are positive and real since both $\rho_t^{(\mathfrak{R}^n)}$ and $\Gamma_{j,\boldsymbol{\alpha}}$ are positive operators. Hence, in order to minimize $\mathrm{Tr}[\Gamma_{\boldsymbol{\alpha}}\rho_t^{(n)}]$, all $\mathrm{Tr}[\Gamma_{j,\boldsymbol{\alpha}}\rho_t^{(\mathfrak{R}^n)}]$ must be minimized

simultaneously. Inserting the definition (4.46) for $\Gamma_{j,\boldsymbol{\alpha}}$ we have

$$\begin{aligned}\mathrm{Tr}\left[\Gamma_{j,\boldsymbol{\alpha}}\rho_t^{(\mathfrak{R}^n)}\right] &= \mathrm{Tr}[(\mathsf{L}_j^\dagger(t)+\alpha_j^*(t))(\mathsf{L}_j(t)+\alpha_j(t))\rho_t^{(\mathfrak{R}^n)}] \\ &= \mathrm{Tr}[(\mathsf{L}_j^\dagger(t)\mathsf{L}_j(t)+|\alpha_j(t)|^2)\rho_t^{(\mathfrak{R}^n)}] + 2\,\mathrm{Re}(\alpha_j^*(t)\,\mathrm{Tr}[\mathsf{L}_j(t)\rho_t^{(\mathfrak{R}^n)}]), \qquad (4.48)\end{aligned}$$

where the first term is always positive, whereas the second term can be positive or negative depending on $\boldsymbol{\alpha}$.

The partial jump rate $\mathrm{Tr}[\Gamma_{j,\boldsymbol{\alpha}}\rho_t^{(\mathfrak{R}^n)}]$ is minimal if the second term in Eq. (4.48) is as negative as possible. This fixes the complex phase of the optimal α_j to

$$\arg(\tilde{\alpha}_j^*(t)) = \pi + \arg(\mathrm{Tr}[\mathsf{L}_j\rho_t^{(\mathfrak{R}^n)}]), \qquad (4.49)$$

where we use the tilde to indicate the optimum. With this phase condition, we can recast Eq. (4.48) at the optimum as a quadratic expression in $|\tilde{\alpha}_j^*(t)|$,

$$\mathrm{Tr}\left[\Gamma_{j,\tilde{\boldsymbol{\alpha}}}\rho_t^{(\mathfrak{R}^n)}\right] = \mathrm{Tr}[(\mathsf{L}_j^\dagger(t)\mathsf{L}_j(t)+|\tilde{\alpha}_j(t)|^2)\rho_t^{(\mathfrak{R}^n)}] - 2|\tilde{\alpha}_j(t)||\,\mathrm{Tr}[\mathsf{L}_j(t)\rho_t^{(\mathfrak{R}^n)}]|. \qquad (4.50)$$

It is minimal for $|\tilde{\alpha}_j(t)| = |\,\mathrm{Tr}[\mathsf{L}_j(t)\rho_t^{(\mathfrak{R}^n)}]|/\,\mathrm{Tr}\,\rho_t^{(\mathfrak{R}^n)}$. Together with the phase condition (4.49), this gives the optimal parameters

$$\tilde{\alpha}_j(t,\mathfrak{R}^n) = -\frac{1}{\mathrm{Tr}\,\rho_t^{(\mathfrak{R}^n)}}\,\mathrm{Tr}[\mathsf{L}_j(t)\rho_t^{(\mathfrak{R}^n)}]. \qquad (4.51)$$

Here, we have explicitly indicated the $\mathfrak{R}^n$-dependence of $\tilde{\alpha}_j$. The optimal partial rates therefore read

$$\mathrm{Tr}\left[\Gamma_{j,\tilde{\boldsymbol{\alpha}}}\rho_t^{(\mathfrak{R}^n)}\right] = \mathrm{Tr}\left[\mathsf{L}_j^\dagger(t)\mathsf{L}_j(t)\rho_t^{(\mathfrak{R}^n)}\right] - \frac{1}{\mathrm{Tr}\,\rho_t^{(\mathfrak{R}^n)}}\left|\mathrm{Tr}\left[\mathsf{L}_j(t)\rho_t^{(\mathfrak{R}^n)}\right]\right|^2. \qquad (4.52)$$

A summation of the optimal partial rates over j and $\mathfrak{R}^n$ yields the optimal total jump rate $\mathrm{Tr}[\Gamma_{\boldsymbol{\alpha}}\rho_t^{(n)}]$. In the following section, we will further investigate the meaning of Eq. (4.52) and, in particular, the conditions for the optimal rates to vanish.

In Sec. 4.2.1 we observed that the jump expansion is composed of different sequences of continuous and jump transformations ($\mathcal{U}_{\boldsymbol{\alpha}}$ and $\mathcal{J}_{j,\boldsymbol{\alpha}}$) of the initial state, *i.e.* different record-conditioned branches, see Eqs. (4.29) and (4.31), and the schematic diagram Fig. 4.1. Equation (4.51), in conjunction with Eqs. (4.22) and (4.23), now shows that the convergence of the jump expansion is optimized by adapting the applied transformations to each specific branch. Specifically, the jump operator $\mathsf{L}_{j,\tilde{\boldsymbol{\alpha}}}$ that defines the optimal $\mathcal{J}_{j,\tilde{\boldsymbol{\alpha}}}$ acquires a shift given by the expectation value in the respective branch. After a jump of type j, the $\mathcal{J}_{j,\tilde{\boldsymbol{\alpha}}}$ are therefore different from the $\mathcal{J}_{j',\tilde{\boldsymbol{\alpha}}}$ after a jump of type j'. The optimal shifts $\tilde{\boldsymbol{\alpha}}$ are hence updated at such branching points depending on the type of jump and on the time when it takes place. After a series of n jumps, $\tilde{\boldsymbol{\alpha}}$ depends on the entire record $\mathfrak{R}^n$ of past jumps.

To summarize, while Dyson-like expansions are usually defined in terms of a fixed decomposition of the generator, we here consider an expansion in which the decomposition changes from one term to the next. Formally, the transformation of the jump expansion to its optimally convergent form can be considered an adaptive resummation in the above sense that it adapts the $\mathcal{L}$-decomposition both to time and to each specific branch.

In view of the fact that the jump expansion was derived in analogy to a usual Dyson series in Sec. 4.1.2, it is not obvious that record conditioned, time dependent decompositions $\mathcal{L}(t) = \mathcal{L}_{\tilde{\boldsymbol{\alpha}}(t,\mathfrak{R}^n)}(t) + \mathcal{J}_{\tilde{\boldsymbol{\alpha}}(t,\mathfrak{R}^n)}(t)$ still generate valid solutions of the master equation. To see that this is indeed the case, we take the time derivative of the n-jump term as we did in Eq. (4.42),

$$\begin{aligned}\partial_t \rho_t^{(n)} = &\sum_{j_1 \cdots j_n} \int_0^{t_n} \mathrm{d}t_{n-1} \ldots \int_0^{t_2} \mathrm{d}t_1 \mathcal{U}_{\tilde{\boldsymbol{\alpha}}(t,\mathfrak{R}^n)}(t,t_n) \mathcal{J}_{j_n,\tilde{\boldsymbol{\alpha}}(t_n,\mathfrak{R}^{n-1})} \ldots \mathcal{U}_{\tilde{\boldsymbol{\alpha}}(t,\mathfrak{R}^0)}(t_1,0)\rho_0 \Big|_{t_n=t} \\ &+ \mathcal{L}_{\tilde{\boldsymbol{\alpha}}(t,\mathfrak{R}^n)}(t) \int_0^{t} \mathrm{d}t_n \ldots \int_0^{t_2} \mathrm{d}t_1 \mathcal{U}_{\tilde{\boldsymbol{\alpha}}(t,\mathfrak{R}^n)}(t,t_n) \mathcal{J}_{j_n,\tilde{\boldsymbol{\alpha}}(t_n,\mathfrak{R}^{n-1})} \ldots \mathcal{U}_{\tilde{\boldsymbol{\alpha}}(t,\mathfrak{R}^0)}(t_1,0)\rho_0.\end{aligned} \tag{4.53}$$

Again, the derivative of the integration limit eliminates the t_n-integration and the derivative of the exponential in the propagator $\mathcal{U}_{\tilde{\boldsymbol{\alpha}}(t,\mathfrak{R}^n)}(t,t_n)$ brings down $\mathcal{L}_{\tilde{\boldsymbol{\alpha}}(t,\mathfrak{R}^n)}(t)$. Now we can substitute back the $\mathfrak{R}^n$- and the $\mathfrak{R}^{n-1}$-conditioned branch (4.30) to obtain

$$\partial_t \rho_t^{(n)} = \sum_{j_n,\{\mathfrak{R}^{n-1}\}} \mathcal{J}_{j_n,\tilde{\boldsymbol{\alpha}}(t,\mathfrak{R}^{n-1})} \rho_t^{(\mathfrak{R}^{n-1})} + \sum_{\{\mathfrak{R}^n\}} \mathcal{L}_{\tilde{\boldsymbol{\alpha}}(t,\mathfrak{R}^n)}(t) \rho_t^{(\mathfrak{R}^n)}. \tag{4.54}$$

The $\mathfrak{R}^n$-conditioned terms of $\partial_t \rho_t^{(n)}$ and of $\partial_t \rho_t^{(n+1)}$ now combine for $\mathcal{L}(t) \sum_{\{\mathfrak{R}^n\}} \rho_t^{(\mathfrak{R}^n)}$, independently of $\tilde{\boldsymbol{\alpha}}$. The sum over all orders thus yields the master equation (2.66).

Vanishing Jump Rates

We have found out that the jump operators $\mathsf{L}_{j,\boldsymbol{\alpha}}$ with the complex shifts $\tilde{\boldsymbol{\alpha}}(t,\mathfrak{R}^n)$ given by Eq. (4.51) lead to an optimally convergent jump expansion. Moreover, since the jump rates $\mathrm{Tr}[\mathsf{\Gamma}_{j,\tilde{\boldsymbol{\alpha}}} \rho_t^{(\mathfrak{R}^n)}]$, Eq. (4.52), quantify how fast higher order terms get populated over time, we can conclude that the smaller the optimal jump rates, the better the convergence of the optimized jump expansion. For non-vanishing jump rates, the number of terms necessary to approximate ρ_t with a given accuracy increases with time t. If, however, all jump rates vanish after some time, the weights of the expansion terms remain constant and it is safe to approximate ρ_t with a fixed number of terms for all t. Let us therefore examine the conditions for $\mathrm{Tr}[\mathsf{\Gamma}_{j,\tilde{\boldsymbol{\alpha}}} \rho_t^{(\mathfrak{R}^n)}]$ to vanish.

First, one notices that without resummation, *i.e.* for $\boldsymbol{\alpha} = 0$, the rate

$$\mathrm{Tr}\left[\mathsf{\Gamma}_{\boldsymbol{\alpha}} \rho_t^{(n)}\right] = \sum_j \mathrm{Tr}\left[\mathsf{\Gamma}_{j,\boldsymbol{\alpha}} \rho_t^{(n)}\right] = \sum_j \mathrm{Tr}[\mathsf{L}_j^\dagger(t) \mathsf{L}_j(t) \rho_t^{(n)}] \tag{4.55}$$

vanishes, by definition, if $\rho_t^{(n)}$ is orthogonal to the positive operators $\mathsf{L}_j^\dagger(t)\mathsf{L}_j(t)$. For pure states $\rho_t^{(n)} = |\psi\rangle\langle\psi|$ this is equivalent to $|\psi\rangle$ belonging to the null space of all jump operators L_j. Generally, this can only occur if the jump map $\mathcal{J}_0(t)$ given by Eq. (4.22) is a contraction to this subspace which is, at the same time, invariant under the dynamics generated by the Hamiltonian $\mathsf{H}(t)$, see Eq. (4.23). That this rather restrictive condition may indeed be fulfilled is shown by the damped harmonic oscillator at $T = 0$, where the entire state space is contracted to the ground state as we saw in Sec. 3.1.

Naturally, the conditions for the optimal rates $\mathrm{Tr}[\mathsf{\Gamma}_{\tilde{\boldsymbol{\alpha}}}\rho_t^{(n)}]$ to vanish are somewhat less restrictive, since they are obtained out of $\mathrm{Tr}[\mathsf{\Gamma}_{\boldsymbol{\alpha}}\rho_t^{(n)}]$ by minimization. It is instructive to first examine the case that the optimal *partial* rate $\mathrm{Tr}[\mathsf{\Gamma}_{j,\tilde{\boldsymbol{\alpha}}}\rho_t^{(\mathfrak{R}^n)}]$ given by Eq. (4.52) vanishes. This implies that

$$\mathrm{Tr}[\mathsf{L}_j^\dagger(t)\mathsf{L}_j(t)\rho_t^{(\mathfrak{R}^n)}]\,\mathrm{Tr}\,\rho_t^{(\mathfrak{R}^n)} = \mathrm{Tr}[\mathsf{L}_j^\dagger(t)\rho_t^{(\mathfrak{R}^n)}]\,\mathrm{Tr}[\mathsf{L}_j(t)\rho_t^{(\mathfrak{R}^n)}]. \tag{4.56}$$

Now consider the state $\rho_t^{(\mathfrak{R}^n)}$ in its eigenbasis, $\rho_t^{(\mathfrak{R}^n)} = \sum_{k=1}^r p_k|k\rangle\langle k|$, with r positive, nonzero real eigenvalues p_k. Labeling the matrix entries of the jump operator in this eigenbasis as $\langle l|\mathsf{L}_j(t)|k\rangle = L_{lk}$, we can rewrite Eq. (4.56) as

$$\begin{aligned}\left(\sum_{k=1}^r p_k\langle k|\mathsf{L}_j^\dagger(t)\mathsf{L}_j(t)|k\rangle\right)\sum_{l=1}^r p_l &= \left(\sum_{k=1}^r p_k\langle k|\mathsf{L}_j^\dagger(t)|k\rangle\right)\left(\sum_{l=1}^r p_l\langle l|\mathsf{L}_j(t)|l\rangle\right)\\ \left(\sum_{k=1}^r p_k\sum_{m=1}^d |L_{mk}|^2\right)\sum_{l=1}^r p_l &= \sum_{k=1}^r p_k L_{kk}^*\sum_{l=1}^l p_l L_{ll},\end{aligned} \tag{4.57}$$

where d is the Hilbert space dimension and we have inserted the identity $\sum_{m=1}^d |m\rangle\langle m| = \mathbb{1}$ on the left hand side between $\mathsf{L}_j^\dagger$ and L_j. If we expand the products of sums on the left and right hand side, terms with $k = l = m$ cancel right away and we are left with

$$\sum_{k=1}^r p_k^2\sum_{m\neq k}^d |L_{mk}|^2 + \sum_{k=1}^r\sum_{l>k}^r p_k p_l\sum_{m=1}^d (|L_{mk}|^2 + |L_{ml}|^2) = \sum_{k=1}^r\sum_{l>k}^r p_k p_l(L_{kk}L_{ll}^* + L_{kk}^* L_{ll}). \tag{4.58}$$

Subtraction of the right hand side leads to

$$\begin{aligned}0 &= \sum_{k=1}^r p_k^2\sum_{m\neq k}^d |L_{mk}|^2 + \sum_{k=1}^r\sum_{l>k}^r p_k p_l\left[-L_{kk}L_{ll}^* - L_{kk}^*L_{ll} + \sum_{m=1}^d (|L_{mk}|^2 + |L_{ml}|^2)\right]\\ &= \sum_{k=1}^r p_k^2\sum_{m\neq k}^d |L_{mk}|^2 + \sum_{k=1}^r\sum_{l>k}^r p_k p_l\left[|L_{kk} - L_{ll}|^2 + \sum_{m\neq k}^d |L_{mk}|^2 + \sum_{l\neq k}^d |L_{ml}|^2\right],\end{aligned} \tag{4.59}$$

where in the second line we have combined terms where either $m = k$ or $m = l$. Now all terms on the right hand side are manifestly nonnegative and must therefore vanish

separately. Since the p_k are nonzero by definition, the factors containing absolute values of L-matrix entries are the ones to vanish. The first condition, $|L_{mk}|^2 = 0$ for $m \neq k$, is equivalent to $|k\rangle$ being an eigenvector of the jump operator $\mathsf{L}_j(t)$. The second condition, $|L_{kk} - L_{ll}|^2 = 0$, implies that the eigenvalues of $|k\rangle$ and $|l\rangle$ must be equal.

To conclude, we saw that the optimal partial jump rate $\mathrm{Tr}[\Gamma_{j,\tilde{\boldsymbol{\alpha}}}\rho_t^{(\mathfrak{R}^n)}]$ vanishes if $\rho_t^{(\mathfrak{R}^n)}$ is a probabilistic mixture of eigenstates of $\mathsf{L}_j(t)$ that correspond to the same eigenvalue. For jump operators with a nondegenerate spectrum of eigenvalues, therefore only pure eigenstates $\rho_t^{(\mathfrak{R}^n)} = p_k|k\rangle\langle k|$ of $\mathsf{L}_j(t)$ lead to a vanishing $\mathrm{Tr}[\Gamma_{j,\tilde{\boldsymbol{\alpha}}}\rho_t^{(\mathfrak{R}^n)}]$.

In order for the total jump rate $\mathrm{Tr}[\Gamma_{\tilde{\boldsymbol{\alpha}}}\rho_t^{(n)}]$ to vanish, all partial rates $\mathrm{Tr}[\Gamma_{j,\tilde{\boldsymbol{\alpha}}}\rho_t^{(\mathfrak{R}^n)}]$ must vanish simultaneously. This is only possible if simultaneous eigenvectors of all jump operators $\mathsf{L}_j(t)$ exist, which is the case if the $\mathsf{L}_j(t)$ commute. In other words, if the jump operators commute, they define a preferred basis in which the optimal jump rates $\mathrm{Tr}[\Gamma_{\tilde{\boldsymbol{\alpha}}}\rho_t^{(n)}]$ vanish.

One may now argue that simultaneous eigenstates of all L_j form a set of measure zero within state space and therefore the above conditions will never be fulfilled. The optimal complex shifts $\tilde{\alpha}_j$ given by Eq. (4.51) are, however, designed to minimize the jump rates $\mathrm{Tr}[\Gamma_{j,\tilde{\boldsymbol{\alpha}}}\rho_t^{(\mathfrak{R}^n)}]$ for all times $t > 0$. Therefore on the one hand, even if we do not start in an L_j-eigenstate, we expect that $\tilde{\alpha}_j$ drives us towards one as time goes by. On the other hand, the system Hamiltonian H prevents us from reaching such an eigenstate unless H commutes with the L_j or, more generally, the set of simultaneous eigenstates of all L_j is invariant under H. At some point, both processes equilibrate resulting in optimal jump rates under the restriction that the total time evolution ρ_t is still realized. Indeed, it was shown in a number of paradigmatic quantum systems, that the fixed points of the nonlinear evolution under $\mathsf{H}_{\tilde{\boldsymbol{\alpha}}}^{\mathrm{eff}}$ given by (4.25) and (4.51) have exactly the above mentioned properties [49, 51, 61].

Further Optimization Based on Initial Pure State Decomposition

So far, we have minimized the jump rates by first decomposing $\mathrm{Tr}[\Gamma_{\boldsymbol{\alpha}}\rho_t^{(n)}]$ into the partial rates $\mathrm{Tr}[\Gamma_{j,\boldsymbol{\alpha}}\rho_t^{(\mathfrak{R}^n)}]$ and then minimizing all partial rates *separately* with suitable complex vectors $\boldsymbol{\alpha} = \tilde{\boldsymbol{\alpha}}(t, \mathfrak{R}^n)$. Now, looking at the $\mathrm{Tr}[\Gamma_{j,\boldsymbol{\alpha}}\rho_t^{(\mathfrak{R}^n)}]$ in Eq. (4.47), we see that their dependence on mixed states $\rho_t^{(\mathfrak{R}^n)}$ leaves room for further optimization. The reason is that $\rho_t^{(\mathfrak{R}^n)}$, as any density matrix, can be decomposed into a probabilistic mixture of pure states, and therefore $\mathrm{Tr}[\Gamma_{j,\boldsymbol{\alpha}}\rho_t^{(\mathfrak{R}^n)}]$ can be further decomposed into even smaller constituents that depend on this pure state decomposition.

Since $\rho_t^{(\mathfrak{R}^n)}$ originates from ρ_0 through a series of pure state transformations $\mathsf{K}_{\mathfrak{R}^n}(t)$, as we have seen in Eq. (4.30), it is natural to consider only pure state decompositions of the initial state,

$$\rho_0 = \sum_k |\varphi_0^k\rangle\langle\varphi_0^k|, \tag{4.60}$$

and decompose $\rho_t^{(\mathfrak{R}^n)}$ into the transformed $|\varphi_0^k\rangle$,

$$\rho_t^{(\mathfrak{R}^n)} = \sum_k |k_t^{(\mathfrak{R}^n)}\rangle\langle k_t^{(\mathfrak{R}^n)}| = \sum_k \mathsf{K}_{\mathfrak{R}^n}(t)|\varphi_0^k\rangle\langle\varphi_0^k|\mathsf{K}_{\mathfrak{R}^n}^\dagger(t)$$

Here, we choose unnormalized pure states $\langle\varphi_0^k|\varphi_0^k\rangle \leq 1$ for brevity. Now we decompose the partial rate $\mathrm{Tr}[\mathsf{\Gamma}_{j,\boldsymbol{\alpha}}\rho_t^{(\mathfrak{R}^n)}]$ based on this pure state decomposition as

$$\begin{aligned}\mathrm{Tr}\left[\mathsf{\Gamma}_{j,\boldsymbol{\alpha}}\rho_t^{(\mathfrak{R}^n)}\right] &= \mathrm{Tr}\left[\mathsf{L}_{j,\boldsymbol{\alpha}}^\dagger(t)\mathsf{L}_{j,\boldsymbol{\alpha}}(t)\rho_t^{(\mathfrak{R}^n)}\right] = \sum_k \langle k_t^{(\mathfrak{R}^n)}|\mathsf{L}_{j,\boldsymbol{\alpha}}^\dagger(t)\mathsf{L}_{j,\boldsymbol{\alpha}}(t)|k_t^{(\mathfrak{R}^n)}\rangle \\ &= \sum_k \langle\varphi_0^k|\mathsf{K}_{\mathfrak{R}^n}^\dagger(t)\mathsf{L}_{j,\boldsymbol{\alpha}}^\dagger(t)\mathsf{L}_{j,\boldsymbol{\alpha}}(t)\mathsf{K}_{\mathfrak{R}^n}(t)|\varphi_0^k\rangle \equiv \sum_k \langle\varphi_0^k|\mathsf{\Gamma}'_{j,\boldsymbol{\alpha}}|\varphi_0^k\rangle, \end{aligned} \tag{4.61}$$

where the partial rates $\langle\varphi_0^k|\mathsf{\Gamma}'_{j,\boldsymbol{\alpha}}|\varphi_0^k\rangle$ depend explicitly on the initial pure state decomposition $\{|\varphi_0^i\rangle\}$. The positivity of the operators $\mathsf{\Gamma}'_{j,\boldsymbol{\alpha}} \equiv \mathsf{K}_{\mathfrak{R}^n}^\dagger(t)\mathsf{L}_{j,\boldsymbol{\alpha}}^\dagger(t)\mathsf{L}_{j,\boldsymbol{\alpha}}(t)\mathsf{K}_{\mathfrak{R}^n}(t)$ ensures that $\langle\varphi_0^k|\mathsf{\Gamma}'_{j,\boldsymbol{\alpha}}|\varphi_0^k\rangle \geq 0$. The rates $\langle\varphi_0^k|\mathsf{\Gamma}'_{j,\boldsymbol{\alpha}}|\varphi_0^k\rangle$ are now minimized analogously to Eqs. (4.48)–(4.52): Insertion of the definition (4.20) for $\mathsf{L}_{j,\boldsymbol{\alpha}}$ into Eq. (4.61) leads to

$$\begin{aligned}\langle\varphi_0^k|\mathsf{\Gamma}'_{j,\boldsymbol{\alpha}}|\varphi_0^k\rangle &= \langle k_t^{(\mathfrak{R}^n)}|(\mathsf{L}_j^\dagger(t) + \alpha_j^*(t))(\mathsf{L}_j(t) + \alpha_j(t))|k_t^{(\mathfrak{R}^n)}\rangle \\ &= \langle k_t^{(\mathfrak{R}^n)}|\mathsf{L}_j^\dagger(t)\mathsf{L}_j(t) + |\alpha_j(t)|^2|k_t^{(\mathfrak{R}^n)}\rangle + 2\,\mathrm{Re}(\alpha_j^*(t)\langle k_t^{(\mathfrak{R}^n)}|\mathsf{L}_j(t)|k_t^{(\mathfrak{R}^n)}\rangle).\end{aligned} \tag{4.62}$$

By introducing the phase condition $\arg(\tilde{\alpha}_j^*(t)) = \pi + \arg(\langle k_t^{(\mathfrak{R}^n)}|\mathsf{L}_j(t)|k_t^{(\mathfrak{R}^n)}\rangle)$ in (4.62), we obtain a quadratic equation in $|\tilde{\alpha}_j(t)|$ for the optimum,

$$\langle\varphi_0^k|\mathsf{\Gamma}'_{j,\tilde{\boldsymbol{\alpha}}}|\varphi_0^k\rangle = \langle k_t^{(\mathfrak{R}^n)}|\mathsf{L}_j^\dagger(t)\mathsf{L}_j(t) + |\tilde{\alpha}_j(t)|^2|k_t^{(\mathfrak{R}^n)}\rangle - 2|\tilde{\alpha}_j^*(t)||\langle k_t^{(\mathfrak{R}^n)}|\mathsf{L}_j(t)|k_t^{(\mathfrak{R}^n)}\rangle|. \tag{4.63}$$

It is easy to see that Eq. (4.63) attains its minimum for

$$\tilde{\alpha}_j(t,\mathfrak{R}^n,\{|\varphi_0^i\rangle\}) = -\frac{\langle k_t^{(\mathfrak{R}^n)}|\mathsf{L}_j(t)|k_t^{(\mathfrak{R}^n)}\rangle}{\langle k_t^{(\mathfrak{R}^n)}|k_t^{(\mathfrak{R}^n)}\rangle} = -\frac{\langle\varphi_0^k|\mathsf{K}_{\mathfrak{R}^n}^\dagger(t)\mathsf{L}_j(t)\mathsf{K}_{\mathfrak{R}^n}(t)|\varphi_0^k\rangle}{\langle\varphi_0^k|\mathsf{K}_{\mathfrak{R}^n}^\dagger(t)\mathsf{K}_{\mathfrak{R}^n}(t)|\varphi_0^k\rangle}, \tag{4.64}$$

so that the optimal partial jump rates are given by

$$\langle\varphi_0^k|\mathsf{\Gamma}'_{j,\tilde{\boldsymbol{\alpha}}}|\varphi_0^k\rangle = \langle\varphi_0^k|\mathsf{K}_{\mathfrak{R}^n}^\dagger(t)\mathsf{L}_j^\dagger(t)\mathsf{L}_j(t)\mathsf{K}_{\mathfrak{R}^n}(t)|\varphi_0^k\rangle - \frac{|\langle\varphi_0^k|\mathsf{K}_{\mathfrak{R}^n}^\dagger(t)\mathsf{L}_j(t)\mathsf{K}_{\mathfrak{R}^n}(t)|\varphi_0^k\rangle|^2}{\langle\varphi_0^k|\mathsf{K}_{\mathfrak{R}^n}^\dagger(t)\mathsf{K}_{\mathfrak{R}^n}(t)|\varphi_0^k\rangle}. \tag{4.65}$$

This resummation of the jump expansion, where $\tilde{\alpha}_j(t,\mathfrak{R}^n,\{|\varphi_0^i\rangle\})$ depends also on the initial pure state decomposition $\{|\varphi_0^i\rangle\}$, see Eq. (4.64), allows minimizing the jump rates $\mathrm{Tr}[\mathsf{\Gamma}_{\boldsymbol{\alpha}}\rho_t^{(n)}]$ on a level of even smaller constituent rates $\langle\varphi_0^k|\mathsf{\Gamma}'_{j,\tilde{\boldsymbol{\alpha}}}|\varphi_0^k\rangle$. In principle, this holds the potential to achieve an even higher convergence of the jump expansion than the resummation with $\tilde{\alpha}_j(t,\mathfrak{R}^n)$, Eq. (4.51), which does not make use of this information. We want to stress here, however, that this additional handle of optimization comes at the price that $\{|\varphi_0^i\rangle\}$ is not defined unambiguously. In general, there exist

infinitely many different decompositions of ρ_0, each resulting, in principle, in a different optimum $\left(\tilde{\alpha}_j, \langle\varphi_0^k|\Gamma'_{j,\tilde{\boldsymbol{\alpha}}}|\varphi_0^k\rangle\right)$ and therefore in different convergence properties of the optimized jump expansion. It is not clear how an additional optimization over $\{|\varphi_0^i\rangle\}$ can be performed since there are no general parametrizations of pure state decompositions available.

There exists one important case however, where the resummations with $\tilde{\alpha}_j(t, \mathfrak{R}^n)$ and with $\tilde{\alpha}_j(t, \mathfrak{R}^n, \{|\varphi_0^i\rangle\})$ coincide, namely for pure initial states $\rho_0 = |\psi_0\rangle\langle\psi_0|$. Then, the summation index k in Eq. (4.64) vanishes and we have

$$\tilde{\alpha}_j(t, \mathfrak{R}^n) = -\frac{\langle\psi_t^{(\mathfrak{R}^n)}|\mathsf{L}_j(t)|\psi_t^{(\mathfrak{R}^n)}\rangle}{\langle\psi_t^{(\mathfrak{R}^n)}|\psi_t^{(\mathfrak{R}^n)}\rangle}, \tag{4.66}$$

equivalent to Eq. (4.51). Note that the states $|\psi_t^{(\mathfrak{R}^n)}\rangle$ involved here are the pure state quantum trajectories defined in Eq. (4.37).

This connection of the pure-state-conditioned resummation (4.66) of the jump expansion to the field of quantum trajectories is interesting in its own right, since it sheds new light on the pointer states introduced in Chap. 2. The reason is that the jump operators $\mathsf{L}_{j,\tilde{\boldsymbol{\alpha}}}$ with $\tilde{\boldsymbol{\alpha}}$ given by Eq. (4.66) have already been used to define the so-called orthogonal unraveling of the master equation, in which jumps occur between orthogonal subspaces [69]. The deterministic, continuous part of this orthogonal unraveling is a nonlinear evolution equation for pure states $|\psi\rangle$ whose fixed points were shown to be the pointer states for several paradigmatic Markovian master equations [49, 51, 61]. It was furthermore conjectured that one can obtain the pointer states of any given master equation in this way, if they exist, see Sec. 3.1.2. In view of these results, one may actually regard the minimality of the jump rates $\mathrm{Tr}[\Gamma_{\boldsymbol{\alpha}}\rho_t^{(n)}]$ in Eq. (4.52) as a proof of the postulate that pointer states should be the states with the slowest increase of entropy due to jumps. Furthermore, the empirical statement that pointer states exist, if the environment singles out a preferred basis, is substantiated by the derivations of the previous section: If the jump operators L_j commute, the system is driven towards the simultaneous eigenstates of all L_j. Only the Hamiltonian H may hinder the system from reaching them. Those states for which the two mentioned processes balance, *i.e.* the fixed points of the continuous nonlinear evolution, can then be identified with the pointer states.

The optimal adaptive jump operators $\mathsf{L}_{j,\tilde{\boldsymbol{\alpha}}}$ for quantum trajectories given by Eq. (4.66) have been applied in yet another context: the have been used to minimize the average algorithmic information in the outcome of a fictitious measurement [70], in the sense of Sec. 4.2.2. Following this line of thought, optimal adaptive updates of the jump operators can also be used to optimize the trajectories for completely different objectives, for example, in optimal control [71]. In contrast, our objective in this section is to derive a highly convergent expansion for ρ_t, and we achieve this with either of the resummations (4.51), (4.64), or (4.66). In this context, the quantum trajectory adapted resummation (4.66) is therefore not the most general way to perform a resummation. In particular, the possibility to condition the adaptive update of L_j on a mixed state density matrix as in

Eq. (4.51) is not contained in Eq. (4.66). This is, for example, a prerequisite for deriving suboptimal resummations of the jump expansion based on incomplete information about the system, which we will demonstrate in the following.

4.3.2 Suboptimal Resummations

The biggest obstacle to an analytical or numerical assessment of the optimal adaptive jump expansion is the need to evaluate the jump time multi-integrals, see Eq. (4.27). In particular, the record-dependent complex shifts $\tilde{\boldsymbol{\alpha}}(t, \mathfrak{R}^n)$ imply that the jump and the continuous evolution superoperators in the integrand depend on all previous jump times. Hence, for the practical purposes of deriving analytic approximations or implementing efficient numerical algorithms for open quantum dynamics, it may be advisable to sacrifice some of the convergence of the optimal resummation for a simpler algebraic structure of the integrand [20]. It is clear how such a simpler, *suboptimal* resummation is related to the optimal one: Some of the dependencies of the optimal complex shifts $\tilde{\boldsymbol{\alpha}}$ of the jump operators must be eliminated, *i.e.* only *part* of the information contained in the jump record $\mathfrak{R}^n$ should be used for a suboptimal $\check{\boldsymbol{\alpha}}$. From the many conceivable choices for such a suboptimal resummation, we will present three different ones: the first only makes use the jump count n, in the second, $\check{\boldsymbol{\alpha}}$ is constant between successive jumps, and in the third, $\check{\boldsymbol{\alpha}}$ is adapted only to the jump times t_n.

The general procedure to obtain a suboptimal $\check{\boldsymbol{\alpha}}$ is predetermined by the derivation of the optimal $\tilde{\boldsymbol{\alpha}}$ in the previous section. There, we noted that weights $w_n(t)$ of the jump terms increase with rates $\mathrm{Tr}[\mathsf{\Gamma}_{\boldsymbol{\alpha}}\rho_t^{(n)}]$. The $\mathrm{Tr}[\mathsf{\Gamma}_{\boldsymbol{\alpha}}\rho_t^{(n)}]$, in turn, are the sum of the positive partial rates $\mathrm{Tr}[\mathsf{\Gamma}_{j,\boldsymbol{\alpha}}\rho_t^{(\mathfrak{R}^n)}]$ that depend on the entire jump record $\mathfrak{R}^n$ and on time. In order to minimize $\mathrm{Tr}[\mathsf{\Gamma}_{\boldsymbol{\alpha}}\rho_t^{(n)}]$, it is therefore necessary to minimize all partial rates separately, which can only be accomplished by a record and time dependent $\tilde{\boldsymbol{\alpha}}(t, \mathfrak{R}^n)$. In contrast, if we do not minimize $\mathrm{Tr}[\mathsf{\Gamma}_{\boldsymbol{\alpha}}\rho_t^{(n)}]$ on the level of the smallest possible partial rates, but minimize a sub-sum of them with a single $\check{\boldsymbol{\alpha}}$, the obtained $\mathrm{Tr}[\mathsf{\Gamma}_{\check{\boldsymbol{\alpha}}}\rho_t^{(n)}]$ will generally be higher than $\mathrm{Tr}[\mathsf{\Gamma}_{\tilde{\boldsymbol{\alpha}}}\rho_t^{(n)}]$ but $\check{\boldsymbol{\alpha}}$ will no longer depend on the full jump record.

The most drastic reduction in the above sense is to minimize $\mathrm{Tr}[\mathsf{\Gamma}_{\boldsymbol{\alpha}}\rho_t^{(n)}]$ in Eq. (4.46) *directly* with a single $\check{\boldsymbol{\alpha}}(t, n)$, *i.e.* to make no decomposition into partial rates at all. Proceeding in the same fashion as for the optimal resummation (4.51), we use the definition (4.20) of $\mathsf{L}_{j,\boldsymbol{\alpha}}$ and expand the product in Eq. (4.46),

$$\mathrm{Tr}\left[\mathsf{\Gamma}_{\boldsymbol{\alpha}}\rho_t^{(n)}\right] = \sum_j \mathrm{Tr}[(\mathsf{L}_j^\dagger \mathsf{L}_j + |\alpha_j|^2)\rho_t^{(n)}] + 2\,\mathrm{Re}(\alpha_j^*\,\mathrm{Tr}[\mathsf{L}_j\rho_t^{(n)}]). \tag{4.67}$$

As before, the phase requirement $\arg(\check{\alpha}_j^*(t,n)) = \pi + \arg(\mathrm{Tr}[\mathsf{L}_j\rho_t^{(n)}])$ makes the second term as negative as possible, which allows us to minimize a real quadratic equation using

$$\check{\alpha}_j(t,n) = -\frac{1}{\mathrm{Tr}\,\rho_t^{(n)}}\,\mathrm{Tr}[\mathsf{L}_j\rho_t^{(n)}]. \tag{4.68}$$

As mentioned above, the corresponding jump rate

$$\mathrm{Tr}\left[\Gamma_{\check{\boldsymbol{\alpha}}}\rho_t^{(n)}\right] = \sum_{j,n}\mathrm{Tr}\left(\mathsf{L}_j^\dagger\mathsf{L}_j\rho_t^{(n)}\right) - \frac{1}{\mathrm{Tr}\,\rho_t^{(n)}}|\,\mathrm{Tr}(\mathsf{L}_j\rho_t^{(n)})|^2 \tag{4.69}$$

is generally higher than the optimum $\mathrm{Tr}[\Gamma_{\tilde{\boldsymbol{\alpha}}}\rho_t^{(n)}]$ in Eq. (4.65). In the examples in Chap. 5 we will see that even this rather drastic deviation from the optimum may still yield a highly convergent jump expansion.

Making a somehow less radical intervention on the optimal resummation, $\tilde{\boldsymbol{\alpha}}(t,\mathfrak{R}^n)$, we may choose to keep the dependence on the jump times. Grouping together all partial rates $\mathrm{Tr}[\Gamma_{j,\boldsymbol{\alpha}}\rho_t^{(\mathfrak{R}^n)}]$ with the same jump times, we obtain a decomposition into $\mathrm{Tr}[\Gamma_{j,\boldsymbol{\alpha}}\rho_t^{(\mathfrak{t}^n)}]$ given by

$$\begin{aligned}\mathrm{Tr}\left[\Gamma_{\boldsymbol{\alpha}}\rho_t^{(n)}\right] &= \sum_j \mathrm{Tr}\left[\mathsf{L}_{j,\boldsymbol{\alpha}}^\dagger(t)\mathsf{L}_{j,\boldsymbol{\alpha}}(t)\rho_t^{(n)}\right] = \sum_{j,\{\mathfrak{R}^n\}}\mathrm{Tr}\left[\mathsf{L}_{j,\boldsymbol{\alpha}}^\dagger(t)\mathsf{L}_{j,\boldsymbol{\alpha}}(t)\rho_t^{(\mathfrak{R}^n)}\right]\\ &= \sum_{j,\{\mathfrak{t}^n\}}\mathrm{Tr}\left[\mathsf{L}_{j,\boldsymbol{\alpha}}^\dagger(t)\mathsf{L}_{j,\boldsymbol{\alpha}}(t)\rho_t^{(\mathfrak{t}^n)}\right] = \sum_{j,\{\mathfrak{t}^n\}}\mathrm{Tr}\left[\Gamma_{j,\boldsymbol{\alpha}}\rho_t^{(\mathfrak{t}^n)}\right].\end{aligned} \tag{4.70}$$

Here, $\mathfrak{t}^n$ denotes the tuple of all jump times $\mathfrak{t}^n = (t_1,\ldots,t_n)$ providing partial information about the entire jump record $\mathfrak{R}^n = (j_1,t_1;\ldots;j_n,t_n)$. The symbol $\sum_{\{\mathfrak{t}^n\}}$ therefore denotes the multi-integral over all jump times. Each rate $\mathrm{Tr}[\Gamma_{j,\boldsymbol{\alpha}}\rho_t^{(\mathfrak{t}^n)}]$ is now minimized by a $\mathfrak{t}^n$-dependent $\check{\boldsymbol{\alpha}}$ derived in the same fashion as above,

$$\check{\alpha}_j(t,\mathfrak{t}^n) = -\frac{1}{\mathrm{Tr}\,\rho_t^{(\mathfrak{t}^n)}}\,\mathrm{Tr}[\mathsf{L}_j\rho_t^{(\mathfrak{t}^n)}]. \tag{4.71}$$

The total jump rates, and hence the convergence of the jump expansion, for this optimization will be generally between the previous suboptimal resummation, Eqs. (4.68) and (4.69), and the optimal resummation, Eqs. (4.51) and (4.52). It should be close to the optimum in cases where all jump operators act similarly on any density matrix ρ.

Another significant simplification of the jump terms can be achieved by leaving $\boldsymbol{\alpha}$ piecewise constant between successive jump. In this case, $\rho_t^{(\mathfrak{R}^n)}$ in Eq. (4.30) evolves under a constant generator between t_i and t_{i+1}, with $\exp[\mathcal{L}_{\boldsymbol{\alpha}}(t_{i+t}-t_i)]$, unless the Hamiltonian H or the jump operators L_j exhibit a time dependence of their own. To achieve this, we simply set $t = t_n$ in the optimal $\tilde{\boldsymbol{\alpha}}(t,\mathfrak{R}^n)$ in Eq. (4.51) and obtain

$$\check{\alpha}_j(\mathfrak{R}^n) = -\frac{1}{\mathrm{Tr}\,\rho_{t_n}^{(\mathfrak{R}^n)}}\,\mathrm{Tr}(\mathsf{L}_j\rho_{t_n}^{(\mathfrak{R}^n)}). \tag{4.72}$$

We note that, within the series of transformations (4.30) leading to $\rho_t^{(\mathfrak{R}^n)}$, instantaneous jumps effect the most drastic changes of the state and therefore of $\tilde{\boldsymbol{\alpha}}(t,\mathfrak{R}^n)$. Hence, we expect that the last suboptimal resummation, where $\check{\boldsymbol{\alpha}}$ is only updated when jumps occur, should be very close to the optimal one, in particular, if the waiting time between

the jumps is smaller than the time scale of the coherent evolution.

Finally, we deduce a suboptimal resummation which makes the jump terms $\rho_t^{(n)}$ analytically accessible, as we will see in Chap. 5. It builds on the resummation (4.72) and, in addition, eliminates the dependence on the jump times [20]. If we forget about the jump times t_n, it makes no sense to condition $\boldsymbol{\alpha}$ on states ρ_t at specific times, as was the case in all previous resummations. To eliminate this state dependence in an unbiased fashion, we assume complete ignorance of the state, except immediately after a jump with index j_n,

$$\rho_t^{(\mathfrak{R}^n)} \propto \mathbb{1} \quad \text{for } t \neq t_n, \tag{4.73}$$

$$\rho_t^{(\mathfrak{R}^n)} \propto \mathsf{L}_{j_n,\boldsymbol{\alpha}(\mathfrak{R}^{n-1})} \mathbb{1} \mathsf{L}^\dagger_{j_n,\boldsymbol{\alpha}(\mathfrak{R}^{n-1})} \quad \text{for } t = t_n. \tag{4.74}$$

Plugging this approximation into Eq. (4.72), we obtain the *state independent* adaptive update

$$\check{\alpha}_j(\mathfrak{j}^n) = -\frac{\mathrm{Tr}\left(\mathsf{L}_j \mathsf{L}_{j_n,\check{\boldsymbol{\alpha}}(\mathfrak{j}^{n-1})} \mathsf{L}^\dagger_{j_n,\check{\boldsymbol{\alpha}}(\mathfrak{j}^{n-1})}\right)}{\mathrm{Tr}\left(\mathsf{L}_{j_n,\check{\boldsymbol{\alpha}}(\mathfrak{j}^{n-1})} \mathsf{L}^\dagger_{j_n,\check{\boldsymbol{\alpha}}(\mathfrak{j}^{n-1})}\right)}. \tag{4.75}$$

Note that $\check{\boldsymbol{\alpha}}$ is now only a function of the sequence $\mathfrak{j}^n = (j_1, \ldots, j_n)$ of past jumps. Of course, one could also choose to eliminate the $\mathfrak{t}^n$-dependence of $\boldsymbol{\alpha}$ while keeping its t-dependence, analogous to Eqs. (4.70) and (4.71). Only the furthest possible reduction of time-dependencies in the jump time multi-integral (4.27) should, however, render the jump terms analytically accessible. We expect the convergence of the resummation (4.75) to be particularly close to that of the optimal resummation if different jumps mutually exclude each other, *i.e.* if a jump with index j_i modifies the system state in such a way that a jump with j_{i+1} is unlikely to occur shortly after. For example, this is the case for a QND measurement as defined in Sec. 2.1.3, where a measurement with outcome j_i enhances the probability to observe the same outcome j_i in second measurement as well.

5 Analytic Approximations to Markovian Dynamics

In the previous section we derived the jump expansion for general Markovian open quantum dynamics and optimized its convergence by means of an adaptive resummation. We now demonstrate in two important open quantum models that this highly convergent series, similarly to the closed system Dyson series, facilitates finding analytical approximations of the system dynamics. First, we consider the spatial detection of a free particle and, second, the Landau-Zener problem with dephasing. The derived approximate descriptions not only exhibit an unprecedented degree of accuracy, but the analytically accessible expansion terms also put forward an intuitive picture of the open system dynamics [20].

5.1 Spatial Detection of a Free Particle

As an application of the jump expansion and its resummations, consider the dynamics of a free particle in one dimension, undergoing continuous spatial detection. Our goal is to find an analytical description of the particle's dynamics during the detection process. Since the complicated time-dependent, adaptive structure of the optimally convergent resummation does not favor an analytical treatment, we will here use the simpler suboptimal resummation, Eq. (4.75) [20]. The present example allows us to illustrate that the resummation (4.75) is simple enough to access its leading order terms analytically, and that it results in a close to optimal convergence of the jump expansion.

The spatial detection setting we have in mind amounts to a continuous measurement of whether the particle is located in the left or in the right half space. This setup was studied by a number of authors since its first proposal in 1969 by Allcock [72–77]. The interest at that time was the determination of the arrival time of a moving quantum particle at a specific position, as an operational approach to a desired, more general quantum time operator. Contrary to our intuition based on classical measurements, Allcock found that the particle eludes detection by being reflected at the measurement boundary [72]. The probability for this to happen approaches unity if one performs this measurement ever more precisely[1]. The failure of this simplest conceivable time measurement highlighted the conceptual difficulties of regarding time as more than a parameter in quantum dynamics [79]. Experimentally, the particle detection described above can be realized, for example, by a laser which is tuned to excite the particle's

[1] This was the first evidence of what today is called the *quantum Zeno effect* [78].

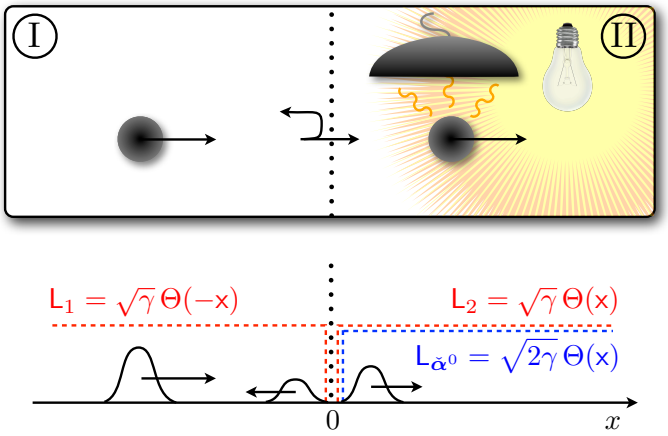

Figure 5.1: Schematic diagram of spatial detection: A free particle coming from the left, $x < 0$, region I, is excited by a suitable light source upon entering the right half space, $x \geq 0$, region II. When a photon detector picks up the scattered light, we know that the particle must be in region II. Surprisingly, the particle is partially reflected at the measurement boundary $x = 0$. Formally, the average, nonselective particle dynamics for an ideal projective left-right measurement applied with rate γ is described by a Markovian master equation with two jump operators, $\mathsf{L}_1 = \sqrt{\gamma}\Theta\,(-\mathsf{x})$ and $\mathsf{L}_2 = \sqrt{\gamma}\Theta\,(\mathsf{x})$, Eq. (5.1). The dynamics under the master equation, in turn, is decomposed by the jump expansion, Eq. (5.2). The adaptive resummation (4.75) of the jump expansion increases the convergence and makes the jump terms analytically accessible.

internal structure and which illuminates only the right half space [80], see the schematic diagram Fig. 5.1.

While the qualitative observation that the particle is partially reflected by the measurement stands for more than four decades, its exact dynamics remains unknown. This may be attributed to the fact that, despite its conceptual and formal simplicity, the continuous left-right detection process is not solvable analytically. As we will see in the following, the resummed jump expansion unveils an analytically accessible approximate description for the detection process which, in particular, allows one to determine the reflection probability as a function of the measurement rate. In facilitating a treatment very similar to the usual quantum reflection at a potential step, this description is not only physically intuitive but also highly accurate.

5.1.1 Jump Expansion for Spatial Detection

In Sec. 3.3 we saw that the average or nonselective dynamics under a continuous measurement, *i.e.* when disregarding the measurement outcomes, is described by a Markovian master equation involving the measurement operators M_i, see Eq. (3.76). Specifically, we here make the assumption of an ideal projective left-right measurement which is de-

scribed by the measurement operators $\mathsf{M}_1 = \Theta(-\mathsf{x}) \propto \mathsf{L}_1$ and $\mathsf{M}_2 = \Theta(\mathsf{x}) \propto \mathsf{L}_2$ ($\Theta(\mathsf{x})$ is the Heaviside step function of the position operator x). Using the Hamiltonian for a free particle of mass m and the measurement rate γ, the nonselective measurement master equation reads

$$\begin{aligned}\partial_t \rho_t &= -\frac{i}{\hbar}\,[\mathsf{H}, \rho_t] + \sum_{i=1}^{2} \left(\mathsf{L}_i \rho_t \mathsf{L}_i^\dagger - \frac{1}{2} \mathsf{L}_i^\dagger \mathsf{L}_i \rho_t - \frac{1}{2} \rho_t \mathsf{L}_i^\dagger \mathsf{L}_i \right) \\ &= -\frac{i}{\hbar} \left[\frac{\mathsf{p}^2}{2m}, \rho_t \right] + \gamma(\Theta(\mathsf{x})\rho_t\Theta(\mathsf{x}) + \Theta(-\mathsf{x})\rho_t\Theta(-\mathsf{x}) - \rho_t), \end{aligned} \tag{5.1}$$

which defines the jump operators $\mathsf{L}_1 = \sqrt{\gamma}\Theta\,(-\mathsf{x})$ and $\mathsf{L}_2 = \sqrt{\gamma}\Theta\,(\mathsf{x})$.

The jump expansion for this master equation, $\rho_t = \sum_n \rho_t^{(n)}$, Eq. (4.27), without resummation, $\boldsymbol{\alpha} = 0$, is composed of the jump terms

$$\begin{aligned}\rho_t^{(n)} = \gamma^n \sum_{j_1 \dots j_n = \pm 1} \int_0^t \mathrm{d}t_n \int_0^{t_n} \mathrm{d}t_{n-1} \dots \int_0^{t_2} \mathrm{d}t_1 e^{-\frac{i}{\hbar}\mathsf{H}^{\mathrm{eff}}(t-t_n)} \Theta(j_n\mathsf{x}) e^{-\frac{i}{\hbar}\mathsf{H}^{\mathrm{eff}}(t_n-t_{n-1})} \Theta(j_{n-1}\mathsf{x}) \\ \dots \times \Theta(j_1\mathsf{x}) e^{-\frac{i}{\hbar}\mathsf{H}^{\mathrm{eff}}t_1} \rho_0 e^{\frac{i}{\hbar}\mathsf{H}^{\mathrm{eff}}t_1} \Theta(j_1\mathsf{x}) \dots \Theta(j_{n-1}\mathsf{x}) e^{\frac{i}{\hbar}\mathsf{H}^{\mathrm{eff}}(t_n-t_{n-1})} \Theta(j_n\mathsf{x}) e^{\frac{i}{\hbar}\mathsf{H}^{\mathrm{eff}}(t-t_n)},\end{aligned} \tag{5.2}$$

with $\mathsf{H}^{\mathrm{eff}} = \mathsf{p}^2/2m - i\hbar\gamma/2$. As described in Sec. 4.2.3, the weights of the expansion terms, $w_n(t) = \operatorname{Tr} \rho_t^{(n)}$, follow a cascaded time evolution which populates the $(n+1)$-th term with the jump rate $\operatorname{Tr}[\Gamma_\alpha \rho_t^{(n)}]$. Since $\operatorname{Tr}[\Gamma_\alpha \rho_t^{(n)}]$ is proportional to the norm decrease under $\mathsf{H}^{\mathrm{eff}}$, see Eq. (4.46), we have $\partial_t w_n(t) = \gamma w_{n-1}(t) - \gamma w_n(t)$ for the above jump terms. Noting that such stepwise transitions at a fixed rate define the Poisson process, we see that the $w_n(t)$ are Poisson-distributed,

$$w_n(t) = \frac{(\gamma t)^n}{n!} e^{-\gamma t}. \tag{5.3}$$

Therefore, at a given time t, terms with an average number of $\bar{n} = \gamma t$ jumps make up the jump expansion for $\boldsymbol{\alpha} = 0$, and we need at least about $2\bar{n}$ terms for a reliable estimate of ρ_t.

Many of these $2\bar{n}$ terms essentially contain redundant information, however. To see this, consider a typical detection setting in which the particle is initially located entirely on one side, say on the left, and moves towards the measurement boundary at $x = 0$. The first jump then projects the particle to the left hand side with near unit probability. Since this projection does not change the wave function nor its dynamics, $\rho_t^{(1)}$ is typically indistinguishable from $\rho_t^{(0)}$. More generally, the jumps have very little effect as long as the particle is far away from the measurement boundary. In fact, the jump expansion will be dominated by those largely redundant terms since a free particle will only spend a small fraction of time near $x = 0$ before going off to the left or to the right. Therefore, the convergence of the expansion $\rho_t = \sum_n \rho_t^{(n)}$ with $\rho_t^{(n)}$ given by Eq. (5.2) is unnecessarily

low which leaves considerable room for an optimization through resummation.

5.1.2 Resummation and Analytical Approximation

Let us now consider a resummation of the jump expansion. Since our goal is to treat the jump terms analytically, we will use the particularly simple suboptimal resummation $\check{\boldsymbol{\alpha}}(\mathsf{j}^n)$ defined by Eq. (4.75). It updates the jump operators $\mathsf{L}_{j,\check{\boldsymbol{\alpha}}}$ whenever a jump occurs conditioned on the sequence of jump indices $\mathsf{j}^n = (j_1, \ldots, j_n)$ of all previous jumps. In the following we will see that the resulting jump terms $\rho_t^{(n)}$ simply describe the n-fold scattering of the initial state at an imaginary potential step. A treatment analogous to the real potential step problem allows us to determine the reflection probability of each separate scattering event as a contribution to the total reflection probability of a particle undergoing the spatial detection process.

As mentioned above, for a particle initially located on the left, the first jump typically occurs with the jump operator L_1, *i.e.* we have $j_1 = 1$. Equation (4.75) with $\mathsf{L}_1 = \sqrt{\gamma}\Theta(-\mathsf{x})$ and $\mathsf{L}_2 = \sqrt{\gamma}\Theta(\mathsf{x})$ then yields the new shifts $\check{\alpha}_1 = -\sqrt{\gamma}$ and $\check{\alpha}_2 = 0$ and therefore the updated jump operators

$$\mathsf{L}_{1,\check{\boldsymbol{\alpha}}} = -\sqrt{\gamma}\Theta(\mathsf{x}), \tag{5.4}$$

$$\mathsf{L}_{2,\check{\boldsymbol{\alpha}}} = \sqrt{\gamma}\Theta(\mathsf{x}). \tag{5.5}$$

In the following, we start the time evolution with the above jump operators instead of L_1 and L_2. This reduces the jump rate from the beginning on. Note that the minus sign in $\mathsf{L}_{1,\check{\boldsymbol{\alpha}}(1)}$ is physically irrelevant—it cancels when inserted into the master equation (5.1). Both $\mathsf{L}_{1,\check{\boldsymbol{\alpha}}}$ and $\mathsf{L}_{2,\check{\boldsymbol{\alpha}}}$ are therefore equivalent and one can use a single jump operator $\mathsf{L}_{\check{\boldsymbol{\alpha}}} = \sqrt{2\gamma}\Theta(\mathsf{x})$ instead. With only one jump operator, j^n reduces to an n-tuple of one and the same jump index so that $\check{\boldsymbol{\alpha}}(\mathsf{j}^n)$ is characterized by a single complex number $\check{\alpha}$ and the length n of the tuple—we hence write $\check{\alpha}^n$ for $\check{\boldsymbol{\alpha}}(\mathsf{j}^n)$.

The Leading Order Term $\rho_t^{(0)}$

The above simplifications hence suggest to a use single initial jump operator given by

$$\mathsf{L}_{\check{\alpha}^0} = \sqrt{2\gamma}\Theta(\mathsf{x}), \tag{5.6}$$

which implies the effective Hamiltonian, see Eq. (4.24),

$$\mathsf{H}^{\text{eff}}_{\check{\alpha}^0} = \mathsf{H} - \frac{i\hbar}{2}\mathsf{L}^\dagger_{\check{\alpha}^0}\mathsf{L}_{\check{\alpha}^0} = \frac{\mathsf{p}^2}{2m} - i\hbar\gamma\Theta(\mathsf{x}). \tag{5.7}$$

The leading order jump term $\rho_t^{(0)}$ is therefore given by

$$\begin{aligned}\rho_t^{(0)} &= \exp\left[-\frac{i}{\hbar}\mathsf{H}_{\check{\alpha}^0}^{\text{eff}} t\right] \rho_0 \exp\left[\frac{i}{\hbar}\mathsf{H}_{\check{\alpha}^0}^{\text{eff}\dagger} t\right] \\ &= \exp\left[\left(-\frac{i}{\hbar}\frac{\mathsf{p}^2}{2m} - \gamma\Theta\left(\mathsf{x}\right)\right) t\right] \rho_0 \exp\left[\left(\frac{i}{\hbar}\frac{\mathsf{p}^2}{2m} - \gamma\Theta\left(\mathsf{x}\right)\right) t\right]. \end{aligned} \tag{5.8}$$

It describes the scattering of a free, one-dimensional quantum particle at a negative imaginary potential step $-i\hbar\gamma\Theta(x)$. With the jump rate $\mathrm{Tr}[\mathsf{L}_{\check{\alpha}^0}^\dagger \mathsf{L}_{\check{\alpha}^0} \rho_t^{(0)}]$ proportional to the norm decay under $\mathsf{H}_{\check{\alpha}^0}^{\text{eff}}$, Eq. (5.7), we see that the first jump can only occur after the particle has at least partially traversed the measurement boundary. Comparing this to the situation without resummation where the jump rate was γ, irrespective of the particle position, we get a first impression of how the resummation increases the convergence of the jump expansion.

To determine the leading order reflection probability R_0, we make a stationary ansatz for scattering off the imaginary potential step in analogy to the real potential step problem. This is done by choosing as initial state $\rho_0 = |\psi_{k_0}\rangle\langle\psi_{k_0}|$, an incoming plane wave from the left in region I (see schematic diagram Fig. 5.1), and a reflected and transmitted wave in region I and region II, respectively. Hence, the initial wave function $|\psi_{k_0}\rangle$ reads, in position representation,

$$\psi_{k_0}(x) = A\exp(ik_0x) + B\exp(-ik_0x), \qquad \text{for } x \leq 0, \text{ (region I)}, \tag{5.9}$$

$$\psi_{k_0}(x) = C\exp(i\kappa x) + D\exp(-i\kappa x), \qquad \text{for } x > 0, \text{ (region II)}. \tag{5.10}$$

With $\psi_{k_0}(x)$ defined as a stationary state and hence an eigenvector of the Hamiltonian $\mathsf{H}_{\check{\alpha}^0}^{\text{eff}}$, the associated eigenvalue in region I, without the potential, is equal to that in region II, with the imaginary potential,

$$\kappa = \sqrt{k_0^2 + i\frac{2m\gamma}{\hbar}}. \tag{5.11}$$

With the imaginary part of the wave vector κ being positive, the solution $\exp(-i\kappa x)$ in region II is not normalizable and therefore $D = 0$. The continuity of the wave function and its first derivative at $x = 0$ yields the following conditions for the coefficients A, B, and C,

$$A + B = C, \tag{5.12}$$

$$k_0(A - B) = \kappa C. \tag{5.13}$$

They allow determining the ratio of A and B,

$$\frac{B}{A} = \frac{k_0 - \kappa}{k_0 + \kappa}, \tag{5.14}$$

the absolute square of which is the probability of reflection R_0 for the leading order jump

term $\rho_t^{(0)}$. Inserting the expression (5.11) for κ we obtain

$$R_0(k_0) = \left| \frac{1 - \sqrt{1 + i\frac{2m\gamma}{\hbar k_0^2}}}{1 + \sqrt{1 + i\frac{2m\gamma}{\hbar k_0^2}}} \right|^2 \equiv \left| \frac{1 - \sqrt{1 + i/\varepsilon}}{1 + \sqrt{1 + i/\varepsilon}} \right|^2 = R_0(\varepsilon), \tag{5.15}$$

where we have introduced the dimensionless parameter[2] ε,

$$\varepsilon \equiv \frac{\hbar k_0^2}{2m\gamma} = \frac{E_{\text{in}}}{\hbar\gamma}. \tag{5.16}$$

Very similar to the reflection probability at a real potential step, $R_0(\varepsilon)$ is monotonically decreasing with the limiting values $R_0(0) = 1$ and $R_0(\varepsilon \to \infty) = 0$, see red dashed line in Fig. 5.4.

The above stationary ansatz is usually the basis for solving the scattering problem of an arbitrary initial wave packet $\rho_0 = |\psi_0\rangle\langle\psi_0|$ analytically [81]. In particular, the reflection probability $R(\psi_0)$ of $|\psi_0\rangle$ is determined by the integral over $R_0(k)$ weighted with the momentum distribution $|\psi_0(k)|^2$,

$$R(\psi_0) = \int \mathrm{d}k R_0(k) |\psi_0(k)|^2. \tag{5.17}$$

Moreover, one obtains the evolved state starting from the initial wave packet by considering the complex phases of the coefficients A, B, and C. For the present demonstration of the analytical treatment of the jump expansion it is however convenient to restrict our attention to plane waves or wave packets that have a sufficiently narrow momentum distribution to be treated as such.

In contrast to conventional scattering, the parts of $\rho_t^{(0)}$ in region II, which define the transmission probability $T_0(k_0)$, decay under the negative imaginary potential, see Eq. (5.8). With reflection and transmission properly defined only for outgoing scattering states, *i.e.* for $t \to \infty$ or $x \to \pm\infty$, the leading order contribution $T_0(k_0)$ to the transmission probability vanishes. In addition, the reflected part of $\rho_t^{(0)}$ goes off to the left, *i.e.* it stays in region I and experiences no further norm decay. Therefore, the weight of the leading order term $w_0(t) = \operatorname{Tr} \rho_t^{(0)}$ is equal to the reflection probability, $w_0(t) = R_0(k_0)$.

Note that the reflection probability $R_0(k_0)$ is conditioned on the absence of jumps as it applies to the leading order jump term $\rho_t^{(0)}$. It is therefore only the leading order contribution to the total reflection probability $R(k_0)$ under the master equation (5.1) and we have $R(k_0) \geq R_0(k_0)$, in general. In the following, we will consider the first order contribution.

[2] In fact, one can show that ε is the only free parameter in Eq. (5.1) for incoming plane waves $\rho_0 = |\psi_{k_0}\rangle\langle\psi_{k_0}|$ by using position coordinates in units of $1/k_0$ and deviding Eq. (5.1) by $E_{\text{in}}/\hbar$.

The First Order Term $\rho_t^{(1)}$

We saw above that the leading order contribution $R_0(k_0)$ to the reflection probability is determined by a stationary ansatz for the leading order jump term $\rho_t^{(0)}$ at an imaginary potential step. The treatment of the first order jump term $\rho_t^{(1)}$ turns out to be more involved, however. The reason is that the first jump projects a plane wave $|\psi_{k_0}\rangle$ in region I onto an exponential tail in region II, see Eqs. (5.9) and (5.10),

$$|\psi'_{k_0}\rangle = \mathsf{L}_{\check{\alpha}^0}|\psi_{k_0}\rangle = \sqrt{2\gamma}\Theta\left(\mathsf{x}\right)|\psi_{k_0}\rangle = \sqrt{2\gamma}\int \mathrm{d}x\Theta(x)\exp(i\kappa x)|x\rangle. \tag{5.18}$$

$|\psi'_{k_0}\rangle$ is now a wave packet that subsequently evolves in time. To determine its time evolution, we apply the update rule (4.75) to the jump operator $\mathsf{L}_{\check{\alpha}^0}$, Eq. (5.6), as is required by the resummation method for the jump expansion. We obtain the new shift $\check{\alpha}^1 = -\sqrt{2\gamma}$ leading to the new jump operator $\mathsf{L}_{\check{\alpha}^1}$ after the first jump,

$$\mathsf{L}_{\check{\alpha}^1} = -\sqrt{2\gamma}\Theta\left(-\mathsf{x}\right). \tag{5.19}$$

This results in the updated effective Hamiltonian

$$\mathsf{H}^{\mathrm{eff}}_{\check{\alpha}^1} = \mathsf{H} - \frac{i\hbar}{2}\mathsf{L}^\dagger_{\check{\alpha}^1}\mathsf{L}_{\check{\alpha}^1} = \frac{\mathsf{p}^2}{2m} - i\hbar\gamma\Theta\left(-\mathsf{x}\right). \tag{5.20}$$

The jump term $\rho_t^{(1)}$ for the initial plane wave $\rho_0 = |\psi_{k_0}\rangle\langle\psi_{k_0}|$ is now given by the wave packet $|\psi'_{k_0}\rangle$ evolved from the jump time t_1 to the final time t under $\mathsf{H}^{\mathrm{eff}}_{\check{\alpha}^1}$, and integrated over t_1,

$$\begin{aligned}\rho_t^{(1)} &= \int_0^t \mathrm{d}t_1 \exp\left[-\frac{i}{\hbar}\mathsf{H}^{\mathrm{eff}}_{\check{\alpha}^1}(t-t_1)\right]\mathsf{L}_{\check{\alpha}^0}|\psi_{k_0}\rangle\langle\psi_{k_0}|\mathsf{L}^\dagger_{\check{\alpha}^0}\exp\left[\frac{i}{\hbar}\mathsf{H}^{\mathrm{eff}\dagger}_{\check{\alpha}^1}(t-t_1)\right] \\ &= \int_0^t \mathrm{d}t_1 \exp\left[-\frac{i}{\hbar}\mathsf{H}^{\mathrm{eff}}_{\check{\alpha}^1}(t-t_1)\right]|\psi'_{k_0}\rangle\langle\psi'_{k_0}|\exp\left[\frac{i}{\hbar}\mathsf{H}^{\mathrm{eff}\dagger}_{\check{\alpha}^1}(t-t_1)\right].\end{aligned} \tag{5.21}$$

We see that, after the first jump, the imaginary potential shifts from the right to the left half space, and the initial stationary state $|\psi_{k_0}\rangle$ continues as a wave packet $|\psi'_{k_0}\rangle$. $|\psi'_{k_0}\rangle$, in turn, is exponentially squeezed to the right flank of the imaginary potential step, see Fig. (5.2). Its rapid dispersion in position space results in the fact that $|\psi'_{k_0}\rangle$ will again be partially scattered at the imaginary potential.

Let us now determine the first order reflection probability $R_1(k_0)$, which is that of the wave packet $|\psi'_{k_0}\rangle$, Eq. (5.18). Equation (5.17) states that the reflection probability of a wave packet is given by the integral over the k-dependent stationary reflection probability $R_0(k)$, weighted with the momentum distribution, $|\psi'_{k_0}(k)|^2$ in the present case. The wave function $\psi'_{k_0}(k)$ in momentum space, in turn, is given by the Fourier transform of the

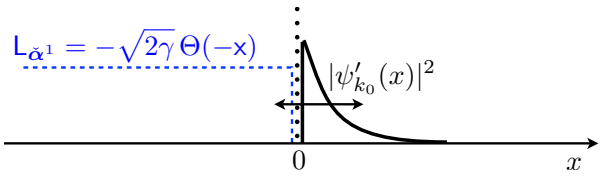

Figure 5.2: Wave function of the first order jump term $\rho_t^{(1)} = |\psi'_{k_0}\rangle\langle\psi'_{k_0}|$, Eq. (5.18), for an initial stationary wave $\rho_0 = |\psi_{k_0}\rangle\langle\psi_{k_0}|$, Eqs. (5.9) and (5.10), and with the resummation defined by Eq. (4.75). The first jump projects $|\psi_{k_0}\rangle$ onto its exponential tail on the right hand side. The jump operator is then updated from $\mathsf{L}_{\check{\alpha}^0} = \sqrt{2\gamma}\Theta\,(\mathsf{x})$ to $\mathsf{L}_{\check{\alpha}^1} = -\sqrt{2\gamma}\Theta\,(-\mathsf{x})$. Due to dispersion, the wave packet $|\psi'_{k_0}\rangle$ is again partially scattered at the imaginary potential step $-i\hbar\gamma\Theta(-x)$ defined by $\mathsf{L}_{\check{\alpha}^1}$.

position representation $\psi'_{k_0}(x)$ determined by Eq. (5.18),

$$\psi'_{k_0}(x) = \mathcal{N}\Theta(x)\exp(i\kappa x), \tag{5.22}$$

$$\psi'_{k_0}(k) = \frac{\mathcal{N}}{\sqrt{2\pi}}\int \mathrm{d}x\Theta(x)\exp[i(\kappa-k)x] = \frac{\mathcal{N}}{\sqrt{2\pi}}\frac{i}{\kappa-k}, \tag{5.23}$$

with κ given by Eq. (5.11). While $\mathcal{N} = \sqrt{2\,\mathrm{Im}(\kappa)}$ yields a normalized wave packet $|\psi'_{k_0}\rangle$, the convention used for the jump expansion is that $\rho_t^{(1)}$ is an unnormalized state, which implies that $\mathcal{N} = \sqrt{2\,\mathrm{Im}(\kappa)(1-R_0(k_0))}$ in the present case. For our intuitive description in terms of reflection probabilities $R_n(k_0)$, however, we will presently work with normalized wave packets $|\psi'_{k_0}\rangle$ and account for the additional factor $(1-R_0(k_0))$ later on.

Using Eq. (5.17) and taking into account that only the negative momentum components of $|\psi'_{k_0}\rangle$ are incident on the potential step, see Fig. (5.2), we obtain the reflection probability

$$\begin{aligned} R_1(k_0) &= \int_{-\infty}^{0}\mathrm{d}k R_0(k)|\psi'_{k_0}(k)|^2 + \int_0^{\infty}\mathrm{d}k|\psi'_{k_0}(k)|^2 \\ &= \int_{-\infty}^{\infty}\mathrm{d}k\left[\left|\frac{1-\sqrt{1+i2m\gamma/\hbar k^2}}{1+\sqrt{1+i2m\gamma/\hbar k^2}}\right|^2\Theta(-k)+\Theta(k)\right]\frac{\mathrm{Im}\left[\sqrt{k_0^2+i2m\gamma/\hbar}\right]}{\pi\left|\sqrt{k_0^2+i2m\gamma/\hbar}-k\right|^2}. \end{aligned} \tag{5.24}$$

Like in the case of the leading order reflection probability, we can recast $R_1(k_0)$ as a function of the dimensionless parameter ε, Eq. (5.16). This is done by using the

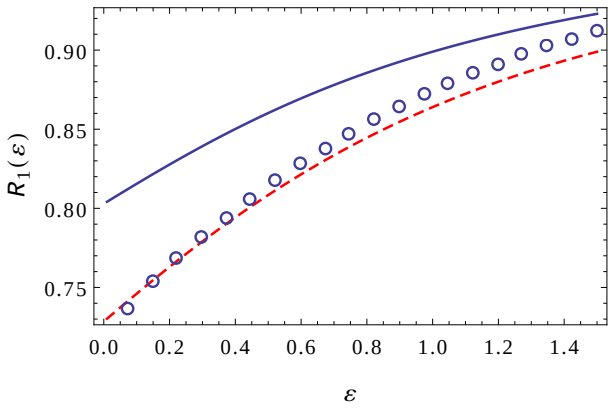

Figure 5.3: First order contribution $R_1(\varepsilon)$ to the reflection probability of a particle described by a plane wave $|\psi_{k_0}\rangle$, Eqs. (5.9) and (5.10), which undergoes spatial detection, Eq. (5.1). $R_1(\varepsilon)$ is determined as the probability for the wave packet $|\psi'_{k_0}\rangle$ after the first jump, Eq. (5.18), to be reflected at the negative imaginary potential step $-i\hbar\gamma\Theta(-\mathsf{x})$. It is a function of the dimensionless parameter $\varepsilon = E_{\rm in}/\hbar\gamma = \hbar k_0^2/2m\gamma$. We plot the numerically exact reflection probability of $|\psi'_{k_0}\rangle$ obtained by propagation on a grid (blue circles), the analytical approximation (5.25) based on the separation of positive and negative momentum components of $|\psi'_{k_0}\rangle$ (blue solid line), and the expression (5.27) which involves an additional correction term.

dimensionless wave vector $q = k/k_0$ in Eq. (5.24), which results in

$$R_1(\varepsilon) = \int_{-\infty}^{\infty} \mathrm{d}q \left[\left| \frac{1-\sqrt{1+i/\varepsilon q^2}}{1+\sqrt{1+i/\varepsilon q^2}} \right|^2 \Theta(-q) + \Theta(q) \right] \frac{\mathrm{Im}\left[\sqrt{1+i/\varepsilon}\right]}{\pi|\sqrt{1+i/\varepsilon}-q|^2}. \tag{5.25}$$

Quite surprisingly, the above analytical expression for $R_1(\varepsilon)$ deviates from its numerically exact value, see Fig. 5.3. The latter can be obtained by propagating the wave packet $|\psi'_{k_0}\rangle$ with the imaginary potential step on a grid. The reason for the deviation is that Eqs. (5.24) and (5.25) assume that interference terms between positive and negative momentum components have no influence on the scattering process. This is only admissible if the wave packet starts at a sufficient distance from the scattering potential so that positive and negative momentum components have time to separate and have no spatial overlap at the time of the scattering process. The wave packet $|\psi'_{k_0}\rangle$, Eqs. (5.22) and (5.23), is very close to the scattering potential, however, and hence these interference terms induce a small but nonvanishing probability current to the left, *i.e.* into region I,

$$|\langle\psi'_{k_0}(t)|\Theta(\mathsf{k})\,\Theta(-\mathsf{x})\,\Theta(-\mathsf{k})\,|\psi'_{k_0}(t)\rangle|^2 = |\langle\psi'_{k_0}|e^{i\mathsf{H}t/\hbar}\Theta(\mathsf{k})\,\Theta(-\mathsf{x})\,\Theta(-\mathsf{k})\,e^{-i\mathsf{H}t/\hbar}|\psi'_{k_0}\rangle|^2, \tag{5.26}$$

for $t > 0$. These parts of the wave packet then decay under the imaginary potential in

region I, which effects a further decrease of the observed reflection probability. Neglecting the detailed dynamics of these interference terms, we assume that their norm decay occurs with rate 2γ. By using again dimensionless coordinates $q = k/k_0$, $r = xk_0$, and $\tau = tE_{\mathrm{in}}/\hbar$, we obtain a small correction term for $R_1(\varepsilon)$, Eq. (5.25),

$$R_1(\varepsilon) = \int_{-\infty}^{\infty} \mathrm{d}q \left[\left| \frac{1-\sqrt{1+i/\varepsilon q^2}}{1+\sqrt{1+i/\varepsilon q^2}} \right|^2 \Theta(-q) + \Theta(q) \right] \underbrace{\frac{\mathrm{Im}\left[\sqrt{1+i/\varepsilon}\right]}{\pi|\sqrt{1+i/\varepsilon}-q|^2}}_{|\varphi_\varepsilon'(q)|^2}$$
$$- \int \mathrm{d}\tau 2\varepsilon^{-1} e^{-2\tau/\varepsilon} \left| \langle \varphi_\varepsilon' | \mathsf{C}(\tau) | \varphi_\varepsilon' \rangle \right|^2, \tag{5.27}$$

with $\mathsf{C}(\tau) = \Theta(\mathsf{k})\,\Theta(-\mathsf{x}-2\mathsf{k}\tau)\,\Theta(-\mathsf{k})$. Here, the state $|\varphi_\varepsilon'\rangle$ denotes $|\psi_{k_0}'\rangle$ in dimensionless coordinates, $\varphi_\varepsilon'(r) = \mathcal{N}\Theta(r)\exp(i\varepsilon r)$ and $\varphi_\varepsilon'(q) = \mathcal{N} i/\sqrt{2\pi}(\sqrt{1+i/\varepsilon}-q)$. Note that, in comparison with Eq. (5.26), we have transferred the time evolution of the wave function to the operator $\mathsf{C}(\tau)$. Figure 5.3 shows that the correction term in Eq. (5.27) improves the analytic approximation, Eq. (5.25), for the first order reflection probability $R_1(\varepsilon)$, particularly for small ε. For large ε, the expression (5.27) for $R_1(\varepsilon)$ approaches unity since $|\varphi_\varepsilon(q)|^2$ in the first term goes to a delta-function $\delta(q-1)$ and the second term vanishes.

Similar to the leading order transmission probability, the transmitted part of $|\psi_{k_0}'\rangle$ vanishes for $t \to \infty$ and $x \to -\infty$ under the influence of the imaginary potential in the left half space. The norm of $|\psi_{k_0}'\rangle$ therefore decays to $R_1(\varepsilon)$ as $t \to \infty$. Accounting for the additional factor $(1 - R_1(\varepsilon))$ in the proper normalization of the jump term $\rho_t^{(1)}$, see Eqs. (5.22) and (5.23), the first order weight therefore goes to

$$w_1(t \to \infty) = (1 - R_0(\varepsilon))R_1(\varepsilon). \tag{5.28}$$

Higher Order Terms

In the previous sections we observed that the first two terms $\rho_t^{(0)}$ and $\rho_t^{(1)}$ of the jump expansion after the resummation (4.75) are conveniently described by the scattering of the initial state at an imaginary potential step. Whereas the imaginary potential was restricted to the right half space for the leading order term, it switched to the left half space for the first order term. This resulted from the fact that the resummation adapts the jump operators in such a way that the first jump amounts to a projection on the right half space while the second one amounts to a projection on the left half space. Continuing this series of jumps and adaptive updates of the jump operator $\mathsf{L}_{\check{\alpha}^n}$, we see that $\mathsf{L}_{\check{\alpha}^n}$ effectively alternates between the projector on the left and the projector on the right half space upon each occurrence of a jump. The imaginary potential hence follows this alternation between left and right, so that the jump terms after the resummation

take the form

$$\rho_t^{(n)} = (2\gamma)^n \int_0^t \mathrm{d}t_n \ldots \int_0^{t_2} \mathrm{d}t_1 e^{\left[-\frac{ip^2}{2m\hbar}-\gamma\Theta((-1)^n\mathsf{x})\right](t-t_n)} \Theta([-1]^{n-1}\mathsf{x}) \ldots \Theta(\mathsf{x}) e^{\left[-\frac{ip^2}{2m\hbar}-\gamma\Theta(\mathsf{x})\right]t_1}$$
$$\times\rho_0 e^{\left[\frac{ip^2}{2m\hbar}-\gamma\Theta(\mathsf{x})\right]t_1} \Theta(\mathsf{x}) \ldots \Theta\left([-1]^{n-1}\mathsf{x}\right) e^{\left[\frac{ip^2}{2m\hbar}-\gamma\Theta((-1)^n\mathsf{x})\right](t-t_n)}. \tag{5.29}$$

Compare this to the jump terms without resummation, Eq. (5.2), which do not exhibit this alternation but involve an additional sum over the jump indices.

As a consequence, the particle state immediately after the $2n$-th jump (with $n = 0, 1, \ldots, \infty$) is a wave packet located on the left, which falls off exponentially as $x \to -\infty$. This wave packet is then scattered at the imaginary potential step to its right. Analogously, after the $(2n+1)$-th jump, the particle is exponentially located on the right and subsequently scattered at the imaginary potential step to its left. Since both situations are very similar to the point of departure for the treatment of $\rho_t^{(1)}$ in the previous section, see Eqs. (5.18), (5.19) with the possible exchange x and $-x$, we will simply assume that the particle dynamics after the n-th jump at time t_n is approximated by the time evolution after the first jump at t_1, Eq. (5.21). In particular, this allows us to approximate the n-th jump term

$$\rho_t^{(n)} \approx \rho_t^{(1)}, \quad (\text{up to } x \leftrightarrow -x) \tag{5.30}$$

and therefore the n-th order reflection probability

$$R_n(\varepsilon) \approx R_1(\varepsilon). \tag{5.31}$$

This spares us the the precise investigation of the time evolution for a given number of jumps and a given set of jump times.

As described above, $\rho_t^{(n)}$ is incident on the imaginary potential step from the left for n even, or from the right for n odd, so that its reflected part goes off to the left or to the right, respectively. The respective transmitted parts decay under the imaginary potential. Therefore, only the even order reflection probabilities R_{2n} contribute to the total reflection probability R under the master equation (5.1) for an incident particle from the left. Moreover, since we have defined the R_n as the reflection probabilities of normalized wave packets, we must account for the norm of the jump term $\rho_t^{(n)}$ which brings in the additional factor $(1-R_0(\varepsilon))(1-R_1(\varepsilon)) \cdot \ldots \cdot (1-R_{n-1}(\varepsilon))$. The total reflection probability therefore reads

$$\begin{aligned} R(\varepsilon) &= R_0(\varepsilon) + [1-R_0(\varepsilon)][1-R_1(\varepsilon)]R_2(\varepsilon) + \ldots \\ &= \sum_{n=0}^{\infty} R_{2n}(\varepsilon) \prod_{m<2n} [1-R_m(\varepsilon)]. \end{aligned} \tag{5.32}$$

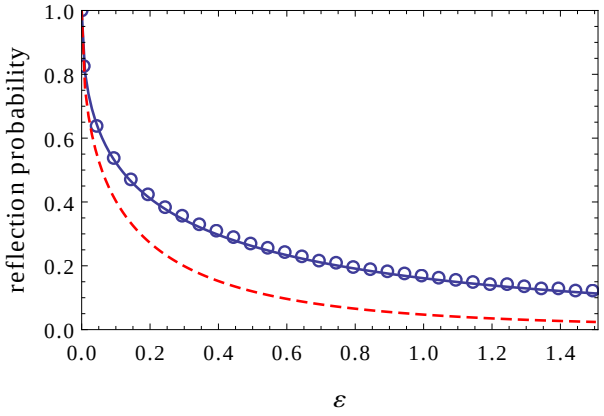

Figure 5.4: Reflection probability $R(\varepsilon)$ of a particle described by a plane wave $|\psi_{k_0}\rangle$, Eqs. (5.9) and (5.10), which undergoes spatial detection, Eq. (5.1), as a function of the dimensionless parameter $\varepsilon = E_{\text{in}}/\hbar\gamma = \hbar k_0^2/2m\gamma$. In solid blue we plot the analytic approximation of $R(\varepsilon)$, Eq. (5.33) with $R_0(\varepsilon)$ and $R_1(\varepsilon)$ given by Eqs. (5.15) and (5.27), and in dashed red we plot the leading order approximation $R_0(\varepsilon)$, Eq. (5.15). Blue circles represent the numerically exact reflection probability obtained by propagation of Eq. (5.1) on a grid. The initial state of the propagation is a sufficiently broad Gaussian wave packet located exclusively on the left, so that $R(\varepsilon)$ varies approximately linearly over its kinetic energy distribution—this effectively approximates a plane wave. We see that the analytic approximation of $R(\varepsilon)$ is asymptotically exact with a maximal deviation of below 1% (at $\varepsilon \approx 0.2$) from the numerical values.

Inserting the approximation (5.31) we obtain

$$\begin{aligned} R(\varepsilon) &= R_0(\varepsilon) - (1 - R_0(\varepsilon)) \left\{ \sum_{n=0}^{\infty} [1 - R_1(\varepsilon)]^{2n+1} \right\} R_1(\varepsilon) \\ &= 1 - \frac{1 - R_0(\varepsilon)}{2 - R_1(\varepsilon)}, \end{aligned} \tag{5.33}$$

where we have used the analytical expression $1/(1-q)$ for the infinite geometric series $\sum_i q^i$. With $R_0(0) = 1$ and $R_1(0) \in [0, 1]$, we have $R(0) = 1$, which is in accord with Allcock's prediction that an infinitely precise measurement ($\gamma \to \infty$) leads to a complete reflection of the detected particle [72]. For a large parameter ε we have $R_0(\varepsilon \to \infty) = 0$ and $R_1(\varepsilon \to \infty) = 1$, see above, so that R approaches unity in this limit. In other words, a free particle without measurement ($\gamma = 0$) experiences no reflection as it should. Therefore, the analytic approximation (5.33) for the total reflection probability $R(\varepsilon)$ by spatial detection is asymptotically exact.

In Fig. 5.4 we plot the expression (5.33) for the reflection probability $R(\varepsilon)$ with $R_0(\varepsilon)$ and $R_1(\varepsilon)$ given by Eqs. (5.15) and (5.27), respectively. In addition, we plot the nu-

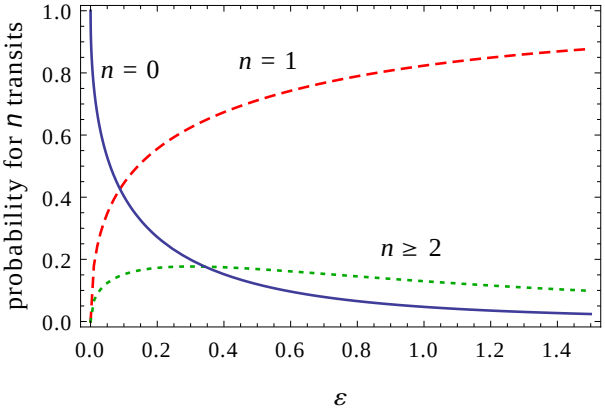

Figure 5.5: Probability for $n = 0, 1$, and $n \geq 2$ transits, w_0, w_1, and $1 - w_0 - w_1$, as a function of the dimensionless energy ε. w_0 and w_1 are equivalent to the weights of the leading order and the first order term in the resummed jump expansion, $w_0 = R_0(\varepsilon)$ and $w_1 = (1 - R_0(\varepsilon))R_1(\varepsilon)$, with $R_0(\varepsilon)$ and $R_1(\varepsilon)$ given by Eqs. (5.15) and (5.27).

merically exact reflection probability under the master equation (5.1). In order for that, we propagate Eq. (5.1) on a grid, with an initial broad Gaussian wave packet located exclusively on the left. The initial state is chosen sufficiently broad so that $R(\varepsilon)$ varies approximately linearly over its kinetic energy distribution and, hence, its scattering probability is equal to that of a plane wave with a momentum equal to the mean momentum of the wave packet. The comparison of the two curves confirms that the analytic approximation (5.33) of $R(\varepsilon)$ is asymptotically exact, and exhibits a maximal deviation of 0.009 from the numerically exact values at $\varepsilon \approx 0.2$.

In conclusion, we obtained a very accurate approximate analytic description for the dynamics of a free particle undergoing spatial detection, Eq. (5.1), by applying the resummation (4.75) of the jump expansion. The jumps in the original jump expansion (5.2) (*i.e.* without resummation) described particle detection events on the right and left, which occur at a constant rate γ. Hence, the weights of the terms in the jump expansion are Poisson distributed and one must take into account at least $2\gamma t$ terms to get a good estimate of ρ_t. In contrast, the jumps in the resummed jump expansion are associated with transits of the particle across the measurement boundary ($x = 0$), which correspond to a series of scattering processes at an imaginary potential step. The advantage of this resummed jump expansion is twofold: On the one hand, the scattering at an imaginary potential step is readily accessible with analytical means. On the other hand, a free particle experiences only a limited number of transits before going off to the left or to the right—in fact, it most likely experiences no or only one transit, see Fig. 5.5. This demonstrates the highly increased convergence of the resummed jump expansion and enables us to obtain a faithful estimate of ρ_t based on the leading order jump terms. In particular, we showed that one can approximate the reflection probability under the

master equation (5.1) with per mil accuracy using only the leading order and the first order reflection probability.

5.2 The Landau-Zener System with Dephasing

As a second example we will apply the adaptive resummation method to the open Landau-Zener system in order to obtain an approximate analytical description [20]. Again we will use the resummation (4.75) which has the ability both to dramatically increase the convergence of the jump expansion and to yield analytically accessible jump terms, as we saw in the spatial detection setting above. For the open Landau-Zener system, however, we cannot evaluate the jump terms as straightforwardly as before. The resummation rather suggests a mapping of the jump expansion to a classical stochastic process, which then yields the desired analytic approximation.

The Landau-Zener system features a pair of coupled energy levels whose energy difference depends linearly on time. It was originally studied as a model for reactive scattering and it was solved in 1932 [82–85]. Later on it was found that the impact of the Landau-Zener problem goes far beyond the field of reactive scattering—it is the paradigmatic model for a quantum system which is subject to a time-dependent external or internal parameter. Depending on the speed of the parameter change, it exhibits two limiting regimes. In the diabatic regime, the parameter changes rapidly compared to the intrinsic system time scales so that the quantum system will stay in its initial energy eigenstate. In the adiabatic regime, the parameter changes slowly compared to the system time scales so that the system constantly adapts to the instantaneous eigenbasis and finally finds itself in the opposite energy eigenstate. Hence, the Landau-Zener tunneling probability ranges from zero in the diabatic regime to unity in the adiabatic regime. Most importantly, besides this qualitative observation, the Landau-Zener system is one of the few analytically solvable quantum problems with a time-dependent Hamiltonian. To this date, the Landau-Zener problem was successfully applied in many different areas of quantum physics, *e.g.* quantum chemistry [86], quantum optics [87], solid state physics [88], or ultracold gases [89].

Given the fact that many systems to which the Landau-Zener model has been applied suffer from environmental decoherence, it is natural to also consider its open system version. And indeed, many analytical and numerical studies of the open Landau-Zener problem have been carried out [90–98]. Almost all of the analytical approaches focus, however, on specific environmental models or asymptotic parameter regimes. So far, no in-depth analytical study of the simplest case of a Markovian master equation, encompassing all dynamical regimes, was carried out[3]. The adaptive resummation method now makes possible such an analytical approach to the Markovian open Landau-Zener system.

[3]The only notable exception is a paper by Lacour *et al.* [99], but the asymptotic regimes of the obtained analytical approximation are incorrect.

5.2.1 The Closed Landau-Zener System

Before we consider the open Landau-Zener system, let us first consider the situation of closed system dynamics and outline its analytical solution. The closed Landau-Zener system is described by a pair of energy levels $|0\rangle$ and $|1\rangle$ with constant coupling c and linear-in-time energy separation vt, see Fig. 5.6. The resulting Schrödinger equation is

$$\partial_t|\psi\rangle = -\frac{i}{\hbar}\left(\frac{vt}{2}\sigma_z + c\sigma_x\right)|\psi\rangle, \tag{5.34}$$

with σ_x and σ_z denoting the first and third Pauli matrix, respectively. The basis $\{|0\rangle, |1\rangle\}$, which is the energy eigenbasis in the absence of the coupling $c\sigma_x$, is called the diabatic basis. The eigenvalues of the time-dependent Hamiltonian in Eq. (5.34) are given by

$$E_\pm(t) = \pm\frac{1}{2}\sqrt{(vt)^2 + (2c)^2}, \tag{5.35}$$

with the respective time-dependent energy eigenstates

$$|+\rangle = \sin\left(\frac{c}{vt}\right)|0\rangle + \cos\left(\frac{c}{vt}\right)|1\rangle, \tag{5.36}$$

$$|-\rangle = \cos\left(\frac{c}{vt}\right)|0\rangle - \sin\left(\frac{c}{vt}\right)|1\rangle. \tag{5.37}$$

This shows that the instantaneous energies in the presence of the coupling are shifted with respect to the uncoupled case so that the crossing at $t = 0$ turns into an avoided crossing with a separation of $2c$, see Fig. 5.6. The basis $\{|+\rangle, |-\rangle\}$ is called the adiabatic basis, but we will use the diabatic basis $\{|0\rangle, |1\rangle\}$ throughout this chapter.

By rescaling time as $\tau = \sqrt{v/\hbar}t$, we obtain the dimensionless form of Eq. (5.34),

$$\partial_\tau|\psi\rangle = \underbrace{-i\left(\frac{\tau}{2}\sigma_z + \sqrt{\delta}\sigma_x\right)}_{\mathsf{H}_{\mathrm{LZ}}(\tau)}|\psi\rangle, \tag{5.38}$$

with only one parameter $\delta = c^2/v\hbar \geq 0$, called the *adiabaticity parameter*. If one starts in either of the two states at $\tau_0 = -\infty$, the probability to experience an adiabatic transition until $\tau = \infty$ is given by [83]

$$P(\delta, 0) = 1 - \exp(-2\pi\delta). \tag{5.39}$$

Consequently, the two limiting cases of small or large δ, corresponding to a slow energy sweep with strong coupling or to a rapid energy sweep with small coupling, respectively, show either complete or no tunneling of the initial populations.

To prove expression (5.39) for the tunneling probability and to lay the ground for treating the open Landau-Zener system, we will outline the full solution of the Schrödinger equation (2.41) following Ref. [100]. Let us first express Eq. (2.41) as a set of coupled

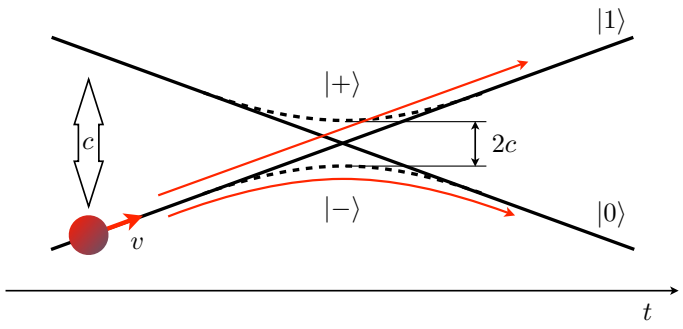

Figure 5.6: Schematic diagram of the Landau-Zener system: two coupled energy levels $|0\rangle$ and $|1\rangle$ are shifted with respect to each other with velocity v. The coupling introduces a shift of the instantaneous energy levels (dashed lines, states $|+\rangle$ and $|-\rangle$, Eqs. (5.36) and (5.37)) with respect to the uncoupled case (solid lines), resulting in an avoided crossing with the separation proportional to the coupling constant c, see Eq. (5.35). A system initially in state $|1\rangle$ (red dot) can stay in $|1\rangle$ or tunnel to $|0\rangle$ in course of the time evolution. In practice, one generally observes partial tunneling and it is more probable to find the system in the final state $|0\rangle$ if the transit of the avoided crossing is slow compared to the energy gap, whereas finding state $|1\rangle$ is more probable for a slow transit, see Eq. (5.39).

differential equations for the coefficients ψ_0 and ψ_1 of state $|\psi\rangle$,

$$i\dot{\psi}_0(\tau) = \frac{\tau}{2}\psi_0(\tau) + \sqrt{\delta}\psi_1(\tau), \tag{5.40}$$

$$i\dot{\psi}_1(\tau) = -\frac{\tau}{2}\psi_1(\tau) + \sqrt{\delta}\psi_0(\tau). \tag{5.41}$$

After solving the first equation for ψ_1, we can insert it into the second to obtain

$$\left(i\frac{\partial}{\partial\tau} + \frac{\tau}{2}\right)\left(i\frac{\partial}{\partial\tau} - \frac{\tau}{2}\right)\psi_0(\tau) = \delta\psi_0(\tau). \tag{5.42}$$

The substitution $\psi_0(\tau) = \exp(-i\tau^2/4)\varphi_0(\tau)$ leads to the simplification

$$\left(\frac{\partial^2}{\partial\tau^2} - i\tau\frac{\partial}{\partial\tau} + \delta\right)\varphi_0(\tau) = 0. \tag{5.43}$$

In the Taylor expansion of $\varphi_0(\tau)$ we see that Eq. (5.43) determines that all coefficients of odd order and, separately, all coefficients of even order are mutually dependent. This structure suggests two independent solutions: an even and an odd function of time, $\varphi_0(\tau) = e(\tau^2) + \tau o(\tau^2)$. The final substitution $\tau^2 = -2iz$ leads to the Kummer differential

equation,

$$\left(z\frac{\partial^2}{\partial z^2} + (b-z)\frac{\partial}{\partial z} - a\right) f(z) = 0, \tag{5.44}$$

with $b = 1/2$, $a = i\delta/2$ and $b = 3/2$, $a = 1/2 + i\delta/2$ for $f(z) = e(z)$ and $f(z) = o(z)$, respectively. Kummer's equation is solved by the confluent hypergeometric function ${}_1F_1(a;b;z)$ and, hence, the general solution to Eq. (5.42) reads

$$\psi_0(\tau) = \left[c_1\, {}_1F_1\left(\frac{i\delta}{2};\frac{1}{2};\frac{i\tau^2}{2}\right) + c_2\tau\, {}_1F_1\left(\frac{1}{2}+\frac{i\delta}{2};\frac{3}{2};\frac{i\tau^2}{2}\right)\right] e^{-i\tau^2/4}. \tag{5.45}$$

Since Eqs. (5.40) and (5.41) remain unchanged under the substitution $\delta \to -\delta$, $\tau \to i\tau$ and exchange of ψ_0 and ψ_1, the solution for $\psi_1(\tau)$ reads

$$\psi_1(\tau) = \left[c_3\, {}_1F_1\left(-\frac{i\delta}{2};\frac{1}{2};-\frac{i\tau^2}{2}\right) + c_4\tau\, {}_1F_1\left(\frac{1}{2}-\frac{i\delta}{2};\frac{3}{2};-\frac{i\tau^2}{2}\right)\right] e^{i\tau^2/4}. \tag{5.46}$$

We can now determine the coefficients c_i by setting $\tau = 0$ in Eqs. (5.45) and (5.46), and in their first derivatives, Eqs. (5.40) and (5.41), $c_1 = \psi_0(0)$, $c_2 = -i\sqrt{\delta}\psi_1(0)$, $c_3 = \psi_1(0)$, $c_4 = -i\sqrt{\delta}\psi_0(0)$. Therefore, the time evolution operator $\mathsf{U}(\tau,0)$ which maps a state at time 0 to a state at time τ reads

$$\mathsf{U}(\tau,0) = \begin{pmatrix} {}_1F_1\left(\frac{i}{2}\delta;\frac{1}{2};\frac{i}{2}\tau^2\right) e^{-i\tau^2/4} & -i\sqrt{\delta}\tau\, {}_1F_1\left(\frac{1}{2}+\frac{i}{2}\delta;\frac{3}{2};\frac{i}{2}\tau^2\right) e^{-i\tau^2/4} \\ -i\sqrt{\delta}\tau\, {}_1F_1\left(\frac{1}{2}-\frac{i}{2}\delta;\frac{3}{2};-\frac{i}{2}\tau^2\right) e^{i\tau^2/4} & {}_1F_1\left(-\frac{i}{2}\delta;\frac{1}{2};-\frac{i}{2}\tau^2\right) e^{i\tau^2/4} \end{pmatrix}. \tag{5.47}$$

The operator $\mathsf{U}(\tau,\tau_0)$ for an arbitrary initial time τ_0 can be obtained from Eq. (5.47) by simply propagating from τ_0 to 0 by means of $\mathsf{U}^{-1}(\tau_0,0)$ and then propagating from 0 to τ,

$$\mathsf{U}(\tau,\tau_0) = \mathsf{U}(\tau,0)\mathsf{U}(0,\tau_0) = \mathsf{U}(\tau,0)\mathsf{U}^{-1}(\tau_0,0) = \mathsf{U}(\tau,0)\mathsf{U}^{\dagger}(\tau_0,0). \tag{5.48}$$

The fact that Eq. (5.47) features confluent hypergeometric functions with parameters $b = 1/2$ and $b = 3/2$ suggests that the solution can also be given in terms of parabolic cylinder functions $D_\nu(z)$ [83, 101]. Indeed, parabolic cylinder functions are solutions to Eq. (5.42) and the particular solution for the initial condition $\psi_0(-\infty) = 0$ is given by

$$\psi_0(\tau) = aD_{i\delta-1}\left(\tau e^{\frac{3\pi}{4}i}\right). \tag{5.49}$$

Using its asymptotic form for $\tau \to -\infty$ [101],

$$D_{i\delta-1}\left(\tau e^{\frac{3\pi}{4}i}\right) \xrightarrow{\tau\to-\infty} e^{\frac{i}{4}\tau^2} e^{\frac{\pi}{4}(1-i\delta)i}(-\tau)^{i\delta-1}, \tag{5.50}$$

in the differential equation (5.40), we obtain

$$|\psi_1(\tau)| = \frac{1}{\sqrt{\delta}} \left| -\frac{\tau}{2}\psi_0(\tau) + i\frac{\partial}{\partial\tau}\psi_0(\tau) \right| \tag{5.51}$$
$$\to \frac{1}{\sqrt{\delta}} \left| a e^{\frac{i}{4}\tau^2} e^{\frac{\pi}{4}(1-i\delta)i} (-\tau)^{i\delta} - iae^{\frac{i}{4}\tau^2} e^{\frac{\pi}{4}(1-i\delta)i} (-\tau)^{i\delta-2} \right|.$$

The initial condition $|\psi_1(-\infty)| = 1$ determines the factor $a = \sqrt{\delta}\exp(-\pi\delta/4 + i\phi)$. Using Eq. (5.49), the coefficient $\psi_1(\tau)$ at arbitrary times τ therefore reads

$$\begin{aligned}\psi_1(\tau) &= \frac{1}{\sqrt{\delta}} \left(-\frac{\tau}{2}\psi_0(\tau) + i\frac{\partial}{\partial\tau}\psi_0(\tau) \right) \\ &= e^{-\frac{\pi}{4}\delta} e^{\left(\phi - \frac{3\pi}{4}\right)i} \left(-\frac{\tau e^{\frac{3\pi}{4}i}}{2} D_{i\delta-1}\left(\tau e^{\frac{3\pi}{4}i}\right) + D'_{i\delta-1}\left(\tau e^{\frac{3\pi}{4}i}\right) \right) \\ &= e^{-\frac{\pi}{4}\delta} e^{\left(\phi + \frac{\pi}{4}\right)i} D_{i\delta}\left(\tau e^{\frac{3\pi}{4}i}\right), \end{aligned} \tag{5.52}$$

where the recursion relations for $D_\nu(z)$ have been inserted in the last step. With the help of expressions (5.49) and (5.52) for ψ_0 and ψ_1, and the initial conditions $\psi_0(-\infty) = 0$, $|\psi_1(-\infty)| = 1$, we can now determine the propagator $\mathsf{U}(\tau, \tau_0)$ for $\tau_0 = -\infty$. It reads

$$\mathsf{U}(\tau, -\infty) = e^{-\frac{\pi}{4}\delta} \begin{pmatrix} e^{-\left(\phi+\frac{\pi}{4}\right)i} D_{-i\delta}\left(\tau e^{-\frac{3\pi}{4}i}\right) & \sqrt{\delta} e^{i\phi} D_{i\delta-1}\left(\tau e^{\frac{3\pi}{4}i}\right) \\ -\sqrt{\delta} e^{-i\phi} D_{-i\delta-1}\left(\tau e^{-\frac{3\pi}{4}i}\right) & e^{\left(\phi+\frac{\pi}{4}\right)i} D_{i\delta}\left(\tau e^{\frac{3\pi}{4}i}\right) \end{pmatrix}, \tag{5.53}$$

and it is determined up an arbitrary phase ϕ at $\tau = -\infty$. Finally, we note that the tunneling probability (5.39) is given by $P(\delta, 0) = |\psi_0(\infty)|^2 = |\langle 0|\mathsf{U}(\infty, -\infty)|1\rangle|^2$. It can therefore be derived from Eq. (5.53) by inserting the asymptotic expression for $D_{i\delta-1}$ for $\tau \to \infty$ [101],

$$D_{i\delta-1}\left(\tau e^{\frac{3\pi}{4}i}\right) \xrightarrow{\tau\to\infty} e^{\frac{i}{4}\tau^2} e^{\frac{3\pi}{4}i(i\delta-1)} \tau^{i\delta-1} + \frac{\sqrt{2\pi}}{\Gamma(1-i\delta)} e^{-\frac{i}{4}\tau^2} e^{-\frac{\pi}{4}\delta} \tau^{-i\delta}. \tag{5.54}$$

While the first term in Eq. (5.54) vanishes for $\tau \to \infty$, the second term gives

$$|\langle 0|\mathsf{U}(\infty, -\infty)|1\rangle|^2 = \delta e^{-\frac{\pi\delta}{2}} \frac{2\pi}{|\Gamma(1-i\delta)|^2} e^{-\frac{\pi\delta}{2}} = \frac{2\pi\delta}{\pi\delta} \sinh(\pi\delta) e^{-\pi\delta} = 1 - e^{-2\pi\delta}, \tag{5.55}$$

the Landau-Zener tunneling probability (5.39).

This concludes our considerations of the closed Landau-Zener system. In the following section we will see that the open Landau-Zener dynamics in the presence of environmental influences can be solved by using the closed system dynamical propagators, Eqs. (5.47) and (5.53), just with a complex time argument.

5.2.2 The Open Landau-Zener System

The simplest conceivable open system extension of the Landau-Zener model is described by a Markovian master equation in standard form (2.66) with the Hamiltonian $\mathsf{H}_{\mathrm{LZ}}(\tau)$, Eq. (5.38), and a single Lindblad operator L. Here we will consider L to be proportional to the third Pauli matrix, $\mathsf{L} = \sqrt{\gamma/2}\sigma_z$. The associated incoherent dynamics goes by the name of *dephasing* [25]. Since L is diagonal in the diabatic basis $\{|0\rangle, |1\rangle\}$, it leads to a decay of the coherences $\langle 0|\rho_t|1\rangle$ and $\langle 1|\rho_t|0\rangle$ in time but does not affect the populations. Dephasing is used to model, for example, rapid fluctuations of the diabatic energy levels or a nonselective measurement that determines whether the system is in state $|0\rangle$ or $|1\rangle$. The analogy to a nonselective measurement in the diabatic basis is applied, in particular, in the incoherent control setting of the visual pigment protein Rhodopsin, see Chap. 7. The corresponding Markovian master equation, expressed in terms of the dimensionless time τ and the adiabaticity parameter δ, see Eq. (5.38), reads

$$\partial_\tau \rho_\tau = -i[\mathsf{H}_{\mathrm{LZ}}(\tau), \rho_\tau] + \frac{\gamma}{2}(\sigma_z \rho_\tau \sigma_z - \rho_\tau) = -i\left[\frac{\tau}{2}\sigma_z + \sqrt{\delta}\sigma_x, \rho_\tau\right] + \frac{\gamma}{2}(\sigma_z \rho_\tau \sigma_z - \rho_\tau). \quad (5.56)$$

Here, γ is called the *dephasing rate* and it is also dimensionless. As in Sec. 5.1, we will apply the resummation (4.75) of the jump expansion to derive an approximate analytic description of the open Landau-Zener dynamics, since the Eq. (5.56) is not analytically solvable. Specifically, we are interested in the transition probability $P(\delta, \gamma)$ as a function of both the adiabaticity parameter δ and the dephasing rate γ.

Strong Dephasing

Before considering the jump expansion, however, let us investigate the limit of strong dephasing $\gamma \gg \sqrt{\delta}$. This limit turns out to be quite instructive since it makes Eq. (5.56) analytically solvable. First, let us rewrite Eq. (5.56) in the Bloch-vector-representation, *i.e.* we expand all operators in the orthonormal Hilbert-Schmidt basis $\{\mathbb{1}, \sigma_x, \sigma_y, \sigma_z\}$. Denoting the expansion coefficients of the density matrix by x, y, and z, $\rho = 1/2(\mathbb{1} + x\sigma_x + y\sigma_y + z\sigma_z)$, we obtain the master equation

$$\begin{pmatrix} \dot{x} \\ \dot{y} \\ \dot{z} \end{pmatrix} = \begin{pmatrix} -\gamma & -\tau & 0 \\ \tau & -\gamma & -2\sqrt{\delta} \\ 0 & 2\sqrt{\delta} & 0 \end{pmatrix} \begin{pmatrix} x \\ y \\ z \end{pmatrix}. \quad (5.57)$$

For $\gamma \gg \sqrt{\delta}$, we can adiabatically eliminate the x- and y-components by setting $\dot{x} = \dot{y} = 0$ and obtain a closed evolution equation for the z-component,

$$\dot{z} = -\frac{4\delta}{\gamma + \frac{\tau^2}{\gamma}} z. \quad (5.58)$$

Integration of Eq. (5.58) for the initial value $z(-\infty) = 1$ yields

$$z(\tau) = \exp\left(-4\delta\left(\frac{\pi}{2} + \arctan\left(\frac{\tau}{\gamma}\right)\right)\right). \tag{5.59}$$

With the arctangent going to $\pi/2$ for $\tau \to \infty$, we can immediately determine the tunneling probability $P(\delta, \infty)$ for infinitely strong dephasing, $\gamma \to \infty$,

$$P(\delta, \infty) = \frac{1}{2}(1 - z(\infty)) = \frac{1}{2}(1 - e^{-4\pi\delta}). \tag{5.60}$$

This result is in agreement with the Landau-Zener tunneling probability in the presence of rapid oscillations of the energy levels [90].

5.2.3 Jump Expansion for the Landau-Zener System with Dephasing

To approximate the tunneling probability $P(\delta, \gamma)$ analytically for arbitrary parameters δ and γ, we now consider the jump expansion for the master equation (5.56) and apply the adaptive resummation (4.75).

Generally, the terms of the jump expansion $\rho_\tau = \sum_n \rho_\tau^{(n)}$ are defined by Eq. (4.27). For the open Landau-Zener system, Eq. (5.56), it is important to take an arbitrary initial time τ_0 instead of $\tau_0 = 0$, since in the end we want to evaluate $P(\delta, \gamma)$ as the tunneling probability between $\tau_0 \to -\infty$ and $\tau \to \infty$. The jump terms $\rho_\tau^{(n)}$ without resummation, $\boldsymbol{\alpha} = 0$, and for the initial state $\rho_{\tau_0} = |1\rangle\langle 1|$ hence take the form

$$\begin{aligned}\rho_\tau^{(n)} = \frac{\gamma^n}{2^n}\int_{\tau_0}^{\tau} \mathrm{d}\tau_n \ldots \int_{\tau_0}^{\tau_2} \mathrm{d}\tau_1 \mathcal{T}_- \exp\left[-i\int_{\tau_n}^{\tau} \mathsf{H}^{\mathrm{eff}}(\tau')\mathrm{d}\tau'\right] \sigma_z \ldots \sigma_z \mathcal{T}_- \exp\left[-i\int_{\tau_0}^{\tau_1} \mathsf{H}^{\mathrm{eff}}(\tau')\mathrm{d}\tau'\right] \\ \times |1\rangle\langle 1| \mathcal{T}_+ \exp\left[i\int_{\tau_0}^{\tau_1} \left\{\mathsf{H}^{\mathrm{eff}}(\tau')\right\}^\dagger \mathrm{d}\tau'\right] \sigma_z \ldots \sigma_z \mathcal{T}_+ \exp\left[i\int_{\tau_n}^{\tau} \left\{\mathsf{H}^{\mathrm{eff}}(\tau')\right\}^\dagger \mathrm{d}\tau'\right],\end{aligned} \tag{5.61}$$

with $\mathsf{H}^{\mathrm{eff}}(\tau) = \mathsf{H}_{\mathrm{LZ}}(\tau) - i\gamma/4$, see Eq. (4.24). Note that the time dependent effective Hamiltonian requires us to integrate $\mathsf{H}^{\mathrm{eff}}(\tau')$ over τ' for the continuous between-jump evolution. This, in turn, entails the use of ascending and descending time ordering operators indicated by $\mathcal{T}_+$ and $\mathcal{T}_-$, respectively. With the jump rate being proportional to the imaginary part of the effective Hamiltonian, the weights $w_n(\tau) = \mathrm{Tr}\,\rho_\tau^{(n)}$ of the jump terms without resummation are again Poisson distributed between τ_0 and τ, as in the previous example, see Eq. (5.3),

$$w_n(\tau) = \frac{[\gamma(\tau - \tau_0)/2]^n}{n!} e^{-\gamma(\tau-\tau_0)/2}. \tag{5.62}$$

We therefore must account for at least $2\bar{n} = \gamma(\tau - \tau_0)$ terms, in order for the jump expansion to provide a good estimate for the density matrix ρ_τ at time τ. Since, as mentioned above, the Landau-Zener tunneling probability $P(\delta, \gamma)$ is defined for the limits $\tau_0 \to -\infty$

and $\tau \to \infty$, this makes the jump expansion practically useless for approximating $P(\delta, \gamma)$.

5.2.4 Adaptive Resummation of the Jump Expansion

The adaptive resummation changes the convergence properties of the jump expansion dramatically. The application of the update rule (4.75) for the jump operator $\mathsf{L} = \sqrt{\gamma/2}\sigma_z$ requires a little caution, however. For example, inserting L into Eq. (4.75) to obtain the complex shift $\check{\alpha}^1$ after the first jump yields[4]

$$\check{\alpha}^1 = \frac{\mathrm{Tr}\left[\left(\frac{\gamma}{2}\right)^{\frac{3}{2}} \sigma_z\sigma_z\sigma_z\right]}{\mathrm{Tr}\left[\frac{\gamma}{2}\sigma_z\sigma_z\right]} = \sqrt{\frac{\gamma}{2}}\frac{\mathrm{Tr}\,\sigma_z}{\mathrm{Tr}\,\mathbb{1}} = 0. \tag{5.63}$$

This would imply that L does not get shifted at all and hence no actual resummation of the jump expansion takes place. Since Eq. (4.75) only determines the *update* of L, however, we are free to choose any *initial* complex shift $\check{\alpha}^0$ of L. In the following we choose $\check{\alpha}^0$ in such a way that all subsequent shifts $\check{\alpha}^n$ do not vanish.

The Leading Order Term

To evaluate the leading order term of the jump expansion, we choose the initial complex shift $\check{\alpha}^0$ in such a way that it is optimal for the initial state $\rho_{\tau_0} = |1\rangle\langle 1|$. The optimal shift for a given state is determined by Eq. (4.51) and, upon inserting ρ_{τ_0} and L, we obtain

$$\check{\alpha}^0 = -\sqrt{\frac{\gamma}{2}}\,\mathrm{Tr}[\sigma_z|1\rangle\langle 1|] = \sqrt{\frac{\gamma}{2}}. \tag{5.64}$$

This initial shift $\check{\alpha}^0$ leads to the optimized jump operator

$$\mathsf{L}_{\check{\alpha}^0} = \mathsf{L} + \check{\alpha}^0 = \sqrt{\frac{\gamma}{2}}(\sigma_z + \mathbb{1}) = \sqrt{2\gamma}|0\rangle\langle 0|. \tag{5.65}$$

Very similar to the example in Sec. 5.1, this initial jump operator is a projector onto a subspace that is orthogonal to ρ_{τ_0}. The associated effective Hamiltonian $\mathsf{H}^{\mathrm{eff}}_{\check{\alpha}^0}(\tau) = \mathsf{H}_{\mathrm{LZ}}(\tau) - i\gamma|0\rangle\langle 0|$ effects a decay of the population in the diabatic state $|0\rangle$, and the leading order jump term reads

$$\begin{aligned}\rho^{(0)}_\tau &= \mathcal{T}_- e^{\left[-i\int_{\tau_0}^{\tau}\mathsf{H}_{\mathrm{LZ}}(\tau')\mathrm{d}\tau' - \gamma(\tau-\tau_0)|0\rangle\langle 0|\right]}\rho_{\tau_0}\mathcal{T}_+ e^{\left[i\int_{\tau_0}^{\tau}\mathsf{H}_{\mathrm{LZ}}(\tau')\mathrm{d}\tau' - \gamma(\tau-\tau_0)|0\rangle\langle 0|\right]} \\ &\equiv \mathsf{U}_{\check{\alpha}^0}(\tau,\tau_0)|1\rangle\langle 1|\mathsf{U}^\dagger_{\check{\alpha}^0}(\tau,\tau_0).\end{aligned} \tag{5.66}$$

Since the jump rate is proportional to the norm decay under the effective Hamiltonian, it is clear that the first jump cannot occur until the population in state $|1\rangle$ starts tunneling to the state $|0\rangle$, *i.e.* at around $\tau \approx 0$.

[4] Due to the fact that we have only one jump operator L, $\check{\boldsymbol{\alpha}}(\mathrm{j}^n)$ is an n-tuple of a single complex number $\check{\alpha}$. We therefore abbreviate $\check{\boldsymbol{\alpha}}(\mathrm{j}^n)$ with $\check{\alpha}^n$.

Despite the additional parameter γ in the effective Hamiltonian, the dynamics of $\rho_\tau^{(0)}$ under $\mathsf{H}_{\check{\alpha}^0}^{\text{eff}}$, Eq. (5.66), can be reformulated to match the closed Landau-Zener Schrödinger equation (5.38) and hence can be solved analytically [100]. The Schrödinger equation for the non-Hermitian Hamiltonian $\mathsf{H}_{\check{\alpha}^0}^{\text{eff}}$ reads

$$\partial_\tau|\psi_\tau\rangle = -i\left(\mathsf{H}_{\text{LZ}}(\tau) - i\gamma|0\rangle\langle 0|\right)|\psi_\tau\rangle = -i\left(\frac{\tau}{2}\sigma_z + \sqrt{\delta}\sigma_x - i\gamma|0\rangle\langle 0|\right)|\psi_\tau\rangle. \tag{5.67}$$

Expressing this in terms of the pure state coefficients ψ_0, ψ_1 we obtain

$$i\dot{\psi}_0(\tau) = \left(\frac{\tau}{2} - i\gamma\right)\psi_0(\tau) + \sqrt{\delta}\psi_1(\tau), \tag{5.68}$$

$$i\dot{\psi}_1(\tau) = -\frac{\tau}{2}\psi_1(\tau) + \sqrt{\delta}\psi_0(\tau). \tag{5.69}$$

After the transformation $|\psi\rangle = e^{-\gamma\tau/2}|\varphi\rangle$, the resulting coupled differential equations,

$$i\dot{\varphi}_0(\tau) = \frac{1}{2}(\tau - i\gamma)\varphi_0(\tau) + \sqrt{\delta}\varphi_1(\tau), \tag{5.70}$$

$$i\dot{\varphi}_1(\tau) = -\frac{1}{2}(\tau - i\gamma)\varphi_1(\tau) + \sqrt{\delta}\varphi_0(\tau), \tag{5.71}$$

can be identified with the closed system equations (5.40) and (5.41) by substituting the complex time $\tau' = \tau - i\gamma$. Since the differential equations (5.40) and (5.41) are solved by the time evolution operator $\mathsf{U}(\tau, 0)$, Eq. (5.47), between $\tau_0 = 0$ and τ, Eq. (5.66) for $\rho_\tau^{(0)}$ is solved by the same operator U with a complex time argument,

$$\mathsf{U}_{\check{\alpha}^0}(\tau, 0) = e^{-\frac{\gamma\tau}{2}}\mathsf{U}(\tau - i\gamma, 0). \tag{5.72}$$

Equivalently, for the initial time $\tau_0 = -\infty$ we can use the time evolution operator $\mathsf{U}(\tau - i\gamma, -\infty)$, Eq. (5.53),

$$\mathsf{U}_{\check{\alpha}^0}(\tau, -\infty) = e^{-\frac{\gamma\tau}{2}}\mathsf{U}(\tau - i\gamma, -\infty). \tag{5.73}$$

As before, for arbitrary initial times τ_0, the operator $\mathsf{U}_{\check{\alpha}^0}(\tau, \tau_0)$ is obtained by propagating from τ_0 to 0 and then from 0 to τ. Care must be taken, however, since the open system time evolution operator $\mathsf{U}_{\check{\alpha}^0}$ is not unitary. The inverse of a general matrix is given by its adjugate over its determinant. In all considered cases, we observed that $\mathsf{U}_{\check{\alpha}^0}$ has unit determinant so that we have

$$\mathsf{U}_{\check{\alpha}^0}(\tau, \tau_0) = \mathsf{U}_{\check{\alpha}^0}(\tau, 0)\left[\mathsf{U}_{\check{\alpha}^0}(\tau_0, 0)\right]^{-1} = \mathsf{U}_{\check{\alpha}^0}(\tau, 0)\,\text{adj}\left[\mathsf{U}_{\check{\alpha}^0}(\tau_0, 0)\right], \tag{5.74}$$

with

$$\text{adj}\left[\begin{pmatrix} a & b \\ c & d \end{pmatrix}\right] = \begin{pmatrix} d & -b \\ -c & a \end{pmatrix}. \tag{5.75}$$

Let us finally determine the asymptotic populations in the leading order jump term, $\langle 0|\rho_\tau^{(0)}|0\rangle$ and $\langle 1|\rho_\tau^{(0)}|1\rangle$, for $\tau_0 \to -\infty$ and $\tau \to \infty$. While it is clear that $\langle 0|\rho_{\tau\to\infty}^{(0)}|0\rangle$ decays completely under the influence of the imaginary part $-i\gamma|0\rangle\langle 0|$ of $\mathsf{H}_{\check{\alpha}_0}^{\text{eff}}$, the pop-

ulation $\langle 1|\rho_\tau^{(0)}|1\rangle = |\langle 1|\mathsf{U}_{\check{\alpha}^0}(\tau,-\infty)|1\rangle|^2$ is determined by Eq. (5.73). The asymptotic expansion (5.54) of the parabolic cylinder function $D_{i\delta}(\tau' \exp[3\pi i/4])$, which is valid for $\mathrm{Re}[\tau'] > 0$, then gives

$$\langle 1|\rho_\tau^{(0)}|1\rangle \xrightarrow{\tau\to\infty} \exp[-2\pi\delta]. \tag{5.76}$$

This is precisely the same value for $\langle 1|\rho_{\tau\to\infty}^{(0)}|1\rangle$ as in the closed Landau-Zener system, *cf.* Eq. (5.39). This is a quite surprising result since one expects that the decay of the coherences $\langle 0|\rho_\tau^{(0)}|1\rangle$ and $\langle 1|\rho_\tau^{(0)}|0\rangle$ under $\mathsf{H}_{\check{\alpha}_0}^{\mathrm{eff}}$ would have an influence on the probability to remain in the initial diabatic state.

Higher Order Jump Terms

With the initial choice for $\mathsf{L}_{\check{\alpha}^0}$, Eq. (5.65), the diabatic state $|0\rangle$ must be populated in order for the first jump to occur. Since coherent transitions between the initial state $|1\rangle$ and state $|0\rangle$ take place only around $\tau \approx 0$, the resummation guarantees that no jumps occur before that time. The first jump with the jump operator $\mathsf{L}_{\check{\alpha}^0}$ then projects the system onto state $|0\rangle$, and Eq. (4.75) determines the new shift $\check{\alpha}^1$,

$$\check{\alpha}^1 = -\frac{\mathrm{Tr}\left[\mathsf{L}\mathsf{L}_{\check{\alpha}^0}\mathsf{L}_{\check{\alpha}^0}^\dagger\right]}{\mathrm{Tr}\left[\mathsf{L}_{\check{\alpha}^0}\mathsf{L}_{\check{\alpha}^0}^\dagger\right]} = -\sqrt{\frac{\gamma}{2}}\frac{\mathrm{Tr}[\sigma_z|1\rangle\langle 1|]}{\mathrm{Tr}[|1\rangle\langle 1|]} = -\sqrt{\frac{\gamma}{2}}. \tag{5.77}$$

This leads to the updated jump operator

$$\mathsf{L}_{\check{\alpha}^1} = \mathsf{L} + \check{\alpha}^1 = \sqrt{\frac{\gamma}{2}}(\sigma_z - \mathbb{1}) = -\sqrt{2\gamma}|1\rangle\langle 1|. \tag{5.78}$$

We see that the jump operator changes from being proportional to the projector onto $|0\rangle$ into an operator proportional to the projector onto $|1\rangle$. Therefore, the new effective Hamiltonian, $\mathsf{H}_{\check{\alpha}_1}^{\mathrm{eff}}(\tau) = \mathsf{H}_{\mathrm{LZ}}(\tau) - i\gamma|1\rangle\langle 1|$, leads to a decay of the population in $|1\rangle$. Hence, the first order jump term reads

$$\begin{aligned}\rho_\tau^{(1)} &= 2\gamma\int_{\tau_0}^{\tau}\mathcal{T}_-\exp\left[-i\int_{\tau_1}^{\tau}\mathsf{H}_{\mathrm{LZ}}(\tau')\mathrm{d}\tau' - \gamma(\tau-\tau_1)|1\rangle\langle 1|\right]|0\rangle\langle 0| \\ &\quad\times\rho_{\tau_1}^{(0)}|0\rangle\langle 0|\mathcal{T}_+\exp\left[i\int_{\tau_1}^{\tau}\mathsf{H}_{\mathrm{LZ}}(\tau')\mathrm{d}\tau' - \gamma\tau|1\rangle\langle 1|\right]\mathrm{d}\tau_1 \\ &\equiv 2\gamma\int_{\tau_0}^{\tau}\mathsf{U}_{\check{\alpha}^1}(\tau,\tau_1)|0\rangle\langle 0|\rho_{\tau_1}^{(0)}|0\rangle\langle 0|\mathsf{U}_{\check{\alpha}^1}^\dagger(\tau,\tau_1)\mathrm{d}\tau_1.\end{aligned} \tag{5.79}$$

With the jump rate proportional to the decay of the population $\langle 1|\rho_\tau^{(1)}|1\rangle$ under $\mathsf{H}_{\check{\alpha}_1}^{\mathrm{eff}}(\tau)$, it is clear that another coherent transition, this time from state $|0\rangle$ back to state $|1\rangle$, must take place before the next jump can occur.

Similar to the leading order jump term, the nonunitary operator $\mathsf{U}_{\check{\alpha}^1}(\tau,\tau_0)$ can be deduced from the time evolution operator $\mathsf{U}(\tau,\tau_0)$ for the closed Landau-Zener system

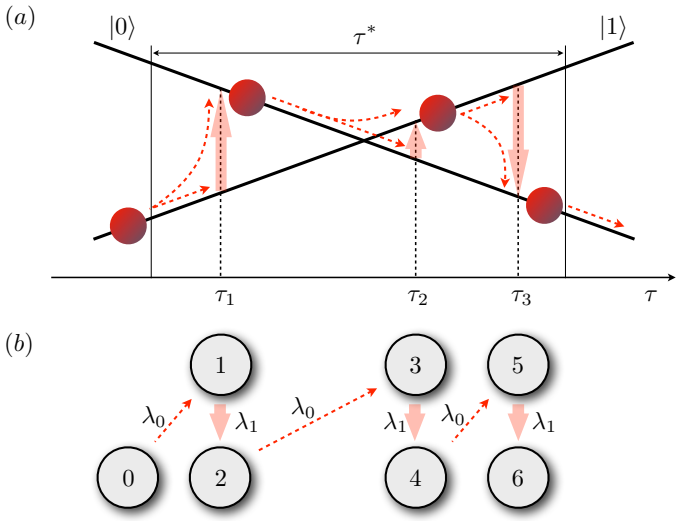

Figure 5.7: Schematic diagram of the jump expansion $\rho_\tau = \sum_n \rho_\tau^{(n)}$ for the open Landau-Zener system after the resummation, Eq. (4.75). The transformations that make up the jump terms $\rho_\tau^{(n)}$, Eq. (5.82), follow a strict alternation of tunnelings between the diabatic states $|0\rangle$ and $|1\rangle$ within a finite time interval τ^*, and jumps to either $|0\rangle$ or $|1\rangle$ are distributed randomly over τ^*. In panel (a) we trace an exemplary series of transformations with the specific jump times τ_1, τ_2, and τ_3. Dashed red and massive reddish arrows here represent tunnelings and jumps, respectively. This dynamics suggests to map the open Landau-Zener system to a classical inhomogeneous Markov chain with two time-dependent, alternating rates $\lambda_0(\tau)$ and $\lambda_1(t)$, see panel (b). The rates in this classical stochastic process, $\lambda_0(\tau)$ and $\lambda_1(t)$, should represent the quantum tunneling and jump rates, respectively.

with an imaginary time argument, see Eqs. (5.72) and (5.73). Here we have

$$\mathsf{U}_{\check{\alpha}^1}(\tau, 0) = e^{-\frac{\gamma\tau}{2}} \mathsf{U}(\tau + i\gamma, 0), \tag{5.80}$$

$$\mathsf{U}_{\check{\alpha}^1}(\tau, -\infty) = e^{-\frac{\gamma\tau}{2}} \mathsf{U}(\tau + i\gamma, -\infty), \tag{5.81}$$

and an expression equivalent to Eq. (5.74) for arbitrary initial times. While the parabolic cylinder functions $D_\nu(z)$ involved in $\mathsf{U}(\tau + i\gamma, -\infty)$ determine the leading order jump term $\rho_\tau^{(0)}$ for $\tau \to -\infty$, the next order $\rho_\tau^{(1)}$ involves an integral over $D_\nu(z)$. This makes it impossible to assess the population $\langle 0|\rho_\tau^{(1)}|0\rangle$ or those of higher orders analytically. One can, however, find an approximate analytical description for the populations in $\rho_\tau^{(n)}$ in terms of a classical stochastic process, as we will see in the following section.

Continuing the series of consecutive jumps and adaptive updates leading to $\rho_\tau^{(n)}$, one sees that $\mathsf{L}_{\check{\alpha}^n}$ alternates between the projector onto $|0\rangle$ and $|1\rangle$ similar to the spatial

detection setting in Sec. 5.1, see schematic diagram Fig. 5.7. In other words, we have $\mathsf{L}_{\check{\alpha}^{2n}} = \mathsf{L}_{\check{\alpha}^0}$ and $\mathsf{L}_{\check{\alpha}^{2n+1}} = \mathsf{L}_{\check{\alpha}^1}$ for $n = 0, 1, \ldots \infty$, with Landau-Zener transitions in between. The jump terms $\rho_\tau^{(n)}$ therefore read

$$\begin{aligned}\rho_\tau^{(n)} = (2\gamma)^n \int_{\tau_0}^{\tau} \mathrm{d}\tau_n \ldots \int_{\tau_0}^{\tau_2} \mathrm{d}\tau_1 \mathsf{U}_{\check{\alpha}^n}(\tau, \tau_n) \ldots |0\rangle\langle 0|\mathsf{U}_{\check{\alpha}^0}(\tau_3, \tau_2)|1\rangle\langle 1|\mathsf{U}_{\check{\alpha}^1}(\tau_2, \tau_1)|0\rangle\langle 0| \\ \times \mathsf{U}_{\check{\alpha}^0}(\tau_1, \tau_0) \underbrace{|1\rangle\langle 1|}_{\rho_{\tau_0}} \mathsf{U}^\dagger_{\check{\alpha}^0}(\tau_1, \tau_0)|0\rangle\langle 0|\mathsf{U}^\dagger_{\check{\alpha}^1}(\tau_2, \tau_1)|1\rangle\langle 1|\mathsf{U}^\dagger_{\check{\alpha}^0}(\tau_3, \tau_2)|0\rangle\langle 0| \ldots \mathsf{U}^\dagger_{\check{\alpha}^n}(\tau, \tau_n),\end{aligned} \tag{5.82}$$

with $\mathsf{U}_{\check{\alpha}^0}(\tau_{i+1}, \tau_i)$ and $\mathsf{U}_{\check{\alpha}^1}(\tau_{i+1}, \tau_i)$ given by Eqs. (5.72), (5.74) and (5.80). The strict alternation between transitions and jumps suggests to map the open Landau-Zener system to an alternating classical stochastic process.

Before doing so, we note that the non-unitary part of $\mathsf{U}_{\check{\alpha}^0}$ and of $\mathsf{U}_{\check{\alpha}^1}$ lead to a decay of the populations in $|0\rangle$ and $|1\rangle$, respectively. Hence, in the limit $\tau \to \infty$, odd jump terms $\rho^{(2n+1)}$ contribute only to the population $\langle 0|\rho_\tau|0\rangle$, and therefore to tunneling, whereas even jump terms $\rho^{(2n)}$ contribute only to $\langle 1|\rho_\tau|1\rangle$. So the total tunneling probability $P(\delta, \gamma)$ is given by the sum of the weights (4.33) of all uneven jump terms,

$$P(\delta, \gamma) = \sum_{n=0}^{\infty} w_{2n+1}(\tau \to \infty). \tag{5.83}$$

Classical Stochastic Process

We saw that the transformations that make up the jump expansion after the resummation, Eq. (5.82), strictly alternate between Landau-Zener tunnelings and jumps. In other words, in order for n jumps to occur, the system must have tunneled n times, and for $(n+1)$ tunnelings n jumps are necessary. This suggests to map the problem to a classical inhomogeneous Markov chain with two alternating rates $\lambda_0(\tau)$ and $\lambda_1(\tau)$, corresponding to the Landau-Zener transfer rate and to the jump rate, respectively, see Fig. 5.7. In addition, we will assume that Landau-Zener tunneling is only possible during a finite time interval of length τ^* (*i.e.* $\lambda_0(\tau > \tau^*) = 0$) during which the two levels are close to each other[5]. Despite the obvious quantum nature of the problem, this classical description will prove to be surprisingly exact.

An inhomogeneous Markov chain is defined by the states $n = 0, 1, 2 \ldots$ and the time-dependent transition rates $\lambda_n(\tau)$ between state n and state $n + 1$, see Fig. 5.8. The

[5]Note that, for simplicity, we here allow tunneling between $\tau = 0$ and $\tau = \tau^*$, although the parametrization of the original Landau-Zener system suggests to use a symmetrical interval around $\tau = 0$, *e.g.* $[-\tau^*/2, \tau^*/2]$. Also, we do not consider $\tau < 0$ at all since the resummation ensures that no jumps take place before the first tunneling.

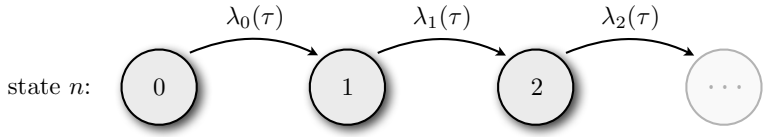

Figure 5.8: Schematic diagram of a classical inhomogeneous Markov chain: The probability $p_n(\tau)$ to find the system in state n at time τ decreases with the time-dependent transition rate $\lambda_n(\tau)$ in favor of $p_{n+1}(\tau)$. This defines the differential equation (5.84). For strictly positive transition rates $\lambda_n(\tau)$, the average jump count $\bar{n}(\tau) = \sum_n np_n(\tau)$ can only increase (this is also called a Markovian birth process). The initial condition $p_n(0) = \delta_{n,0}$ leads to Eq. (5.85).

differential equations that govern its dynamics are therefore

$$\dot{p}_n(\tau) = \lambda_{n-1}(\tau)p_{n-1}(\tau) - \lambda_n(\tau)p_n(\tau), \tag{5.84}$$

$$\text{with } p_0(\tau) = e^{-\int_0^\tau \lambda_0(\tau')\mathrm{d}\tau'}. \tag{5.85}$$

In the following, we use the abbreviation $\Lambda_n(\tau)$ for $\int_0^\tau \lambda_n(\tau')\mathrm{d}\tau'$. Since here we assume positive transition rates $\lambda_n(\tau)$, the average count $\bar{n}(\tau) = \sum_n np_n(\tau)$ strictly increases with time. This type of dynamics is also called a *Markovian birth process*. Equation (5.84) can be reformulated by multiplication with $\exp(\Lambda_n(\tau))$,

$$e^{\Lambda_n(\tau)}\lambda_{n-1}(\tau)p_{n-1}(\tau) = e^{\Lambda_n(\tau)}(\dot{p}_n(\tau) + \lambda_n(\tau)p_n(\tau)) = \frac{\mathrm{d}}{\mathrm{d}\tau}(e^{\Lambda_n(\tau)}p_n(\tau)), \tag{5.86}$$

and integrated to obtain

$$p_n(\tau) = e^{-\Lambda_n(\tau)} \int_0^\tau e^{\Lambda_n(\tau')}\lambda_{n-1}(\tau')p_{n-1}(\tau')\mathrm{d}\tau'. \tag{5.87}$$

Adopting two alternating transition rates, we fix $\lambda_{2n}(\tau) = \lambda_0(\tau)$ and $\lambda_{2n+1}(\tau) = \lambda_1(\tau)$ in the following. If the transition rate λ_0 vanishes after time τ^* ($\lambda_0(\tau > \tau^*) = 0$), the Markov chain is interrupted at every second link. Hence, after τ^* we can register at most one more transition from state $2n-1$ to $2n$, if $\lambda_1(\tau) \neq 0$, before the evolution ceases entirely. For the probabilities at infinite time we thus have

$$p_{2n-1}(\infty) = 0, \tag{5.88}$$

$$p_{2n}(\infty) = p_{2n-1}(\tau^*) + p_{2n}(\tau^*). \tag{5.89}$$

For the mapping between the inhomogeneous Markov chain and the open Landau-Zener jump expansion, we identify the state $2n$ with the system state after n tunnelings plus n jumps, see Fig. 5.7 (b). At $\tau \to \infty$, the weight $w_n(\tau)$ of the n-th order term $\rho_\tau^{(n)}$, which involves exactly n jumps, is therefore given by

$$w_n(\infty) = p_{2n}(\infty) = p_{2n-1}(\tau^*) + p_{2n}(\tau^*). \tag{5.90}$$

This, together with Eq. (5.83), allows deducing the total tunneling probability from the Markov chain.

After defining the mapping of the open Landau-Zener system to the alternating inhomogeneous Markov chain, we want to ensure that the latter satisfies the exact limits for the tunneling probability at infinitely strong and at zero dephasing as given by Eqs. (5.39) and (5.60). Zero dephasing corresponds to $\lambda_1(\tau) = 0$, which causes the Markov chain to stop after the first transition. In this case $p_1(\tau) = 1 - p_0(\tau)$, so that Eqs. (5.85) and (5.90) lead to

$$P(\delta, 0) = 1 - p_0(\tau^*) = 1 - e^{-\Lambda_0(\tau^*)}. \tag{5.91}$$

The comparison with Eq. (5.39) immediately yields the requirement

$$\Lambda_0(\tau^*) = 2\pi\delta. \tag{5.92}$$

For strong dephasing, $\lambda_1(\tau) \gg \lambda_0(\tau)$, every second transition of the alternating Markov chain occurs immediately after the previous one. Adiabatic elimination of the p_{2n+1} hence leads to an inhomogeneous Poisson process with rate $\lambda_0(\tau)$ with the well-known probability distribution

$$p_{2n}(\tau) = \frac{\Lambda_0(\tau)^n}{n!} e^{-\Lambda_0(\tau)}. \tag{5.93}$$

Adding up every second of these probabilities as prescribed by Eqs. (5.83) and (5.90) we see that the condition (5.92) automatically leads to the correct strong dephasing limit (5.60),

$$P(\delta, \infty) = \sum_{n=0}^{\infty} \frac{\Lambda_0(\tau^*)^{2n+1}}{(2n+1)!} e^{-\Lambda_0(\tau^*)} = \frac{1}{2}(1 - e^{-4\Lambda_0(\tau^*)}) = \frac{1}{2}(1 - e^{-4\pi\delta}). \tag{5.94}$$

By symmetry, the alternating Markov chain reduces to an inhomogeneous Poisson process with rate $\lambda_1(\tau)$ in the limit of very strong Landau-Zener tunneling, $\lambda_0(\tau) \gg \lambda_1(\tau)$. In contrast to the strong dephasing limit, here the even probabilities $p_{2n}(\tau)$ vanish while the odd ones, $p_{2n+1}(\tau)$, converge to a Poisson distribution,

$$p_{2n+1}(\tau) = \frac{\Lambda_1(\tau)^n}{n!} e^{-\Lambda_1(\tau)}. \tag{5.95}$$

To obtain the probability distribution in the intermediate regime, $\lambda_0(\tau) \approx \lambda_1(\tau)$, under the condition that it converges to the Poissonian distributions, Eqs. (5.93) and (5.95), in the respective limits, we make the following ansatz. First, we only consider sums $p_{2n-1}(\tau) + p_{2n}(\tau)$ of consecutive even and odd probabilities, since they ultimately determine the tunneling probability $P(\delta, \gamma)$, see Eq. (5.90). This saves us the task of considering the limits of even and odd probabilities separately. Second, we take $p_{2n-1}(\tau) + p_{2n}(\tau)$ so that it fulfills the limit (5.93) by definition, and that it decays exponentially with $\Lambda_1(\tau)$ for $\Lambda_1(\tau) \to \infty$ in analogy to the exponential decay of the Poissonian probabilities (5.95). Third, for simplicity we make the additional assumption that $p_{2n-1}(\tau) + p_{2n}(\tau)$ does not depend the transition rates $\lambda_0(\tau)$ and $\lambda_1(\tau)$ explicitly,

as one would expect for $\lambda_0(\tau) \approx \lambda_1(\tau)$, but only on their integrals $\Lambda_0(\tau)$ and $\Lambda_1(\tau)$. We therefore have,

$$p_{2n-1}(\tau) + p_{2n}(\tau) = \frac{\Lambda_0(\tau)^n}{n!} e^{-\Lambda_0(\tau)} (1 + f_n[\Lambda_1(\tau)] e^{-\Lambda_1(\tau)}), \tag{5.96}$$

where $f_n[\Lambda_1(\tau)]$ is a polynomial in $\Lambda_1(\tau)$ of finite order,

$$f_n[\Lambda_1(\tau)] = c_{n,0} + c_{n,1}\Lambda_1(\tau) + c_{n,2}[\Lambda_1(\tau)]^2 + \ldots, \tag{5.97}$$

with coefficients $c_{n,i}$ that depend on $\Lambda_0(\tau)$. In the absence of dephasing, $\Lambda_1(\tau^*) = 0$, the values of expression (5.96) for $\tau = \tau^*$ are determined by Eq. (5.91),

$$p_0(\tau^*) = e^{-\Lambda_0(\tau^*)} = e^{-\Lambda_0(\tau^*)}(1 + c_{0,0}), \tag{5.98}$$

$$p_1(\tau^*) + p_2(\tau^*) = 1 - e^{-\Lambda_0(\tau^*)} = \Lambda_0(\tau^*) e^{-\Lambda_0(\tau^*)}(1 + c_{1,0}), \tag{5.99}$$

$$p_{2n-1}(\tau^*) + p_{2n}(\tau^*) = 0, \quad \text{for } n > 1. \tag{5.100}$$

This determines the coefficients $c_{0,0} = 0$ and $c_{1,0} = 0$ and we have, in addition, $c_{i,0} = 0$ for $i > 0$ since $p_0(\tau^*)$ is independent of dephasing and therefore of $\Lambda_1(\tau)$.

For small but nonvanishing $\Lambda_1(\tau^*)$, the asymptotic behavior of the Markov chain, Eq. (5.95), requires that

$$p_{2n-1}(\tau^*) + p_{2n}(\tau^*) \propto [\Lambda_1(\tau^*)]^{n-1} + \mathcal{O}([\Lambda_1(\tau^*)]^n), \quad \text{for } n > 1. \tag{5.101}$$

In order for this condition to be fulfilled, the Taylor expansion of $1 + f_n[\Lambda_1(\tau)]e^{-\Lambda_1(\tau)}$ must vanish to $(n-2)$-th order, which determines the coefficients $c_{i,n}$ for $i < n-1$. If we ask for the specific polynomial f_n which yields the required asymptotic behavior with the smallest possible order, *i.e.* we take $c_{n,i} = 0$ for $i > n$, then the highest order coefficient $c_{n,n}$ is determined by the norm of the probability distribution, $\sum_n p_{2n-1}(\tau^*) + p_{2n}(\tau^*) = 1$. Taken together, this yields

$$\begin{aligned} p_{2n}(\infty) &= p_{2n-1}(\tau^*) + p_{2n}(\tau^*) \\ &= \frac{\Lambda_0^n(\tau^*)}{n!} e^{-\Lambda_0(\tau^*)} \left[1 - \frac{\Gamma(n, \Lambda_1(\tau^*))}{(n-1)!}\right] + \frac{\Lambda_1^{n-1}(\tau^*)}{(n-1)!} e^{-\Lambda_1(\tau^*)} \left[1 - \frac{\Gamma(n, \Lambda_0(\tau^*))}{(n-1)!}\right]. \end{aligned} \tag{5.102}$$

The expression (5.102) shows the anticipated symmetry in Λ_0 and Λ_1 and reduces to a Poissonian probability distribution in the limit of large Λ_0 and large Λ_1. The difference appearing in the order of the Poissonian factors (n for Λ_0 and $n-1$ for Λ_1) indicates that the order of the alternation in the Markov chain distinguishes Λ_0 from Λ_1.

While the limiting tunneling probabilities $P(\delta, 0)$ and $P(\delta, \infty)$, Eqs. (5.91) and (5.94), determine the value of $\Lambda_0(\tau^*)$ as a function of the Landau-Zener parameter δ, Eq. (5.92), we assume $\Lambda_1(\tau^*)$ to be proportional to the dephasing rate γ and time τ^*,

$$\Lambda_1(\tau^*) = \gamma\tau^*. \tag{5.103}$$

The probability distribution (5.102) for the alternating inhomogeneous Markov chain, together with the integrated transition probabilities, Eqs. (5.92) and (5.103), now allows us to determine the the open Landau-Zener tunneling probability $P(\delta, \gamma)$, Eq. (5.83), as a function of the parameters γ, δ, and τ^*.

The Landau-Zener Time

Among the parameters γ, δ, and τ^*, the Landau-Zener tunneling time τ^* is the only one which does not appear in the original quantum master equation (5.56). It therefore remains to be determined to complete the mapping between the classical inhomogeneous Markov chain and the open quantum system.

The Landau-Zener time τ^* can be obtained from the classical Markov chain by means of the integrated transition probabilities given by Eqs. (5.92) and (5.103). Specifically, the probability $p_2(\infty)$ for two transitions, determined by Eq. (5.102), reads

$$p_2(\infty) = 2\pi\delta e^{-2\pi\delta}(1 - e^{-\gamma\tau^*}) + e^{-\gamma\tau^*}(1 - e^{-2\pi\delta}). \tag{5.104}$$

We see that τ^* is here determined by the derivative of $p_2(\infty)$ with respect to γ, at $\gamma = 0$,

$$\partial_\gamma p_2(\infty)|_{\gamma=0} = ((1 + 2\pi\delta)e^{-2\pi\delta} - 1)\tau^*. \tag{5.105}$$

As one expects, the characteristic time during which Landau-Zener tunneling takes place depends only on the parameter δ of the coherent evolution and not on the incoherent dephasing rate γ. The derivative (5.105), in turn, can be assessed by means of the correspondence between the classical Markov chain and the Landau-Zener jump expansion. In particular, Eq. (5.90) states that $p_2(\infty)$ is equal to the weight $w_1(\infty)$ of the first order term $\rho_\infty^{(1)}$ of the jump expansion. Using Eq. (5.79) for $\rho_\tau^{(1)}$ and inserting Eq. (5.66) gives, for $\tau_0 = -\infty$,

$$\rho_\infty^{(1)} = 2\gamma \int_{-\infty}^{\infty} \mathrm{d}\tau_1 \mathsf{U}_{\check{\alpha}^1}(\infty, \tau_1)|0\rangle\langle 0|\mathsf{U}_{\check{\alpha}^0}(\tau_1, -\infty)|1\rangle\langle 1|\mathsf{U}^\dagger_{\check{\alpha}^0}(\tau_1, -\infty)|0\rangle\langle 0|\mathsf{U}^\dagger_{\check{\alpha}^1}(\infty, \tau_1). \tag{5.106}$$

The first order weight is therefore given by

$$\begin{aligned} w_1(\infty) = \mathrm{Tr}[\rho_\infty^{(1)}] &= \langle 0|\rho_\infty^{(1)}|0\rangle + \underbrace{\langle 1|\rho_\infty^{(1)}|1\rangle}_{=0} \\ &= 2\gamma \int_{-\infty}^{\infty} \mathrm{d}\tau_1 \langle 0|\mathsf{U}_{\check{\alpha}^1}(\infty, \tau_1)|0\rangle\langle 0|\mathsf{U}_{\check{\alpha}^0}(\tau_1, -\infty)|1\rangle\langle 1|\mathsf{U}^\dagger_{\check{\alpha}^0}(\tau_1, -\infty)|0\rangle\langle 0|\mathsf{U}^\dagger_{\check{\alpha}^1}(\infty, \tau_1)|0\rangle \\ &= 2\gamma \int_{-\infty}^{\infty} \mathrm{d}\tau_1 \left|\langle 0|\mathsf{U}_{\check{\alpha}^1}(\infty, \tau_1)|0\rangle\right|^2 \left|\langle 0|\mathsf{U}_{\check{\alpha}^0}(\tau_1, -\infty)|1\rangle\right|^2, \end{aligned} \tag{5.107}$$

where we have used that the nonunitary part of $\mathsf{U}_{\check{\alpha}^1}$ leads to a complete decay of the population $\langle 1|\rho_\infty^{(1)}|1\rangle$. Note here, that the closed Landau-Zener problem is invariant under the permutation of $|0\rangle$ and $|1\rangle$ plus time reversal. For the between-jump dynamics, Eqs. (5.68) and (5.69), of the open system, this transformation simply effects a

change of the nonunitary part from $-i\gamma|0\rangle\langle 0|$ to $-i\gamma|1\rangle\langle 1|$. We can therefore substitute $\langle 0|\mathsf{U}_{\check{\alpha}^1}(\infty,\tau_1)|0\rangle$ with $\langle 1|\mathsf{U}_{\check{\alpha}^0}(-\tau_1,-\infty)|1\rangle$ in Eq. (5.107) and insert the closed system propagator U in imaginary time $\pm\tau_1 - i\gamma$, Eq. (5.73),

$$w_1(\infty) = 2\gamma \int_{-\infty}^{\infty} \mathrm{d}\tau_1 \left|\langle 1|\mathsf{U}_{\check{\alpha}^0}(-\tau_1,-\infty)|1\rangle\right|^2 \left|\langle 0|\mathsf{U}_{\check{\alpha}^0}(\tau_1,-\infty)|1\rangle\right|^2 \tag{5.108}$$

$$= 2\gamma \int_{-\infty}^{\infty} \mathrm{d}\tau_1 \left|\langle 1|\mathsf{U}(-\tau_1 - i\gamma,-\infty)|1\rangle\right|^2 \left|\langle 0|\mathsf{U}(\tau_1 - i\gamma,-\infty)|1\rangle\right|^2 . \tag{5.109}$$

This expression for $w_1(\infty)$ now allows us to rewrite the derivative of $p_2(\infty)$ with respect to γ as

$$\begin{aligned}\partial_\gamma p_2(\infty) = \partial_\gamma w_1(\infty) = 2\int_{-\infty}^{\infty} \mathrm{d}\tau_1 \Big\{ &\left|\langle 1|\mathsf{U}(-\tau_1 - i\gamma,-\infty)|1\rangle\right|^2 \left|\langle 0|\mathsf{U}(\tau_1 - i\gamma,-\infty)|1\rangle\right|^2 \\ &+\partial_\gamma \left|\langle 1|\mathsf{U}(-\tau_1 - i\gamma,-\infty)|1\rangle\right|^2 \left|\langle 0|\mathsf{U}(\tau_1 - i\gamma,-\infty)|1\rangle\right|^2 \Big\} .\end{aligned} \tag{5.110}$$

The chain rule for the second summand implies the derivative of the propagator with respect to its first (time) argument, for which we can insert the closed system Schrödinger equation, $\partial_\tau \mathsf{U}(\tau,\tau_0) = -i\mathsf{H}_{\mathrm{LZ}}(\tau)\mathsf{U}(\tau,\tau_0)$. For brevity we omit the initial time $\tau_0 = -\infty$ as the second argument of U and use $\mathsf{H}_{\mathrm{LZ}}(\tau) = \tau/2\sigma_z + \sqrt{\delta}\sigma_x$ to obtain

$$\begin{aligned}\partial_\gamma w_1(\infty) = 2\int_{-\infty}^{\infty} \mathrm{d}\tau_1 \Big\{ &\left|\langle 1|\mathsf{U}(-\tau_1 - i\gamma)|1\rangle\right|^2 \left|\langle 0|\mathsf{U}(\tau_1 - i\gamma)|1\rangle\right|^2 - 2\gamma \left|\langle 0|\mathsf{U}(\tau_1 - i\gamma)|1\rangle\right|^2 \\ &\times \mathrm{Re}\left[\langle 1|\mathsf{H}_{\mathrm{LZ}}(-\tau_1 - i\gamma)\mathsf{U}(-\tau_1 - i\gamma)|1\rangle\langle 1|\mathsf{U}(-\tau_1 - i\gamma)|1\rangle^*\right] - 2\gamma \\ &\times \left|\langle 1|\mathsf{U}(-\tau_1 - i\gamma)|1\rangle\right|^2 \mathrm{Re}\left[\langle 0|\mathsf{H}_{\mathrm{LZ}}(\tau_1 - i\gamma)\mathsf{U}(\tau_1 - i\gamma)|1\rangle\langle 0|\mathsf{U}(\tau_1 - i\gamma)|1\rangle^*\right]\Big\} \\ = 2\int_{-\infty}^{\infty} \mathrm{d}\tau_1 \Big\{ &(1 - 2\gamma\tau_1) \left|\langle 1|\mathsf{U}(-\tau_1 - i\gamma)|1\rangle\right|^2 \left|\langle 0|\mathsf{U}(\tau_1 - i\gamma)|1\rangle\right|^2 \\ &-2\gamma\sqrt{\delta}\Big(\mathrm{Re}\left[\langle 0|\mathsf{U}(-\tau_1 - i\gamma)|1\rangle \left(\langle 1|\mathsf{U}(-\tau_1 - i\gamma)|1\rangle\right)^*\right] \left|\langle 0|\mathsf{U}(\tau_1 - i\gamma)|1\rangle\right|^2 \\ &+ \left|\langle 1|\mathsf{U}(-\tau_1 - i\gamma)|1\rangle\right|^2 \mathrm{Re}\left[\langle 1|\mathsf{U}(\tau_1 - i\gamma)|1\rangle \left(\langle 0|\mathsf{U}(\tau_1 - i\gamma)|1\rangle\right)^*\right]\Big)\Big\} .\end{aligned} \tag{5.111}$$

The second and the third term of this expression vanish for $\gamma = 0$. In contrast, the first term, integrated from $\tau_1 = -\infty$ to ∞, is ill defined since the integrand asymptotically behaves as $(1 - 2\gamma\tau_1)(1 - e^{-2\pi\delta})e^{-\gamma\tau_1}$ for large τ_1, which yields a constant for $\gamma = 0$. Subtracting this asymptotic expression on the positive half axis, however, and noting that $\int_0^\infty (1 - 2\gamma\tau_1)e^{-\gamma\tau_1}\mathrm{d}\tau_1 = 0$, one obtains a well defined integral for all values of γ,

$$\begin{aligned}\partial_\gamma w_1(\infty) = 2\int_{-\infty}^{\infty} \mathrm{d}\tau_1 \Big\{ &(1 - 2\gamma\tau_1) \left|\langle 1|\mathsf{U}(-\tau_1 - i\gamma)|1\rangle\right|^2 \left|\langle 0|\mathsf{U}(\tau_1 - i\gamma)|1\rangle\right|^2 \\ &-\Theta(\tau_1)(1 - 2\gamma\tau_1)(1 - e^{-2\pi\delta})e^{-\gamma\tau_1}\Big\}.\end{aligned} \tag{5.112}$$

Setting $\gamma = 0$, as is required for the determination of τ^* in Eq. (5.105), we obtain

$$\begin{aligned}\partial_\gamma w_1(\infty)\Big|_{\gamma=0} &= 2\int_{-\infty}^{\infty} \mathrm{d}\tau_1 \left\{ |\langle 1|\mathsf{U}(-\tau_1)|1\rangle|^2 \, |\langle 0|\mathsf{U}(\tau_1)|1\rangle|^2 - \Theta(\tau_1)(1-e^{-2\pi\delta}) \right\} \\ &= 2\int_{-\infty}^{\infty} \mathrm{d}\tau_1 \left\{ \left|\langle 1|\mathsf{U}(-\tau_1)|1\rangle\right|^2 \left(1 - \left|\langle 1|\mathsf{U}(\tau_1)|1\rangle\right|^2\right) - \Theta(\tau_1)(1-e^{-2\pi\delta}) \right\} \\ &= 2\int_{-\infty}^{\infty} \mathrm{d}\tau_1 \left\{ \left|e^{-\frac{\pi\delta}{4}} D_{i\delta}\left(-\tau_1 e^{\frac{3\pi}{4}i}\right)\right|^2 \left[1 - \left|e^{-\frac{\pi\delta}{4}} D_{i\delta}\left(\tau_1 e^{\frac{3\pi}{4}i}\right)\right|^2\right] \right. \\ &\quad \left. -\Theta(\tau_1)(1-e^{-2\pi\delta}) \right\}, \end{aligned} \tag{5.113}$$

where in the second equality we have used the conservation of the norm under U.

With Eqs. (5.105) and (5.113), we have derived an explicit expression for the Landau-Zener interaction time τ^* in terms of an integral over parabolic cylinder functions and as a function of the adiabaticity parameter δ. Unfortunately, the integral in Eq. (5.113) has no known analytic solution. In what follows, we will approximate the integral by solving it analytically for large and small δ and then interpolating between the two limits with an appropriate analytic function. We start with the lowest order approximation of the parabolic cylinder function for large parameters [102],

$$D_{\frac{1}{2}\mu^2-\frac{1}{2}}\left(\sqrt{2}\mu z\right) \xrightarrow{|\mu|\to\infty} g(\mu)\frac{e^{\mu^2\xi(t)}}{(t^2-1)^{\frac{1}{4}}}, \tag{5.114}$$

with $g(\mu)^{-1} = 2^{\mu^2/4+1/4} e^{1/4\mu^2} \mu^{-\mu^2/2+1/2}$ and $2\xi(t) = t\sqrt{t^2-1} - \ln[t+\sqrt{t^2-1}]$. For the specific parabolic cylinder function $D_{i\delta}(-\tau \exp[3\pi i/4])$ involved in Eq. (5.113), this expression simplifies to

$$\begin{aligned} D_{i\delta}\left(-\tau e^{\frac{3\pi}{4}i}\right) \xrightarrow{\delta\to\infty} & \frac{2^{-\frac{1}{2}-i\delta} e^{-\frac{1}{4}-\frac{i\delta}{2}}}{(-2-i\tau^2-4i\delta)^{\frac{1}{4}}} \exp\left[\sqrt{-2-i\tau^2-4i\delta}\frac{\tau}{4} e^{\frac{3\pi}{4}i}\right] \\ & \times \left(-\tau e^{\frac{3\pi}{4}i} + \sqrt{-2-i\tau^2-4i\delta}\right)^{\frac{1}{2}+i\delta}. \end{aligned} \tag{5.115}$$

The absolute square of expression (5.115) can be further approximated for large δ by

$$\left|e^{-\frac{\pi\delta}{4}} D_{i\delta}\left(-\tau e^{\frac{3\pi}{4}i}\right)\right|^2 \xrightarrow{\delta\to\infty} \frac{1}{2}\left(1+\frac{\tau}{\sqrt{a+\tau^2}}\right)\left(1-b+\frac{b\tau}{\sqrt{a+\tau^2}}\right), \tag{5.116}$$

with $a = \left(\sqrt{1+4\delta}-2\delta\right)^{-1}$ and $b = 1/2 - \pi\delta/4 - \delta \arctan[(1-2\delta)/(1+2\delta)]$. In this limit, the integral in Eq. (5.113) can be evaluated analytically. After substituting the asymptotic expression, Eq. (5.116), for the parabolic cylinder function and using the new

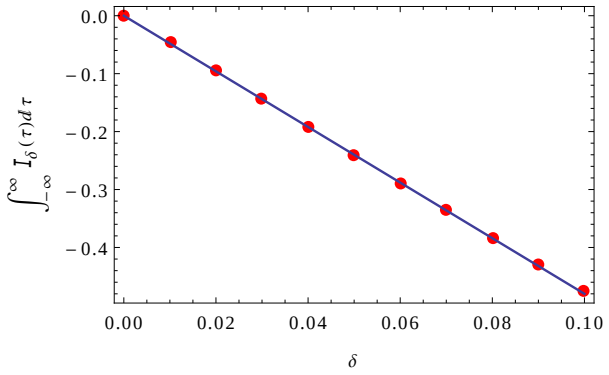

Figure 5.9: Numerical values for the integral $\int_{-\infty}^{\infty} I_\delta(\tau)\mathrm{d}\tau$, Eq. (5.118), as a function of δ (red dots). Since $\int_{-\infty}^{\infty} I_0(\tau)\mathrm{d}\tau = 0$, the linear fit (blue line) gives the first order expansion coefficient $c_1 \approx -4.8$ for small δ.

limiting value 2τ instead of $(1 - e^{-2\pi\delta})$, we obtain

$$\begin{aligned}\partial_\gamma w_1(\infty)|_{\gamma=0} &\xrightarrow{\delta\to\infty} \left[\sqrt{a+\tau^2} + \tau - \frac{ab^2\tau}{4(a+\tau^2)} - \frac{\sqrt{a}}{4}(b^2+2)\arctan\frac{\tau}{\sqrt{a}} - 2\tau\Theta(\tau)\right]_{-\infty}^{\infty} \\ &= -\frac{\pi}{4}\sqrt{a}(2+b^2) = -\pi\sqrt{\delta} + \mathcal{O}\left(\delta^{-\frac{3}{2}}\right). \end{aligned} \tag{5.117}$$

This asymptotic expression for the tunneling time in the limit $\delta \gg 1$ is in agreement with previous studies on that matter [103].

Let us consider the opposite limit of a small adiabaticity parameters δ. Fist, setting $\delta = 0$ we see that both the integrand and and the integral in Eq. (5.113) vanish, since $D_0(z) = e^{-z^2/4}$, which implies $|D_0(\tau e^{3\pi i/4})| = 1$. Second, if we divide Eq. (5.113) by the asymptotic value $1 - e^{-2\pi\delta}$ for $\tau \to \infty$, we can apply l'Hôpital's rule to obtain the new integrand at $\delta = 0$,

$$\begin{aligned} I_\delta(\tau) &\equiv \frac{\delta e^{-\pi\delta}}{1-e^{-2\pi\delta}} \left|D_{i\delta}\left(-\tau e^{\frac{3\pi}{4}i}\right)\right|^2 \left|D_{i\delta-1}\left(\tau e^{\frac{3\pi}{4}i}\right)\right|^2 - \Theta(\tau) \\ &\xrightarrow{\delta\to 0} \frac{1}{2\pi}\left|D_{-1}\left(\tau e^{\frac{3\pi}{4}i}\right)\right|^2 - \Theta(\tau), \end{aligned} \tag{5.118}$$

which is nonvanishing. The integral of $I_0(\tau)$ from $\tau = -\infty$ to ∞ does vanish, however, as can be seen by inserting the identity $D_{-1}(z) = \sqrt{\pi/2}e^{z^2/4}\,\mathrm{erfc}\left(z/\sqrt{2}\right)$ into Eq. (5.118). This implies that the integral in Eq. (5.113) and therefore $\partial_\gamma w_1(\infty)|_{\gamma=0}$ behaves asymptotically as

$$\partial_\gamma w_1(\infty)|_{\gamma=0} \xrightarrow{\delta\to 0} (1 - e^{-2\pi\delta})(c_1\delta + \mathcal{O}(\delta^2)), \tag{5.119}$$

where the coefficient c_1 remains to be determined. This is done by integrating $I_\delta(\tau)$, Eq. (5.118), numerically from $\tau = -\infty$ to ∞ for small δ, see Fig. 5.9. A linear fit to the numerical values gives $c_1 \approx -4.8$.

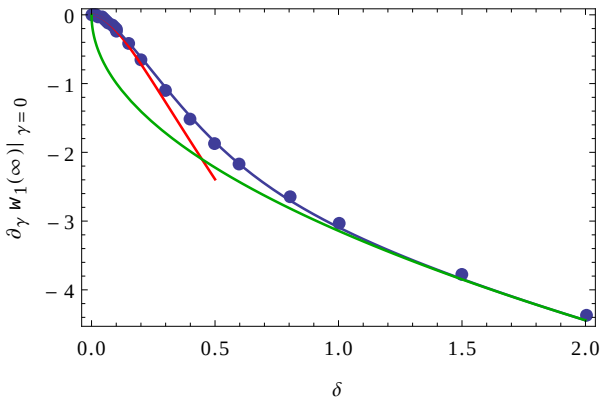

Figure 5.10: Numerically exact values of $\partial_\gamma w_1(\infty)|_{\gamma=0}$ (blue dots) as given by Eq. (5.113) are compared to the analytic approximation, Eq. (5.120), with $c_1 = 4.8$ and $c_2 = 5/2$ (blue line). We see that the analytic approximation has the required asymptotic behavior for large and small δ, Eq. (5.117) (green line) and Eq. (5.119) (red line), and shows only small deviations from the numerically exact values in between.

With the asymptotic expressions for $\partial_\gamma w_1(\infty)|_{\gamma=0}$ in the limits $\delta \gg 1$ and $\delta \ll 1$, Eqs. (5.117) and (5.119), we now use a suitable connecting function in between to finally assess the tunneling time τ^* with the help of Eq. (5.105). A suitable connecting function for $\partial_\gamma w_1(\infty)|_{\gamma=0}$, Eq. (5.113), which has the required asymptotic behavior is given by

$$\partial_\gamma w_1(\infty)|_{\gamma=0} \approx -\pi \tanh(c_2\delta)\sqrt{\delta\left(1 - e^{-4\left(\frac{c_1}{c_2}\right)^2\delta}\right)}. \tag{5.120}$$

Here, the parameter c_2 determines where the transition between the two limiting asymptotic expressions occurs. The error of the approximation (5.120) is minimal for $c_2 = 5/2$, see Fig. 5.10. With the help of Eq. (5.105) we can now approximate the Landau-Zener time τ^* with

$$\tau^* = \frac{\partial_\gamma w_1(\infty)|_{\gamma=0}}{(1+2\pi\delta)e^{-2\pi\delta} - 1} \approx \frac{-\pi \tanh(c_2\delta)}{(1+2\pi\delta)e^{-2\pi\delta} - 1}\sqrt{\delta\left(1 - e^{-\left(\frac{2c_1}{c_2}\right)^2\delta}\right)}. \tag{5.121}$$

This expression for τ^* completely determines the probabilities $p_{2n}(\infty)$, Eq. (5.102), of the alternating, inhomogeneous Markov chain with the integrated transition rates $\Lambda_0(\tau^*) = 2\pi\delta$ and $\Lambda_1(\tau^*) = \gamma\tau^*$, Eqs. (5.92) and (5.103). This classical stochastic process was constructed as an approximate description for the resummed open Landau-Zener jump expansion, $\rho_\tau = \sum_n \rho_\tau^{(n)}$ with $\rho_\tau^{(n)}$ given by Eq. (5.82). It therefore allows, in particular, to calculate the weights $w_n(\tau)$ of the constituent terms $\rho_\tau^{(n)}$ at $\tau = \infty$, see

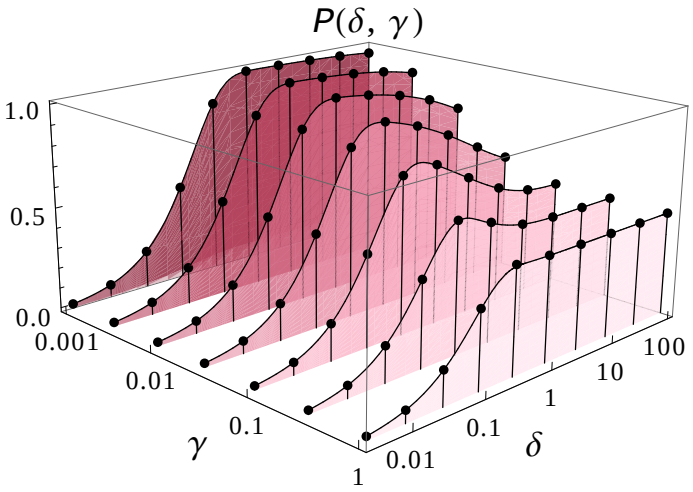

Figure 5.11: Landau-Zener tunneling probability $P(\delta,\gamma)$ in the presence of dephasing as a function of the dephasing rate γ and the adiabaticity parameter δ. The numerically exact $P(\delta,\gamma)$ (black dots) is compared to the analytic approximation (black lines), Eq. (5.122) with τ^* given by (5.121), which is based on a classical stochastic model. The model was constructed to yield the exact asymptotics for $\delta \to 0$ and $\delta \to \infty$, Eqs. (5.91) and (5.94). Deviations from the numerically exact values are below 0.005 over all ranges of the parameters δ and γ (note the logarithmic axes).

Eq. (5.90), and therefore the tunneling probability $P(\delta,\gamma)$ using Eq. (5.83),

$$\begin{aligned} P(\delta,\gamma) &= \sum_{n=0}^{\infty} w_{2n+1}(\infty) \approx \sum_{n=0}^{\infty} p_{4n+2}(\infty) \\ &\approx \sum_{n=0}^{\infty} \frac{(2\pi\delta)^{2n+1}}{(2n+1)!} e^{-2\pi\delta}\left[1 - \frac{\Gamma(2n+1,\gamma\tau^*)}{(2n)!}\right] + \frac{(\gamma\tau^*)^{2n}}{(2n)!} e^{-\gamma\tau^*}\left[1 - \frac{\Gamma(2n+1,\gamma\tau^*)}{(2n)!}\right]. \end{aligned} \tag{5.122}$$

In Fig. (5.11) we compare this analytic approximation to the numerically exact values of $P(\delta,\gamma)$ in a logarithmic plot over all ranges of the parameters δ and γ. The plot shows that the approximation, Eq. (5.122) with τ^* given by Eq. (5.121), is asymptotically exact by construction and shows deviations below 0.005 at intermediate regimes of δ and γ. The approximate classical stochastic description of the open Landau-Zener system, which was derived from the resummation of the jump expansion, proves to be highly accurate.

In conclusion, we have applied the jump expansion and its resummation (4.75) to the Landau-Zener tunneling in the presence of dephasing. Similar to the treatment of spatial detection in Sec. 5.1, the resummation significantly increased the convergence of the jump expansion and yielded analytically accessible jump terms. Here the jump

terms, given in terms of integrals over special functions, exhibited a strict alternation of tunnelings and jumps and could hence be solved by means of an alternating classical stochastic description. This approximate description then yielded a highly accurate analytical approximation to the tunneling probability.

6 Efficient Numerical Simulations of Markovian Dynamics

The dynamics of Markovian open quantum systems is described by a master equation in standard form, Eq. (2.66), for the system density matrix ρ_t. While only a handful of the simplest master equations are solvable analytically[1], the resummation method for the jump expansion can generally be used as a starting point for deriving an analytic approximation to a given model system, see Chap. 5. Usually the solution of an arbitrary master equation is, however, assessed most easily with numerical means.

In Chap. 5, for example, we used a straightforward numerical propagation of the master equations (5.1) and (5.56) on a grid to estimate the quality of our analytic approximations. The direct propagation usually becomes impractical, however, if more complicated, higher dimensional master equations are considered. This is due to the fact that a density matrix ρ_t has N^2-1 independent real variables, where N is the Hilbert space dimension. N, in turn, scales exponentially with the physical degrees of freedom of the considered quantum system.

In the first part of the present chapter we introduce two iterative numerical approximation schemes for Markovian master equations which are more efficient than a direct propagation. The first scheme, called the *Monte Carlo wave function approach* is a well established technique [28, 44, 104]. It is based on the fact that any evolving density matrix ρ_t can be represented as an ensemble of stochastic quantum trajectories $|\psi_t^j\rangle$ corresponding to N-dimensional complex vectors, see Chap. 2, Sec. 2.3. Conversely, this implies that ρ_t can be approximated by the probabilistic mixture of pure states, $\rho_t \approx 1/n \sum_{i=1}^{n} |\psi_t^j\rangle\langle\psi_t^j|$, to which all stochastic realizations $|\psi_t^j\rangle$ contribute equally. This is at present the standard method to solve a Markovian master equation numerically. The second approximation scheme, which is in some sense complementary to the quantum Monte Carlo approach, is derived from the jump expansion of the density matrix, $\rho_t = \sum_n \rho_t^{(n)}$, introduced in Chap. 4. The constituent mixed state terms $\rho_t^{(n)}$ are successively approximated using the Monte Carlo integration method with importance sampling [21]. The possibility to optimize the convergence of the jump expansion using resummation implies here that one can maximally bias the weights of the constituent terms and then calculate the most important ones first.

In the second part of this chapter we demonstrate our novel numerical integration method in three exemplary Markovian open systems. Specifically, we will use it to approximate the dynamics of the damped quantum harmonic oscillator, Eqs. (3.5) and

[1] Two notable analytically solvable Markovian open systems are the two-level system with dephasing [25] and the harmonic oscillator in a bosonic heat bath at zero temperature [28], see Sec. 3.1.

(3.12), of quantum Brownian motion, Eqs. (3.55) and (3.67), and of a continuous, non-selective measurement with feedback, Eq. (3.76). Besides serving as testbeds for the newly derived approximation scheme, these examples show that the optimal resummation increases the convergence of the jump expansion dramatically. Specifically, for the considered open systems we observe convergence within the lowest two to five orders [21]. On the one hand, this indicates that the resummation method may well facilitate analytic approximations to other Markovian open systems than those treated in Chap. 5. On the other hand, it underscores the potential of the jump expansion to yield highly efficient numerical approximation schemes.

6.1 Numerical Methods

6.1.1 Monte Carlo Wave Function Approach

In Sec. 2.3 we saw that the time evolution of the mixed state density matrix ρ_t under a general Markovian master equation,

$$\partial_t \rho_t = -\frac{i}{\hbar}\left[\mathsf{H}, \rho_t\right] + \sum_i \gamma_i(t)\left(\mathsf{L}_i \rho_t \mathsf{L}_i^\dagger - \frac{1}{2}\mathsf{L}_i^\dagger \mathsf{L}_i \rho_t - \frac{1}{2}\rho_t \mathsf{L}_i^\dagger \mathsf{L}_i\right), \tag{6.1}$$

is equivalent to the ensemble average of the pure states $|\psi_t^j\rangle\langle\psi_t^j|$ evolving under the stochastic differential equation (2.113). The superscript j here labels different realizations of the stochastic dynamics. Therefore, a finite size ensemble $\{|\psi_t^1\rangle\langle\psi_t^1|, \ldots |\psi_t^n\rangle\langle\psi_t^n|\}$ approximates ρ_t as

$$\rho_t \approx \frac{1}{n}\sum_{j=1}^{n} |\psi_t^j\rangle\langle\psi_t^j|, \tag{6.2}$$

with the approximation becoming exact in the limit $n \to \infty$. In other words, we can approximate ρ_t by propagating the initial state, say $\rho_0 = |\psi_0\rangle\langle\psi_0|$, with the corresponding stochastic differential equation n times and then mixing the obtained realizations $|\psi_t^j\rangle$ uniformly.

In order to outline a procedure for obtaining single realizations $|\psi_t^j\rangle$ of the stochastic dynamics that gives ρ_t on average, let us first write down the corresponding stochastic differential equation, Eq. (2.113),

$$\begin{aligned} |\mathrm{d}\psi_t\rangle = &-\frac{i}{\hbar}\mathsf{H}|\psi_t\rangle \mathrm{d}t - \frac{1}{2}\sum_i \gamma_i(t)\left[\mathsf{L}_i^\dagger \mathsf{L}_i - \langle \mathsf{L}_i^\dagger \mathsf{L}_i\rangle_\psi\right]|\psi_t\rangle \mathrm{d}t \\ &+ \sum_i \left[\frac{\mathsf{L}_i|\psi_t\rangle}{\langle\psi_t|\mathsf{L}_i^\dagger \mathsf{L}_i|\psi_t\rangle} - |\psi_t\rangle\right]\mathrm{d}N_i(t). \end{aligned} \tag{6.3}$$

It consists of a piecewise deterministic evolution with interspersed random jump transformations governed by the independent Poisson processes $N_i(t)$. Here, the average of

the Poisson increments must satisfy

$$\mathbb{E}[\mathrm{d}N_i(t)] = \gamma_i(t)\langle \mathsf{L}_i^\dagger \mathsf{L}_i\rangle \mathrm{d}t, \tag{6.4}$$

which is equal to the probability for a jump of type i to occur within the time interval $[t, t+\mathrm{d}t]$. Equations (6.3) and (6.4) together imply that one must execute the following iterative procedure. Assume that at time t' we have the pure state $|\psi_{t'}\rangle$, which is either the initial state, for $t'=0$, or a state that was obtained from the execution of a jump, see step 2 below. Then execute the following steps:

1. For the (piecewise) deterministic evolution, first line in Eq. (6.3), propagate $|\psi_{t'}\rangle$ with the nonlinear equation

$$\partial_t|\psi_t\rangle = -\frac{i}{\hbar}\left[\mathsf{H}^{\mathrm{eff}}(t) + \frac{1}{2}\left\langle\psi_t|\mathsf{H}^{\mathrm{eff}}(t) - \mathsf{H}^{\mathrm{eff}}(t)^\dagger|\psi_t\right\rangle\right]|\psi_t\rangle, \tag{6.5}$$

with the non-Hermitian effective Hamiltonian

$$\mathsf{H}^{\mathrm{eff}}(t) = \mathsf{H} - \frac{i\hbar}{2}\sum_i \gamma_i(t)\mathsf{L}_i^\dagger\mathsf{L}_i. \tag{6.6}$$

Note that the second, nonlinear term in Eq. (6.5) simply compensates for the norm decay under the non-Hermitian part of $\mathsf{H}^{\mathrm{eff}}$ in the first term. This propagation is performed until the time t'' of the next jump. The latter is determined by drawing a random number r uniformly from the interval $[0,1]$, and solving the equation

$$r = \langle\psi_{t'}|e^{\frac{i}{\hbar}\int_{t'}^{t''}\mathsf{H}^{\mathrm{eff}}(t)^\dagger \mathrm{d}t}e^{-\frac{i}{\hbar}\int_{t'}^{t''}\mathsf{H}^{\mathrm{eff}}(t)\mathrm{d}t}|\psi_{t'}\rangle. \tag{6.7}$$

This guarantees that the probability of performing a jump between t and $t+\mathrm{d}t$ is equal to the norm decay under $\mathsf{H}^{\mathrm{eff}}$ at time t, $\langle\psi_t|\sum_i\gamma_i(t)\mathsf{L}_i^\dagger\mathsf{L}_i|\psi_t\rangle$, and therefore to the sum of the independent Poissonian jump probabilities, Eq. (6.4).

In practice, the above nonlinear propagation between t' and t'' can be realized by propagating $|\psi_t\rangle$ with $\exp\left(-i\mathsf{H}^{\mathrm{eff}}(t)\Delta t/\hbar\right)$ and a small time step Δt. After each step, the state vector must then be renormalized, *i.e.* we must divide $|\psi_{t+k\Delta t}\rangle$ after, say, k steps by $\sqrt{d_k} = \sqrt{\langle\psi_{t+k\Delta t}|\psi_{t+k\Delta t}\rangle}$. Before performing the next step, we can then check the jump condition (6.7) easily as the right hand side is given by $\prod_{j=1}^k d_j$.

2. Randomly apply a jump, corresponding to one of the independent Poisson processes $N_i(t)$, to the state $|\psi_{t''}\rangle$. The probability p_i to have a jump in the process $N_i(t)$ at time t'' is proportional to $\gamma_i(t'')\langle\mathsf{L}_i^\dagger\mathsf{L}_i\rangle$, see Eq. (6.4). With the normalization of the probability distribution p_i, we have

$$p_i = \frac{\gamma_i(t'')\langle\psi_{t''}|\mathsf{L}_i^\dagger\mathsf{L}_i|\psi_{t''}\rangle}{\sum_i\gamma_i(t'')\langle\psi_{t''}|\mathsf{L}_i^\dagger\mathsf{L}_i|\psi_{t''}\rangle}. \tag{6.8}$$

Hence, we draw the index i randomly from the probability distribution p_i. Then, we apply the jump transformation of type i,

$$|\psi'_{t''}\rangle = \frac{\mathsf{L}_i|\psi_{t''}\rangle}{\langle\psi_{t''}|\mathsf{L}_i^\dagger\mathsf{L}_i|\psi_{t''}\rangle}. \tag{6.9}$$

Note that, by dividing by the expectation value $\langle\psi_{t''}|\mathsf{L}_i^\dagger\mathsf{L}_i|\psi_{t''}\rangle$, we conserve the norm of $|\psi_{t''}\rangle$. On average, the jumps given by Eq. (6.9) lead to the stochastic part of the dynamics, as described by the second line of Eq. (6.3). After performing a random jump, we continue the next interval of deterministic evolution, *i.e.* we go back to step 1, substituting $|\psi'_{t''}\rangle$ with $|\psi_{t'}\rangle$. These two steps are iterated until we reach the final time t of the stochastic evolution.

After generating a sufficiently large number of realizations $|\psi_t^j\rangle$ of the above stochastic propagation, their ensemble average, Eq. (6.2), converges to the solution ρ_t of the master equation. Since the ensemble average is, however, performed uniformly, *i.e.* all realizations $|\psi_t^j\rangle$ contribute equally, this convergence is by no means guaranteed to be rapid. This motivates a second method for the numerical approximation of ρ_t based on the jump expansion, whose convergence can be optimized with the adaptive resummations derived in Chap. 4.

6.1.2 Monte Carlo Integral Estimate of the Jump Expansion

The jump expansion introduced in Chap. 4 decomposes solutions ρ_t of a Markovian master equation into an infinite sum of mixed state terms $\rho_t^{(n)}$. Analogous to the Monte Carlo wave function approach discussed above, we can approximate ρ_t by the sum of the lowest m terms,

$$\rho_t \approx \sum_{n=0}^{m} \rho_t^{(n)}. \tag{6.10}$$

The advantage of using the jump expansion is that each term $\rho_t^{(n)}$ has its own specific weight, $w_n(t) = \operatorname{Tr}\rho_t^{(n)}$, and one can maximize the lowest order weights by applying the adaptive resummations derived in Sec. 4.3 [21]. The approximation (6.10) for ρ_t therefore allows one to calculate the constituent terms $\rho_t^{(n)}$ systematically, starting with the most important ones. In the standard trajectory-based approximation (6.2), in contrast, all terms contribute equally and the importance of one specific trajectory arises only from the frequency of its (stochastic) occurrence.

Let us demonstrate how one can calculate the approximation terms $\rho_t^{(n)}$ numerically. First note that the $\rho_t^{(n)}$ are composed of the branches $\rho_t^{(\mathfrak{R}^n)}$ which originate from the initial state ρ_0 by a sequence of continuous propagations $\mathcal{U}_{\boldsymbol{\alpha}}(t_{i+1}, t_i)$ and jump transformations $\mathcal{J}_{j_i,\boldsymbol{\alpha}}(t_i)$, see Eqs (4.29)–(4.31). The branches $\rho_t^{(\mathfrak{R}^n)}$ are completely determined by an associated jump record $\mathfrak{R}^n = (j_1, t_1; j_2, t_2; \ldots; j_n, t_n)$, containing the times t_i and the types j_i of jumps taking place, and by the complex shifts $\boldsymbol{\alpha}$ of the jump operators. With the jump times t_i distributed over the entire propagation interval $[0, t]$, the decomposition

of $\rho_t^{(n)}$ into its branches involves a multi-integral over the t_i and a sum over the jump indices j_i. For the numerical evaluation of the jump time multi-integral, it is advantageous to group those branches with the same t_i but with different j_i,

$$\rho_t^{(n)} = \int_0^t \mathrm{d}t_n \int_0^{t_n} \mathrm{d}t_{n-1} \ldots \int_0^{t_2} \mathrm{d}t_1 \sum_{j_1 \ldots j_n} \rho_t^{(\mathfrak{R}^n)} \equiv \int_0^t \mathrm{d}t_n \int_0^{t_n} \mathrm{d}t_{n-1} \ldots \int_0^{t_2} \mathrm{d}t_1 \rho_t^{(\mathfrak{t}^n)}, \tag{6.11}$$

with $\mathfrak{t}^n = (t_1, t_2, \ldots, t_n)$.

Monte Carlo Integration with Importance Sampling

Generally, multi-integrals such as the one in Eq. (6.11) are evaluated numerically efficiently using Monte Carlo integration [105]. The Monte Carlo integration method prescribes that the integral of a function $f(\mathfrak{t}^n)$ over the finite n-dimensional volume V is approximated by V times the arithmetic mean of f at N randomly chosen sample points $\mathfrak{t}_i^n$,

$$\int_V f(\mathfrak{t}^n)\mathrm{d}\mathfrak{t}^n \approx V\langle f\rangle_N \pm V\sqrt{\frac{\langle f^2\rangle_N - \langle f\rangle_N^2}{N}}. \tag{6.12}$$

Here, the mean and the second moment are defined as usual,

$$\langle f\rangle_N = \frac{1}{N}\sum_{i=1}^N f(\mathfrak{t}_i^n) \qquad \langle f^2\rangle_N = \frac{1}{N}\sum_{i=1}^N f^2(\mathfrak{t}_i^n). \tag{6.13}$$

It is important to note that the $\mathfrak{t}_i^n$ are here assumed to be distributed uniformly over V.

Naturally, the approximation (6.12) converges particularly fast with the number N of sample points, if f varies slowly over the integration volume V. If this is not the case, the convergence of the Monte Carlo estimate with N can be improved with importance sampling [105]. Suppose that the integrand f can be written as a product of the function h, which is almost constant on V, times another, positive function p,

$$\int_V f(\mathfrak{t}^n)\mathrm{d}\mathfrak{t}^n = \int_V \frac{f(\mathfrak{t}^n)}{p(\mathfrak{t}^n)} p(\mathfrak{t}^n)\mathrm{d}\mathfrak{t}^n \equiv \int_V h(\mathfrak{t}^n)p(\mathfrak{t}^n)\mathrm{d}\mathfrak{t}^n. \tag{6.14}$$

Changing variables from $\mathrm{d}\mathfrak{t}^n$ to $\mathrm{d}\mathfrak{s}^n = p(\mathfrak{t}^n)\mathrm{d}\mathfrak{t}^n$ and assuming that the integral over $p(\mathfrak{t}^n)$ is normalized,

$$\int_V p(\mathfrak{t}^n)\mathrm{d}\mathfrak{t}^n = 1, \tag{6.15}$$

we see that Eq. (6.14) together with Eq. (6.12) implies that we can approximate the integral of f by sampling the function h. In contrast to Eq. (6.12), the sample points must then be distributed nonuniformly, with the probability distribution $p(\mathfrak{t}^n)$. In this case, we obtain

$$\int_V f(\mathfrak{t}^n) \approx \left\langle \frac{f}{p} \right\rangle \pm \sqrt{\frac{\langle f^2/p^2\rangle - \langle f/p\rangle^2}{N}}, \tag{6.16}$$

and we recognize in Eq. (6.12) the special case of $p(\mathfrak{t}^n) = 1$. What is more, we can determine the optimal $p(\mathfrak{t}^n)$ by minimizing the numerator in the square root of Eq. (6.16), which is simply the variance of the Monte Carlo estimate per sampling point. In order for that, we note that $\langle f^2/p^2\rangle$ and $\langle f/p\rangle$ are themselves estimators of integrals,

$$\begin{aligned}\langle f^2/p^2\rangle - \langle f/p\rangle^2 &\approx \int_V \frac{f^2(\mathfrak{t}^n)}{p^2(\mathfrak{t}^n)} p(\mathfrak{t}^n)\mathrm{d}\mathfrak{t}^n - \left[\int_V \frac{f^2(\mathfrak{t}^n)}{p(\mathfrak{t}^n)} p(\mathfrak{t}^n)\mathrm{d}\mathfrak{t}^n\right]^2 \\ &= \int_V \frac{f^2(\mathfrak{t}^n)}{p(\mathfrak{t}^n)}\mathrm{d}\mathfrak{t}^n - \left[\int_V f^2(\mathfrak{t}^n)\mathrm{d}\mathfrak{t}^n\right]^2. \end{aligned} \tag{6.17}$$

The optimal p is now identified by a vanishing functional derivative,

$$\frac{\delta}{\delta p}\left(\int_V \frac{f^2(\mathfrak{t}^n)}{p(\mathfrak{t}^n)}\mathrm{d}\mathfrak{t}^n - \left[\int_V f^2(\mathfrak{t}^n)\mathrm{d}\mathfrak{t}^n\right]^2 + \lambda\int_V p(\mathfrak{t}^n)\mathrm{d}\mathfrak{t}^n\right) = 0, \tag{6.18}$$

with the Lagrange multiplier λ. With the middle term independent of p and after interchanging functional derivative and integral, we obtain $-f^2(\mathfrak{t}^n)/\tilde{p}^2(\mathfrak{t}^n) + \lambda = 0$, or

$$\tilde{p}(\mathfrak{t}^n) = \frac{|f(\mathfrak{t}^n)|}{\sqrt{\lambda}} = \frac{|f(\mathfrak{t}^n)|}{\int_V |f(\mathfrak{t}^n)|\mathrm{d}\mathfrak{t}^n}, \tag{6.19}$$

In the second equality we used $\sqrt{\lambda} = \int_V |f(\mathfrak{t}^n)|\mathrm{d}\mathfrak{t}^n$, to ensure the normalization condition, Eq. (6.15), and the tilde indicates the optimum.

The Jump Time Multi-Integral

Let us come back to the terms $\rho_t^{(n)}$ that constitute the approximation for ρ_t, see Eq. (6.10). Equation (6.11) states that $\rho_t^{(n)}$ is determined by a multi-integral of $\rho_t^{(\mathfrak{t}^n)}$ over the jump times $t_1, \ldots, t_n$. Hence, for a numerical approximation to $\rho_t^{(n)}$ we substitute $f(\mathfrak{t}^n)$ with $\rho_t^{(\mathfrak{t}^n)}$ and the modulus $|f(\mathfrak{t}^n)|$ with $\mathrm{Tr}\,\rho_t^{(\mathfrak{t}^n)}$ in the above Monte Carlo scheme [21],

$$\rho_t^{(n)} = \int_0^t \mathrm{d}t_n \int_0^{t_n} \mathrm{d}t_{n-1} \ldots \int_0^{t_2} \mathrm{d}t_1 \rho_t^{(\mathfrak{t}^n)} \approx \frac{1}{N}\sum_{i=1}^{N} \frac{\rho_t^{(\mathfrak{t}_i^n)}}{p(\mathfrak{t}_i^n)}. \tag{6.20}$$

As above, $p(\mathfrak{t}_i^n)$ is the probability density for drawing a specific jump time sample. The new integrand $\rho_t^{(\mathfrak{t}^n)}$ is a density matrix defined as the sum of those record-conditioned branches $\rho_t^{(\mathfrak{R}^n)}$ which exhibit the same jump times $t_1, \ldots, t_n$, see Eq. (6.11). With $\rho_t^{(\mathfrak{R}^n)}$ determined by Eqs (4.29)–(4.31), we see that $\rho_t^{(\mathfrak{t}^n)}$ is obtained from the initial state ρ_0 by a series of t_i-dependent transformations,

$$\rho_t^{(\mathfrak{t}^n)} = \mathcal{U}_{\boldsymbol{\alpha}}(t, t_n)\mathcal{J}_{\boldsymbol{\alpha}}(t_n)\mathcal{U}_{\boldsymbol{\alpha}}(t_n, t_{n-1})\mathcal{J}_{\boldsymbol{\alpha}}(t_{n-1}) \ldots \mathcal{J}_{\boldsymbol{\alpha}}(t_1)\mathcal{U}_{\boldsymbol{\alpha}}(t_1, 0)\rho_0. \tag{6.21}$$

Here, the $\mathcal{J}_{\boldsymbol{\alpha}}(t)$ are mixtures of abrupt jump transformations determined by the jump operators $\mathsf{L}_{j,\boldsymbol{\alpha}}(t)$, while the $\mathcal{U}_{\boldsymbol{\alpha}}(t_{i+1},t_i)$ effect a continuous propagation from t_i to t_{i+1} under the effective Hamiltonian $\mathsf{H}^{\text{eff}}_{\boldsymbol{\alpha}}(t)=\mathsf{H}_{\boldsymbol{\alpha}}(t)-i\hbar/2\sum_j \mathsf{L}^\dagger_{j,\boldsymbol{\alpha}}(t)\mathsf{L}_{j,\boldsymbol{\alpha}}(t)$, see Eqs. (4.22)–(4.25). The explicit expressions for $\mathcal{J}_{\boldsymbol{\alpha}}$ and $\mathcal{U}_{\boldsymbol{\alpha}}$ read

$$\mathcal{J}_{\boldsymbol{\alpha}}(t_i)\rho=\sum_{j_i}\mathcal{J}_{j_i,\boldsymbol{\alpha}}(t_i)\rho=\sum_{j_i}\mathsf{L}_{j_i,\boldsymbol{\alpha}}(t_i)\rho\mathsf{L}_{j_i,\boldsymbol{\alpha}}(t_i)^\dagger, \tag{6.22}$$

$$\mathcal{U}_{\boldsymbol{\alpha}}(t_{i+1},t_i)\rho=\mathcal{T}\exp\left[-\frac{i}{\hbar}\int_{t_i}^{t_{i+1}}\mathsf{H}^{\text{eff}}_{\boldsymbol{\alpha}}(t')\mathrm{d}t'\right]\rho\mathcal{T}\exp\left[\frac{i}{\hbar}\int_{t_i}^{t_{i+1}}\mathsf{H}^{\text{eff}}_{\boldsymbol{\alpha}}(t')^\dagger\mathrm{d}t'\right]. \tag{6.23}$$

It is important to recall that $\boldsymbol{\alpha}$ indicates both a shift of the original jump operators $\mathsf{L}_j(t)$, appearing in the master equation (2.66), by arbitrary complex numbers α_j, see Eq. (4.20), and an appropriate transformation of the Hamiltonian, see Eq. (4.21). At a given time t, these shifts may depend both on t and on the record $\mathfrak{R}^n$ of previous jumps, see Eq. (4.51), or on any subset of these parameters, see Eq. (4.75), for example.

The Jump Time Distribution

The jump time samples $\mathfrak{t}_i^n$ necessary for the Monte Carlo estimate, Eq. (6.20), are drawn from the probability distribution $p(\mathfrak{t}^n)$ on an n-dimensional simplex satisfying $0<t_1<\ldots<t_n<t$. The normalization condition for $p(\mathfrak{t}^n)$ hence reads

$$\int_0^t \mathrm{d}t_n\int_0^{t_n}\mathrm{d}t_{n-1}\ldots\int_0^{t_1}\mathrm{d}t_1 p(\mathfrak{t}^n)=1. \tag{6.24}$$

Crucially, the Monte Carlo estimate for $\rho_t^{(n)}$, Eq. (6.20), is valid for any $p(\mathfrak{t}^n)$ fulfilling the normalization condition (6.24). Nevertheless, we argued above that the convergence[2] of the estimate with the number N of jump time samples $\mathfrak{t}_i^n$ depends on $p(\mathfrak{t}^n)$. Moreover, we saw that the convergence is optimal if $p(\mathfrak{t}^n)$ is proportional to the trace norm of the integrand,

$$\tilde{p}(\mathfrak{t}^n)\propto\operatorname{Tr}\rho_t^{(\mathfrak{t}^n)}. \tag{6.25}$$

Let us try to evaluate the optimal jump time distribution $\tilde{p}(\mathfrak{t}^n)$. Consider, for example, the master equations of collisional decoherence, Eq. (3.67), and of a nonselective measurement, Eq. (3.76). Here we have $\int\mathsf{L}_Q^\dagger\mathsf{L}_Q\mathrm{d}Q=\gamma$ and $\sum_j\mathsf{L}_j^\dagger\mathsf{L}_j=\gamma$, respectively. This implies that for $\boldsymbol{\alpha}=0$ jumps $\mathcal{J}_{\boldsymbol{\alpha}}(t_i)$, Eq. (6.22), change of the norm by γ and continuous evolutions $\mathcal{U}_{\boldsymbol{\alpha}}(t_{i+1},t_i)$, Eq. (6.23), by $\exp[-\gamma(t_{i+1}-t_i)]$. With the entire series of transformations (6.21) comprising n jumps and piecewise continuous evolutions between

[2] In the present chapter, we must not confuse the meanings of "convergence of the jump expansion" and "convergence of the Monte Carlo estimate". Formally, the former describes how fast the series $\sum_{n=0}^m\rho_t^{(n)}$ approaches ρ_t with increasing expansion order m, while the latter means how fast the arithmetic mean of the sample matrices $\rho_t^{(\mathfrak{t}_i^n)}$ $(i=1,\ldots,N)$, Eq. (6.20), approaches $\rho_t^{(n)}$ with the number N of jump time samples.

0 to t in total, the final trace norm reads

$$\operatorname{Tr} \rho_t^{(\mathfrak{t}^n)} = \gamma^n \exp[-\gamma t], \tag{6.26}$$

which is independent of the individual jump times t_i. This final norm also implies that for collisional decoherence and nonselective measurements, the jump times must be distributed uniformly over the interval $[0, t]$ to obtain an optimal convergence of the Monte Carlo estimate, Eq. (6.20). This can be seen by evaluating $\operatorname{Tr} \rho_t^{(n)}$ via the multi-integral, Eq. (6.11), which gives a homogeneous Poissonian distribution,

$$\operatorname{Tr} \rho_t^{(n)} = \frac{(\gamma t)^n}{n!} \exp[-\gamma t], \tag{6.27}$$

for the number n of jumps between 0 and t.

As another example, consider the damped harmonic oscillator at $T = 0$, Eq. (3.12), where $\mathsf{L} = \sqrt{\gamma_0}\mathsf{a}$ and a coherent initial state $\rho_0 = |\alpha_0\rangle\langle\alpha_0|$ remains coherent, $\rho_t = |\alpha_t\rangle\langle\alpha_t|$, see Eqs. (3.15) and (3.16). In this case we have, for $\boldsymbol{\alpha} = 0$,

$$\operatorname{Tr} \rho_t^{(\mathfrak{t}^n)} = \gamma_0^n \exp\left[-\gamma_0 \int_0^t |\alpha_{t'}|^2 \mathrm{d}t'\right] \prod_i |\alpha_{t_i}|^2. \tag{6.28}$$

While here $\operatorname{Tr} \rho_t^{(\mathfrak{t}^n)}$ does depend on the individual t_i, this dependence is governed by the unique function $|\alpha_t|^2$. The evaluation of $\operatorname{Tr} \rho_t^{(n)}$ via Eq. (6.11) shows that for the harmonic oscillator at $T = 0$, an inhomogeneous Poisson distribution for the t_i leads to an optimal convergence of the Monte Carlo estimate,

$$\operatorname{Tr} \rho_t^{(n)} = \frac{\left(\gamma_0 \int_0^t |\alpha_{t'}|^2 \mathrm{d}t'\right)^n}{n!} \exp\left[-\gamma_0 \int_0^t |\alpha_{t'}|^2 \mathrm{d}t'\right]. \tag{6.29}$$

We see that for some, relatively simple master equations, optimal convergence of the Monte Carlo integration method is ensured by drawing the jump times t_i from a homogeneous or inhomogeneous Poisson distribution. In practice, this is done by drawing the individual jump times $t_1, \ldots, t_n$ independently from one and the same 1-dimensional probability distribution $p_1(t') = R(t')/R(t)$, where $t' \in (0, t)$ and R is the antiderivative of the (possibly time-dependent) rate characterizing the Poisson process. Subsequently, we must sort the t_i to ensure the increasing order $0 < t_1 < \ldots < t_n < t$, as is required by the jump time integral, Eq. (6.20). Taking into account that in this case there are $n!$ possibilities to obtain the same sequence of jump times, we obtain the total n-dimensional probability distribution

$$p(\mathfrak{t}^n) = n! \prod_{j=1}^{n} p_1(t_j). \tag{6.30}$$

It is important to note that this jump time distribution is not optimal for general master equations. It is, however, simple and straightforward enough to be implemented in

practice without any additional numerical overhead. In fact, in the following section we will use the distribution (6.30) for approximating a set of exemplary master equations, where it yields a sufficient convergence of the Monte Carlo estimate.

The optimal jump time distribution $\tilde{p}(\mathfrak{t}^n) \propto \operatorname{Tr} \rho_t^{(\mathfrak{t}^n)}$ for a general master equation will depend on the number n of jumps and on the jump times $t_1, \ldots, t_n$ in some complicated fashion. The problem of evaluating $\tilde{p}(\mathfrak{t}^n)$ is here tantamount to performing the series (6.21) of transformations of the initial state ρ_0 for any n-tuple of jump times. It is clear that this is practically impossible with analytical means and, in most cases, it is numerically expensive. Although $\tilde{p}(\mathfrak{t}^n)$ may be unknown *a priori* in practice, however, one may approximate $\tilde{p}(\mathfrak{t}^n)$ successively with each iteration of the Monte Carlo integration method. The reason is that in each iteration we evaluate $\rho_t^{(\mathfrak{t}_i^n)}$ for one specific jump time sample $\mathfrak{t}_i^n$ and hence obtain $\operatorname{Tr} \rho_t^{(\mathfrak{t}_i^n)}$ for free. For the $(i+1)$-th iteration we can then use a piecewise constant jump time distribution $p_i(\mathfrak{t}^n)$ which assumes the values $\operatorname{Tr} \rho_t^{(\mathfrak{t}_1^n)}, \ldots, \operatorname{Tr} \rho_t^{(\mathfrak{t}_i^n)}$ in the neighborhood of $\mathfrak{t}_1^n, \ldots, \mathfrak{t}_i^n$, respectively. Interpreting the n-tuples $\mathfrak{t}_j^n$ as n-dimensional vectors, we can use the vector norm $|\mathfrak{t}^n - \mathfrak{t}_j^n|$ to specify the neighborhood of $\mathfrak{t}_j^n$ and, hence, write $p_i(\mathfrak{t}^n)$ as

$$p_i(\mathfrak{t}^n) = \mathcal{N}^{-1} \begin{cases} \operatorname{Tr} \rho_t^{(\mathfrak{t}_1^n)}, & \text{for} |\mathfrak{t}^n - \mathfrak{t}_1^n| < |\mathfrak{t}^n - \mathfrak{t}_j^n|, j = 2, \ldots, i \\ \operatorname{Tr} \rho_t^{(\mathfrak{t}_2^n)}, & \text{for} |\mathfrak{t}^n - \mathfrak{t}_2^n| < |\mathfrak{t}^n - \mathfrak{t}_j^n|, j = 1, 3, \ldots, i \\ \quad \vdots & \\ \operatorname{Tr} \rho_t^{(\mathfrak{t}_i^n)}, & \text{for} |\mathfrak{t}^n - \mathfrak{t}_i^n| < |\mathfrak{t}^n - \mathfrak{t}_j^n|, j = 1, \ldots, i-1 \end{cases}, \tag{6.31}$$

with the normalization $\mathcal{N}$, see Eq. (6.24). This guarantees that we approach the optimal jump time distribution after a large number of iterations, $p_i(\mathfrak{t}^n) \to \tilde{p}(\mathfrak{t}^n)$ for $i \to \infty$, with only little additional numerical effort.

The Iterative Procedure

The above considerations suggest to iterate the following steps for approximating the n-th order term $\rho_t^{(n)}$ of the jump expansion of ρ_t, Eq. (6.10):

1. Draw a jump time sample $\mathfrak{t}_i^n$ comprising n real numbers t_i between 0 and t from the probability distribution $p(\mathfrak{t}^n)$. Sort the numbers in increasing order $t_1 < \ldots < t_n$.

2. Propagate ρ_0 with $\mathcal{U}_{\boldsymbol{\alpha}}(t_1, 0)$, Eq. (6.23). Depending on whether the complex shift $\boldsymbol{\alpha}$ of the jump operators ($\mathsf{L}_{j,\boldsymbol{\alpha}} \equiv \mathsf{L}_j + \alpha_j$) is conditioned on the previous *types* of jumps j_i, continue with one of the following alternatives

   a) If $\boldsymbol{\alpha}$ is not conditioned on j_i, apply $\mathcal{J}_{\boldsymbol{\alpha}}(t_1)$, Eq. (6.22). Continue switching between stepwise propagations from t_k to t_{k+1} (step 2) and jumps at times t_k (step 2 a) until reaching the final state $\rho_t^{(\mathfrak{t}_i^n)}$.

   b) If $\boldsymbol{\alpha}$ is conditioned on j_i, choose one specific jump index j_1 and apply $\mathcal{J}_{\boldsymbol{\alpha},j_1}(t_1)$, see Eq. (6.22). Continue switching between stepwise propagations from t_k to t_{k+1}

(step 2) and jumps $\mathcal{J}_{\boldsymbol{\alpha},j_k}(t_k)$ of specific types (step 2 b) until reaching the final time t to obtain the record conditioned branch $\rho_t^{(\mathfrak{R}_i^n)}$. Iterate this record conditioned propagation over all possible combinations of jump indices. Take the sum of the obtained record conditioned branches to obtain $\rho_t^{(\mathfrak{t}_i^n)}$.

3. Possibly update the jump time distribution with $\operatorname{Tr}\rho_t^{(\mathfrak{t}_i^n)}$, see Eq. (6.31).

4. Having reiterated the above steps N times, Monte Carlo integration prescribes to take the weighted mean of all $\rho_t^{(\mathfrak{t}_i^n)}$ for $i = 1, \ldots, N$ to obtain $\rho_t^{(n)}$, see Eq. (6.20).

To finally approximate ρ_t with the jump expansion, Eq. (6.10), up to k-th order, the above procedure must be repeated for $n = 0, \ldots, k$ jumps.

After specifying the iterative procedure to obtain a Monte Carlo integral estimate of the jump expansion (MIJE), let us compare it briefly to the previously discussed Monte Carlo wave function approach (MCWF) based on quantum trajectories. Despite their different formal derivations, they are strikingly similar. And yet, they exhibit a few significant differences.

In both methods one starts with the initial state ρ_0 and applies jump transformation at randomly chosen times $(t_1, \ldots, t_n)$ that make up the jump time sample $\mathfrak{t}_i^n$. In between, one propagates the state piecewise continuously with a non-Hermitian effective Hamiltonian[3] H^{eff}. The numerical effort for obtaining one realization of this stochastic propagation is hence comparable in both methods. In the end, ρ_t is approximated by the statistical mean of the stochastic propagations of the initial state.

There are three significant differences between the two numerical approximation methods, however. The first is that in the MCWF approach the t_j are chosen on the fly based on the time-local norm decay under H^{eff}, while the MIJE method prescribes to draw the entire jump time sample at once from a predetermined probability distribution $p(\mathfrak{t}^n)$. Therefore, the propagation in the MCWF approach must be performed stepwise, in general, and the number n of jumps is not determined beforehand. In contrast, the MIJE method allows to carry out the entire propagation at once and for one specific n. Also, in MCWF the determination of the t_j via the norm decay under H^{eff}, Eq. (6.24), is obligatory. In MIJE, any jump time distribution $p(\mathfrak{t}^n)$ leads to a correct Monte Carlo estimate for ρ_t, although the convergence of the estimate with the number of iterations is optimal if $p(\mathfrak{t}^n)$ is proportional to the trace norm after a propagation with $\mathfrak{t}^n$. The second major distinction is that, in MCWF, one compensates for the norm decay under H^{eff} after each step so that at the end of each iteration, one obtains a normalized state. In MIJE, this is not the case and the norm or weight of the final state generally differs from one iteration to the next. The third and most important distinction is that in MIJE, we can optimize the weights of the lowest order terms $\rho_t^{(n)}$ of the approximation (6.10) for ρ_t, by applying the resummations of the jump expansion derived in Chap. 4. As a reminder, this is done by adapting the complex shifts $\boldsymbol{\alpha}$ of the jump operators. The possibility to fix the

[3] Note that in Eqs. (6.22) and (6.23) we use the notation from Chap. 4, where we incorporated the jump rates $\gamma_i(t)$ in the operators $\mathsf{L}_i(t)$.

number n therefore implies that the we can evaluate the estimate for ρ_t systematically, starting with the terms with the highest weights. In contrast, in MCWF all stochastic realizations contribute equally to the ρ_t-estimate, due to the continuous renormalization of the propagated state.

In conclusion, the possibility to optimize the weights of the terms constituting the approximation to ρ_t and the possibility to evaluate them systematically implies a clear advantage of MIJE over MCWF, in terms of efficiency. It should be kept in mind, however, that the evaluation of the optimal jump time distribution $\tilde{p}(\mathfrak{t}^n)$ in MIJE is numerically demanding in general, so that one would usually content oneself with a suboptimal $p(\mathfrak{t}^n)$. The method of drawing the jump times in MCWF is optimal, by definition, but it implies a stepwise propagation. It would therefore be interesting to benchmark MCWF and MIJE systematically against each other. In the following section, we only demonstrate the general validity of the MIJE-estimate for ρ_t and the optimization of the weights of its approximation terms.

6.2 Application of the Monte Carlo Integration Method

Let us now demonstrate the Monte Carlo integration method for the jump expansion $\rho_t = \sum_n \rho_t^{(n)}$, as well as the optimization of the weights of the terms $\rho_t^{(n)}$ by means of the adaptive resummation $\tilde{\boldsymbol{\alpha}}$ derived in Chap. 4, Sec. 4.3.1. As testbeds for the numerical integration scheme we consider the three exemplary Markovian open quantum problems introduced in Chap. 3: (i) the damped harmonic oscillator, (ii) spatial decoherence of a particle, and (iii) a continuous quantum measurement with feedback. We saw that they display many different facets of Markovian quantum dynamics such as decoherence, dissipation, thermalization, and pointer states. Moreover, these examples involve both discrete and continuous Hilbert spaces and feature finite and continuous sets of Hermitian or non-Hermitian jump operators. The demonstration and optimization of the Monte Carlo integration scheme in the considered model systems, can hence be taken as an indication of its wide range of applicability [21].

To demonstrate that the numerical estimate defined by Eqs. (6.10) and (6.20) indeed converges to the solution ρ_τ of a given master equation at a given time τ, we must perform two steps: first, we must evaluate the expansion terms $\rho_\tau^{(n)}$ by approximating the involved jump time multi-integral with the Monte Carlo estimate, Eq. (6.20), for a sufficiently large number N of jump time samples. Then we must show that the series $\sum_{n=0}^{k} \rho_\tau^{(n)}$ converges to the exact ρ_τ with increasing expansion order k. For the relatively simple model systems considered here, we can obtain the exact ρ_τ by direct numerical propagation of the corresponding master equation on a grid. For the Monte Carlo estimate, Eq. (6.20), we use the jump time distribution $p(\mathfrak{t}^n)$ given by Eq. (6.30), with varying functions $p_1(t)$, see below. The time τ of comparison is chosen to be around the intrinsic incoherent time scale of the considered master equation.

To identify convergence of the series $\sum_{n=0}^{k} \rho_\tau^{(n)}$ to ρ_τ, we use a natural distance measure

on state space, the so-called *fidelity*,

$$\mathcal{F}(\sigma,\rho) = \mathrm{Tr}\,\sqrt{\sqrt{\sigma}\rho\sqrt{\sigma}}. \tag{6.32}$$

It quantifies the operational distinguishability of two density matrices σ and ρ by a series of measurements. It ranges between zero and unity and is maximal for $\sigma = \rho$. The fidelity between ρ_τ and the expansion up to the k-th order will be denoted as

$$\mathcal{F}_k \equiv \mathcal{F}\left(\rho_\tau, \mathcal{N}_k^{-1}\sum_{n=0}^{k}\rho_\tau^{(n)}\right), \tag{6.33}$$

with $\mathcal{N}_k = \mathrm{Tr}\sum_{n=0}^{k}\rho_\tau^{(n)}$. Due to the properties of the fidelity mentioned above, we know that $\sum_{n=0}^{k}\rho_\tau^{(n)}$ converges to the correct state ρ_τ if we have $\mathcal{F}_k \to 1$ for $k \to \infty$.

Moreover, for a highly convergent jump expansion, $\rho_\tau = \sum_n \rho_\tau^{(n)}$, we expect that already the lowest order terms are very close to the true ρ_τ, so that $\mathcal{F}_k$ rapidly reaches values close to unity. In contrast, the lowest orders of an expansion with poor convergence differ appreciably from the true ρ_τ, so that $\mathcal{F}_k$ should increase more slowly with k. This allows us to compare the *speed* of convergence of the numerically estimated jump expansion for $\boldsymbol{\alpha} = 0$, *i.e.* without resummation, and for the optimal resummation $\boldsymbol{\alpha} = \tilde{\boldsymbol{\alpha}}(t,\mathfrak{R}^n)$, Eq. (4.51). We will see that the optimal resummation generally converges within the lowest two to five orders, whereas the jump expansion with $\boldsymbol{\alpha} = 0$ converges only within the lowest 20 to 80 orders, depending on the considered model system. This gives an impression of the performance gain of the Monte Carlo integration scheme due to the optimization of the weights of the expansion terms.

6.2.1 Exemplary Master Equations

The Damped Harmonic Oscillator

As the first exemplary Markovian open system, consider the damped harmonic oscillator discussed in Sec. 3.1. Here, the harmonic oscillator is coupled to a surrounding bosonic heat bath which describes, for example, the situation of a cavity field mode in contact with the modes of an environmental electromagnetic field. The dynamics of the damped harmonic oscillator is described by the master equation

$$\begin{aligned}\partial_t\rho_t = &-i\left[\omega_0\mathsf{a}^\dagger\mathsf{a},\rho_t\right] + (1+N_{\mathrm{th}})\,\gamma_0\left\{\mathsf{a}\rho_t\mathsf{a}^\dagger - \frac{1}{2}\mathsf{a}^\dagger\mathsf{a}\rho_t - \frac{1}{2}\rho_t\mathsf{a}^\dagger\mathsf{a}\right\}\\ &+N_{\mathrm{th}}\gamma_0\left\{\mathsf{a}^\dagger\rho_t\mathsf{a} - \frac{1}{2}\mathsf{a}\mathsf{a}^\dagger\rho_t - \frac{1}{2}\rho_t\mathsf{a}\mathsf{a}^\dagger\right\},\end{aligned} \tag{6.34}$$

where γ_0 is the spontaneous emission rate and N_{th} is the thermal occupation number of the surrounding modes at the environmental temperature. Here, jumps correspond to absorptions (jump operator $\mathsf{a}^\dagger$) and emissions (jump operator a) of single quanta from and to the environment.

For the numerical solution of Eq. (6.34) and of all following examples, we first propagate the master equation in a finite basis to obtain ρ_τ and, second, we apply the Monte Carlo integration method to approximate the terms $\rho_\tau^{(n)}$ of the jump expansion, $\rho_\tau = \sum_n \rho_\tau^{(n)}$. Here, the finite basis consists of 20 Fock states and we use the final time $\tau = 6/\gamma_0$. The parameters are chosen as $\omega_0/\gamma_0 = 2$ and $N_{\text{th}} = 0.5$, and the exemplary initial state, $\rho_0 = |\psi_0\rangle\langle\psi_0|$, is a superposition of four Fock states, $|\psi_0\rangle = (|19\rangle + |18\rangle + |17\rangle + |16\rangle)/2$.

The Monte Carlo estimate, Eq. (6.20), is calculated for $\boldsymbol{\alpha} = 0$, *i.e.* for the jump expansion without resummation, and for the optimal resummation $\boldsymbol{\alpha} = \tilde{\boldsymbol{\alpha}}(t, \mathfrak{R}^n)$, Eq. (4.51). We use a number N of jump time samples that guarantees convergence of the Monte Carlo estimate. For $\boldsymbol{\alpha} = 0$ we draw the jump time samples $\mathfrak{t}_i^n$ from the distribution $p(\mathfrak{t}^n)$, Eq. (6.30), with $p_1(t)$ proportional to the average jump rate $\text{Tr}[\sum_j \mathsf{L}_j^\dagger \mathsf{L}_j \rho_t]$, see Eqs. (4.40) and (4.46), as suggested by Eq. (6.29). For $\boldsymbol{\alpha} = \tilde{\boldsymbol{\alpha}}(t, \mathfrak{R}^n)$ the jump operators $\mathsf{L}_{j,\boldsymbol{\alpha}}$ and hence the jump rate depends strongly on time t and on the jump record $\mathfrak{R}^n$. Since the optimal resummation $\tilde{\boldsymbol{\alpha}}$ minimizes the overall jump rate, however, we expect that the latter is approximately homogeneous, *i.e.* we take $p_1(t) = \text{const}$. Note that we use the above jump time distributions in the following examples as well, *i.e.* $p(\mathfrak{t}^n)$ given by Eq. (6.30) with $p_1(t) \propto \text{Tr}[\sum_j \mathsf{L}_j^\dagger \mathsf{L}_j \rho_t]$ for $\boldsymbol{\alpha} = 0$ and $p_1(t) = \text{const}$ for $\boldsymbol{\alpha} = \tilde{\boldsymbol{\alpha}}$.

In Fig. 6.1 (a) we plot the fidelity $\mathcal{F}_k$, Eq. (6.33), between ρ_τ and the jump expansion up to k-th order. We see that both for $\boldsymbol{\alpha} = 0$ and for $\boldsymbol{\alpha} = \tilde{\boldsymbol{\alpha}}$, $\mathcal{F}_k$ approaches unity with increasing expansion order k which implies that the numerically estimated jump expansion converges to ρ_τ, as intended. We also see that $\mathcal{F}_k$ increases rapidly for the optimal resummation (solid purple line), reaching values around 0.95 after $k = 3$ orders. The jump expansion without resummation, in contrast, needs $k \approx 19$ orders to attain comparable values of $\mathcal{F}_k$ (dashed blue line), indicating a much slower convergence.

As a specific limiting case of the damped harmonic oscillator, let us consider a zero temperature environment, *i.e.* Eq. (6.34) with $N_{\text{th}} = 0$,

$$\partial_t \rho_t = -i\left[\omega_0 \mathsf{a}^\dagger \mathsf{a}, \rho_t\right] + \gamma_0 \left\{ \mathsf{a}\rho_t \mathsf{a}^\dagger - \frac{1}{2}\mathsf{a}^\dagger \mathsf{a}\rho_t - \frac{1}{2}\rho_t \mathsf{a}^\dagger \mathsf{a} \right\}. \tag{6.35}$$

This limit is particularly interesting since Eq. (6.35) exhibits pointer states, *i.e.* a preferred set of basis states that the open system rapidly decays to, see Sec. 3.1.2. In particular, these pointer states are here the coherent states $|\alpha\rangle$ exhibiting a vanishing jump rate, and they are attained on the time scale τ_{dec}, Eq. (3.25). In Sec. 2.3 we saw that the branches of the optimally convergent jump expansion evolve rapidly towards these pointer states, which implies that a particularly low number of jumps or expansion orders is necessary to approximate ρ_t.

In Fig. 6.1 (b) we plot the convergence of the numerically estimated jump expansion for the initial superposition of two coherent states $|\psi_0\rangle = (|0\rangle + |6\rangle)/\sqrt{2}$ and for the parameters $\omega_0/\gamma_0 = 2$ and $\tau = 2/\gamma_0$. Again, the fidelity $\mathcal{F}_k$ approaches unity with increasing expansion order k both for $\boldsymbol{\alpha} = 0$ and for $\boldsymbol{\alpha} = \tilde{\boldsymbol{\alpha}}$. Moreover, this is also the case for all other master equations considered in the following. This proves the general validity of the Monte Carlo integration scheme outlined in Sec. 6.1.2 for approximating

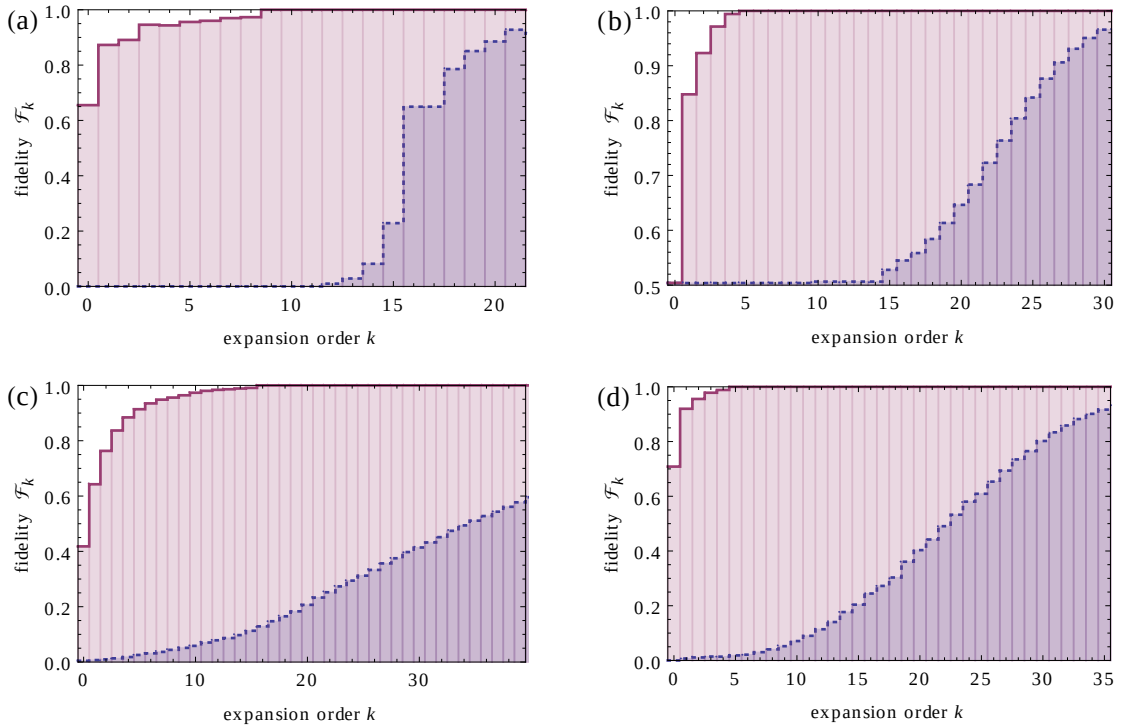

Figure 6.1: Convergence of the numerical estimate of the jump expansion $\rho_\tau = \sum_n \rho_\tau^{(n)}$, without resummation, $\boldsymbol{\alpha} = 0$, (dashed blue line) and for the optimal resummation $\tilde{\boldsymbol{\alpha}}$, Eq. (4.64) (solid purple line). The terms $\rho_\tau^{(n)}$ are obtained by Monte Carlo integration, Eq. (6.20). The convergence is quantified by the fidelity $\mathcal{F}_k$ between ρ_τ with the expansion $\rho_\tau^{(0)} + \ldots + \rho_\tau^{(k)}$ up to k-th order, see Eq. (6.33). The four panels represent different master equations: (a) the damped harmonic oscillator, Eq. (6.34), for a finite temperature corresponding to a thermal occupation $N_{\text{th}} = 0.5$, and (b) for zero temperature, $N_{\text{th}} = 0$, (c) the diffusive limit of quantum Brownian motion, Eq. (6.36), and (d) the nonselective measurement with feedback, Eq. (3.73). One observes that in all cases the resummation leads to a highly improved convergence.

the dynamics ρ_t under Markovian master equations. In the present case, the optimally resummed jump expansion converges within $k \approx 3$ orders (solid purple line) while for $\boldsymbol{\alpha} = 0$ it takes $k \approx 30$ order to reach comparable values of $\mathcal{F}_k$ (dashed blue line). Due to the existence of pointer states with vanishing jump rates, the difference between $\boldsymbol{\alpha} = \tilde{\boldsymbol{\alpha}}$ and $\boldsymbol{\alpha} = 0$ in terms of convergence is here even more pronounced than in the finite temperature case. Also note that here $\mathcal{F}_k$ is never below 0.5, which is a special feature of the initial state.

Quantum Brownian Motion

As the second exemplary Markovian open system, we consider the diffusive limit of quantum Brownian motion. As we saw in Sec. 3.2, there are two distinct models that can be used to describe Brownian motion. The first is the Caldeira-Leggett model which is obtained by coupling the position coordinate of the Brownian particle to a bosonic heat bath, see Sec. 3.2.1. In the diffusive limit of large Brownian mass and high temperatures, the dynamics is described by the master equation

$$\partial_t \rho_t = -\frac{i}{\hbar}\left[\frac{\mathsf{p}^2}{2m}, \rho_t\right] - \frac{4\pi\gamma}{\Lambda_{\mathrm{th}}^2}\left[\mathsf{x}, [\mathsf{x}, \rho_t]\right]. \tag{6.36}$$

Here, Λ_{th} is the thermal de Broglie wavelength of the Brownian particle, γ the rate of friction, and the jump operator is equal the position operator x.

For the numerical propagation of Eq. (6.36) on a grid, we use the split-operator technique. The parameters are here chosen to satisfy $\hbar/8\pi m\gamma = 15\Lambda_{\mathrm{th}}^2$. Moreover, we use the final time $\tau = 1/3\gamma$ and an initial Gaussian wave packet of width $\sigma_x = 3\Lambda_{\mathrm{th}}$ centered at $x_0 = 0$. Figure 6.1 (c) confirms the strong convergence gain of the optimal resummation, already observed in the damped harmonic oscillator, for spatial decoherence. Again, the optimal resummation converges after a few orders, here around $k \approx 5$, whereas the jump expansion without resummation requires around $k \approx 80$ orders to attain comparable values of $\mathcal{F}_k$ (not shown on the scale of the plot).

The second model that can be used to describe quantum Brownian motion is called collisional decoherence, see Sec. 3.2.2. It describes the interaction of the Brownian particle with its environment by individual scattering events with background gas particles. The corresponding master equation reads, in the limit of large Brownian mass,

$$\partial_t \rho_t = -\frac{i}{\hbar}\left[\frac{\mathsf{p}^2}{2m}, \rho_t\right] + \gamma \int G(q) e^{iq\mathsf{x}/\hbar} \rho_t e^{-iq\mathsf{x}/\hbar} \mathrm{d}q - \gamma\rho_t, \tag{6.37}$$

with the momentum transfer distribution $G(q)$ and the average collision rate γ. In contrast to Eq. (6.36), here the jumps or collision events effect momentum kicks of magnitude q.

We simulate the above linear coupling master equation for a Gaussian momentum transfer distribution $G(q)$ of width σ_G and parameters satisfying $2m\hbar\gamma = 4\sigma_G^2$. Here we choose the final time $\tau = 20/\gamma$ and again an initial Gaussian wave packet of width $\sigma_x = 3\hbar/\sigma_G$ centered at $x_0 = 0$. As in the previous examples, the optimal resummation converges rapidly within the lowest $k \approx 4$ orders, see Fig. 6.2 (a), solid purple line. The difference is that here also for $\boldsymbol{\alpha} = 0$ the fidelity shows a rapid increase at small k (dashed blue line). While one still needs around $k \approx 13$ orders to reach a fidelity of 0.95, we observe that already the lowest orders yield a fairly good estimate for ρ_τ. Therefore, we also plot the cumulative weight distribution $\mathcal{W}_k = w_0(\tau) + \ldots + w_k(\tau)$ in Fig. 6.2 (b), which shows that the lowest order weights are strongly suppressed for $\boldsymbol{\alpha} = 0$ and that the convergence for the optimal $\tilde{\boldsymbol{\alpha}}$ is clearly superior.

The above result indicates that a strong increase of the fidelity does not necessarily

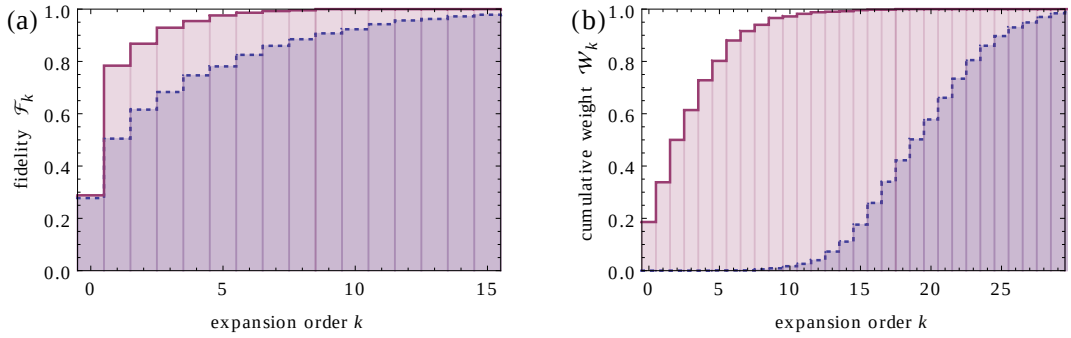

Figure 6.2: Convergence of the jump expansion for collisional decoherence, Eq. (6.37), for the optimal resummation $\tilde{\boldsymbol{\alpha}}$ (purple solid line) and without resummation, $\boldsymbol{\alpha} = 0$ (blue dashed line). In (a) we plot the fidelity $\mathcal{F}_k$ analogous to Fig. 6.1, whereas (b) shows the cumulative sum of the weights of the expansion terms up to k-th order, $\mathcal{W}_k = w_0(t) + \ldots + w_k(t)$. Note that, here, the fidelity shows a strong increase even for $\boldsymbol{\alpha} = 0$. The comparison of (a) and (b) however shows that this rapid increase of $\mathcal{F}_k$ does not imply a strong convergence of the jump expansion without resummation. It is rather a special feature of collisional decoherence (compare to $\mathcal{F}_k$ for different exemplary master equations, Fig. 6.1).

imply a rapid convergence of the jump expansion. In the above collisional decoherence example, all orders lower than $k = 5$ have very small weights and hence the jump expansion is far from converged. The fidelity between the exact ρ_τ and the *normalized* expansion up to 5-th order gives $\mathcal{F}_5 \approx 0.75$, however, which means that the lowest orders are quite similar to ρ_τ despite their low weights. This behavior was not observed in the other exemplary master equations, see Fig. 6.1, which implies that it is a special feature of collisional decoherence. Note that the weights $w_k(\tau)$ are the actual subject of optimization by the resummation $\tilde{\boldsymbol{\alpha}}$ and not the fidelity, see Sec. 4.3.1. The optimal resummation therefore works as well for collisional decoherence as for the other master equations. Also note that, if we cannot propagate ρ_t directly, for example for more complicated master equations or higher dimensional Hilbert spaces, $\mathcal{F}_k$ is not available. In this case the weights $w_k(\tau)$ are the only available criterium by which one can estimate whether the jump expansion has converged or not.

But what causes this specific behavior of collisional decoherence? The short answer is that collisional decoherence does not do much to the initial state besides destroying its spatial coherences. Since here we have a set of continuously distributed momentum kicks for $\boldsymbol{\alpha} = 0$, a probabilistic mixture of all single-jump transformations has exactly this property and there is only very small room for optimization by $\tilde{\boldsymbol{\alpha}}$. Compare this to the damped harmonic, where the initial state changes completely, or to the Caldeira-Leggett model, where we have only a single jump operator.

Nonselective Measurements

As the last example, we consider the nonselective measurement of an electromagnetic cavity with feedback, see Sec. 3.3.1. This measurement is realized by sending two-level atoms as probes through the cavity, which gives the master equation

$$\partial_t \rho_t = -i\left[\omega \mathsf{a}^\dagger \mathsf{a}, \rho_t\right] + \gamma\left[\sum_l (\mathsf{M}_{+,l}\rho_t \mathsf{M}_{+,l}^\dagger + \mathsf{M}_{-,l}\rho_t \mathsf{M}_{-,l}^\dagger) - \rho_t\right], \tag{6.38}$$

with $\mathsf{M}_{\pm,l} = \sum_n \langle \pm_l + _n\rangle\langle n|$, $|\pm_l\rangle = \exp(i\pi l\sigma_z/2d)|\pm\rangle$, and $|\pm\rangle = (|0\rangle \pm |1\rangle)/\sqrt{2}$. Here, the index $l = 0, 1, \ldots, d$ stems from the different bases in which the atomic probes can be measured, and any single l defines a valid cavity measurement. To increase the amount of extracted information one can also vary l from one measurement to the next which gives the sum in Eq. (6.38). We will here use $d = 19$ and the exemplary probe measurements with $l = 0$ and $l = 10$, *i.e.* we have the four jump operators $\mathsf{M}_{+,0}$, $\mathsf{M}_{-,0}$, $\mathsf{M}_{+,10}$, and $\mathsf{M}_{-,10}$. In addition, we will apply the feedback operation $\mathsf{a}^\dagger$ whenever we detect the outcome $+, 0$, which changes the first jump operator to $\mathsf{M}_{+,0}^{\mathrm{fb}} = \mathsf{a}^\dagger \mathsf{M}_{+,0}$, and stabilizes the cavity in the Fock state $|19\rangle$, see Sec. 3.3.1.

For the numerical simulation of Eq. (6.38) we use the parameters $\gamma = 2\omega$, $\tau = 40/\gamma$, and the initial coherent state $|\beta\rangle$ with $\beta = 2$. In Fig. 6.1 (d) we plot the fidelity between ρ_τ and the Monte Carlo estimate for the jump expansion for $\boldsymbol{\alpha} = 0$ and for $\boldsymbol{\alpha} = \tilde{\boldsymbol{\alpha}}$ as a function of the expansion order k. Again, the high convergence of the optimal resummation observed in the previous examples is confirmed. It converges within $k \approx 2$ orders, whereas one needs to take into account $k \approx 40$ orders for $\boldsymbol{\alpha} = 0$ to obtain a faithful estimate of ρ_τ.

In conclusion, we saw that the Monte Carlo integration method successfully approximates the time evolution ρ_t of a wide variety of Markovian open systems. Being based on the jump expansion, the adaptive resummations derived in Chap. 4 can be used to optimize the efficiency of this approximation method. In the examples considered here, we saw that, making use of the optimal resummation, one can obtain a reliable estimate of ρ_t by evaluating only the lowest 2 to 5 expansion terms. It would be quite interesting, as mentioned above, to benchmark this approximation method against the standard Monte Carlo wave function approach which does not incorporate such a possibility of optimization. The strong convergence of the optimized jump expansion observed in the present chapter also indicates that it may facilitate new analytic approximations to Markovian open systems besides those derived in Chap. 5.

7 Incoherent Control of the Retinal Isomerization in Rhodopsin

In the previous chapters we have pursued a deeper understanding of the incoherent evolution of Markovian open quantum systems based on an adaptive resummation of the associated master equation dynamics. Our expressed goal was to find approximate analytical models that can be used for a purposeful implementation of incoherent dynamics, or short, for incoherent control. Based on the specific analytical description of the Landau-Zener problem in the presence of dephasing derived in Chap. 5 [20], we now outline a simple and robust method to control the isomerization dynamics of the large biomolecule rhodopsin under ambient conditions [22].

The underlying motivation is that physicists have pursued to control the dynamics of quantum systems in a coherent fashion since the advent of lasers. The coherent nature of the laser light allows one to take direct influence on the Hamiltonian of a given quantum system and thereby manipulate constructive or destructive interferences to obtain specific target quantum state [106, 107]. As the logical extension of conventional photochemistry, this *coherent quantum control* was first applied to the selective making and breaking of chemical bonds in molecules [108–110]. Later on, it proved to be useful in other areas such as solid state physics [111] or quantum information [8] as well.

Coherent control usually considers a closed quantum system that is to be steered towards a specific final state by means of a time-dependent control Hamiltonian. This framework is particularly successful when applied to small systems that involve a limited number of discrete energy levels and are well isolated from their surroundings. A small molecule, for example, can be guided through its Born-Oppenheimer potential landscape towards a specific target configuration by applying time-separated femtosecond optical pulses in a deliberate fashion. This can be used, for example, to change the branching ratio for a given chemical reaction of that molecule [112]. In larger systems, however, it becomes more and more difficult to address a specific quantum state with a single optical pulse. Take, for example, a large polyatomic molecule with its multitude of densely spaced electronic and rovibrational energy levels. Moreover, the couplings among system states lead to a rapid redistribution of the energy, initially localized in a specific excited state, to other unwanted states.

To some extent, these obstacles can be overcome by *optimal control* where the control pulses are shaped in the time and energy domain. Crucially, the pulse shapes that one applies are optimized for a desired target quantity. This can be done either numerically, by an *a priori* simulation of the system dynamics, or experimentally, by measuring the target quantity for a given pulse shape and updating the latter adaptively, for example by using evolutionary optimization algorithms. Even though one hardly understands

why this or that complicated pulse shape is optimal for a given task, optimal control was found to achieve good results for astonishingly complex quantum systems [23, 113, 114]. Optimal control is, however, also limited in terms of the number of degrees of freedom it can address, since larger and larger systems call for ever more refined pulse shapes.

Another problem for coherent control is the often unavoidable influence of a large uncontrollable environment on the controlled system. The ensuing decoherence generally leads to a loss of purity which one must compensate if the target of control is a pure state [8, 115]. Moreover, the environment can result in noisy system parameters or imperfect control fields. This implies additional restrictions on the accuracy of the control process, and it can even be prohibitive for certain targets, especially in large systems [116].

One possibility to avoid the discussed limitations of coherent quantum control in terms of system-size and robustness to environmental noise is to exploit the incoherent dynamics of open quantum systems. This is called *incoherent control* as a complement to the coherent control described above. It can be realized by controlling how the system interacts with the surrounding environment [117, 118], by engineering the environmental state [9, 119, 120], or by implementing additional incoherent processes such as a quantum measurement [121, 122].

To illustrate the advantages of incoherent control, remember that the open system dynamics due to a Markovian environment differs qualitatively from the dynamics of closed systems under the Schrödinger equation, see Chap. 2. For example, a Markovian master equation,

$$\partial_t \rho_t = -\frac{i}{\hbar}[\mathsf{H}, \rho_t] + \sum_i \mathsf{L}_i \rho \mathsf{L}_i^\dagger - \frac{1}{2}\mathsf{L}_i^\dagger \mathsf{L}_i \rho_t - \frac{1}{2}\rho_t \mathsf{L}_i^\dagger \mathsf{L}_i, \tag{7.1}$$

generally effects a contraction on state space. Unlike the Schrödinger equation, it can therefore exhibit fixed points or steady states which are independent of the initial state and of the specific dynamics at intermediate times.

A prominent method that relies on the existence of such fixed points in open systems is optical pumping. Here, Hamiltonian driving is used to single out a specific fixed point. Another example is the damped harmonic oscillator, Eq. (3.5). Here one can manipulate the jump operators or, more precisely, the rates of absorption and emission of a photon, Eq. (3.10), by changing the environmental temperature. The fixed point is then given by the corresponding thermal state, Eq. (3.18). The idea of engineering the steady state of an open quantum system has attracted quite some attention of late [9, 11, 119, 120, 123–128], since it implies robustness both to the intricate evolution of a large number of coupled quantum states and to small imperfections due to environment coupling. In practice however, it can only be realized in highly engineered systems [117, 118, 129], in which one can access and design suitable environmental couplings and thus choose the jump operators L_i.

A different way of controlling an open system incoherently is by means of quantum measurements. Generally, there are two ways to do so. One can apply specific system transformations conditioned on the outcomes of a series of measurements [54, 121, 130, 131]—this is called *feedback control*. It requires, however, that one can actually detect the

measurement outcomes with high resolution and that the measurement is repeatable, *i.e.* that the system state is not destroyed. Again, these conditions are usually satisfied only in highly engineered model systems [63, 122, 132–134]. Alternatively one can implement a measurement without actually reading off the outcomes which is called a *nonselective measurement*, see Secs. 2.1.3 and 3.3[1]. This method is robust and more widely applicable than those mentioned above, since the demands on the measurement are quite low: It must only in principle allow one to distinguish between different states. If the nonselective measurement is carried out in a continuous fashion, one effectively implements a Markovian master equation (7.1) with the jump operators given by the measurement operators, see Eq. (3.76). First proof of principles studies of incoherent control by nonselective measurements have already been carried out [12, 135] and we will here apply it to control a prototypical biomolecular reaction, the isomerization of the visual pigment protein rhodopsin.

7.1 Coherent and Incoherent Isomerization Dynamics

Let us demonstrate how incoherent control works by means of a specific example: the isomerization reaction of rhodopsin. Rhodopsin is the pigment protein contained in the rod and cone cells of the vertebrate retina. It detects the incidence of photons by absorbing them in an isomerization reaction of its cofactor[2] retinal, see Fig. 7.1. As a result of the isomerization of retinal, rhodopsin changes its three-dimensional structure, setting off a biochemical reaction chain that culminates in the creation of an action potential in the sensory neurons [137–140]. The isomerization of rhodopsin or, more precisely, that of retinal therefore constitutes the primary event in the process of vision [141, 142]. After some time and under consumption of biochemical energy, rhodopsin changes back to its initial structure with the retinal cofactor back to the original isomer so that it is rearmed for absorbing another photon [142–144]. A quite similar protein called bacteriorhodopsin is responsible for light harvesting in certain bacteria such as halophilic archae [145], which are unable to carry out photosynthesis. Instead of setting off a sensory reaction chain, bacteriorhodopsin spends the energy of the incident photon for proton pumping and thereby acts as the primary source of energy in the mentioned bacteria.

Retinal is a relatively small organic molecule consisting of a phenyl-ring and a fourfold unsaturated polyene chain. Due to the four double bonds, there exists a variety of retinal isomers. Only two of them are of importance in the isomerization that takes place in the visual pigment rhodopsin: the 11-cis isomer and the all-trans isomer, see Fig. 7.2. Retinal starts in the 11-cis state corresponding to the minimum of the lowest

[1] In this sense, the analytical examples in Chap. 5 can also be considered incoherent control setups: In the first example one controls the reflection of a particle by a nonselective left-right measurement and in the second example one controls tunneling by a nonselective measurement of the populations of a two state system.

[2] A cofactor is a non-protein molecule that is responsible for the biological functionality of the protein it is attached to. A protein and its cofactor are not necessarily covalently bound and organic cofactors are often vitamins.

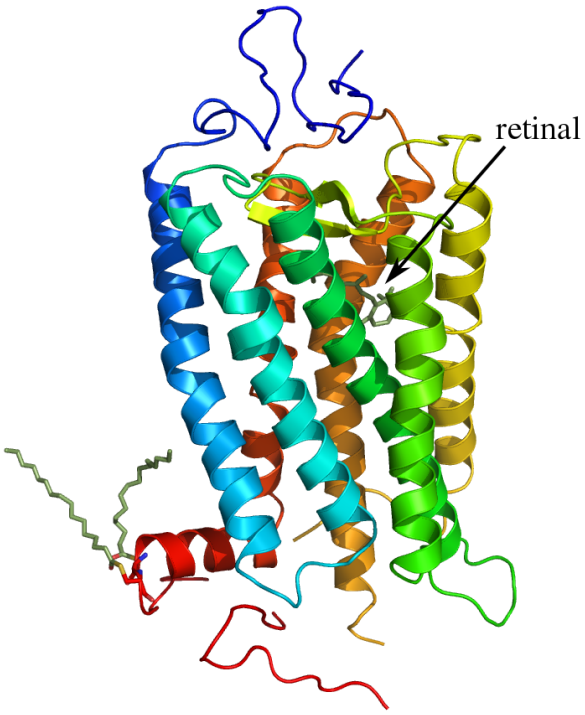

Figure 7.1: The 3D structure model of bovine rhodopsin, as obtained from crystal structure analysis [136] (see also pdb.org). At the center of the protein is the covalently bound cofactor retinal, depicted in gray, which is responsible for the absorption of visual light.

lying Born-Oppenheimer potential. Femtosecond spectroscopy experiments [146, 149] indicate that an absorption of a 500 nm photon leads to a transition of the ground state wave packet to the surface of the first excited electronic state, where it starts to evolve. Figure 7.2 presents a schematic picture of the ensuing evolution of the wave packet in the isomerization coordinate. Crucially, it reaches an avoided crossing with the electronic ground state potential after about 110 fs [147]. At this point, part of the population stays in the excited electronic state, proceeding towards the potential minimum associated with the all-trans isomer which is reached after about 200 fs [146, 149]. The other part of the wave packet tunnels to the initial Born-Oppenheimer surface and proceeds uphill until it reaches a turning point and then goes back in the opposite direction. It therefore reaches the avoided crossing of the two potential surfaces for a second time, where now part of the population proceeds towards the initial 11-cis isomer and the other part tunnels to the excited state potential. Gradually dissipating its vibrational energy to other vibrational degrees of freedom and to the environment, the molecule reaches either the 11-cis or the all-trans isomer without any further return to the avoided crossing. The coherent tunnelings described above continue for about 1 to 2 ps [148].

In the end, about 65% of the total population of retinal is found in the all-trans isomer

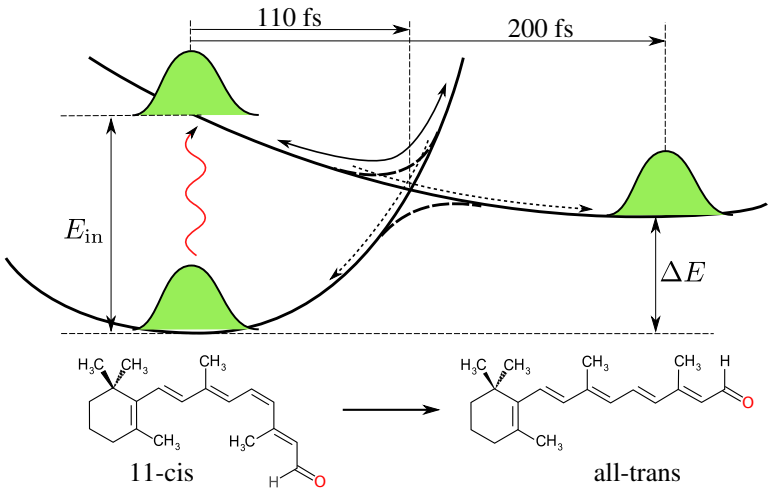

Figure 7.2: Schematic of the isomerization dynamics of retinal. Starting at the minimum of the lowest electronic potential which corresponds to the 11-cis isomer, retinal is excited by a 500 nm photon, $E_{\text{in}} = hc/500\,\text{nm}$ [146]. On the excited electronic potential, the wave packet starts to evolve along the isomerization coordinate (x-axis) and reaches an avoided crossing after 110 fs [147]. There, one part stays in the excited electronic state and the other part tunnels back to the electronic ground state potential. Whereas the former proceeds within 200 fs [146] to the minimum of the excited electronic potential which corresponds to the all-trans isomer, the latter proceeds uphill, turns back, and eventually reaches the avoided crossing for a second time. Again, the wave packet experiences partial tunneling with one part going back to the 11-cis isomer. This coherent tunneling continues for about 1 to 2 ps [148]. Once the wave packet has reached either one of the two potential minima, it dissipates the excess vibrational energy to the environment preventing it from returning to the avoided crossing.

[147, 150]. This isomerization yield is much higher than that of comparable isomerization reactions in solution [150, 151] since the protein architecture surrounding retinal was optimized by natural selection over billions of years. The high isomerization yield can be attributed to the extremely fast 200 fs time scale, which makes the retinal-isomerization in rhodopsin one of the fastest biochemical reactions ever observed [146]. It should be mentioned, however, that within 200 fs it is impossible to perform the rotation of the complete C_4H_4O-tail of retinal as the structural formulas for the two isomers in Fig. 7.2 suggest. The actual 3-dimensional shape after 200 fs is highly twisted and carries lots of excess vibrational energy—this intermediate product is called *photorhodopsin*. The transformation from photorhodopsin to the relaxed all-trans isomer called *bathorhodopsin* then occurs with near unit efficiency on a picosecond time scale [146, 152].

But how can one perform a nonselective measurement in this highly complex biomole-

cule? To see this, note that the fundamental difference between the all-trans and the 11-cis isomer of retinal is the arrangement of the constituent atoms in 3-dimensional space. Due to the structural differences, the two isomers have completely different vibrational eigenmodes and hence, for example, different absorption spectra in the infrared [152]. In other words, while one isomer may be transparent to a given infrared photon, the other one may have a finite absorption cross section at that frequency. Detecting the absorption of one such photon therefore constitutes a measurement of the retinal configuration state. What is more, for a nonselective measurement one need not worry about the actual recording of the absorption event—one can simply shine in infrared light at the relevant frequency to induce decoherence described by the master equation (7.1).

To be more specific, the infrared absorption spectra of rhodopsin show two things [152]: First, the absorption spectra of the electronic ground state and of the first excited state differ sharply in the vibrational modes associated with the concerted hydrogen-out-of-plane (HOOP) motion. In the corresponding spectral region between 800 and 950 cm^{-1}, the electronic ground state shows almost no absorption, whereas the first electronic state exhibits a pronounced structure involving three absorption peaks. Second, it was shown that the absorption spectra evolve along the isomerization coordinate [152]. For the present purpose of controlling the isomerization yield of rhodopsin, we here make use of the first aspect, *i.e.* the different infrared absorption cross sections of the involved electronic states, to implement a nonselective measurement of the electronic state during the isomerization dynamics [22]. Experimentally, several ways of making retinal absorb photons in the desired HOOP-mode have been demonstrated—one, by directly shining in infrared laser light [153], and two, by using a two-photon-process in the visual domain to implement a stimulated Raman transition [152].

7.1.1 The Closed Two-State Model for the Isomerization of Rhodopsin

To simulate the time evolution of rhodopsin under the influence of a nonselective measurement, we choose the simplest conceivable Hamiltonian model. The Born-Oppenheimer potential energy landscape depicted in Fig. 7.2 is represented by two coupled quantum mechanical oscillators with frequencies ω_1 and ω_2. Hence, the Schrödinger equation describing the closed isomerization dynamics of retinal reads

$$\begin{aligned}\partial_t|\psi_t\rangle = -\frac{i}{\hbar}\Bigg[&\frac{\hbar^2\mathsf{k}^2}{2m}\otimes\mathbb{1} + \frac{1}{2}m\omega_1^2\mathsf{x}^2\otimes|1\rangle\langle 1| + \left(\Delta E + \frac{1}{2}m\omega_2^2\left(\mathsf{x}-\Delta x\right)^2\right)\otimes|2\rangle\langle 2| \\ &+ \mathbb{1}\otimes\alpha(|1\rangle\langle 2| + |2\rangle\langle 1|)\Bigg]|\psi_t\rangle. \end{aligned} \tag{7.2}$$

Here, the states $|1\rangle$ and $|2\rangle$ are the ground and first excited electronic state, x is the isomerization coordinate, and ΔE and Δx are the energy and isomerization coordinate offset between the electronic potential curves, see Fig. 7.2. In agreement with experimental data [146], we set the energy difference E_{in} of the harmonic potentials at $x = 0$ to $E_{\mathrm{in}} = hc/\lambda = hc/500\,\mathrm{nm}$, and the offset of their minima to $\Delta E = 0.6E_{\mathrm{in}}$. This

determines the isomerization coordinate offset Δx,

$$m(\Delta x)^2 = \frac{2\,(E_{\text{in}} - \Delta E)}{\omega_2^2} = \frac{0.8 E_{\text{in}}}{\omega_2^2}. \tag{7.3}$$

The initial state $|\psi_0\rangle$ of the isomerization dynamics is the state immediately after the excitation due to an incoming 500 nm photon, *i.e.* the vibrational ground state $|v_{0,1}\rangle$ of the lowest electronic potential promoted to the first electronic potential surface,

$$|\psi_0\rangle = |v_{0,1}\rangle \otimes |2\rangle, \tag{7.4}$$

with

$$v_{0,1}(x) = \left(\frac{m\omega_1}{\pi\hbar}\right)^{\frac{1}{4}} \exp\left[-\frac{m\omega_1}{2\hbar}x^2\right]. \tag{7.5}$$

Note that in Eqs. (7.2) to (7.5), the mass m only appears as a factor of x^2 and as a divisor of k^2. In other words, it simply rescales the position coordinate and hence all numerical results discussed below are independent of m.

The only remaining parameters in the above two state model, Eqs. (7.2)–(7.5), for the isomerization dynamics of retinal are the frequencies of the harmonic electronic potentials ω_1 and ω_2, and the coupling constant α. Note that $\omega_1 = 2\pi/T_1$ and $\omega_2 = 2\pi/T_2$ should be chosen in such a way that a given initial wave packet evolves according to the above mentioned, experimentally determined time scales. Specifically, it should reach the avoided crossing after about 110 fs and it should reach the minimum of the excited electronic potential after about 200 fs. These requirements are fulfilled by choosing $T_1 = 300\,\text{fs}$ and $T_2 = 600\,\text{fs}$.

The adequate coupling constant α is determined in the following way: first, we assume that the transits through the avoided crossing occur completely coherently until about 1.1 ps, in agreement with experimental results [148]. Second, if the wave packet reaches one of the potential minima corresponding to the 11-cis and the all-trans isomer, it does not come back to the avoided crossing. We can therefore propagate the initial wave packet, Eqs. (7.4) and (7.5), with the Schrödinger equation (7.2) for 1.1 ps, with an absorbing, imaginary potential located at the bottom of each potential. In Fig. 7.3 we plot the resulting population in the all trans isomer as a function of time. This population shows a steplike behavior involving four steps between 0 and 1.1 ps. We conclude that the wave packet experiences seven transits of the avoided crossing (four from left to right and three from right to left), with each left-to-right-transit depositing a finite population to the all-trans isomer state. The adequate coupling constant α must then result in the experimentally determined final all-trans population (0.65). For the chosen model parameters we have $\alpha/\hbar = 0.1\,\text{fs}^{-1}$, see Fig. 7.3. Also, we see that the last step is only about 0.01 high, which means that after 1.1 ps almost the entire population has been transferred either to the all-trans or to the 11-cis isomer.

The evaluation of the all-trans population as a function of the coupling constant α suggests that the partition ratio for each individual transit of the avoided crossing is well described by the Landau-Zener tunneling probability, Eq. (5.39), as indicated by

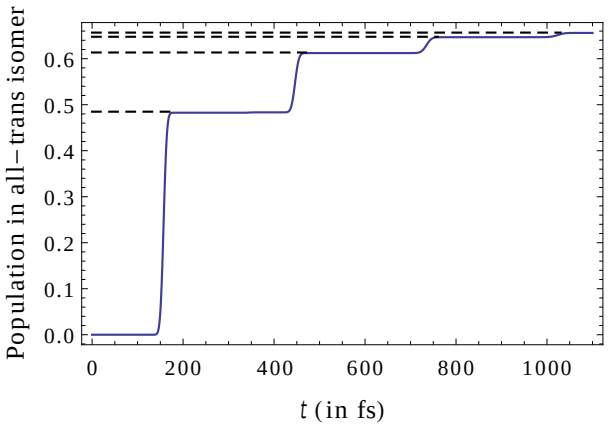

Figure 7.3: Population in the all-trans isomer as a function of time, blue solid line, obtained by numerical propagation of the initial wave packet, Eqs. (7.4) and (7.5), under the Schrödinger equation (7.2), with an absorbing potential at the bottom of the two harmonic potentials. In Eq. (7.2), $\Delta E = 0.6E_{\text{in}}$ and Δx, Eq. (7.3), are fixed by the experimentally determined excitation energy $E_{\text{in}} = ch/500\,\text{nm}$ [146]. Moreover, we use the parameters $\omega_1 = 2\pi/300\,\text{fs}$, $\omega_2 = 2\pi/600\,\text{fs}$, and $\alpha/\hbar = 0.1\,\text{fs}^{-1}$ to reproduce the experimentally observed time scales and the final isomerization yield (see text). In addition, the plot confirms the experimental observation that a single transit of the avoided crossing of the electronic potentials is well described by coherent Landau-Zener tunneling [148]: The dashed black lines in the plot represent the probabilities $P_n(\delta)$, Eq. (7.6), for n independent Landau-Zener transits for $n = 1, 3, 5, 7$, where the adiabaticity parameter, $\delta = 0.115$, is fixed by the wave packet velocity at the avoided crossing.

experimental studies [154]. This can be seen in Fig. 7.4, where we plot the numerically obtained all-trans populations after a single transit (from left to right) and after three transits (left-right, right-left, left-right) and compare this to the probability $P_n(\delta)$ for experiencing $n-1$ tunnelings plus one no-tunneling transition in an odd number n of independent Landau-Zener cycles. Here, $P_n(\delta)$ is determined by the Landau-Zener probability, Eq. (5.39),

$$P_n(\delta) = \exp[-2\pi\delta] \sum_{i=0}^{(n-1)/2} (1 - \exp[-2\pi\delta])^{2i}, \text{ for } n \text{ odd}. \tag{7.6}$$

The relevant adiabaticity parameter for our two state model, $\delta = 11.5(\alpha/\hbar)^2\,\text{fs}^2$, is fixed by the wave packet velocity at the avoided crossing which, in turn, is determined by the potential energy offset between the initial position on the excited Born-Oppenheimer surface and the crossing point. We see that $P_1(\delta)$ and $P_3(\delta)$ (solid lines in Fig. 7.4) are in very good agreement with the numerically obtained populations (dotted lines). This

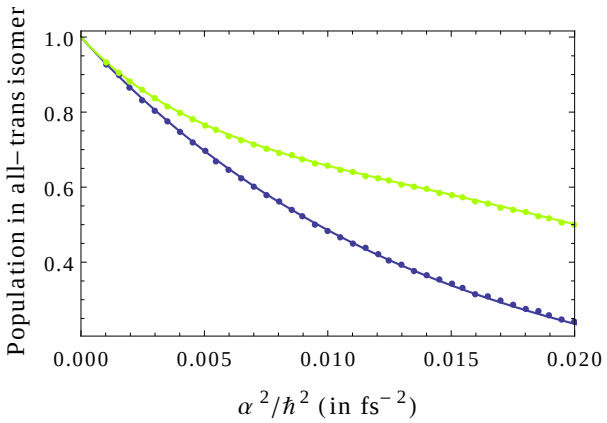

Figure 7.4: Population in the all-trans isomer obtained by numerical propagation of the initial wave packet, Eqs. (7.4) and (7.5), under the Schrödinger equation (7.2) as a function of the coupling constant $\alpha/\hbar$ between the electronic potentials. Blue dots represent the population after one transit (from left to right) of the avoided crossing and light green dots that after three transits (left-right, right-left, left-right). Compare this to the probabilities $P_1(\delta)$ and $P_3(\delta)$ (with $\delta = 11.5(\alpha/\hbar)^2\,\mathrm{fs}^2$, see text), Eq. (7.6), for ending up in the initial diabatic state after one and three independent Landau-Zener transits (blue line and light green line, respectively).

observation can be confirmed in Fig. 7.3 , where we mark the Landau-Zener predictions $P_n(\delta)$ for $n = 1, 3, 5, 7$ and $\delta = 0.115$ (*i.e.* for $\alpha = 0.1$) by dashed horizontal lines.

7.1.2 The Rhodopsin Isomerization under Nonselective Measurements

As mentioned above, the basic idea to implement a nonselective measurement in rhodopsin is to shine in infrared light. This must be done at a specific wavelength which is scattered or absorbed differently by the two electronic states involved in the isomerization reaction. Experimental studies show that the hydrogen-out-of-plane modes between 800 and $950\,\mathrm{cm}^{-1}$ are particularly suited for this purpose: while the electronic ground state $|1\rangle$ is transparent to infrared photons at $850\,\mathrm{cm}^{-1}$, the first excited electronic state $|2\rangle$ exhibits a finite cross section [152]. Consequently, if one could unambiguously detect whether a single $850\,\mathrm{cm}^{-1}$ probe photon was absorbed by retinal or not, then the detection of an absorption event would project retinal onto $|2\rangle$. Even if one does not have the ability to detect single measurement outcomes, the continuous illumination of retinal with $850\,\mathrm{cm}^{-1}$ photons constitutes a nonselective measurement of the electronic state,

see Secs. 2.1.3 and 3.3. It therefore gives rise to the master equation

$$\begin{aligned}\partial_t \rho_t &= -\frac{i}{\hbar}\left[\mathsf{H}_{\mathrm{ret}}, \rho_t\right] + \gamma\left\{(\mathbb{1}\otimes|2\rangle\langle 2|)\rho_t(\mathbb{1}\otimes|2\rangle\langle 2|) - \frac{1}{2}(\mathbb{1}\otimes|2\rangle\langle 2|)\rho_t - \frac{1}{2}\rho_t(\mathbb{1}\otimes|2\rangle\langle 2|)\right\} \\ &= -\frac{i}{\hbar}\left[\mathsf{H}_{\mathrm{ret}}, \rho_t\right] + \frac{\gamma}{2}\left\{(\mathbb{1}\otimes|2\rangle\langle 2|)\rho_t(\mathbb{1}\otimes|2\rangle\langle 2|) + (\mathbb{1}\otimes|1\rangle\langle 1|)\rho_t(\mathbb{1}\otimes|1\rangle\langle 1|) - \rho_t\right\},\end{aligned} \tag{7.7}$$

where $\mathsf{H}_{\mathrm{ret}}$ is determined by Eq. (7.2),

$$\mathsf{H}_{\mathrm{ret}} = \frac{\hbar^2\mathsf{k}^2}{2m}\otimes\mathbb{1} + \frac{m}{2}\omega_1^2\mathsf{x}^2\otimes|1\rangle\langle 1| + \left[\Delta E + \frac{m}{2}\omega_2^2\left(\mathsf{x}-\Delta x\right)^2\right]\otimes|2\rangle\langle 2| + \mathbb{1}\otimes\alpha(|1\rangle\langle 2| + |2\rangle\langle 1|). \tag{7.8}$$

Here, the nonselective measurement rate γ is given by the intensity of the incoming infrared radiation times the absorption cross section of the first excited electronic state. Equations (7.7) and (7.8) constitute our open quantum model for the isomerization of retinal under the influence of a continuous nonselective measurement of the electronic state.

Before propagating the master equation (7.7) and determining the isomerization yield for various measurement rates γ, let us give a short outlook on what to expect qualitatively. We saw in the previous section that the final isomerization yield is determined by the transits of the excited state wave packet through the avoided crossing of the two electronic potentials. These transits, in turn, are well described by consecutive Landau-Zener tunnelings. Furthermore, in Sec. 5.2 we found that Landau-Zener tunneling is suppressed in the presence of dephasing or a nonselective measurement. Specifically, the tunneling probability $P(\delta,\gamma)$ decreases monotonically from its coherent value of $1-\exp(-2\pi\delta)$ (for $\gamma = 0$) to the lower limit $(1-\exp[-4\pi\delta])/2$ in the case of infinitely strong dephasing and the analytic expressions (5.121) and (5.122), that were found by means of an adaptive resummation of the open Landau-Zener jump expansion, interpolate between the two limits. Therefore, equivalently to Eq. (7.6) for a series of coherent Landau-Zener tunnelings, the open Landau-Zener probability after an odd number n of transits reads

$$P_n(\delta,\gamma) = P(\delta,\gamma)\sum_{i=0}^{(n-1)/2}\left(1-P(\delta,\gamma)\right)^{2i}, \tag{7.9}$$

with $P(\delta,\gamma)$ given by Eq. (5.122).

The Landau-Zener analogy suggests to enhance the isomerization yield by applying the nonselective measurement dynamics, Eq. (7.7), whenever the excited state wave packet transits the avoided crossing from left to right. We have to keep in mind, however, that the Landau-Zener problem describes an idealized avoided crossing of two states whose energy difference varies linearly from $-\infty$ to ∞. In contrast, our two-state model for the isomerization of retinal, Eq. (7.2), involves the continuous isomerization coordinate x, *i.e.* it governs the evolution of wave packets on a potential energy landscape. Moreover, unlike in the Landau-Zener problem our initial state $|\psi_0\rangle$ as given by Eqs. (7.4) and (7.5),

will explore only a finite region of the entire coordinate space and hence experience only a finite energy difference between the electronic potentials.

Single Transit

Let us first look into the numerically exact γ-dependence of a single transit through the avoided crossing in retinal. In order for that, we propagate Eq. (7.7) until about 200 fs and determine the population in the all-trans isomer. The blue line in Fig. 7.5 shows the all-trans population as a function of γ on a semi-logarithmic plot. For comparison, we also plot the analytic open Landau-Zener probability (dashed black line) given by Eq. (7.9) for $\delta = 0.115$ (see above). We see that initially, for measurement rates $\gamma \in [0, 2\,\mathrm{fs}^{-1}]$, the all-trans population behaves as predicted by the analytic open Landau-Zener model. When, however, γ exceeds the inverse of the smallest coherent time scale, indicated by Ω on the abscissa, the all-trans population starts rising above its Landau-Zener limit of $1/2 + \exp[-4\pi\delta]/2$ and eventually approaches unity. Here, the inverse of the smallest coherent time scale is given by the Rabi frequency Ω of the coupled electronic potentials immediately after the initial excitation pulse,

$$\Omega = \sqrt{(E_{\mathrm{in}}/\hbar)^2 + (\alpha/\hbar)^2} \approx E_{\mathrm{in}}/\hbar. \tag{7.10}$$

Note that the Landau-Zener model involves no such maximal coherent frequency since the energy offset of the considered levels varies between $-\infty$ and ∞. The finite energy offset in the more realistic two state model, Eq. (7.7), therefore implies that we have more possibilities for controlling the isomerization yield of retinal.

An intuitive explanation why the passage through the avoided crossing increases with growing rate γ is given by the quantum Zeno effect: Frequent measurements of the electronic state prevent the system from evolving away from an eigenstate of the uncoupled Hamiltonian, which in turn enhances the diabatic transition. In practice, the measurement rate cannot be increased arbitrarily since retinal can absorb only a finite amount of infrared photons without disintegrating. The corresponding maximal sustainable infrared radiation power is determined both by the number of absorbing modes and by the time scale on which the excess vibrational energy is redistributed to other modes. In case of the HOOP frequencies between 800 and 950 cm^{-1} we have three modes corresponding to the wagging motion of C_{10}–H, C_{11}–H, and C_{12}–H. In view of the C–H bond energy ($\approx 4\,\mathrm{eV}$) and the energy of a photon at HOOP frequency ($\approx 0.1\,\mathrm{eV}$), a rate of $\gamma = 100\,\mathrm{fs}^{-1}$ (see Fig. 7.5) applied over a 200 fs interval would be too much.

A simple way to reduce the energy absorbed by retinal is to only induce infrared absorption during the actual transit of the avoided crossing. If we apply a measurement with rate $\gamma > 0$ within the time interval of the transit, $t \in [90\,\mathrm{fs}, 120\,\mathrm{fs}]$, and switch it off otherwise, we reduce the vibrational energy transferred to the retinal molecule by 85% compared to the continuous measurement over the entire 200 fs interval. The required femtosecond infrared or Raman pulses are feasible with present day technology [152, 153, 155–158]. What is more, the all-trans population for this pulsed measurement exceeds that of a continuous measurement by as much as 0.2, see purple line in Fig. 7.5. This

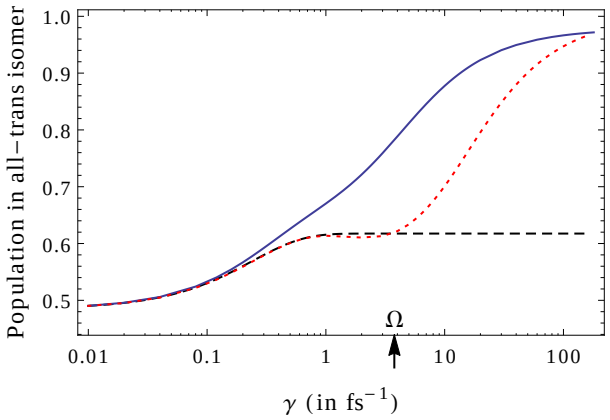

Figure 7.5: Population of the all-trans isomer after the first 200 fs as a function of the measurement rate γ. The red dotted line corresponds to the *continuous* nonselective measurement dynamics over the entire 200 fs time interval. The black dashed line depicts the corresponding prediction of the analytical open Landau-Zener model, Eq. (7.9). One observes that the isomerization yield increases strongly once γ exceeds the characteristic coherent system time scale Ω. The blue solid line shows the result of a *pulsed* nonselective measurement, applied only during the time period $t \in [90\,\text{fs}, 120\,\text{fs}]$ when the wave packet passes the avoided crossing. Note that the isomerization yield gets enhanced substantially in the pulsed case, even at moderate measurement rates $\gamma \simeq \Omega$.

further increase of the diabatic transition probability results from the fact that besides suppressing Landau-Zener tunneling, dephasing stretches the characteristic tunneling interval, see Eq. (5.59) for example. Hence, in the case of pulsed dephasing we limit the suppressed, incoherent tunneling to a small time period.

Multiple Transits

Having described the effect of a nonselective measurement on a single transit through the avoided crossing of the electronic potentials, let us consider the final all-trans population after 1.1 ps and seven transits in total. In Fig. 7.6 we plot the all-trans population (solid line) resulting from pulsed measurements applied during the transits of the avoided crossing, *i.e.* in the time intervals [90 fs, 120 fs], [390 fs, 420 fs], [670 fs, 700 fs], and [960 fs, 990 fs]. The inset depicts the time-dependent switching of the measurement. Note that in this case only the left-to-right transits are addressed since they are the ones that contribute to the final all-trans population. A measurement-induced suppression of tunneling during the right-to-left transits would lead to a higher population in the unwanted 11-cis isomer.

The final all-trans population after seven transits is naturally higher than that after a single transit. It increases monotonically with γ, starting from its experimentally observed value of 65% at $\gamma = 0$, and eventually approaches unity. Note that the mea-

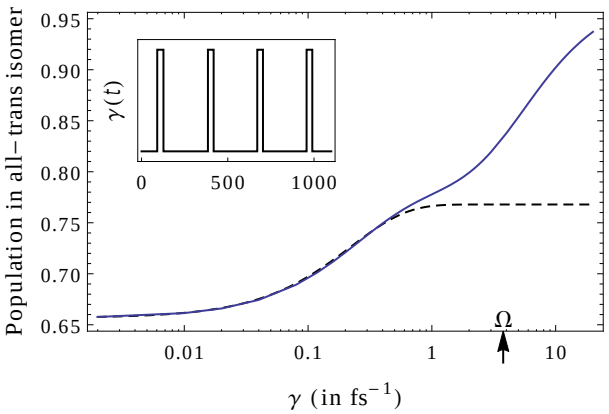

Figure 7.6: Final isomerization yield for a pulsed nonselective measurement with rate γ (solid line). For comparison, the dashed line shows the result of the analytical open Landau-Zener model, Eq. (7.9). The inset indicates the periods when the measurement is switched on (abscissa in fs), corresponding to times when the excited state wave packet transits the avoided crossing from left to right. An all-trans population of 80% is obtained already at a moderate measurement rate of $2\,\mathrm{fs}^{-1}$.

surement rate γ, necessary for achieving a given population, is roughly one order of magnitude lower than in the previous section. For example, a moderate rate of $2\,\mathrm{fs}^{-1}$ leads to a yield of 80%. Again, we plot the prediction of the open Landau-Zener model, Eq. (7.9), for comparison (dashed line).

In conclusion, we saw that adequately timed infrared or two photon Raman pulses can be used to optimize the isomerization dynamics of the visual pigment protein rhodopsin, which constitutes the primary event in human vision. The underlying incoherent dynamics boosting the natural isomerization yield of 65% up to unity, in principle, is based on the back action of a nonselective measurement. The measurement distinguishes the electronic states involved in the isomerization by means of their unique spectral signatures between 800 and $950\,\mathrm{cm}^{-1}$. This purposeful implementation of decoherence was inspired by the Landau-Zener analogy for the avoided electronic potential surface crossing and ultimately facilitated by the analytical description of Landau-Zener tunneling in the presence of dephasing, see Chap. 5.

The performance of the proposed incoherent control scheme surpasses that of comparable coherent control schemes [23]. What is more, the necessary optical controls are simpler to implement since they only require a pulsed laser source and no advanced pulse shaping techniques, and the underlying incoherent control mechanism is more robust as it is not prone to environmental noise. With these advantages over coherent control schemes, the measurement based, incoherent approach not only offers a new powerful handle on the biological processes of photon detection and energy harvesting, but on the chemical reaction dynamics of large molecules under ambient conditions in general.

8 Conclusions

This thesis was aimed at deriving new analytical and numerical tools for a deeper understanding of open quantum dynamics. To summarize, in Chapter 4 we saw that one obtains a nonperturbative jump expansion of general Markovian open quantum dynamics by decomposing the Lindblad generator into two parts, similar to the Dyson series for weakly perturbed closed quantum systems. The absence of a small parameter in the jump expansion made it necessary to ensure its convergence in a second step by resummation. Motivated by the invariance properties of the master equation, this was realized by introducing a complex shift to the jump operators. We found that the convergence after the resummation is optimal if these shifts are adapted to time and to all previously occurred jumps. Besides this optimal adaptive resummation, there exists a variety of suboptimal resummations with a simpler algebraic structure, so that one can tailor the jump expansion to one's specific needs.

Based on a particularly simple but strongly convergent resummation of the jump expansion, we were able to derive highly accurate analytic approximations to two longstanding open quantum problems in Chapter 5: the spatial detection of a free particle and the open Landau-Zener system. In both systems we showed that the adaptive resummation method provides a compelling, intuitive dynamical picture which facilitates an analytic description: The spatial detection setting is mapped to the multiple quantum scattering at an imaginary potential step and the open Landau-Zener problem is mapped to a classical alternating Markov chain. Comparing the obtained analytic approximations to the numerically exact results, we found that the former are accurate to the per mil level.

In Chapter 7 we used the newly gained intuition about the open Landau-Zener system to design a robust control scheme based on the incoherent parts of the system dynamics. In particular, we studied the isomerization dynamics of the visual pigment protein rhodopsin and saw that it can be controlled by a continuous or pulsed nonselective measurement in the infrared. While this scheme requires pulsed laser sources but no advanced pulse shaping techniques and the underlying incoherent dynamics is not prone to environmental noise, it may boost the isomerization yield from its natural value of 0.65, which is already the result of evolutionary optimization, up to values close to unity. Measurement based incoherent control therefore offers a new, powerful handle not only on the biological processes of photon detection and energy harvesting, but on the chemical reaction dynamics of large molecules in general.

Besides facilitating analytic descriptions of Markovian open systems, the adaptive resummation scheme can also be used as a new, efficient method for the numerical simulation of their dynamics. In Chapter 6 we derived the corresponding numerical algorithm which approximates the jump expansion terms by standard Monte Carlo integration

with importance sampling. The strong convergence after the resummation implies that one can evaluate the contributions to the dynamics one by one, in the order of their importance. This contrasts with the standard simulation method based on quantum trajectories which approximates the time evolution with a single indiscriminate sum. We demonstrated the general validity and the efficiency of the Monte Carlo integration scheme in three exemplary, paradigmatic open systems. More specifically, we saw that the optimal resummation converges within the lowest two to five orders.

Based on the strong convergence of the optimal resummation for all considered Markovian master equations, we expect that this technique can advance our understanding of other open quantum systems as well. On the one hand, the strong convergence implies a generally high efficiency of the Monte Carlo integration method. In this respect, a systematic comparison to the performance of the standard quantum Monte Carlo wave function approach would be illuminating. On the other hand, it implies that we have considerable room for adapting the jump expansion to other master equations in order to obtain specific simple and yet strongly convergent suboptimal resummations. This, in turn, would facilitate the mapping of the system dynamics to analytically accessible stochastic processes, similar to those treated in Chapter 5. The physical intuition that comes along with such analytic descriptions could then be employed for designing new, robust incoherent control techniques, as we showed in Chapter 7.

One can also think of extending the present expansion and resummation scheme to other quantum control scenarios. For example, one could optimize the jump expansion to effect a rapid increase of a desired target functional of the evolved quantum state. This was already considered for expansions of open system dynamics into quantum trajectories [71]. To result in an increased target functional for the final density matrix, such an optimal control scenario should of course go beyond the invariant transformations of the master equation and associated jump operators, Eqs. (4.20) and (4.21). One can also extend the range of application of the adaptive resummation method to non-Markovian open systems. This can be done by mapping a system coupled to a bath with finite correlation times to an extended system with additional quantum degrees of freedom which couple to a memoryless environment [159]. Then, the resulting Markovian system is again directly accessible with the jump expansion. Furthermore, given the similarity of the jump expansion to perturbative expansions of closed systems and therefore to quantum scattering theory, one could use the former for deriving an incoherent quantum scattering approach. Such a formalism has possible applications in inelastic nuclear scattering, where the multitude of collective motional states of the nucleus act as an environment to the actual scattering process [160]. In this line of thought, the reflection of a free particle at a measurement boundary described in Chapter 5 can be seen as a simple incoherent scattering example.

Finally, the optimal resummation of the jump expansion has implications for the study of pointer states, *i.e.* the distinguished set of basis states with presumably classical properties that any open system ultimately decays to. At present, the pointer states of a given open system can be identified as the solitonic or steady state solutions of a specific nonlinear evolution equation for pure states. This nonlinear equation was established

based on empirical observations in certain paradigmatic open systems [14, 49, 51], and it can be associated with the deterministic part of a specific unraveling of the master equation into quantum trajectories called the orthogonal unraveling [16, 53, 61]. Here, we proved the minimality of the jump rates, a defining property of the pointer states, for the optimal resummation and obtained exactly the same jump operators as in the orthogonal unraveling. We therefore have additional support for the above mentioned method for identifying pointer states. Moreover, with the pointer states of realistic open systems expected to exhibit small but nonvanishing jump rates, the emergence of classical properties should be described most adequately by means of mixed states. Since the jump expansion, in contrast to the quantum trajectory approach, decomposes the open system dynamics into mixed states, it may well allow for new conclusions about the quantum-to-classical transition.

All in all, with its use for the analytical and numerical study of general Markovian dynamics and its implications for quantum control and for the emergence of classicality, the adaptive resummation method promises to be a valuable addition to the standard open systems toolbox.

Bibliography

[1] W. H. Zurek, *Pointer basis of quantum apparatus: Into what mixture does the wave packet collapse?*, Phys. Rev. D **24**, 1516–1525 (1981).

[2] E. Joos and H. D. Zeh, *The emergence of classical properties through interaction with the environment*, Z. Phys. B Con. Mat. **59**, 223–243 (1985).

[3] E. Joos, H. D. Zeh, C. Kiefer, D. Giulini, J. Kupsch, and I. O. Stamatescu, *Decoherence and the Appearance of a Classical World in Quantum Theory*, Springer, Berlin, 2nd edition, 2003.

[4] W. H. Zurek, *Decoherence, einselection, and the quantum origins of the classical*, Rev. Mod. Phys. **75**, 715–775 (2003).

[5] M. Brune, E. Hagley, J. Dreyer, X. Maître, A. Maali, C. Wunderlich, J. M. Raimond, and S. Haroche, *Observing the Progressive Decoherence of the "Meter" in a Quantum Measurement*, Phys. Rev. Lett. **77**, 4887–4890 (1996).

[6] L. Hackermüller, K. Hornberger, B. Brezger, A. Zeilinger, and M. Arndt, *Decoherence of matter waves by thermal emission of radiation*, Nature **427**, 711–714 (2004).

[7] I. L. Chuang, R. Laflamme, P. W. Shor, and W. H. Zurek, *Quantum Computers, Factoring, and Decoherence*, Science **270**, 1633–1635 (1995).

[8] L. Viola and S. Lloyd, *Dynamical suppression of decoherence in two-state quantum systems*, Phys. Rev. A **58**, 2733–2744 (1998).

[9] S. Clark, A. Peng, M. Gu, and S. Parkins, *Unconditional Preparation of Entanglement between Atoms in Cascaded Optical Cavities*, Phys. Rev. Lett. **91**, 177901 (2003).

[10] A. Pechen and H. Rabitz, *Teaching the environment to control quantum systems*, Phys. Rev. A **73**, 062102 (2006).

[11] F. Verstraete, M. M. Wolf, and J. I. Cirac, *Quantum computation and quantum-state engineering driven by dissipation*, Nat. Phys. **5**, 633–636 (2009).

[12] O. V. Prezhdo, *Quantum Anti-Zeno Acceleration of a Chemical Reaction*, Phys. Rev. Lett. **85**, 4413–4417 (2000).

[13] R. Wu, A. Pechen, C. Brif, and H. Rabitz, *Controllability of open quantum systems with Kraus-map dynamics*, J. Phys. A: Math. Theor. **40**, 5681 (2007).

[14] W. T. Strunz, *Decoherence in Quantum Physics*, in *Coherent Evolution in Noisy Environments*, edited by A. Buchleitner and K. Hornberger, volume 611 of *Lect. Notes Phys.*, chapter 5, pages 199–233, Springer, Berlin, 2002.

[15] J. Eisert, *Exact Decoherence to Pointer States in Free Open Quantum Systems is Universal*, Phys. Rev. Lett. **92**, 210401 (2004).

[16] M. Busse and K. Hornberger, *Emergence of pointer states in a non-perturbative environment*, J. Phys. A: Math. Theor. **42**, 362001 (2009).

[17] A. S. Holevo, *Statistical Structure of Quantum Theory*, volume 67 of *Lect. Notes Phys. M*, chapter 3, pages 71–96, Springer, Berlin, 2001.

[18] B. Vacchini, *Theory of Decoherence due to Scattering Events and Lévy Processes*, Phys. Rev. Lett. **95**, 230402 (2005).

[19] K. Hornberger, *Introduction to Decoherence Theory*, in *Entanglement and Decoherence*, edited by A. Buchleitner, C. Viviescas, and M. Tiersch, volume 768 of *Lect. Notes Phys.*, chapter 5, pages 221–276, Springer, Berlin, 2009.

[20] F. Lucas and K. Hornberger, *Adaptive Resummation of Markovian Quantum Dynamics*, Phys. Rev. Lett. **110**, 240401 (2013).

[21] F. Lucas and K. Hornberger, *Optimally convergent quantum jump expansion*, Phys. Rev. A **89**, 012112 (2014).

[22] F. Lucas and K. Hornberger, *Incoherent Control of the Retinal Isomerization in Rhodopsin*, ArXiv e-prints (2014), arXiv:1403.3203.

[23] V. I. Prokhorenko, A. M. Nagy, S. A. Waschuk, L. S. Brown, R. R. Birge, and R. J. D. Miller, *Coherent Control of Retinal Isomerization in Bacteriorhodopsin*, Science **313**, 1257–1261 (2006).

[24] C. Cohen-Tannoudji, B. Diu, and F. Laloë, *Quantum Mechanics*, volume 1, Wiley, New York, 2nd edition, 2005.

[25] M. A. Nielsen and I. L. Chuang, *Quantum Computation and Quantum Information*, Cambridge University Press, Cambridge, 2000.

[26] S. J. Freedman and J. F. Clauser, *Experimental Test of Local Hidden-Variable Theories*, Phys. Rev. Lett. **28**, 938–941 (1972).

[27] A. Aspect, P. Grangier, and G. Roger, *Experimental Tests of Realistic Local Theories via Bell's Theorem*, Phys. Rev. Lett. **47**, 460–463 (1981).

[28] H. P. Breuer and F. Petruccione, *The Theory of Open Quantum Systems*, Oxford University Press, Oxford, 2002.

[29] S. Nimmrichter and K. Hornberger, *Macroscopicity of Mechanical Quantum Superposition States*, Phys. Rev. Lett. **110**, 160403 (2013).

[30] U. Weiss, *Quantum Dissipative Systems*, World Scientific, Singapore, 1999.

[31] H. Grabert, P. Schramm, and G.-L. Ingold, *Quantum Brownian motion: The functional integral approach*, Phys. Rep. **168**, 115–207 (1988).

[32] R. Horodecki, P. Horodecki, M. Horodecki, and K. Horodecki, *Quantum entanglement*, Rev. Mod. Phys. **81**, 865–942 (2009).

[33] R. Alicki and K. Lendi, *Quantum Dynamical Semigroups and Applications*, volume 286 of *Lect. Notes Phys.*, Springer, Berlin, 1987.

[34] D. Chruściński and A. Kossakowski, *From Markovian semigroup to non-Markovian quantum evolution*, Europhys. Lett. **97**, 20005 (2012).

[35] M. Wolf and J. I. Cirac, *Dividing Quantum Channels*, Commun. Math. Phys. **279**, 147–168 (2008).

[36] Á. Rivas, S. F. Huelga, and M. B. Plenio, *Entanglement and Non-Markovianity of Quantum Evolutions*, Phys. Rev. Lett. **105**, 050403 (2010).

[37] H.-P. Breuer, E.-M. Laine, and J. Piilo, *Measure for the Degree of Non-Markovian Behavior of Quantum Processes in Open Systems*, Phys. Rev. Lett. **103**, 210401 (2009).

[38] D. Chruściński, A. Kossakowski, and Á. Rivas, *Measures of non-Markovianity: Divisibility versus backflow of information*, Phys. Rev. A **83**, 052128 (2011).

[39] V. Gorini, A. Kossakowski, and E. C. G. Sudarshan, *Completely positive dynamical semigroups of N-level systems*, J. Math. Phys. **17**, 821–825 (1976).

[40] G. Lindblad, *On the generators of quantum dynamical semigroups*, Comm. Math. Phys. **48**, 119–130 (1976).

[41] M. Reed and B. Simon, *Methods of Modern Mathematical Physics*, volume 2, Fourier Analysis, Self-Adjointness, Academic Press, London, 1975.

[42] K. Hornberger, *Monitoring approach to open quantum dynamics using scattering theory*, Europhys. Lett. **77**, 50007 (2007).

[43] A. Barchielli and V. P. Belavkin, *Measurements continuous in time and a posteriori states in quantum mechanics*, J. Phys. A: Math. Gen. **24**, 1495 (1991).

[44] J. Dalibard, Y. Castin, and K. Mølmer, *Wave-function approach to dissipative processes in quantum optics*, Phys. Rev. Lett. **68**, 580–583 (1992).

[45] C. W. Gardiner, A. S. Parkins, and P. Zoller, *Wave-function quantum stochastic differential equations and quantum-jump simulation methods*, Phys. Rev. A **46**, 4363–4381 (1992).

[46] H. J. Carmichael, *An Open Systems Approach to Quantum Optics*, volume 18 of *Lect. Notes Phys. M*, Springer, Berlin, 1993.

[47] W. Nagourney, J. Sandberg, and H. Dehmelt, *Shelved optical electron amplifier: Observation of quantum jumps*, Phys. Rev. Lett. **56**, 2797–2799 (1986).

[48] T. Sauter, W. Neuhauser, R. Blatt, and P. E. Toschek, *Observation of Quantum Jumps*, Phys. Rev. Lett. **57**, 1696–1698 (1986).

[49] N. Gisin and M. Rigo, *Relevant and irrelevant nonlinear Schrodinger equations*, J. Phys. A: Math. Gen. **28**, 7375 (1995).

[50] A. O. Caldeira and A. J. Leggett, *Path integral approach to quantum Brownian motion*, Physica A **121**, 587–616 (1983).

[51] L. Diósi and C. Kiefer, *Robustness and Diffusion of Pointer States*, Phys. Rev. Lett. **85**, 3552–3555 (2000).

[52] K. Hornberger and J. E. Sipe, *Collisional decoherence reexamined*, Phys. Rev. A **68**, 012105 (2003).

[53] M. Busse, *Emergence and Dynamics of Pointer States*, PhD thesis, Ludwig-Maximilians-Universität, München, 2010.

[54] H. M. Wiseman and G. J. Milburn, *Quantum Measurement and Control*, Cambridge University Press, Cambridge, 2010.

[55] L. Hörmander, *An introduction to complex analysis in several variables*, North-Holland Publishing, Amsterdam, 3rd revised edition, 1990.

[56] F. M. Ramazanoglu, *The approach to thermal equilibrium in the Caldeira–Leggett model*, J. Phys. A: Math. Theor. **42**, 265303 (2009).

[57] W. H. Zurek, *Decoherence and the Transition from Quantum to Classical*, Phys. Today **44**, 36–44 (1991).

[58] J. R. Taylor, *Scattering Theory*, pages 262–265, John Wiley & Sons, New York, 1972.

[59] B. Vacchini and K. Hornberger, *Quantum linear Boltzmann equation*, Phys. Rep. **478**, 71–120 (2009).

[60] K. Hornberger, S. Gerlich, P. Haslinger, S. Nimmrichter, and M. Arndt, *Colloquium: Quantum interference of clusters and molecules*, Rev. Mod. Phys. **84**, 157–173 (2012).

[61] M. Busse and K. Hornberger, *Pointer basis induced by collisional decoherence*, J. Phys. A: Math. Theor. **43**, 015303 (2010).

[62] C. Guerlin, J. Bernu, S. Deleglise, C. Sayrin, S. Gleyzes, S. Kuhr, M. Brune, J.-M. Raimond, and S. Haroche, *Progressive field-state collapse and quantum non-demolition photon counting*, Nature **448**, 889–893 (2007).

[63] C. Sayrin, I. Dotsenko, X. Zhou, B. Peaudecerf, T. Rybarczyk, S. Gleyzes, P. Rouchon, M. Mirrahimi, H. Amini, M. Brune, J.-M. Raimond, and S. Haroche, *Real-time quantum feedback prepares and stabilizes photon number states*, Nature **477**, 73–77 (2011).

[64] X. Zhou, I. Dotsenko, B. Peaudecerf, T. Rybarczyk, C. Sayrin, S. Gleyzes, J. M. Raimond, M. Brune, and S. Haroche, *Field Locked to a Fock State by Quantum Feedback with Single Photon Corrections*, Phys. Rev. Lett. **108**, 243602 (2012).

[65] J. Fourier, *Théorie Analytique de la Chaleur*, Firmin Didot, Paris, 1822.

[66] B. Taylor, *Methodus Incrementorum Directa et Inversa*, Gul. Innys, London, 1715.

[67] C. Delaunay, *La Théorie du Mouvement de la Lune*, Mallet-Bachelier, Paris, 1860.

[68] A. Messiah, *Quantum Mechanics*, volume 2, chapter XVII, North-Holland, Amsterdam, 1961.

[69] L. Diósi, *Stochastic pure state representation for open quantum systems*, Phys. Lett. A **114**, 451–454 (1986).

[70] J. K. Breslin, G. J. Milburn, and H. M. Wiseman, *Optimal Quantum Trajectories for Continuous Measurement*, Phys. Rev. Lett. **74**, 4827–4830 (1995).

[71] H. M. Wiseman and A. C. Doherty, *Optimal Unravellings for Feedback Control in Linear Quantum Systems*, Phys. Rev. Lett. **94**, 070405 (2005).

[72] G. R. Allcock, *The time of arrival in quantum mechanics I. Formal considerations*, Ann. Phys. New York **53**, 253–285 (1969).

[73] J. G. Muga, S. Brouard, and D. Macias, *Time of Arrival in Quantum Mechanics*, Ann. Phys. New York **240**, 351–366 (1995).

[74] Y. Aharonov, J. Oppenheim, S. Popescu, B. Reznik, and W. G. Unruh, *Measurement of time of arrival in quantum mechanics*, Phys. Rev. A **57**, 4130–4139 (1998).

[75] J. J. Halliwell, *Arrival Times in Quantum Theory from an Irreversible Detector Model*, Prog. Theor. Phys. **102**, 707 (1999).

[76] J. Echanobe, A. del Campo, and J. G. Muga, *Disclosing hidden information in the quantum Zeno effect: Pulsed measurement of the quantum time of arrival*, Phys. Rev. A **77**, 032112 (2008).

[77] J. B. Mackrory, K. Jacobs, and D. A. Steck, *Reflection of a particle from a quantum measurement*, New J. Phys. **12**, 113023 (2010).

[78] B. Misra and E. C. G. Sudarshan, *The Zeno's paradox in quantum theory*, J. Math. Phys. **18**, 756–763 (1977).

[79] J. G. Muga and C. R. Leavens, *Arrival time in quantum mechanics*, Phys. Rep. **338**, 353–438 (2000).

[80] J. A. Damborenea, I. L. Egusquiza, G. C. Hegerfeldt, and J. G. Muga, *Measurement-based approach to quantum arrival times*, Phys. Rev. A **66**, 052104 (2002).

[81] C. Cohen-Tannoudji, B. Diu, and F. Laloë, *Quantum Mechanics*, volume 2, chapter 7, John Wiley & Sons, New York, 2005.

[82] L. D. Landau, *On the theory of transfer of energy at collisions II*, Phys. Z. Sowjetunion **2**, 46 (1932).

[83] C. Zener, *Non-Adiabatic Crossing of Energy Levels*, Proc. R. Soc. London A **137**, 696–702 (1932).

[84] E. Majorana, *Atomi orientati in campo magnetico variabile*, Nuovo Cimento **9**, 43 (1932).

[85] E. C. G. Stueckelberg, *Theorie der unelastischen Stösse zwischen Atomen*, Helv. Phys. Acta **5**, 369 (1932).

[86] L. D. Zusman, *Outer-sphere electron transfer in polar solvents*, Chem. Phys. **49**, 295–304 (1980).

[87] N. V. Vitanov, T. Halfmann, B. W. Shore, and K. Bergmann, *Laser-Induced Population Transfer by Adiabatic Passage Techniques*, Annu. Rev. Phys. Chem. **52**, 763–809 (2001), PMID: 11326080.

[88] W. Wernsdorfer and R. Sessoli, *Quantum Phase Interference and Parity Effects in Magnetic Molecular Clusters*, Science **284**, 133–135 (1999).

[89] T. Köhler, K. Góral, and P. S. Julienne, *Production of cold molecules via magnetically tunable Feshbach resonances*, Rev. Mod. Phys. **78**, 1311–1361 (2006).

[90] Y. Kayanuma, *Nonadiabatic Transitions in Level Crossing with Energy Fluctuation. I. Analytical Investigations*, J. Phys. Soc. Jpn. **53**, 108–117 (1984).

[91] Y. Kayanuma, *Nonadiabatic Transitions in Level Crossing with Energy Fluctuation. II. Numerical Investigations*, J. Phys. Soc. Jpn. **53**, 118–122 (1984).

[92] Y. Kayanuma, *Stochastic Theory for Nonadiabatic Level Crossing with Fluctuating Off-Diagonal Coupling*, J. Phys. Soc. Jpn. **54**, 2037–2046 (1985).

[93] Y. Kayanuma, *Population Inversion in Optical Adiabatic Rapid Passage with Phase Relaxation*, Phys. Rev. Lett. **58**, 1934–1936 (1987).

[94] P. Ao and J. Rammer, *Quantum dynamics of a two-state system in a dissipative environment*, Phys. Rev. B **43**, 5397–5418 (1991).

[95] V. M. Akulin and W. P. Schleich, *Landau-Zener transition to a decaying level*, Phys. Rev. A **46**, 4110–4113 (1992).

[96] V. L. Pokrovsky and N. A. Sinitsyn, *Fast noise in the Landau-Zener theory*, Phys. Rev. B **67**, 144303 (2003).

[97] K. Saito, M. Wubs, S. Kohler, Y. Kayanuma, and P. Hänggi, *Dissipative Landau-Zener transitions of a qubit: Bath-specific and universal behavior*, Phys. Rev. B **75**, 214308 (2007).

[98] G. Tayebirad, R. Mannella, and S. Wimberger, *Engineering interband transport by time-dependent disorder*, Phys. Rev. A **84**, 031605 (2011).

[99] X. Lacour, S. Guérin, L. P. Yatsenko, N. V. Vitanov, and H. R. Jauslin, *Uniform analytic description of dephasing effects in two-state transitions*, Phys. Rev. A **75**, 033417 (2007).

[100] V. M. Akulin, *Coherent Dynamics of Complex Quantum Systems*, Springer, Berlin, 2006.

[101] F. W. J. Olver, D. W. Lozier, R. F. Boisvert, and C. W. Clark, editors, *NIST Handbook of Mathematical Functions*, Cambridge University Press, New York, NY, 2010.

[102] J. Olver, *Uniform Asymptotic Expansions for Weber Parabolic Cylinder Functions of Large Orders*, J. Res. NBS **63 B**, 131 (1959).

[103] K. Mullen, E. Ben-Jacob, Y. Gefen, and Z. Schuss, *Time of Zener tunneling*, Phys. Rev. Lett. **62**, 2543–2546 (1989).

[104] M. B. Plenio and P. L. Knight, *The quantum-jump approach to dissipative dynamics in quantum optics*, Rev. Mod. Phys. **70**, 101–144 (1998).

[105] W. H. Press, S. A. Teukolsky, W. T. Vetterling, and B. P. Flannery, *Numerical Recipes*, Cambridge University Press, Cambridge, 3 edition, 2007.

[106] W. S. Warren, H. Rabitz, and M. Dahleh, *Coherent Control of Quantum Dynamics: The Dream Is Alive*, Science **259**, 1581–1589 (1993).

[107] H. Rabitz, R. de Vivie-Riedle, M. Motzkus, and K. Kompa, *Whither the Future of Controlling Quantum Phenomena?*, Science **288**, 824–828 (2000).

[108] A. H. Zewail and R. B. Bernstein, *Real-Time Laser Femtochemistry Viewing the transition from reagents to products*, Chem. Eng. News **66**, 24–43 (1988).

[109] A. H. Zewail, *Laser Femtochemistry*, Science **242**, 1645–1653 (1988).

[110] M. Shapiro and P. Brumer, *Principles of the Quantum Control of Molecular Processes*, John Wiley & Sons, New York, 2003.

[111] L. Childress, M. V. Gurudev Dutt, J. M. Taylor, A. S. Zibrov, F. Jelezko, J. Wrachtrup, P. R. Hemmer, and M. D. Lukin, *Coherent Dynamics of Coupled Electron and Nuclear Spin Qubits in Diamond*, Science **314**, 281–285 (2006).

[112] A. Assion, T. Baumert, M. Bergt, T. Brixner, B. Kiefer, V. Seyfried, M. Strehle, and G. Gerber, *Control of Chemical Reactions by Feedback-Optimized Phase-Shaped Femtosecond Laser Pulses*, Science **282**, 919–922 (1998).

[113] J. Herek, W. Wohlleben, R. Cogdell, D. Zeidler, and M. Motzkus, *Quantum control of energy flow in light harvesting*, Nature **417**, 533–535 (2002).

[114] M. Roth, L. Guyon, J. Roslund, V. Boutou, F. Courvoisier, J.-P. Wolf, and H. Rabitz, *Quantum Control of Tightly Competitive Product Channels*, Phys. Rev. Lett. **102**, 253001 (2009).

[115] L. Viola, *Advances in decoherence control*, J. Mod. Optic. **51**, 2357–2367 (2004).

[116] M. Khasin and R. Kosloff, *Noise and Controllability: Suppression of Controllability in Large Quantum Systems*, Phys. Rev. Lett. **106**, 123002 (2011).

[117] H. Krauter, C. A. Muschik, K. Jensen, W. Wasilewski, J. M. Petersen, J. I. Cirac, and E. S. Polzik, *Entanglement Generated by Dissipation and Steady State Entanglement of Two Macroscopic Objects*, Phys. Rev. Lett. **107**, 080503 (2011).

[118] J. T. Barreiro, M. Müller, P. Schindler, D. Nigg, T. Monz, M. Chwalla, M. Hennrich, C. F. Roos, P. Zoller, and R. Blatt, *An open-system quantum simulator with trapped ions*, Nature **470**, 486–91 (2011).

[119] J. F. Poyatos, J. I. Cirac, and P. Zoller, *Quantum Reservoir Engineering with Laser Cooled Trapped Ions*, Phys. Rev. Lett. **77**, 4728–4731 (1996).

[120] S. Pielawa, G. Morigi, D. Vitali, and L. Davidovich, *Generation of Einstein-Podolsky-Rosen-Entangled Radiation through an Atomic Reservoir*, Phys. Rev. Lett. **98**, 240401 (2007).

[121] A. Negretti, U. V. Poulsen, and K. Mølmer, *Quantum Superposition State Production by Continuous Observations and Feedback*, Phys. Rev. Lett. **99**, 223601 (2007).

[122] M. S. Blok, C. Bonato, D. J. Markham, M. L. Twitchen, V. V. Dobrovitski, and R. Hanson, *Manipulating a qubit through the backaction of sequential partial measurements and real-time feedback*, Nat. Phys. **10**, 189 (2014).

[123] M. B. Plenio, S. F. Huelga, A. Beige, and P. L. Knight, *Cavity-loss-induced generation of entangled atoms*, Phys. Rev. A **59**, 2468–2475 (1999).

[124] A. S. Parkins, E. Solano, and J. I. Cirac, *Unconditional Two-Mode Squeezing of Separated Atomic Ensembles*, Phys. Rev. Lett. **96**, 053602 (2006).

[125] S. Diehl, A. Micheli, A. Kantian, B. Kraus, H. P. Buchler, and P. Zoller, *Quantum states and phases in driven open quantum systems with cold atoms*, Nat. Phys. **4**, 878–883 (2008).

[126] F. Ticozzi and L. Viola, *Analysis and synthesis of attractive quantum Markovian dynamics*, Automatica **45**, 2002–2009 (2009).

[127] S. G. Schirmer and X. Wang, *Stabilizing open quantum systems by Markovian reservoir engineering*, Phys. Rev. A **81**, 062306 (2010).

[128] M. J. Kastoryano, F. Reiter, and A. S. Sørensen, *Dissipative Preparation of Entanglement in Optical Cavities*, Phys. Rev. Lett. **106**, 090502 (2011).

[129] Y. Lin, J. P. Gaebler, F. Reiter, T. R. Tan, R. Bowler, A. S. Sørensen, D. Leibfried, and D. J. Wineland, *Dissipative production of a maximally entangled steady state of two quantum bits*, Nature **504**, 1476–4687 (2013).

[130] A. C. Doherty and K. Jacobs, *Feedback control of quantum systems using continuous state estimation*, Phys. Rev. A **60**, 2700–2711 (1999).

[131] J. Wang and H. M. Wiseman, *Feedback-stabilization of an arbitrary pure state of a two-level atom*, Phys. Rev. A **64**, 063810 (2001).

[132] R. Vijay, C. Macklin, D. H. Slichter, S. J. Weber, K. W. Murch, R. Naik, A. N. Korotkov, and I. Siddiqi, *Stabilizing Rabi oscillations in a superconducting qubit using quantum feedback.*, Nature **490**, 77–80 (2012).

[133] D. Ristè, C. C. Bultink, K. W. Lehnert, and L. DiCarlo, *Feedback Control of a Solid-State Qubit Using High-Fidelity Projective Measurement*, Phys. Rev. Lett. **109**, 240502 (2012).

[134] S. Brakhane, W. Alt, T. Kampschulte, M. Martinez-Dorantes, R. Reimann, S. Yoon, A. Widera, and D. Meschede, *Bayesian Feedback Control of a Two-Atom Spin-State in an Atom-Cavity System*, Phys. Rev. Lett. **109**, 173601 (2012).

[135] G. A. Álvarez, D. D. B. Rao, L. Frydman, and G. Kurizki, *Zeno and Anti-Zeno Polarization Control of Spin Ensembles by Induced Dephasing*, Phys. Rev. Lett. **105**, 160401 (2010).

[136] T. Okada, Y. Fujiyoshi, M. Silow, J. Navarro, E. M. Landau, and Y. Shichida, *Functional role of internal water molecules in rhodopsin revealed by x-ray crystallography*, P. Natl. Acad. Sci. USA **99**, 5982–5987 (2002).

[137] L. Stryer, *Cyclic GMP Cascade of Vision*, Annu. Rev. Neurosci. **9**, 87–119 (1986).

[138] M. Chabre and P. Deterre, *Molecular mechanism of visual transduction*, Eur. J. Biochem. **179**, 255–266 (1989).

[139] L. Stryer, *Visual excitation and recovery*, J. Biol. Chem. **266**, 10711–10714 (1991).

[140] I. B. Leskov, V. A. Klenchin, J. W. Handy, G. G. Whitlock, V. I. Govardovskii, M. D. Bownds, T. D. Lamb, E. N. P. J. , and V. Y. Arshavsky, *The Gain of Rod Phototransduction: Reconciliation of Biochemical and Electrophysiological Measurements*, Neuron **27**, 525–537 (2000).

[141] T. Yoshizawa and G. Wald, *Pre-Lumirhodopsin and the Bleaching of Visual Pigments*, Nature **197**, 1279 (1963).

[142] G. Wald, *Molecular Basis of Visual Excitation*, Science **162**, 230–239 (1968).

[143] N. L. Mata, R. A. Radu, R. S. Clemmons, and G. H. Travis, *Isomerization and Oxidation of Vitamin A in Cone-Dominant Retinas: A Novel Pathway for Visual-Pigment Regeneration in Daylight*, Neuron **36**, 69–80 (2002).

[144] T. D. Lamb and E. N. Pugh Jr., *Dark adaptation and the retinoid cycle of vision*, Progr. Retin. Eye Res. **23**, 307–380 (2004).

[145] U. Haupts, J. Tittor, and D. Oesterhelt, *Closing in on Bacteriorhodopsin: Progress in Understanding the Molecule*, Annu. Rev. Bioph. Biom. **28**, 367–399 (1999).

[146] R. W. Schoenlein, L. A. Peteanu, R. A. Mathies, and C. V. Shank, *The first step in vision: femtosecond isomerization of rhodopsin*, Science **254**, 412–415 (1991).

[147] D. Polli, P. Altoè, O. Weingart, K. M. Spillane, C. Manzoni, D. Brida, G. Tomasello, G. Orlandi, P. Kukura, R. A. Mathies, M. Garavelli, and G. Cerullo, *Conical intersection dynamics of the primary photoisomerization event in vision*, Nature **467**, 440–3 (2010).

[148] Q. Wang, R. W. Schoenlein, L. A. Peteanu, R. A. Mathies, and C. V. Shank, *Vibrationally coherent photochemistry in the femtosecond primary event of vision*, Science **266**, 422–424 (1994).

[149] L. A. Peteanu, R. W. Schoenlein, Q. Wang, R. A. Mathies, and C. V. Shank, *The first step in vision occurs in femtoseconds: complete blue and red spectral studies*, P. Natl. Acad. Sci. USA **90**, 11762–11766 (1993).

[150] J. Kim, M. Tauber, and R. Mathies, *Wavelength dependent cis-trans isomerization in vision*, Biochemistry **40**, 13774–13778 (2001).

[151] H. J. A. Dartnall, *The photosensitivities of visual pigments in the presence of hydroxylamine*, Vision Res. **8**, 339–358 (1968).

[152] P. Kukura, D. W. McCamant, S. Yoon, D. B. Wandschneider, and R. A. Mathies, *Structural observation of the primary isomerization in vision with femtosecond-stimulated Raman*, Science **310**, 1006–9 (2005).

[153] J. Herbst, K. Heyne, and R. Diller, *Femtosecond infrared spectroscopy of bacteriorhodopsin chromophore isomerization*, Science **297**, 822–5 (2002).

[154] R. W. Schoenlein, L. A. Peteanu, Q. Wang, R. A. Mathies, and C. V. Shank, *Femtosecond dynamics of cis-trans isomerization in a visual pigment analog: isorhodopsin*, J. Phys. Chem. **97**, 12087–12092 (1993).

[155] S. E. Bromberg, H. Yang, M. C. Asplund, T. Lian, B. K. McNamara, K. T. Kotz, J. S. Yeston, M. Wilkens, H. Frei, R. G. Bergman, and C. B. Harris, *The Mechanism of a C-H Bond Activation Reaction in Room-Temperature Alkane Solution*, Science **278**, 260–263 (1997).

[156] M. C. Asplund, M. T. Zanni, and R. M. Hochstrasser, *Two-dimensional infrared spectroscopy of peptides by phase-controlled femtosecond vibrational photon echoes*, P. Natl. Acad. Sci. USA **97**, 8219–8224 (2000).

[157] C. J. Fecko, J. D. Eaves, J. J. Loparo, A. Tokmakoff, and P. L. Geissler, *Ultrafast Hydrogen-Bond Dynamics in the Infrared Spectroscopy of Water*, Science **301**, 1698–1702 (2003).

[158] M. D. Fayer, editor, *Ultrafast Infrared and Raman Spectroscopy*, Practical Spectroscopy, Marcel Dekker, New York, 2001.

[159] A. Imamoḡlu, *Stochastic wave-function approach to non-Markovian systems*, Phys. Rev. A **50**, 3650–3653 (1994).

[160] A. Săndulescu and H. Scutaru, *Open quantum systems and the damping of collective modes in deep inelastic collisions*, Ann. Phys. New York **173**, 277–317 (1987).